Analysis of coupling interface problems for bi-domain diffusion equations

Dissertation
zur Erlangung des akademischen Grades

Doktor rerum naturalium
(Dr. rer. nat.)

von M.Sc. Taj Munir

geb. am 01.01.1988 in Swat, Pakistan

genehmigt durch die Fakultät für Mathematik
der Otto-von-Guericke-Universität Magdeburg, Deutschland

Gutachter: Prof. Dr. Gerald Warnecke
Prof. Dr. Nagaiah Chamakuri

eingereicht am : 28.09.2020
Verteidigung am: 30.11.2020

Analysis of coupling interface problems for bi-domain diffusion equations

Dissertation
Submitted for the academic degree

Doctor rerum naturalium
(Dr. rer. nat.)

by: M.Sc. Math. Taj Munir
born on: 01.01.1988 in Swat, Pakistan

approved from the Faculty of Mathematics
Otto-von-Guericke-University, Magdeburg, Germany

Referees: Prof. Dr. Gerald Warnecke
Prof. Dr. Nagaiah Chamakuri

Submitted on: 28.09.2020
Defended on: 30.11.2020

Acknowledgment

I would like to express my sincere appreciation to my supervisor Prof. Dr. Gerald Warnecke who provided me an opportunity to work in his research group at Otto von Guericke University Magdeburg, Germany. During the PhD process, he encouraged me at every step through valuable and constructive criticism which helped me throughout my research work. I am very fortunate to have Prof. Warnecke as my adviser and can never thank him for all he has done for me during this journey. Even many time he came to the institute only for me. I would like particularly to thank him for his support during the difficult Corona period.

I am also very thankful to my co-supervisor Prof. Dr. Nagaiah Chamakuri for his personal and Skype meetings to guide me towards the required results. He is also a sincere person. In the beginning he give the specific task of my PhD thesis to expedite the process. Some of his suggested concepts made the thesis compact. Further I am grateful to all members of the Prof. Warnecke's research group and other institute members. My special thanks goes Dr. Ferdinand Thein, Dr. Carlos Cueto Camejo, Prof. Friedhelm Schieweck, Prof. Thomas Richter, Dr. Piotr Minakowski, Christoph Matern, Adnan Hayat and Hazem Yaghi for their generous help and discussions. I am also very thankful to the computer technical team Mr. Pieter kr secretaries of the institute Ms. Stephanie Wernicke and Ms. Birgit Dahlstrom for helping in administration issues.

I am also thankful to Prof. Dr. Muhammad Yousaf Malik and Prof. Dr. Shamsul Qamar for the guidance towards the PhD degree in Germany and they support me a lot during the tough situations in the doctoral study too. Further to motivate towards mathematics I was especially impressed from my college teacher, Prof. Ahmad Zeb. I have special thanks to him for his early stage learning motivation, who taught me the several ways that how to read " limit x tends to 0".

I have made many Pakistani, Afghani and Arabic friends during my stay in Magdeburg. I am very thankful to all of them to make my social life so memorable. Special thanks to Dr. Usman Farid, Dr. Muhammad Zaman, Dr. Muhammad Haneef, Hussan Zeb, Muhammad Ali, Fazal Khaliq, Zakir Ullah, Shahid Ali, Wahid Ullah and Tahir Khan to help me like family member. Further I am grateful to the Higher Education commission (HEC) of Pakistan and the German Academic Exchange Service (Deutscher Akademischer Austausch Dienst-DAAD) for funding this work.

Finally, a special profound acknowledgment go to my parents, wife, brothers and sisters and all of my villagers whose forbearance and their prayers have been invaluable. I dedicated this thesis to my beloved daughter Zoya Munir.

Abstract

In this thesis we study various numerical interface coupling conditions for diffusion equations in bio-physics or heat conduction problems. For this we take a one-dimensional case of a 3D model of Falcke [7] with two coupling conditions. The coupling interface conditions are given in Thul [37]. Originally they considered a system that models the intracellular calcium dynamics in a realistic fashion between the cytosolic region and the endoplasmic reticulum (ER) region of a living cell via channels on the membrane which separates both regions.

The phenomenon of calcium dynamics is a multi-domain phenomenon. We analyze a numerical mathematical problem related to the calcium transport, i.e. a bi-domain problem with coupling conditions. In order to understand fundamental numerical issues better, we make an analytical and computational study of the one dimensional case derived from the three dimensional model of Falcke [7]. We compare these with other related coupling conditions. The coupling conditions that we consider in this thesis include the well-known Dirichlet-Neumann coupling, the heat flux coupling, a channel pumping, a simplified channel pumping, a membrane pumping and its special cases simplified membrane pumping and linearized membrane pumping conditions.

We implemented three coupling algorithms namely, an explicit coupling algorithm (A1), an implicit monolithic coupling algorithm (A2), an implicit partitioned iterative coupling algorithm (A3) for the various coupling conditions with bi-domain diffusion equations. The partitioned iterative approach is a bit more complicated because we have the two unknowns corresponding to the each sub-domain. Despite this problem we manage to achieve a numerical solution via sub-iterations. Such algorithms may be useful for parallel computation.

The main emphasis of this work is to study the numerical properties of coupling conditions. We give a detailed account of the Godunov-Ryabenkii stability theory for coupling conditions that was introduced by Giles [10] for this purpose. An important point is to maintain conservativity of the overall scheme. Therefore, we first study this property for the coupling conditions. Unfortunately, Giles neglected to maintain conservativity of his scheme and by using an inconsistent scheme produced artificial instabilities. We show how conservativity is maintained in nodal based as well as finite volume type discretizations. Nodal based schemes need a central difference approximation with respect to the node at the coupling boundary. Finite volume schemes have to use one sided difference with respect to the cell center. It is a central difference with respect to the cell boundary which is also the interface boundary. An analogous result is shown for the homogeneous Neumann outer boundary condition.

We then proceed to prove stability for these coupling conditions. For this purpose we prove a lemma that describes in detail properties of the solutions to the normal mode equations that are useful to Godunov-Ryabenkii analysis of the coupling conditions. For comparison we first treat some boundary conditions related to flux coupling conditions. The simplest coupling, which was the one considered by Giles [10], is Dirichlet-Neumann coupling. The more complex couplings considered in this thesis lead to additional conditional stability conditions. The theoretical results on conservativity and stability are confirmed in computations for a variety of test cases.

Zusammenfassung

In dieser Arbeit werden verschiedene Kopplungsbedingungen für die Diffusionsgleichung aus der Biophysik oder aus Problemen im Bereich der Wärmeleitung numerisch untersucht. Hierfür wird ein eindimensionaler Fall des 3D Modells von Falcke [7] mit zwei Kopplungsbedingungen verwendet. Die Kopplungsbedingungen an der Grenzfläche sind Thul [37] entnommen. Ursprünglich betrachteten sie ein System, das die intrazelluläre Kalziumdynamik in realistischer Weise zwischen der zytosolischen Region und der Region des Endoplasmatischen Retikulums (ER) einer lebenden Zelle über Kanäle auf der Membran, welche die beide Regionen trennt, modelliert.

Das Phänomen der Kalziumdynamik ist ein Phänomen mehrerer gekoppelter Gebiete. Wir untersuchen ein mathematisches Problem, das mit dem Kalziumtransport zusammenhängt. Es ist ein Problem mit Kopplungsbedingungen zwischen zwei Teilintervallen. Um grundlegende numerische Fragen besser zu verstehen, führen wir analytische und rechnerische Untersuchungen des eindimensionalen Falls durch, der aus dem dreidimensionalen Modell von Falcke abgeleitet wurde [7]. Wir vergleichen diese mit anderen verwandten Kopplungsbedingungen. Die Kopplungsbedingungen, die wir in dieser Arbeit betrachten, umfassen die bekannte Dirichlet-Neumann-Kopplung, die Wärmeflusskopplung, ein Kanalpumpen, ein vereinfachtes Kanalpumpen, ein Membranpumpen und seine Spezialfälle vereinfachtes Membranpumpen sowie linearisiertes Membranpumpen.

Wir implementierten drei Kopplungsalgorithmen, nämlich einen expliziten Kopplungsalgorithmus (A1), einen impliziten monolithischen Kopplungsalgorithmus (A2), sowie einen impliziten partitionierten iterativen Kopplungsalgorithmus (A3) für die verschiedenen Kopplungensbedingungen. Der partitionierte iterative Ansatz ist dabei etwas komplizierter, da wir zwei unbekannte Vektoren haben, die den jeweiligen Unterbereichen entsprechen. Trotz dieser Schwierigkeiten erhalten wir eine numerische Lösung des Problems mithilfe sogenannter sub-Iterationen. Derartige Vorgehensweisen können für paralleles Rechnen nützlich sein.

Der Schwerpunkt dieser Arbeit liegt auf der Untersuchung der numerischen Eigenschaften von Kopplungsbedingungen. Wir geben eine detaillierte Darstellung der Godunov-Ryabenkii-Stabilitätstheorie für Kopplungsbedingungen, die von Giles [10] zu diesem Zweck eingeführt wurde. Ein wichtiger Punkt ist die Aufrechterhaltung der Erhaltungseigenschaft des Gesamtsche-mas. Deshalb untersuchen wir zunächst die Kopplungsbedingungen auf diese Eigenschaft. Leider hat Giles es versäumt, eben diese Eigenschaft seines Schemas beizubehalten, und durch die Verwendung eines inkonsistenten Schemas künstliche Instabilitäten erzeugt. Wir zeigen, wie die Erhaltungseigenschaft sowohl bei knotenbasierten als auch bei finite Volumen Diskretisierungen beibehalten wird. Knotenbasierte Schemata benötigen eine zentrale Differenzenapproximation in Bezug auf den Knoten an der Kopplungsgrenze. Finite Volumen Verfahren müssen eine einseitige Differenz in Bezug auf das Zellzentrum verwenden. Dies kann auch als eine zentrale Differenz in Bezug auf die Zellgrenze, welche gleichzeitig die Grenzfläche darstellt, aufgefasst werden. Ein analoges Resultat gilt auch für homogene Neumann Randbedingungen

Wir fahren fort mit dem Nachweis der Stabilität für diese Kopplungsbedingungen. Zu diesem Zweck beweisen wir ein Lemma, welches Eigenschaften der Lösungen der Nor-

malmodengleichungen, die für die Godunov-Ryabenkii-Analyse der Kopplungsbedingungen nützlich sind, detailliert beschreibt. Zum Vergleich behandeln wir zunächst einige Randbedingungen, die mit den Kopplungsbedingungen der Wäremleitung zusammenhängen. Die einfachste Kopplung, die von Giles [10] betrachtet wurde, ist die Dirichlet-Neumann-Kopplung. Die in dieser Arbeit betrachteten komplexeren Kopplungen führen zu zusätzlichen Stabilitätsbedingungen. Die theoretischen Ergebnisse zur Erhaltungseigenschaft und Stabilität werden für eine Vielzahl von Testfällen durch numerische Berechnungen bestätigt.

Contents

Chapter 1

Introduction

1.1 The subject of this thesis

The subject of this thesis is to study various numerical interface coupling conditions related to diffusion systems in bio-physics or problems in heat conduction. For this we take a one-dimensional case of a 3D model of Falcke [7] with various coupling conditions. The coupling interface conditions are given in Thul [37]. Originally they considered a system that models the intracellular calcium dynamics in a realistic fashion between the cytosolic region and the endoplasmic reticulum (ER) region of a living cell via channels on the membrane which separates both regions. The phenomenon of calcium dynamics is a multi-domain phenomenon. We analyze a numerical mathematical problem related to the calcium transport, i.e. a bi-domain problem with coupling conditions. In order to understand fundamental numerical issues better, we make an analytical and computational study of the one dimensional case derived from the three dimensional model of Falcke [7], Thul [37] and Chamakuri [26].

Many important real world problems in physics, engineering and biology are modeled via bi-domain or multi-domain partial differential equations (PDEs) with coupling conditions. These have several applications that arise in medical, biological and environmental sciences, economics as well as many others. These applications include e.g. heat conduction in composite material, heat conduction through skin, transdermal drug delivery and green house gas emission.

The coupling conditions that we consider include the well-known Dirichlet-Neumann coupling, the heat flux coupling, a channel pumping, a simplified channel pumping, a membrane pumping and its special cases simplified membrane pumping and linearized membrane pumping conditions. These problems cannot be typically solved directly, but must be approximated numerically. We use numerical approximations to study our bi-domain diffusion equations with coupling interface conditions. We consider explicit and implicit coupling methods. We give their numerical implementations mainly in three algorithms, namely the explicit, implicit monolithic and implicit partitioned coupling approaches.

The specific task of this thesis is to study a bi-domain diffusion equation with various coupling interface conditions via numerical methods and numerical analysis. Moreover we will also calculate the L_1-error and its numerical order of convergence for the Dirichlet-

Neumann condition with equal diffusion coefficient, since we know an exact solution for this case. Also we show the essential property for the concentration or heat flow, a discrete mass conservativity for the various coupling conditions with bi-domain diffusion equations. Further, we consider the Godunov-Ryabenkii stability based on the normal mode solutions for the coupling schemes as well as for the boundary conditions.

In the numerical discretization of the outer boundaries as well as for the interface boundary conditions the ghost values are appearing in the schemes. To find these ghost values we use the central difference method with respect to the boundary points. For this alternatively we can use the one sided difference method too, but later we will show that only the central difference method maintains the conservativity for a nodal based scheme. The one sided difference is conservative for a finite volume cell based scheme.

1.2 Literature review and state of the art

In this thesis we consider boundary value problems for bi-domain diffusion equations with various coupling interface conditions between two sub-domains. Our study is motivated by certain bi-domain diffusion problems from bio-physics with specific coupling conditions that we go into below. The simplest coupling conditions are the Dirichlet-Neumann (DN) coupling conditions that have been extensively used in domain decompositioning methods, see e.g. Quarteroni and Quarteroni [29, Ch. 19]. The same type of problems also arise in heat flow where heat flux coupling conditions are well established, see e.g. Carslaw and Jaeger [18].

The coupling conditions in which we are mainly interested in are the channel pumping and membrane pumping conditions modeling calcium transport within cells. These pumping conditions were previously considered in Thul [37] and first introduced by Falcke [7], see these conditions in (2.4) and (2.7) below. These are the extension of the heat flux coupling conditions by addition of a non-linear pumping term.

Further, Carr and March [4] considered various coupling conditions based on the heat flux coupling conditions. They studied these various coupling interface conditions with multilayer diffusion problems via a semi-analytic approach. Also they derived the convergence rate for the solution of the various couplings and studied the effect of changing the interface conditions on the solution behavior. We will discuss these and other coupling conditions in Section 2.3.

Concerning basic numerical methods and concepts for single domain diffusion equations we refer to Morton and Mayers [24]. We use concepts such as von Neumann stability and truncation error analysis. We recall the von Neumann stability analysis for a single domain diffusion equation with homogeneous Neumann boundary conditions. This will be explained in Chapter 6.

Also we use the method of Godunov-Ryabenkii (GR) for the stability of boundary conditions, see Godunov and Ryabenkii [11]. Further details of the general theory for the normal mode solutions given in Gustafsson et al. [13], see also the Gustafsson [12] for the GR stability condition "the beginning of a new stability theory". We apply the methods of normal mode analysis to the various coupling interface conditions too. This use for coupling conditions was pioneered by Giles [10]. The discussion of stability for the single

domain as well as for the bi-domain diffusion equations with various coupling conditions is given in Chapter 6.

For the numerical implementation we follow Giles [10] only up-to a certain degree. He considered one dimensional bi-domain parabolic thermal diffusion equations with Dirichlet-Neumann coupling conditions. In his equations he used the heat capacity and the conductivity while we will at first only consider the simpler diffusion equation. He implemented explicit and implicit coupling methods for the interior sub-domains as well as for the coupling interface conditions. Further, for the boundary conditions he used the Dirichlet conditions in his computations. Also he considered different grid sizes for the two sub-domains. As we will see, the discretization of the coupling by Giles has a flaw that leads to loss of conservativity.

Roe et al. [32] discussed other cases of the problem of Giles with a moving interface. In this article they used two types of discretization methods for the sub-domains, a finite difference/finite difference (FD/FD) as well as finite volume/finite element method the (FV/FEM) configuration. In this study it was concluded that FV/FEM discretization has a larger destabilizing effect than the FD/FD. They also discussed the GR-stability using the asymptotic approach introduced by Giles.

A second similar study of Roe et al. [33] considered the model equations of Giles and used the higher order combined interface methods of explicit and implicit methods. They discuss the GR-stability for their formulations. They also published more on the various other special cases of such kind coupling schemes and on the GR-stability. Further references may be found in the above two papers.

Errera and Chemin [6] also considered the equations in Giles [10]. They studied an optimal solution of the numerical Dirichlet-Robin and Robin-Robin coupling conditions. They derived the GR-stability for these coupling conditions. Then a similar study of Errera with Moretti et al. [23] also discussed the stability, convergence and optimization for various coupling conditions. They introduced a parameter, namely the numerical Biot number that controls the stability effect, and optimal coupling coefficients that guarantee unconditional stability. They discussed coupling conditions including Dirichlet-Robin and Neumann-Robin conditions too. For the stability analysis the Godunov-Ryabenkii stability method has been used in this article via asymptotic considerations. Also this group published several other research articles on the same problem, see their references.

Henshaw and Chand [15] considered a heat transfer problem as a multi-domain problem with Dirichlet-Neumann coupling and mixed Robin interface conditions. They discuss the applications in fluid-solid systems. The explicit and implicit coupling methods have been used in this article and the GR-stability was derived. Further, they proposed that the interface equations are discretized via the central difference to determine the ghost point values adjacent to the interface node. It was concluded that generally this gives more accurate and stable approximation as compared to the one sided difference methods.

We will give a more clear insight about this by studying the discrete mass conservation or energy conservation for the various coupling conditions. We conclude that only to discretize the coupling conditions via the central differences method maintains the discrete mass conservativity and the one sided differences method does not maintain it. This will be explained in Chapter 5 for the various coupling conditions.

In an interesting paper ocean-atmosphere coupling conditions were studied by Lemarié et al. [22]. For the numerical discretization they also used a nodal based implicit method as well as an explicit cell based method. For the numerical computations and stability analysis a one dimensional diffusion with DN-coupling has been considered in this paper. For the GR-stability they follow the method of Giles to derive the asymptotic stability conditions.

Another recent study of Zhang et al. [40] is also on the ocean-atmosphere coupling. They considered a multi-domain partial differential equation arising in general circulation models used in climate simulations. They claim that in recent years these two systems became increasingly important in climate change assessment. They also used the explicit and implicit coupling descritization methods in their paper. It was addressed that numerical stability issues arise due to the different time step strategies applied to the coupled partial differential equation. For the stability analysis they also used a GR-stability analysis via using the normal mode solutions. Alternatively, to verify their stability results they also calculated the stability via matrix eigenvalue type methods. Further they point out that the scheme Giles used is not correct.

1.3 Results of the thesis summarized

In this thesis we study three types of coupling algorithms namely explicit, implicit monolithic and partitioned iterative coupling approach. The first two approaches are straight forward. While the implicit partitioned is a bit more complicated. In this we separate the domain into two sub sets on which we want to solve separate linear systems of equations, that are coupled at the interface boundary. We use e.g. the Neumann condition for the left sub-domain and the Dirichlet condition for the other domain. We sub-iterate until the coupled convergence is reached.

Further we calculate the first order L_1-error and its numerical order of convergence for the single domain diffusion as well as for the bi-domain diffusion equations with Dirichlet-Neumann condition with identical diffusion coefficients. Also we show the essential property for the concentration or heat flow, a discrete mass conservativity for the various coupling conditions with bi-domain diffusion equations. Further, we consider the Godunov-Ryabenkii stability based on the normal mode solutions for the coupling schemes as well as for the boundary conditions.

In our above review of the literature several authors, e.g. Giles [10], Roe et al. [33], Errera et al. [6], Henshaw and Chand [15] and many others discussed the Godunov-Ryabenkii stability (GR) analysis for the coupling conditions with bi-domain equations in complicated ways using asymptotic considerations. They took some special assumptions and asymptotic solutions to derive the stability conditions for the complete system of the normal mode equations of the interiors together with coupling schemes. While we proved some of their assumptions on the roots of the quadratic equation obtained after applying the normal mode solutions to the scheme for the interior nodes of the sub-domain. The choice of the roots $q_1(\lambda)$ and $q_2(\lambda)$ that which one is greater than 1 and smaller than 1 in absolute value.

We used the concept of normal mode solution from the Godunov-Ryabenkii [11] for

the boundary conditions as well as for the schemes of the various coupling conditions via explicit and implicit coupling methods. It is very clear that for the schemes of the interior sub-domains we have the von Neumann stability. We considered the von Neumann boundary condition as this helped us in the derivation of the stability analysis for the coupling conditions.

Moreover, we also get the instabilities for the heat flux and linearized coupling conditions for the larger value of spatial mesh size Δx. We get a stability when Δx is small enough. This whole discussion is given in Chapter 6 and also shown the results in Chapter 7.

The main achievements of this thesis are summarized as follows:

1. We modified the 3D model of Falcke [7], Thul [37] to a one dimensional model with various coupling conditions namely the channel pumping and membrane pumping coupling conditions from Thul [37] to a bi-domain coupled interface model. This model the natural behavior of calcium signalling in multi-domain way. This signalling occurs as a multi-domain problem. But in this thesis we study it as a bi-domain modeling with various coupling interface conditions. The two sub-domains are corresponding to the cytosolic and endoplasmic reticulum (ER) regions and the common interface modeled a membrane from which the calcium moves from higher to lower concentration via pore through calcium channels.

2. We give three coupling algorithms namely the explicit coupling algorithm A1, implicit monolithic coupling A2 and the implicit partitioned coupling approach A3. We implemented these algorithms for the various coupling conditions with bi-domain diffusion equations. We implemented slightly different formulation as described by Giles [10], Roe et al. [33], Errera et al. [6] and others. To verify and test our algorithms for the various coupling conditions we fixed the diffusion coefficients $D_- = D_+$ in the DN-coupling to get the identical solution as a standard single domain diffusion equation. These detail are given in Chapter 4.

3. We computed the L_1 error and the numerical order of convergence for the single domain diffusion equation as well as for the bi-domain diffusion equations with Dirichlet-Neumann coupling for the identical diffusion coefficients.

4. We derived the discrete mass conservation for the discretized schemes of the single domain diffusion equation as well as for the bi-domain diffusion equations with homogeneous Neumann boundary conditions as well as the various coupling conditions considered in this thesis. We used explicit nodal based and cell based methods and implicit discretization methods.

   We emphasize that in such kind of coupling interface conditions with bi-domain diffusion equations it is necessary to maintain the mass conservation for concentration (calcium concentration) problems. This is the analogue of energy conservation in case of the same type of equations modeling for heat flow. For the discretization of coupling conditions we used two approaches namely one the sided differences method and the central differences with respect to the boundary points. The central

difference method maintains the conservativity in the case of the nodal based discretization, while the one sided difference maintains it in the case of the cell based finite volume discretization.

5. We recall the well known von Neumann stability analysis for the explicit as well as for the implicit discretization methods. Also we derived the Godunov-Ryabenkii stability conditions for the single domain diffusion equation with zero flux boundary conditions.

   We obtain more precise stability results as compared to the similar literature described above, e.g Giles [10], Roe et al. [33] and others for the coupling conditions. In all these articles they derive the stability results with combined system of the normal mode system for the interior of the sub-domains together with the coupling conditions. This leads a very complicated system. Then there is only one way to discuss the stability analysis with the help of asymptotic considerations or to take some special cases.

   These all essential concepts such as implementations of the various discretization methods, error analysis, numerical order of convergence, discrete mass conservation and stability analysis are necessary to study for the one dimensional case. Then this can be use in the application of the study of the higher space dimensions, i.e. in 2D and 3D case. So, this study will be provide a ground for the implementation of these type complex coupling conditions in two and three space dimensional study.

1.4 Layout of the thesis

This thesis is organized as follows:

In Chapter 2 we give a bi-domain modeling and coupling conditions for the bi-domain diffusion equations. A three dimensional calcium dynamics model with various coupling conditions is given in the first section. In the second section we explain a bi-domain modeling. In Section 3 the one dimensional case of the bi-domain 3D calcium model Falcke[7] and Thul [37] with various coupling interface conditions.

Chapter 3 is devoted to the various discretization methods for the single domain diffusion equation with homogeneous Neumann boundary conditions. The discretization methods include an explicit (nodal based), an implicit and a finite volume (cell based) discretization method. In the first section we explain the single domain diffusion equation with boundary conditions. In the second section we explain the explicit discretization method. The implicit discretization with Thomas algorithm and iterative methods will be explained in the third section. The finite volume (cell based) discretization will be explained in Section 4. The exact solution with truncation error for the single domain diffusion equation is given in the fifth section. The L_1 error analysis with numerical order of convergence will be explained Section 6.

In Chapter 4 we focus on the numerical approximation of the bi-domain diffusion equations with various coupling interface conditions. We use three coupling approximation methods. In the first section we give the explicit discretization method and in the second section we explain the coupling procedures for the implicit monolithic and partitioned iterative coupling approach. In third section we explain the numerical error in L_1 norm and the order of convergence for the bi-domain diffusion equation with Dirichlet-Neumann coupling with identical diffusion coefficients for the nodal as well as for the cell based discretization method.

In Chapter 5 we derive the discrete mass conservation for the various discretization methods for the single domain diffusion equation with homogeneous Neumann boundary conditions. The discretization methods includes an explicit, an implicit and finite volume discretization methods. Also we derive the discrete mass conservation for the various coupling schemes of the bi-domain diffusion equations derived in Chapter 4 via an explicit nodal based as well cell based scheme, implicit coupling. In the last section we give the numerical tables and plots for the all coupling conditions considered in this thesis.

In Chapter 6 we discussed the well-known von Neumann stability for the single domain diffusion equation with explicit and implicite discretization methods. Also we derived the Godunov-Ryabenkii stability for the single domain diffusion equation with homogeneous boundary conditions. Further we derived the GR-stability for the various coupling conditions via explicit and implicit methods.

In Chapter 7 we discuss the numerical results with error analysis of the single domain diffusion equations with homogeneous boundary conditions. Also we discuss the numerical results for the bi-domain diffusion equations with various coupling conditions. In the first section we discuss the numerical results for the single domain diffusion equation. In the second section we give for the Dirichlet-Neumann (DN) coupling the error in the L_1 norm as well the numerical order of convergence. In the third section we explain the various test cases for the stable and unstable solutions for the heat flux coupling conditions. In the fourth section we give a comparison of the results for the heat flux, membrane pumping as well as for the simplified membrane pumping.

We explain the results for the channel pumping conditions and its special case simplified channel pumping conditions in Section 5. Section 6 contains the results for the membrane pumping conditions, its special case simplified membrane pumping and the linearized membrane pumping condition. The details for the solution times and iterations counts will be presented in Section 7.

In Chapter 8 we give the summary and conclusion of the thesis, while in the last Chapter 9 we give the open problems or question arises and future work of this thesis.

Chapter 2

Bi-domain modeling and coupling conditions for diffusion equations

In this chapter we give some details of a three dimensional calcium dynamics model and modify the three dimensional model to a one dimensional bi-domain model with coupling conditions. This is a motivation for the study of coupling conditions.

2.1 Three dimensional bi-domain calcium model with coupled interface conditions

In this section we describe the mathematical modeling of a calcium model in $3D$. A detailed mathematical description is given in Chamakuri [26] and Thul [37], see also Falcke [7]. Here, we just want to recall the model as a motivation to study the various analytic and numerical coupling conditions. In a cell, Ca^{2+} is transported through channels by pumps, it diffuses into the cytosol as well as into the endoplasmic reticulum and it reacts with buffers. A stationary profile can be reached by imposing boundary conditions, which guarantee that the current entering through the channels is equal to the current leaving through the volume surface.

The release process is described by the reaction-diffusion equations for the cytosolic Ca^{2+} concentration c and the Ca^{2+} concentration E in the ER as well as the buffer concentrations b_i and $b_{E,j}$, in the cytosol and ER respectively. We have $i = s, d, m$ and $j = s, m$, where s denotes a stationary, d a dye and m a mobile buffers. These equations are in cartesian coordinates. As a simplification we do not consider the full three-dimensional cytosolic and ER space in this subsection but instead consider thin sheets below and above an idealized planar ER membrane of finite extension. In this thesis we study a one dimensional case of the $3D$ model. For this we take a one dimensional cut along the z-axis. The details are given in Section 2.3.

2.1.1 Problem description

Consider an open domain $\Omega = \Omega_c \cup \Omega_E \cup \Gamma_c \subset \mathbb{R}^3$, composed of two mutually exclusive sets $\Omega_c \cap \Omega_E = \emptyset$, where Ω_c is a cytosolic and Ω_E is an endoplasmic region. Further, Γ_c

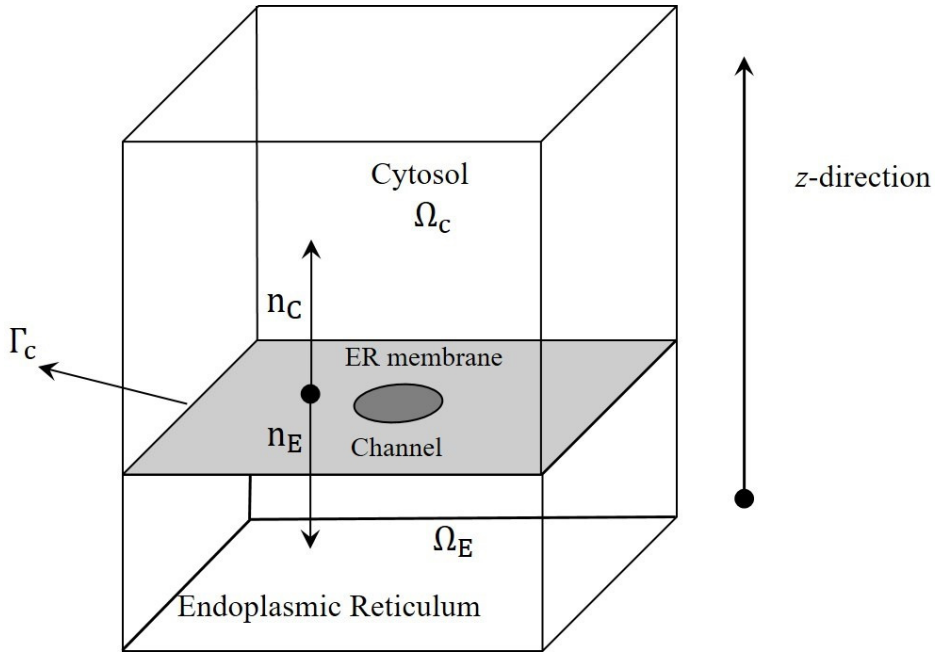

Figure 2.1: Bi-domain cubic volume distribution of ER and cytosolic domains, modification of a figure from [26].

is the coupling interface. The coupling interface Γ_c has $\mathbf{n}_c$ and $\mathbf{n}_E$ as inward and outward normal respectively. The space and time domains are denoted by $Q_1 = \Omega_c \times [0, t_f]$ and $Q_2 = \Omega_E \times [0, t_f]$, t_f denotes the final time. The unknown variables in the following models are $c(x,t) : Q_1 \to \mathbb{R}$ cytosolic Ca^{2+} concentration, $E(x,t) : Q_2 \to \mathbb{R}$, Ca^{2+} concentration in the ER. The buffer concentrations in the cytosol are $b_i : Q_1 \to \mathbb{R}$ and $b_{E,j} : Q_2 \to \mathbb{R}$ are buffer concentrations in the ER, $i = s, m, d$, $j = s, m$, where $b_s(x,t)$ denotes stationary, $b_m(x,t)$ mobile and $b_d(x,t)$ dye buffers.

The model for the calcium concentration flow is described by a system of coupled time dependent reaction-diffusion equations in three space dimensions as follows

$$\begin{aligned}
\frac{\partial c}{\partial t} &= D_c \Delta c - \sum_i H_i(c, b_i) && \text{on} \quad \Omega_c \times \mathbb{R}_{\geq 0}, \\
\frac{\partial E}{\partial t} &= D_E \Delta E - \sum_i K_j(E, b_{e,j}) && \text{on} \quad \Omega_E \times \mathbb{R}_{\geq 0}, \\
\frac{\partial b_i}{\partial t} &= D_c \Delta b_i + H_i(c, b_i) && \text{on} \quad \Omega_c \times \mathbb{R}_{\geq 0} \quad \text{for} \quad i = s, m, d, \\
\frac{\partial b_{E,j}}{\partial t} &= D_c \Delta b_{E,j} + K_j(E, b_{E,j}) && \text{on} \quad \Omega_E \times \mathbb{R}_{\geq 0} \quad \text{for} \quad j = s, m.
\end{aligned} \tag{2.1}$$

More details regarding $3D$ modeling can be found in Chamakuri [26] and Thul [37]. The equations include diffusion of free Ca^{2+} described by $D\Delta c$, diffusion of dye buffers b_d denoted by $D_d \Delta b_d$, diffusion of mobile buffers b_m described by $D_m \Delta b_m$ and the reactions

of stationary buffer b_s, dye buffer b_d and mobile buffer b_m with free Ca^{2+} given by $k_i^+(B_i - b_i)c - k_i^- b_i$ where $i = s, d, m$. The total concentration of stationary, dye and mobile buffers B_i, $i = s, d, m$ is usually homogeneous before the experiments begin. Therefore, the concentration of free buffer, i.e. buffer with no Ca^{2+} bound, can be expressed as $(B_i - b_i)$ at any point in space.

The release of Ca^{2+} is simulated in a cube volume divided by the lumenal membrane perpendicular to the z-axis shown in Figure 2.1. The smaller part represents the ER and the larger part, the cytosol. The channel is a pore in the center of the ER membrane with radius R_s, see Figure 2.1. The initial condition is the stationary Ca^{2+} - distribution resulting from the pumps and the leak flux P_l. The buffer binding and unbinding terms given in the right hand side of the system (2.1) modeled by the usual mass-action kinetic terms given in

$$\begin{aligned} H_i &= k_{b,i}^+(B_i - b_i)c - k_{b,i}^- b_i \\ K_j &= k_{E,j}^+(G_i - b_{E,j})c - k_{E,j}^- b_{E,j}. \end{aligned} \tag{2.2}$$

Further no flux boundary conditions were applied at the outer surface of the domain. For more details regarding 3D modeling see Thul and Falcke [38] as well as Thul [37].

Pumping coupling interface conditions

Channel pumping conditions

The channel flux J_{ch} through the interface membrane which separates the ER and cytosolic regions is given as

$$J_{ch} = \psi \frac{E - \alpha c}{\beta + \gamma E + \delta c}, \qquad r \leq R. \tag{2.3}$$

Here ψ, α, β, γ, δ are non-zero constants and R denotes the cluster radius, cp. Thul [37, (2.2)]. They are given in Table 2.1. Here, the values of E and c have to be taken at the membrane. The currents are incorporated into the volume dynamics by setting the coupling condition on the interface Γ_c at the ER membrane to be

$$D_c \frac{\partial c}{\partial z} = \frac{1}{\gamma} D_E \frac{\partial E}{\partial z} = -J_{ch} \tag{2.4}$$

Membrane pumping conditions

In the calcium dynamics model the membrane pumping flux J_{pump} is a gradient parallel to the z-direction as shown in Figure 2.1. It is given by Thul [37, (2.2)] as

$$J_{pump} = (P_l + P_c(r))(E - c) - P_p \frac{c^2}{K_d^2 + c^2}, \qquad r > R. \tag{2.5}$$

The coefficient of the leak flux density is P_l and P_p the maximal pump strength. Further, k_d is a positive constant and $P_c(r)$ is described below.

The currents are incorporated into the volume dynamics by setting the coupling condition on the interface Γ_c at the ER membrane to be

$$D_c \frac{\partial c}{\partial z} = \frac{1}{\gamma} D_E \frac{\partial E}{\partial z} = -J_{pump} \tag{2.6}$$

or more generally

$$D_c \nabla c \cdot \mathbf{n}_c = \frac{1}{\gamma} D_E \nabla E \cdot \mathbf{n}_E = -J_{pump}. \tag{2.7}$$

The transport through the ER membrane comprises three contributions. Calcium is moved from the ER into the cytosol through a leak current $P_l(E - c)$, and the channels $P_c(r)(E - c)$. The latter term will be discussed in more detail below. Calcium is re-sequestered into the ER by a pumps modeled by term proportional to P_p . The action of pumps was found to be cooperative in calcium. The parameter K_d is the dissociation constant of the pumps.

The term proportional to P_c in equation (2.5) models the current through an open channel. This current was found to depend on the cross-membrane difference. For differences found in cell-physiological conditions, the current can be approximated by a linear dependence on $(E - c)$. The current is modeled as a source with constant density in a specified channel cluster region. A model to calculate the cluster radius is proposed by Thul and Falcke [38].

The position of the cluster is given by a fixed position x_n. Then the flux term is given by

$$P_c(r_n) = \begin{cases} P_{ch} & \text{if } ||r_n - x_n|| < R_n \qquad \text{for a channel with radius } R_n \\ 0 & \text{otherwise.} \end{cases} \tag{2.8}$$

Note that in practice, we want to spontaneously open and close channels. This is predominantly a stochastic process. Further detail can be found on this in Putney et al. [28] and Taylor et al. [36]. Here we do not take this issue into consideration. For a detailed biophysical analysis of the model, see Falcke and Thul [38]. Note that in a model including the dynamics of channel gating the number of open channels is time-dependent. The corresponding value of P_{ch} can be found in Table 2.1. The opening and closing of the calcium channels are a stochastic process. The clusters in turn are randomly scattered across the ER membrane. The average distance of clusters is typically larger than the Ca^{2+} diffusion length. Stochastic behavior, i.e. random opening and closing of channels, manifests itself as spontaneous release events through single channels or several channels in a cluster, see Putney et al. [28] and Taylor et al. [36].

2.2 Bi-domain modeling and solution methods

A bi-domain problem is a problem in which multiple physical models or phenomena are handled simultaneously occurring in two different sub-domains interacting via coupling interface conditions. Many of the real world phenomena in engineering, physics and biology are based on multiple processes which are modeled via mathematical equations mainly by

coupled PDEs, ODEs or with PDE-ODE systems with necessary initial, boundary and coupled interface conditions.

These kind of models allow us to analyze certain complex behavior and visualize a real structure of the phenomena via a single system, which is not possible in single scale modeling. This type of problem occurs frequently in real-world physics, most notably in bio-mechanical or biomedical engineering. The bi-domain model that we are studying is a setting in a similar fluid-structural interactions (FSI) were do not consider a moving boundary through. Although many researchers addressed this class of problems for decades, solving FSI problems numerically is still a challenging task.

In this thesis we also dealing with calcium dynamics modeling which is a multi-domain phenomenon. But we focus on its bi-domain case which is corresponding to the cytosolic and endoplasmic reticulum domains separated by the ER. The interaction take place on the porous ER membrane. We define our coupling interface conditions between two diffusion equations. The two equations are coupled via a common interface boundary on the membrane coupling conditions. The various coupling conditions are given in this chapter and the detail implementation of these coupling conditions are explained in Chapter 4. Their discrete mass conservation is studied in Chapter 5 and the stability analysis for the coupling conditions with bi-domain diffusion equations is given in Chapter 6.

2.2.1 Coupled problems and solution method

Processes in which physically or computationally heterogeneous components interact dynamically are known as coupled problem. The interaction between the components of the problem is multiple in the sense that the solution has to be obtained by a simultaneous analysis of all coupled equations which model the problem.

The increasing necessity to solve complex problems in numerical mathematics, engineering and physics accounting for all the coupling occurring on the different scales of the problem requires the ongoing development of new ideas and methods which can effectively provide accurate numerical solutions with affordable computing times. At this, challenges are given by coupled problems for which the computation of coupling phenomena are difficult to accomplish or with vastly different time constants, e.g. stiff problems, and long-time duration of transient responses.

Solution methods

The theoretical models of the coupled problems usually take mathematical expressions of some conservation principle in the form of coupled partial differential equations (PDEs) in space and time. The partial differential equations by their very nature deal with continuous functions and hence, have to be discretized in space and time for the computational solution. In particular for the numerical solution, the spatial semi-discretization is commonly achieved by finite difference method (FDM), finite element method (FEM) or finite volume methods (FVM).

Further, after applying the spatial discretization scheme, the model is transformed into a system of algebraic, non-linear algebraic or ordinary differential equations (ODEs) in the time dependent case. For real scale problems these may comprise millions of evolution

equations that have to be deal with numerically. In principle, four approaches to the time integration of such coupled systems are feasible. The details can be found in Felippa et al. [8], Spencer et al. [35], Zienkiewicz et al. [41].

Numerical methods for the discretized coupled interface systems

The following four approaches are commonly used for the solution of the discretized coupled problems. Details can be found in Felippa et al. [8].

1. *Monolithic or direct approach*: In this approach the whole problem is treated as a monolithic entity. All components are advanced simultaneously in time by the same time stepping method. For some problems this approach may be computationally too expensive.

2. *Partitioned iterative approach*: In this approach the system components are treated as isolated entities that are separately advanced in time. In this approach we use the available information from the initial data and achieve the advance of time levels via sub-iteration. We will explain this for the implicit case of the coupling conditions in Chapter 4.

3. *Fractional-step approach*: In this approach the coupled systems are decomposed into simpler sub-problems via advancing each time step in multiple steps. Then the split parts are handled via special composition algorithms such, e.g. predictor-corrector or projection schemes.

4. *Field variable elimination approach*: In this approach one or more variables are eliminated with integral transformation or reduction. But this method destroys the sparseness of matrix. So, this approach is the less important in the sense of computational perspective.

We are considering the first and second approach. To achieve the result via partitioned iterative procedure is a bit more complicated because we have the two unknowns corresponding to the each sub-domain. Despite this problem we manage to achieve a numerical solution via sub-iteration.

These kind of approaches has been used for different well known models in Steffen [25], Hairer et al. [39], Khul et al. [20], Brenan et al. [3], Blom and Frederic [2].

Further, Okiro [19] proved global existence for 4×4 system of calcium dynamics model. The development of the theory of ordinary differential equations with discontinuous right hand sides has been to a great extent stimulated by its many applications. A large number of problems from mechanics, the theory of automatic control, electrical engineering are described by these equations, see Heikkila et al [14] . More results in this direction can be found in Hu [17], Lang [21], Heikkila [34], Lakshmikantham [14] and the references therein.

2.3 The one dimensional bi-domain diffusion equation and the coupling conditions

In this section we describe various coupling interface conditions for bi-domain diffusion equations. The coupling conditions includes the Dirichlet-Neumann coupling, perfect contact coupling, heat flux coupling, partition coupling, channel pumping coupling, simplified channel pumping, membrane pumping coupling and simplified membrane pumping coupling conditions.

Here, we consider a bi-domain one-dimensional diffusion model which is a one dimensional reduction of the three dimensional model of Falcke [7] described in Section 2.1. We assume that the concentration only varies in the vertical z-direction and use x as our one dimensional variable. We restrict ourselves to one diffusion equation in order to study the coupling conditions.

We consider as domain the interval $\Omega = [a, b]$ in one space dimension. We divide the domain into two sub-domains by the mid point $c = (a + b)/2$, which is the common interface boundary. The two sub-domains are $\Omega_1 = [a, c]$ and $\Omega_2 = [c, b]$. We are interested in interface coupling conditions. The bi-domain diffusion equations for $w : \Omega \times \mathbb{R}_{\geq 0} \to \mathbb{R}$ are defined as

$$\frac{\partial w}{\partial t} = D_i \frac{\partial^2 w}{\partial x^2} \quad \text{on} \quad \Omega_i \times \mathbb{R}_{\geq 0}, \quad \text{for } i = 1, 2. \tag{2.9}$$

Here $D_i > 0$ for $i = 1, 2$ are the diffusion coefficients which may differ. For $x \in \Omega$, $t > 0$, we consider w to be the solution which describes a concentration or temperature at position x and time t in the sub domains. It satisfies the initial condition

$$w(x, 0) = w_0(x)$$

for given initial data $w_0 : \Omega \to \mathbb{R}$. We take the outer boundary conditions to be the homogeneous no flux Neumann conditions

$$\frac{\partial}{\partial x} w(a, t) = \frac{\partial}{\partial x} w(b, t) = 0.$$

For the consideration of the coupling conditions we set $u = w|_{\Omega_1}$, $v = w|_{\Omega_2}$. A sketch is shown in Figure 4.1. The bi-domain model for the respective sub-domains becomes

$$\frac{\partial u}{\partial t} = D_- \frac{\partial^2 u}{\partial x^2} \quad \text{for all} \quad u \in \Omega_1 \times \mathbb{R}_{\geq 0}, \qquad \frac{\partial v}{\partial t} = D_+ \frac{\partial^2 v}{\partial x^2} \quad \text{for all} \quad v \in \Omega_2 \times \mathbb{R}_{\geq 0}. \tag{2.10}$$

We aim to solve a well posed problem by coupling u and v across the interface $x = c$. The problem defined in (2.9) additionally needs to be coupled with two appropriate internal coupling conditions at the interface between the sub-domains. There are a number of well known coupling conditions in the literature, see e.g. Carslaw and Jaeger [18], Giles [10], Roe et al. [33], or Carr and March [4]. Some of these we want to consider here for comparison. In addition we consider pumping conditions given by Thul [37] as well as Falcke and Thul [7].

2.3.1 Basic coupling conditions

In this subsection we will explain some well known coupling conditions namely the Dirichlet-Neumann coupling, partitioned coupling and the heat flux coupling conditions.

Dirichlet-Neumann coupling

The simplest case is to assume continuity of the solution and the flux at the interface

$$0 = u(c,t) - v(c,t), \qquad D_- \frac{\partial u(c,t)}{\partial x} = D_+ \frac{\partial v(c,t)}{\partial x}. \tag{2.11}$$

Note that in case $D_- = D_+ = D$ this coupling will give a solution w to the original single domain problem (3.1), (3.2) to be considerd below. The common factor D then drops out of (2.11). This type of coupling is used in domain decomposition methods, see e.g. Quarteroni and Valli in [31].

Partition coupling condition

For completeness we mention a more general case than the previous two coupling conditions. The partition condition given by Carslaw and Jaeger [18] on an interface is

$$0 = u(c,t) - \theta v(c,t), \qquad D_- \frac{\partial u(c,t)}{\partial x} = D_+ \frac{\partial v(c,t)}{\partial x}. \tag{2.12}$$

for $t > 0$. If $\theta = 1$ the first interface condition is (2.11). It is called the perfect contact condition in Carr and March [4]. Here $\theta > 0$ is the partition coefficient at $x = c$. The interface condition defined in case $\theta \neq 1$ maintains a constant ratio between the discontinuous solutions at the interface which is applicable in analyte transport in porous media or drug release from multi-layer capsules, see Carslaw and Jaeger [18] as well as Miguel et al. [9].

Heat flux coupling conditions

Carslaw and Jaeger [18, p. 23,(20)] give the following interface conditions known as heat flux conditions which are defined as

$$-D_- \frac{\partial u(c,t)}{\partial x} = H(u(c,t) - v(c,t)), \qquad D_- \frac{\partial u(c,t)}{\partial x} = D_+ \frac{\partial v(c,t)}{\partial x} \tag{2.13}$$

for $t > 0$. Here $H > 0$ is the contact transfer coefficient at $x = c$.

Note that the Dirichlet-Neumann coupling (2.11) is a limiting case of the heat flux coupling (2.13) where we take $H \to \infty$.

As in Fourier's law the heat flux J_{heat} is always in the direction of the negative gradient of the temperature. Therefore, a positive slope of the solution must correspond to a

negative flux. In the coupling conditions this means that the derivatives of the solution equal to minus the flux. Thereby (2.13) can be written equivalently as

$$D_-\frac{\partial u(c,t)}{\partial x} = H(v(c,t)-u(c,t)) = -J_{heat}, \qquad D_+\frac{\partial v(c,t)}{\partial x} = H(v(c,t)-u(c,t)) = -J_{heat}. \tag{2.14}$$

Analogously, this will also be the case for the pumping conditions.

2.3.2 Bi-domain calcium dynamics model with pumping interface conditions

As mentioned, we reduce the single domain 3D model of Thul [37] discussed in Section 2.1 to a bi-domain coupled interface model on the interval $\Omega = [a, b]$ representing a part of the vertical axis in 3D space. Thul [37] considered the flux through the membrane which separates the endoplasmic reticulum and the cytosolic domains along the z-axis. Here we consider $z = x$. When we are dealing with a calcium dynamics model, we take as a special case that $u = E$ and $v = c$, where E is the calcium concentration in endoplasmic reticulum (ER) domain and c is the calcium concentration in the cytosolic domain and in (2.10). The general combined coupled interface conditions for the above model are defined as

$$D_-\frac{\partial u(c,t)}{\partial x} = D_+\frac{\partial v(c,t)}{\partial x} = -J(u(c,t), v(c,t)), \tag{2.15}$$

with a given flux function J. Six different examples are introduced below.

Channel pumping conditions

The channel pumping conditions were defined in (2.6) or (2.7). The channel flux J_{ch} was defined in (2.3) as follows

$$D_-\frac{\partial u}{\partial x} = D_+\frac{\partial v}{\partial x} = -J_{ch} = \psi\frac{\alpha v - u}{\beta + \gamma u + \delta v}. \tag{2.16}$$

Specific values of the parameters ψ, α, β, γ, δ are given in Table 2.1.

Simplified channel pumping conditions

For $\beta + \gamma u + \delta v = 1$ the channel pumping flux J_{ch} gives us the simplified channel flux $J_{sch} = \psi(u - \alpha v)$ and the conditions are defined as

$$D_-\frac{\partial u}{\partial x} = D_+\frac{\partial v}{\partial x} = -J_{sch} = \psi(\alpha v - u). \tag{2.17}$$

We can write these coupling conditions separately as

$$D_-\frac{\partial u}{\partial x} = \psi(\alpha v - u) \qquad \text{or} \qquad D_+\frac{\partial v}{\partial x} = \psi(\alpha v - u). \tag{2.18}$$

For $\psi \to \infty$ we obtain the partition coupling conditions (2.12) as limiting case. For $\alpha = 1$, $\psi = H$ We have the heat flux coupling.

Membrane pumping conditions

We consider the calcium dynamics pumping case with the flux J_{pump} defined in (2.5). It is a membrane and non-linear pumping flux condition for the modified calcium dynamics model taken from the 3D model discussed in Section 2.1 and Thul [37]. We take the flux J_{pump} with a minus sign, see Thul [37]. Then the membrane pumping coupling conditions will take the following form

$$D_-\frac{\partial u}{\partial x} = D_+\frac{\partial v}{\partial x} = -J_{pump}. \tag{2.19}$$

Also we can write these coupling conditions separately as

$$D_-\frac{\partial u}{\partial x} = (P_l+P_c(t))(v-u)+P_p\frac{v^2}{k_d^2+v^2} \qquad \text{and} \qquad D_+\frac{\partial v}{\partial x} = (P_l+P_c(t))(v-u)+P_p\frac{v^2}{k_d^2+v^2}. \tag{2.20}$$

Here, $P_l > 0$ is the coefficient of the leak flux density, $P_c(t) \in [0, P_c]$ is a flux depending on the opening of a channel $P_c > 0$, $P_p > 0$ is the maximal pump strength and $k_d > 0$ is the dissociation constant of the pumps. These coupling conditions contain a nonlinear function of u. For the comparison of coupling conditions we introduce two additional simplified cases.

Simplified membrane pumping conditions

This a special case of the membrane pumping conditions (2.19) obtained by setting $P_l + P_c(t) = H$ and $P_p = P$ and $k_d = 1$ to give

$$D_-\frac{\partial u}{\partial x} = H(v-u) + P\frac{v^2}{1+v^2}, \qquad D_-\frac{\partial u}{\partial x} = D_+\frac{\partial v}{\partial x} = -J_{pump}. \tag{2.21}$$

Heat flux conditions

This is also a special case of the membrane pumping conditions (2.19) obtained by setting $P_l + P_c(t) = H$, $P_p = 0$ to give the following

$$D_-\frac{\partial u}{\partial x} = D_+\frac{\partial v}{\partial x} = -J_{pump} = H(v-u). \tag{2.22}$$

This is also a special case of the heat flux coupling conditions (2.13) for $H = 1$.

Linearized membrane pumping coupling conditions

Here we linearize the non-linear simplified membrane pumping conditions. For this we take the right hand side of (2.21) to be $f(v) = H_{ch}(v-u) + P_p\frac{v^2}{1+v^2}$. To linearized it we use a Taylor series for $g(v) = \frac{v^2}{1+v^2}$, this implies $g(v) = g(1) + g'(1)(v-1) + h.o.t$ which gives $g(v) = \frac{1}{2} + \frac{1}{2}(v-1) + h.o.t = \frac{1}{2}v + h.o.t$. The expansion about $v = 1$ gives $g(v) \approx \frac{1}{2}v$.

The new form of $f(v) = H_{ch}(v-u) + \frac{P_p}{2}v$. We obtain the linearized pumping membrane conditions as

$$D_- \frac{\partial u}{\partial x} = H_{ch}\Big(\Big(1 + \frac{P_p}{2H_{ch}}\Big)v - u\Big), \qquad D_+ \frac{\partial v}{\partial x} = H_{ch}\Big(\Big(1 + \frac{P_p}{2H_{ch}}\Big)v - u\Big). \tag{2.23}$$

This is a special case of the simplified channel pumping (2.17) for $\psi = H$ and $\alpha = 1 + \frac{P_p}{2H_{ch}}$.

Table 2.1: Dimensions of system (2.1) and values of all the parameters. The units are: s second, $\mu M = 10^{-6}\ M$ molar, $\mu m = 10^{-6}\ m$ meters.

Quantity	Value	Unit
concentrations u, v	$0.06, 700$	μMol
leak flux coefficient P_l	3.3613	nms^{-1}
channel flux coefficient P_c	$6.32E6$	nms^{-1}
pump flux coefficient P_p	40000	μMs^{-1}
pump dissociation coefficient K_d	0.2	μM
diffusion coefficient D_-	200	$\mu m^2 s^{-1}$
diffusion coefficient D_+	199	$\mu m^2 s^{-1}$
channel flux constant ψ	9.3954	μms^{-1}
channel flux constant α	1.497	
channel flux constant β	$1.1949E-04$	
channel flux constant γ	$1.1444E-07$	μM^{-1}
channel flux constant δ	$1.1556E-07$	μM^{-1}

Chapter 3

Discretization of single domain diffusion models with boundary conditions

In this chapter we discuss numerical methods for the discretization of the single domain diffusion equation with homogeneous Neumann boundary conditions in one space dimension. We discretize the diffusion equation with Dirichlet and Neumann boundary conditions for an explicit, an implicit finite difference and finite volume discretization method.

The single domain diffusion equation with initial and boundary conditions are explained in the first section. The explicit time discretization method with boundary conditions are discussed in the second section. In the third section we give the implicit time discretization with boundary conditions. In fourth section we derive the finite volume discretization, in fifth section we recall the exact solution and in section six we calculate the L_1 error analysis and the order of convergence. In the last section seven we show the results via these methods and the error analysis for the single domain diffusion equation with homogeneous Neumann boundary conditions.

3.1 Single domain diffusion equation

We consider a single domain diffusion equation on the domain or interval $\Omega = [a, b]$, with $a, b \in \mathbb{R}$ and $a < b$. It is given as

$$\frac{\partial w}{\partial t} = D\frac{\partial^2 w}{\partial x^2} \quad \text{on} \quad \Omega \times \mathbb{R}_{\geq 0}. \tag{3.1}$$

Here $D > 0$ is the diffusion coefficient. The unknown function $w : \mathbb{R}_{\geq 0} \to \mathbb{R}$ describes the physical state $w(x, t)$ at each point $(x, t) \in \Omega \times \mathbb{R}_{\geq 0}$. The physical state may be a concentration or a temperature. In order to have meaningful solutions we must specify initial and boundary data. The initial data are taken to be

$$w(x, 0) = w_0(x) \quad \text{for } x \in \Omega. \tag{3.2}$$

Boundary conditions

As boundary conditions we could impose the Dirichlet conditions

$$w(a,t) = w_L(t), \qquad w(b,t) = w_R(t). \tag{3.3}$$

for all $t > 0$. Here $w_{L,R} : \mathbb{R}_{\geq 0} \to \mathbb{R}$ are given functions prescribing a concentration or temperature at the boundary. This means that we could prescribe a varying concentration or temperature at the boundary.

Alternatively we could consider Neumann or flux boundary conditions

$$D\frac{\partial w(a,t)}{\partial x} = J_1(t), \qquad D\frac{\partial w(b,t)}{\partial x} = J_2(t). \tag{3.4}$$

Here $J_1, J_2 : \mathbb{R}_{\geq 0} \to \mathbb{R}$ are given fluxes. We could also mix the two types of boundary conditions.

As another alternative, we can consider the radiation boundary condition. We assume that the flux across the boundary is proportional to the difference between the value w at boundary and the value $\overline{w}$ in the surrounding medium. We have to consider the outer normal derivative $\frac{\partial w}{\partial n}$ which equal to $\frac{\partial w}{\partial x}$ at the right hand boundary and $-\frac{\partial w}{\partial x}$ at a left hand boundary. So the boundary condition is given by

$$\frac{\partial}{\partial n} w(x,t) = H(w(x,t) - \overline{w}) \tag{3.5}$$

where $H > 0$ is a constant. Some background on determining H for problems of heat conduction may be found in the first chapter of Carslaw and Jaeger [18]. The flux boundary conditions for the outer boundaries a and b become

$$-\frac{\partial w(a,t)}{\partial x} + H_a(w(a,t) - w_a) = 0, \qquad \frac{\partial w(b,t)}{\partial x} + H_b(w(b,t) - w_b) = 0 \tag{3.6}$$

with appropriate H_a, H_b, w_a, $w_b > 0$. As $H \to 0$ (3.5) tends to the no flux boundary condition, i.e. $\partial w/\partial x = 0$. As $H \to \infty$ we obtain the Dirichlet boundary condition.

In the further studies we will concentrate on the homogeneous Neumann conditions with $J_1(t) = J_2(t) = 0$.

3.2 An explicit time discretization method for the single domain diffusion equation

As a first step we are using an explicit finite difference scheme which is a forward difference in time and a central second order difference in space for the discretization of a single domain diffusion equation. The model is defined on the interval $\Omega = [a,b] \times [0,T]$ for some final time $T > 0$ given as

$$\frac{\partial w}{\partial t} = D\frac{\partial^2 w}{\partial x^2} \tag{3.7}$$

with homogeneous Neumann boundary condition. Since the problem is known to be stiff we will be also consider implicit schemes later.

We choose $N \in \mathbb{N}_{\geq 2}$ and define grid points for $\Omega = [a, b]$ by

$$x_j = j\Delta x, \qquad \text{for} \quad j = 0, 1, ..., N, \qquad \text{with} \qquad \Delta x = (b-a)/N.$$

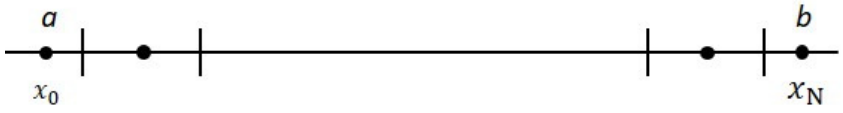

Figure 3.1: One dimensional grid points for the single domain finite difference.

The grid points x_j are related to cells σ_j. At the boundary we have $\sigma_0 = [a, \frac{\Delta x}{2}]$, $\sigma_N = [b - \frac{\Delta x}{2}, b]$ and in the interior $\sigma_j = [x_j - \frac{\Delta x}{2}, x_j + \frac{\Delta x}{2}]$ for $j = 1, \cdots, N-1$. We want to reach the time T in $M \in \mathbb{N}$ time steps. We define the time step $\Delta t = T/M$. For $n = 0, ..., M$ we set $t_n = n\Delta t$. We have to choose M large enough to guarantee the CFL condition $D\Delta t/(\Delta x)^2 \leq 1/2$, i.e. $\Delta t \leq (\Delta x)^2/2D$, in the explicit computations we will consider.

We assume continuous initial data with well defined values of w_0 at the node x_j for $j = 0, \ldots, N$. We set $w_j^0 = w_0(x_j)$.

The numerical approximation at time $t = t_n$ is denoted by w^n. The approximation is defined on the grid points as

$$w_j^n \approx w(x_j, t_n).$$

The forward difference to evaluate the time derivative at $t = t_n$ is given by

$$\frac{\partial w}{\partial t}\Big|_{(t_n, x_j)} \approx \frac{w_j^{n+1} - w_j^n}{\Delta t} + O(\Delta t). \tag{3.8}$$

We take the approximation of the second spatial derivative with the second order central difference

$$\frac{\partial^2 w}{\partial x^2}\Big|_{(t_n, x_j)} \approx \frac{w_{j-1}^n - 2w_j^n + w_{j+1}^n}{(\Delta x)^2} + O((\Delta x)^2). \tag{3.9}$$

Substituting (3.8) and (3.9) in (3.7) we obtain

$$\frac{w_j^{n+1} - w_j^n}{\Delta t} = D\frac{w_{j-1}^n - 2w_j^n + w_{j+1}^n}{h^2} + O(\Delta t) + O((\Delta x)^2). \tag{3.10}$$

By dropping the truncation error terms. We prove the above order of the scheme first order in time and second order in space in the sub-subsection 3.5.1 for the local truncation error. We get the following scheme

$$\frac{w_j^{n+1} - w_j^n}{\Delta t} = D\frac{w_{j-1}^n - 2w_j^n + w_{j+1}^n}{(\Delta x)^2}. \tag{3.11}$$

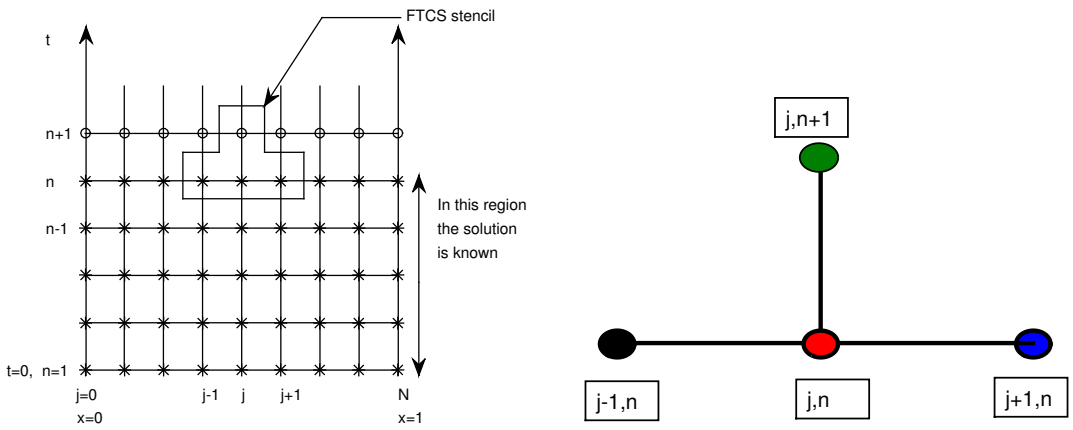

Figure 3.2: The figure in the left panel the spatio-temporal frame for forward in time and central in space (FTCS) scheme, while in the right panel the FTCS stencil is given.

We solve for w_j^{n+1} and set $\nu = D\frac{\Delta t}{(\Delta x)^2}$ to get

$$\begin{aligned} w_j^{n+1} &= \nu w_{j+1}^n + (1-2\nu)w_j^n + \nu w_{j-1}^n \\ &= w_j^n + \nu(w_{j+1}^n - w_j^n) - \nu(w_j^n - w_{j-1}^n). \end{aligned} \tag{3.12}$$

Both forms of the scheme have different advantages depending on the context in which they are used. We refer to the terms containing ν in the second form as numerical fluxes.

The FTCS scheme is explicit because it provides a formula to update w_j^{n+1} independently of the other nodal values at time t_{n+1}. A sketch for the FTCS scheme and stencil can be seen in Figure 3.2. We also apply this procedure for the bi-domain model with initial, boundary and coupling interface conditions will be explain in the next chapter.

Note that we obtain the same scheme (3.12) by using the finite element method with piecewise linear element on this equidistant mesh.

Discretization of non-homogeneous Dirichlet boundary conditions

When applying the Dirichlet boundary conditions

$$w(a,t) = w_L(t), \qquad w(b,t) = w_R(t)$$

for $t > 0$ we would take for $j = 0$

$$w_0^n = w_L(t_n). \tag{3.13}$$

On the right boundary we would have

$$w_N^n = w_R(t_n). \tag{3.14}$$

To implement the homogeneous Dirichlet boundary conditions we set $w_L(t) = w_R(t) = 0$ in (3.13) and in (3.14), with the values for ${w_0}^n = 0$, ${w_N}^n = 0$ known due to the boundary condition we use (3.12) to compute ${w_1}^{n+1}, ..., w_{N-1}^{n+1}$ only.

Discretization of non-homogeneous Neumann boundary condition

More commonly used are the Neumann boundary conditions with time dependent flux as J_L, J_R for the left boundary $\frac{\partial w(a,t)}{\partial x} = J_L(t)$ and the right boundary $\frac{\partial w(b,t)}{\partial x} = J_R(t)$. We introduce the ghost points $x_{-1} = -\Delta x$, $x_{N+1} = (N+1)\Delta x$ and the ghost point values at these points are w^n_{-1} and w^n_{N+1}. Now we apply a central differences with respect to the left boundary point x_0 as follows

$$\frac{w^n_1 - w^n_{-1}}{2\Delta x} = J_L(t_n). \tag{3.15}$$

This gives the ghost value $w^n_{-1} = w^n_1 - 2\Delta x J_L(t_n)$. With this the discretized scheme (3.12) at $j = 0$ will take the form

$$\begin{aligned} w^{n+1}_0 &= \nu w^n_1 + (1-2\nu)w^n_0 + \nu(w^n_1 - 2\Delta x J_L(t_n)) \\ &= 2\nu w^n_1 + (1-2\nu)w^n_0 - 2\nu\Delta x J_L(t_n). \end{aligned} \tag{3.16}$$

For $j = N$, the analogous central differences with respect to the right boundary point x_N is used to obtained w^n_{N+1} which is $w^n_{N+1} = w^n_{N-1} + 2\Delta x J_R(t_n)$. In this case the scheme (3.12) will take the form

$$\begin{aligned} w^{n+1}_N &= \nu w^n_{N-1} + (1-2\nu)w^n_N + \nu(w^n_{N-1} + 2\Delta x J_R(t_n)) \\ &= 2\nu w^n_{N-1} + (1-2\nu)w^n_N + 2\nu\Delta x J_R(t_n). \end{aligned} \tag{3.17}$$

For $j = 1, ..., N-1$ the scheme (3.12) will be used.

To implement the homogeneous Neumann boundary conditions we set the fluxes $J_L(t_n) = J_R(t_n) = 0$ in (3.16) and in (3.17). In this case we write together the explicit discretization scheme with homogeneous Neumann boundary conditions in simplified form as follows

$$\begin{aligned} w^{n+1}_0 &= w^n_0 + 2\nu(w^n_1 - w^n_0) && \text{for } j = 0 \\ w^{n+1}_j &= w^n_j + \nu(w^n_{j+1} - w_j) - \nu(w^n_j - w^n_{j-1}) && \text{for } 0 < j < N \\ w^{n+1}_N &= w^n_N - 2\nu(w^n_N - w^n_{N-1}) && \text{for } j = N. \end{aligned} \tag{3.18}$$

We can write the above system (3.18) in a matrix equation

$$\mathbf{w^{n+1}} = \mathbf{A}\mathbf{w^n}. \tag{3.19}$$

Here $\mathbf{w^n}$=$(w^n_0 \cdots, w^n_N)^T$ and the $(N+1)\times(N+1)$ matrix $\mathbf{A}$ has the following tri-diagonal structure

$$\mathbf{A} = \begin{pmatrix} 1-2\nu & 2\nu & \dots & & 0 \\ \nu & 1-2\nu & \nu & & \vdots \\ \vdots & \ddots & \ddots & \ddots & \\ & & \nu & 1-2\nu & \nu \\ 0 & \dots & & 2\nu & 1-2\nu \end{pmatrix}.$$

Alternatively, we can derive other schemes for the outer boundaries when we discretize the Neumann boundary conditions via one sided differences. The discretization of the left Neumann boundary condition is $\frac{w_0^n - w_{-1}^n}{\Delta x} = J_L(t_n)$. This implies that $w_{-1}^n = w_0^n - \Delta x J_L(t_n)$. We substitute this in (3.12) for $j = 0$ to obtain

$$w_0^{n+1} = \nu w_1^n + (1-\nu)w_0^n - \nu(w_0^n + \Delta x J_L(t_n). \tag{3.20}$$

For the zero flux $J_L(t_n) = 0$ we will get the scheme $w_0^{n+1} = \nu w_1^n + (1-\nu)w_0^n$.

Analogously, we discretize the Neumann boundary condition on the right hand side $\frac{w_{N+1}^n - w_N^n}{\Delta x} = J_R(t_n)$. This implies that $w_{N+1}^n = w_N^n + \Delta x J_R(t_n)$. We substitute this in (3.12) and obtain the following scheme

$$w_N^{n+1} = \nu w_{N-1}^n + (1-\nu)w_N^n + \Delta x J_R(t_n). \tag{3.21}$$

For the zero flux $J_R(t_n) = 0$ we will get the scheme $w_N^{n+1} = \nu w_{N-1}^n + (1-\nu)w_N^n$. We will later see that this alternative is not so good because it violates conservativity of the scheme.

3.3 Implicit time discretization method

Again we consider the diffusion equation defined in (3.7) with Neumann boundary conditions. When we derived the explicit scheme we used the forward difference approximation for the time derivative. Here we use the backward Euler difference approximation method because the problem is stiff and the implicit method allows us to take larger time steps. It is unconditionally stable. But each time step is more costly, since a linear system of equations has to be solved.

3.3.1 Backward in time and central in space

We apply the implicit time discretization method as the backward in time and central in space (BTCS) scheme to the diffusion equation (3.7) given by

$$\frac{w_j^{n+1} - w_j^n}{\Delta t} = D\frac{w_{j-1}^{n+1} - 2w_j^{n+1} + w_{j+1}^{n+1}}{(\Delta x)^2}.$$

We solve for w_j^n on the right hand side and set $\nu = D\frac{\Delta t}{(\Delta x)^2}$ to get the following scheme

$$-\nu w_{j+1}^{n+1} + (1+2\nu)w_j^{n+1} - \nu w_{j-1}^{n+1} = w_j^n. \tag{3.22}$$

Discretization of the homogeneous Neumann boundary conditions

Now we apply the Neumann boundary conditions. For sake of simplicity we consider the homogeneous case $w_x(a,t) = 0$ and $w_x(b,t) = 0$. To discretize these conditions we use the central differences with respect to the left hand boundary point a. We approximate

$\frac{w_1^{n+1}-w_{-1}^{n+1}}{\Delta x^2}=0$, which implies that $w_1^{n+1}=w_{-1}^{n+1}$. Inserting this into the scheme (3.22) we obtain the following scheme for the left hand boundary

$$(1+2\nu)w_0^{n+1}-2\nu w_1^{n+1}=w_0^n. \tag{3.23}$$

Analogously, for $j=N$ we discretize the right hand boundary condition with respect to the boundary point b. We obtain $w_{N-1}^{n+1}=w_{N+1}^{n+1}$. Inserting this into the scheme (3.22) for $j=N$ we obtain the following scheme

$$-2\nu w_{N-1}^{n+1}+(1+2\nu)w_N^{n+1}=w_N^n. \tag{3.24}$$

We write together the fully implicit scheme derived above with the homogeneous outer Neumann boundary conditions as follows

$$\begin{aligned}(1+2\nu)w_0^{n+1}-2\nu w_1^{n+1}&=w_0^n \qquad \text{for } j=0\\ -\nu w_{j+1}^{n+1}+(1+2\nu)w_j^{n+1}-\nu w_{j-1}^{n+1}&=w_j^n \qquad \text{for } 0<j<N\\ (1+2\nu)w_N^{n+1}-2\nu w_{N-1}^{n+1}&=w_N^n \qquad \text{for } j=N.\end{aligned} \tag{3.25}$$

The implicit discretized scheme derived in (3.25) can be written in a matrix equation for $j=0,1,...,N$ as

$$\mathbf{A}\mathbf{w}^{n+1}=\mathbf{w}^n \tag{3.26}$$

Here $\mathbf{w^n}$=$(w_0^n\cdots,w_N^n)^T$ and the $(N+1)\times(N+1)$ matrix $\mathbf{A}$ has the following tri-diagonal structure

$$\mathbf{A}=\begin{pmatrix} 1+2\nu & -2\nu & \dots & & 0\\ -\nu & 1+2\nu & -\nu & & \vdots\\ \vdots & \ddots & \ddots & \ddots & \\ & & -\nu & 1+2\nu & -\nu\\ 0 & \dots & & -2\nu & 1+2\nu \end{pmatrix}.$$

By using an implicit scheme we have to solve the linear system for the matrix $\mathbf{A}$. This is computationally more expensive than the explicit case.

This method is stable for $\nu>0$ so larger time steps can be used for implicit methods than explicit methods. Solving the above matrix system for time level $n+1$, i.e. $\mathbf{w}^{n+1}$ is then just the solution of the above linear system. We used two linear solvers, the direct solver which uses the Thomas algorithm and the Gauss-Seidel iterative method.

Alternatively, we may discretize the homogeneous Neumann boundary conditions via one sided differences. We will get the scheme for the left hand Neumann boundary conditions as

$$w_0^n=(1+\nu)w_0^{n+1}-\nu w_1^{n+1} \tag{3.27}$$

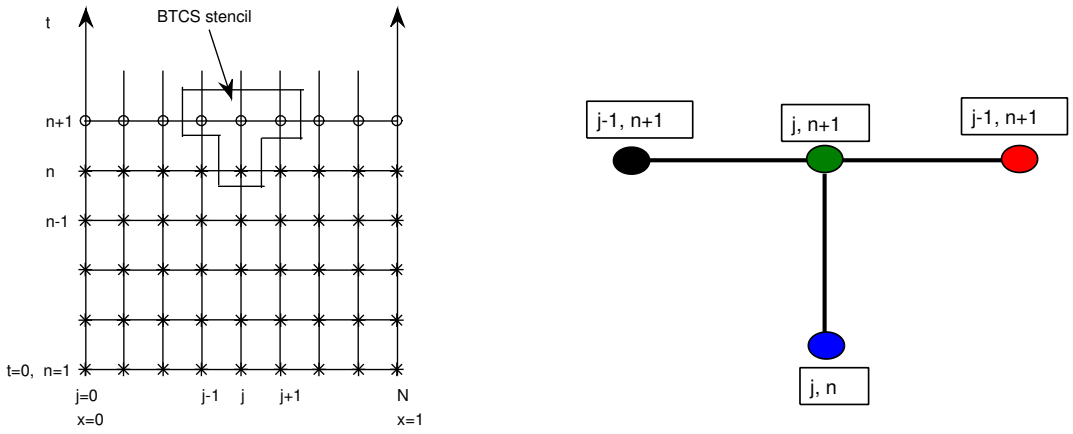

Figure 3.3: The figure in the left panel the spatio-temporal frame for (BTCS) scheme, while in the right panel the BTCS stencil is given.

and for the right hand Neumann boundary condition as

$$w_N^n = (1+\nu)w_N^{n+1} - \nu w_{N-1}^n. \tag{3.28}$$

Again we will see that conservativity is violated in this case.

3.3.2 The Thomas algorithm

The Thomas algorithm, also known as tridiagonal matrix algorithm (TDMA), is used to solve a tridiagonal system of equations. This is a simplified form of the Gaussian elimination. Let the matrix form of the tridiagonal system be $\mathbf{Aw} = \mathbf{d}$. The general form of the equations may given as

$$a_i w_{i-1} + b_i w_i + c_i w_{i+1} = d_i \qquad \text{for} \qquad i = 0, \cdots, N. \tag{3.29}$$

Here $a_0 = 0$ and $c_N = 0$. Then tridiagonal matrix $\mathbf{A}$ is given by

$$\mathbf{A} = \begin{pmatrix} b_0 & c_0 & & & & 0 \\ a_1 & b_1 & c_1 & & & \\ & a_2 & b_2 & c_2 & & \\ & & \ddots & \ddots & \ddots & \\ & & & a_{N-1} & b_{N-1} & c_{N-1} \\ 0 & & & & a_N & b_N \end{pmatrix}$$

and the unknown column matrix is $\mathbf{w}=(w_0, w_1, \cdots, w_N)^T$ and the vector of the known values is $\mathbf{d}=(d_0, d_1, \cdots, d_N)$. This algorithm achieves the required solution in $O(N)$ operations, while the Gaussian elimination in general needs $O(N^3)$. A first sweep eliminates the a_i, and then a backward substitution is used to get the solution. The new variables are denoted with primes. This algorithm uses two sweeps. One is the forward sweep given by eliminating $a_1, \cdots a_N$ and normalizing the $b'_i = b_i - c'_{i-1}$ to 1. This gives an upper triangular matrix with all diagonal entries equal to 1. This leads the new coefficients

$$c'_i = \begin{cases} \dfrac{c_0}{b_0} & \text{for } i = 0 \\ \dfrac{c_i}{b_i - c'_{i-1}a_i} & \text{for } i = 1, 2, , \ \ldots, N-1 \end{cases}$$

and modified right hand side coefficients

$$d'_i = \begin{cases} \dfrac{d_0}{b_0} & \text{for } i = 0 \\ \dfrac{d_i - d'_{i-1}a_i}{b_i - c'_{i-1}a_i} & \text{for } i = 1, 2, \ldots, N. \end{cases}$$

Then the second sweep one is the backward substitution, via this we obtain the required solution

$$\begin{aligned} w_N &= d'_N \\ w_i &= d'_i - c'_i w_{i+1}, \qquad i = N-1, N-2, \cdots, 0. \end{aligned}$$

For further detail regarding stability, proof and other requirements see the books of Higham [16] or Datta [5]. In case of explicit and implicit methods we have such a tridiagonal matrix system of linear equations. We use the above algorithm to obtain the required solution. In this thesis we also consider an iterative approach for comparison. It is given below.

3.3.3 Iterative methods

Consider the linear system (3.26) with $\mathbf{A} \in \mathbb{R}^{(N+1)\times(N+1)}$ and $\mathbf{w^n} \in \mathbb{R}^{\mathbf{N+1}}$. An iterative method for the solution of matrix form $\mathbf{A}\mathbf{w}^{n+1} = \mathbf{w}^n$ consists of a sequence of vectors $(\mathbf{w^{(k)}})_{\mathbf{k\geq 0}}$ of $\mathbb{R}^N$ which converges to the exact solution $\mathbf{w^{n+1}}$, that is $\mathbf{w^{(k)}} \to \mathbf{w^{n+1}}$ for $k \to \infty$.

In the literature the commonly used iterative methods for solving the linear system of equation include the Jacobi method, Gauss-Seidel, and other relaxation methods. Some of the basic explanations, propositions for the convergence analysis and some basic definition are given in Quarteroni et al. [30, Ch. 5]. Here we are using the Gauss-Seidel iterative method which is a commonly used iterative method.

First we give some necessary idea that how iterative methods work: The iterative methods begins with an initial guess for the solution $\mathbf{w^0}$ to the matrix equation $\mathbf{A}\mathbf{w}^{n+1} = \mathbf{w}^n$ that we are trying to solve. Each iteration updates the new k^{th} estimate $\mathbf{w^{(k)}}$ which

converges to the exact solution described above. The different methods have different convergence times and for big inverse matrix problems are much faster than direct matrix inverse methods, see Olsen-Kettle [27].

Gauss-Seidel iterative method

To start the scheme it is necessary to use an initial guess $\mathbf{w}^{(0)}$. We choose a tolerance TOL, e.g. $TOL = 10^{-6}$. We take $\mathbf{w}^{(0)} = \mathbf{w}^n$. The iteration process will be repeated until the residual satisfies $|\mathbf{w}^n - \mathbf{A}\mathbf{w}^{(k+1)}| < TOL$. In the Gauss-Seidel method we have the update

$$w_i^{(k+1)} = \frac{1}{a_{ii}}\big(w_i^{(k)} - \sum_{j=1}^{i-1} a_{ij} w_j^{(k+1)} - \sum_{j=i+1}^{N} a_{ij} w_j^{(k)}\big) \tag{3.30}$$

for $i = 1, \ldots, N+1$. Let $\mathbf{A} = \mathbf{L} + \mathbf{D} + \mathbf{U}$ with $\mathbf{D}$ containing the diagonal terms, $\mathbf{U}$ containing the terms above the diagonal and $\mathbf{L}$ those below the diagonal of the matrix $\mathbf{A}$. Then the above equation can be written in matrix form as $\mathbf{w}^{(k+1)} = \mathbf{D}^{-1}(\mathbf{b} - \mathbf{L}\mathbf{w}^{(k+1)} - \mathbf{U}\mathbf{w}^{(k)})$ or $(\mathbf{D} + \mathbf{L})\mathbf{w}^{(k+1)} = \mathbf{b} - \mathbf{U}\mathbf{w}^{(k)}$. The solution converges $\mathbf{w}^{(k)} \to \mathbf{w}$ as $k \to \infty$ if $||(\mathbf{D} + \mathbf{L})^{-1}\mathbf{U}|| < 1$ for some matrix norm [30].

Implicit versus explicit methods

In the explicit methods we obtain an explicit formula for the values of the unknown function at the new time level for every spatial mesh points. While in the implicit methods we obtain a coupled system of equations for the unknown function at a new time level.

The implicit methods are more elaborate to code since they require the solution of coupled equations, i.e. a matrix system, at each time level. Further, in the explicit methods we have a closed-form formula for the value of the unknown at each mesh point which is comparatively easy in terms of coding and computation. Further, the implicit methods may be unconditionally stable, while the explicit schemes have a restriction on the size of the time step.

3.4 Finite volume discretization of the diffusion equation

Now we consider the finite volume method to discretize the one-dimensional diffusion equation (3.1), with homogenous Neumann boundary conditions.

Spatio-temporal discretization

Now discretize the space interval $[a, b]$ into N equal size grid cells τ of size $\Delta x = (b-a)/N$. Let $x_j = a + (j - 1/2)\Delta x$ be the center of cell $\tau_j = [x_j + \frac{\Delta}{2}, x_j + \frac{\Delta}{2}]$ for $j = 1, 2, \ldots, N$. The edges of cell τ_j are then $x_{j\pm 1/2} = a + (j - 1/2)\Delta x \pm \frac{\Delta x}{2}$. In a finite volume method the unknown is approximated by the average of the solution over a grid cell. We seek an

approximation by cell averages at each time t_n, i.e.

$$w_j^n \approx \frac{1}{\Delta x}\int_{x_{j-\frac{1}{2}}}^{x_{j+\frac{1}{2}}} w(x,t_n)\,dx \qquad \text{for} \qquad j=1,2,\ldots,N. \tag{3.31}$$

We can use the integral averages also to discretize the initial data. The integral may be replaced by a quadrature rule.

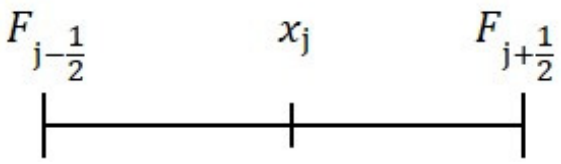

Figure 3.4: Sketch of the finite volume flux.

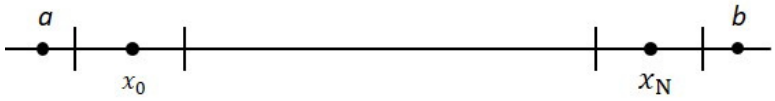

Figure 3.5: Finite volume flux representation for the interior and outer boundaries.

We discretize the time derivative via the forward difference. Then we write the scheme for (3.1) in the **flux form** as follows

$$\frac{w_j^{n+1}-w_j^n}{\Delta t} = D\frac{F_{j+\frac{1}{2}}-F_{j-\frac{1}{2}}}{\Delta x} \tag{3.32}$$

where the **numerical fluxes** are given as

$$F_{j-\frac{1}{2}} = \frac{w_j^n - w_{j-1}^n}{\Delta x}, \qquad F_{j+\frac{1}{2}} = \frac{w_{j+1}^n - w_j^n}{\Delta x}.$$

Using these fluxes in (3.32) we obtain the scheme

$$\begin{aligned} w_j^{n+1} &= w_j^n + \frac{D\Delta t}{\Delta x}\Big(\frac{w_{j+1}^n - w_j^n}{\Delta x} - \frac{w_j^n - w_{j-1}^n}{\Delta x}\Big) \\ &= w_j^n + \nu(w_{j+1}^n - w_j^n) - \nu(w_j^n - w_{j-1}^n). \end{aligned} \tag{3.33}$$

The formula is the same as in (3.12) for the interior nodes. But the interpretation is different, since the nodal points at the cell centers are at different locations.

Implementation of the Neumann boundary conditions on the outer boundaries

Here we derive the update for the boundary cells τ_1 and τ_N. We use the central difference with respect to the boundary points a and b. We introduce the ghost cells τ_0 and τ_{N+1} of length Δx which are adjacent to the domain. The boundary conditions are used to

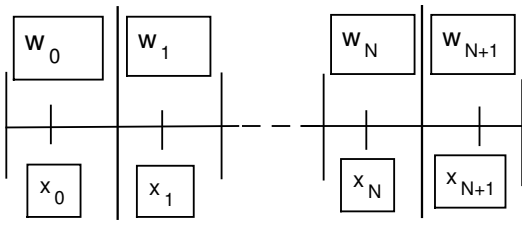

Figure 3.6: Sketch for the finite volume flux representation on the outer boundaries.

determine the value of w_0 and w_{N+1} based on the values w_j in the interior cells. We take the update formula (3.33) for $j = 1$ and $j = N$. First we consider the homogeneous Neumann boundary condition $w_x = 0$ at $x_{1/2} = a$. We take as discretization

$$\frac{w_1^n - w_0^n}{\Delta x} = 0, \qquad \text{for } j = 1. \tag{3.34}$$

This implies that $w_1^n = w_0^n$. We substitute this for $j = 1$ into (3.33) and obtain the following update for the left boundary cell

$$w_1^{n+1} = w_1^n + \nu(w_2^n - w_1^n) = (1-\nu)w_1^n + \nu w_2^n.$$

This is equivalent to taking $F_{1/2} = 0$ at $x = 0$. Analogously, we implement $w_x = 0$ at $x_{N+1/2} = b$. We use

$$\frac{w_{N+1}^n - w_N^n}{\Delta x} = 0, \qquad \text{for } j = N.$$

This gives $w_N^n = w_{N+1}^n$ and $F_{N+1/2} = 0$ at $x = 1$. We substitute this for $j = N$ into (3.33) and obtain the following update for the right boundary cell

$$w_N^{n+1} = w_N^n - \nu(w_N^n - w_{N-1}^n) = (1-\nu)w_N^n + \nu w_{N-1}^n.$$

We write the discretized system with together the homogeneous Neumann boundary conditions as follows

$$\begin{aligned} w_1^{n+1} &= w_1^n + \nu(w_2^n - w_1^n) && \text{for } j = 1 \\ w_j^{n+1} &= w_j^n + \nu(w_{j+1}^n - w_j^n) - \nu(w_j^n - w_{j-1}^n) && \text{for } 1 < j < N \\ w_N^{n+1} &= w_N^n - \nu(w_N^n - w_{N-1}^n) && \text{for } j = N. \end{aligned} \tag{3.35}$$

Here, we derived the same formula as we obtained for the finite difference method in (3.18) for the interior nodes. We can obtain the same scheme as (3.35) for the nodal based approach if we use one sided differences for the outer boundary conditions as mentioned in Section 3.2. Analogously, if we use here the central difference $\frac{w_2^n - w_0^n}{2\Delta x} = 0$ for the outer boundary cells then we can derive the analogous formulation as we derived in (3.18). For the finite difference scheme we used a central difference w.r.t. the nodes. Here we are using a central difference w.r.t. domain boundary.

A discussion why (3.18) and (3.35) have the respective correct numerical boundary conditions will be given in Chapter 5. There we show that switching the numerical boundary conditions leads to a violation of conservativity.

3.5 An exact solution for the single domain diffusion equation

Here we recall an exact solution of the one dimensional single domain diffusion equation. This can be found in any standard text book on the solution of PDEs. This is needed in order to test the accuracy of our numerical solutions obtained for the single domain diffusion equation as well as later for bi-domain diffusion equations with Dirichlet-Neumann coupling for identical diffusion coefficients. With it we may compute the L_1 error for these solutions.

The diffusion equation (3.1) has the following exact solutions

$$w_n(x,t) = e^{-D(\frac{n\pi}{L})^2 t}\cos\Big(\frac{n\pi}{L}x\Big) + 1$$

for $n \in \mathbb{N}$ on the interval $[0, L]$. We will use $L = 1$ and $n = 1$ as a test case. This solution satisfies the homogeneous Neumann boundary conditions at 0 and L. Clearly it satisfies the diffusion equation (3.1). The initial values are $w_0(x) = \cos(\pi x) + 1$.

3.5.1 Truncation error for the single domain diffusion equation

For any numerical method it is necessary to derive the truncation error (TE) for the descritized numerical. Here we derive for the FTCS scheme which is an explicit method of getting the unknown numerical solution. For this we consider the discretized scheme (3.11) as

$$\frac{w_j^{n+1} - w_j^n}{\Delta t} - D\frac{w_{j-1}^n - 2w_j^n + w_{j+1}^n}{(\Delta x)^2} = 0.$$

Using an exact solution w we replace w_j^n by $w(t_n, x_j)$ and use a Taylor's series to expand around (t_n, x_j). We obtain

$$\begin{aligned}
TE &= \frac{w(t_n+\Delta t, x_j) - w(t_n, x_j)}{\Delta t} - D\frac{w(t_n, x_j-\Delta x) - 2w(t_n, x_j) + w(t_n, x_j+\Delta x)}{(\Delta x)^2} \\
&= \frac{1}{\Delta t}\Big(w + \Delta t w_t + \frac{1}{2}(\Delta)^2 w_{tt} + \ldots - w\Big)\Big|_{(t_n,x_j)} \\
&\quad - \frac{D}{(\Delta x)^2}\Big(w - \Delta x w_x + \frac{1}{2}(\Delta x)^2 w_{xx} - \frac{1}{6}(\Delta x)^3 w_{xxx} + \frac{1}{24}(\Delta x)^4 w_{xxxx}\ldots \\
&\quad - 2w + w + \Delta x w_x + \frac{1}{2}(\Delta x)^2 w_{xx} + \frac{1}{6}(\Delta x)^3 w_{xxx} + \frac{1}{24}(\Delta x)^4 w_{xxxx} + \ldots\Big)\Big|_{(t_n,x_j)} \\
&= w_t + \frac{1}{2}\Delta t w_{tt} - D w_{xx} - \frac{D}{12}(\Delta x)^2 w_{xxxx} + \ldots.
\end{aligned} \tag{3.36}$$

As we described that w and its derivatives are evaluated at (t_j, x_j). So, clearly w satisfy the diffusion equation (3.1). Now after cancellation of the identical terms we obtain

$$TE = \frac{1}{2}w_{tt}\Delta t - \frac{1}{12}w_{xxxx}(\Delta x)^2 + O((\Delta t)^2, (\Delta x)^4). \tag{3.37}$$

This shows that the truncation error of FTCS scheme is first order in time and second order in space. In our numerical computations we used a fixed CFL-number $\nu = \frac{1}{3}$. Using $\frac{D\Delta t}{(\Delta x)^2} = \nu = \frac{1}{3}$, we obtain $\Delta t = \frac{1}{3D}(\Delta x)^2$.

Note that from the diffusion equation (3.1) we have $u_t = Du_{xx}$, then $u_{tt} = D^2 u_{xxxx}$. In this case the equation (3.37) will become

$$TE = \Big(\frac{D^2\Delta t}{2} - \frac{D(\Delta x)^2}{12}\Big)w_{xxxx} + O((\Delta t)^2, (\Delta x)^4). \tag{3.38}$$

Inserting the CFL-number ν that we are using to obtain

$$TE = \frac{D}{12}w_{xxxx}(\Delta x)^2 + O((\Delta t)^2, (\Delta x)^4). \tag{3.39}$$

This is a second order convergence. This we also observed in the numerical results, see Table 7.5. Analogously we can derive such a result for the BTCS scheme.

3.6 L_1-error analysis

It is useful, in order to assess the quality of our numerical solutions, to compute the error for a test case with an explicit solution. We consider the L_1-norm of the error. Let $w \in L^1(a, b)$ then the L_1-norm is given as

$$\|w\|_{1,(a,b)} = \int_a^b |w(x)|\, dx. \tag{3.40}$$

Our numerical solution may be interpreted as a step function. For any set A let χ_A be the indicator function of A, i.e. $\chi(x) = 1$ for $x \in A$ and $\chi(x) = 0$ for $x \notin A$. Then the step functions for the finite difference and for the finite volume method at time $t \in [t_n, t_{n+1}[$ are given by

$$w_h(t, \cdot) = \sum_{i=0}^{N} w_i^n \chi_{\sigma_i}$$

and

$$w_h(t, \cdot) = \sum_{i=1}^{N} w_i^n \chi_{\tau_i}$$

respectively. Let us consider the error $\|w_h(t_n, \cdot) - w(t_n, \cdot)\|$ at time t_n, where $w(t_n, \cdot)$ is the exact solution at time t_n and $w_h(t_n, \cdot)$ is the numerical solution defined as a step function above.

The L_1 error for the finite difference solution is given by

$$\begin{aligned}\|w_h(t_n, \cdot) - w(t_n, \cdot)\|_{1,(a,b)} &= \int_a^b |w_h(t_n, x) - w(t_n, x)|\, dx \\ &= \sum_{i=0}^{n} \int_{\sigma_i} |w_i^n - w(t_n, x)|\, dx.\end{aligned}$$

On σ_0 we use left hand rectangle rule, on σ_N the right hand rectangle rule and the mid point rule for $i = 1, \cdots, N-1$. Using the notation $\overline{w}_j^n = w(t_n, x_j)$ this leads to

$$\|w_h(t_n,\cdot) - w(t_n,\cdot)\|_{1,(a,b)} \approx E_n(h) := \frac{\Delta x}{2}|w_0^n - \overline{w}_0^n| + \Delta x \sum_{i=1}^{N-1} |w_i^n - \overline{w}_i^n| + \frac{\Delta x}{2}|w_N^n - \overline{w}_N^n|. \tag{3.41}$$

The L_1 error for the finite volume method is given by

$$\|w_h(t_n,\cdot) - w(t_n,\cdot)\|_{1,(a,b)} = \sum_{i=1}^{n} \int_{\tau_i} |w_i^n - w(t_n,x)|\, dx.$$

In this case we use the mid point rule on all cells. This implies that

$$\|w_h(t_n,\cdot) - w(t_n,\cdot)\|_{1,(a,b)} \approx E_n(h) := \Delta x \sum_{i=1}^{N} |w_i^n - \overline{w}_i^n|. \tag{3.42}$$

3.6.1 Numerical order of convergence

A numerical method is said to be of order α if there is a constant C independent of mesh size $h = \Delta x$ such that at any time $t > 0$

$$\|w_h(t,\cdot) - w(t,\cdot)\| \leq Ch^\alpha$$

in some given norm norm, e.g. the L^1-norm. This estimate should be satisfied for h small enough.

In order to determine the order of converge α of a numerical method we choose a time T and calculate a sequence of approximations giving errors $\|w_{h_0}(T,\cdot) - w(T,\cdot)\|$, $\|w_{h_1}(T,\cdot) - w(T,\cdot)\|, \ldots, \|w_{h_N}(T,\cdot) - w(T,\cdot)\|$ where $h_k < \cdots < h_1 < h_0$ are increasingly small step sizes. Then a formula for the numerical order of convergence is given by

$$\alpha_j = \frac{\log\left(\frac{\|w_{h_j}(t,\cdot) - w(t,\cdot)\|}{\|w_{h_{j-1}}(t,\cdot) - w(t,\cdot)\|}\right)}{\log \frac{h_j}{h_{j-1}}}. \tag{3.43}$$

for $j \in \{1, \cdots, k\}$. Note that the corresponding time steps $\Delta t_0, \cdots, \Delta t_k$ should be chosen such that $T/\Delta t_0, \cdots, T/\Delta t_k \in \mathbb{N}$. When we are working with a fixed CFL number between h and Δt this means that the h_j have to be chosen accordingly.

Chapter 4

Discretization of coupling conditions for the bi-domain diffusion equations

In this chapter we explain the various discretization methods for the coupling conditions given in Chapter 2. The discretization methods we use include the explicit and implicit finite difference method (nodal based), i.e. finite element type, finite volume (cell based) only for Dirichlet-Neumann coupling. The implicit methods further include the monolithic and the partitioned coupling iterative approaches. The explicit discretizations are explained in the first section, while the implicit discretizations are explained in the second section.

4.1 Explicit discretizations

In this section we discretize the bi-domain diffusion equations and various coupling conditions given in Chapter 2 for the bi-domain diffusion equation in one space dimension using explicit discretizations.

4.1.1 Explicit discretization by using ghost point methods

In this subsection we are considering internal coupling conditions using ghost points. As a first step the numerical implementations of the coupling conditions for Dirichlet-Neumann coupling are explained in the following two algorithms which we then will extend to the other coupling conditions.

Spatio-temporal discretization of the bi-domain equation

For simplicity we take $\Omega = [a, b] = [0, 1]$. We introduce grid points for the spatio-temporal discretization of the bi-domain diffusion system on the interval $[0, 1]$ with coupling boundary at $c = \frac{1}{2}$ via a finite difference scheme. We consider $N = 2m$ even for some $m \in \mathbb{N}$ and set $\Delta x = 1/N$. Grid points for the two sub-domains $\Omega_1 = [0, 1/2]$ and $\Omega_2 = [1/2, 1]$ are defined as

$$x_j = j\Delta x, \quad \text{for} \quad j = 0, 1, ..., m-1, j = m+1, ..., N = 2m.$$

At the interface $c = \frac{1}{2}$ we introduce the double node $x_{m_-} = x_{m_+} = m\Delta x$, see Figure 4.1 below. The node x_{m_-} is used in conjunction with Ω_1 and x_{m_+} with Ω_2. Later we will make use of cell boundary points $x_{j\pm\frac{1}{2}} = x_j \pm \frac{\Delta x}{2}$. We then consider the nodal values to represent the value of the solution on a cell $[x_{j-\frac{1}{2}}, x_{j+\frac{1}{2}}]$. For the functions u and v

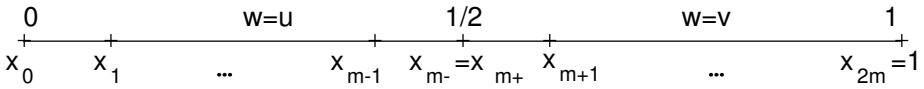

Figure 4.1: Geometry of one dimensional grid points for bi-domain equations

introduced in Section 2.3 we set

$$\begin{aligned} u_j^n &\approx u(x_j, t_n), \qquad \text{for } \; j = 0, 1, ..., m-1, \\ v_j^n &\approx v(x_j, t_n), \qquad \text{for } \; j = m+1, 1, ..., N, \end{aligned}$$

as well as $u_m^n \approx u(x_{m_-}, t_n)$ and $v_m^n \approx v(x_{m_+}, t_n)$. The discretization of the first equation of the system (2.10) via the forward in time and central in space explicit scheme (3.12) using $\nu_- = D_- \frac{\Delta t}{(\Delta x)^2}$ and $\nu_+ = D_+ \frac{\Delta t}{(\Delta x)^2}$ is given by

$$u_j^{n+1} = \nu_- u_{j+1}^n + (1 - 2\nu_-) u_j^n + \nu_- u_{j-1}^n \tag{4.1}$$

The above scheme can be written as

$$u_j^{n+1} = u_j^n + \nu_-(u_{j+1}^n - u_j^n) - \nu_-(u_j^n - u_{j-1}^n) \tag{4.2}$$

for the interior points x_j with $j = 1, ..., m-1$. Analogously, for x_j with $j = m+1, ..., N-1$, we get the following scheme

$$v_j^{n+1} = \nu_+ v_{j+1}^n + (1 - 2\nu_+) v_j^n + \nu_+ v_{j-1}^n. \tag{4.3}$$

Due to the homogeneous outer Neumann boundary conditions we use the numerical boundary conditions (3.16), (3.17) with $J_L = J_R = 0$. They are as follows

$$u_0^{n+1} = 2\nu_- u_1^n + (1 - 2\nu_-) u_0^n \tag{4.4}$$

for the left out boundary and

$$v_N^{n+1} = 2\nu_+ v_{N-1}^n + (1 - 2\nu_+) v_N^n \tag{4.5}$$

for the right outer boundary. It remains to determine u_m^{n+1} and v_m^{n+1} via various numerical coupling conditions below.

4.1.2 Dirichlet-Neumann coupling conditions

As a first step we consider the Dirichlet-Neumann conditions for the bi-domain diffusion model. The algorithm for this is explained as follows.

Explicit coupled discretization scheme

We begin with an explicit discretization scheme. Its computational steps are given in Algorithm A1 and are represented graphically in Figure 4.2

We follow Giles [10] only to a certain degree. He considered explicit and implicit coupled scheme to solve the coupled bi-domains interface models numerically. A slightly more general version is given in Roe et al. [33]. In partitioned procedure schemes the coupled discretization scheme is considered as one of the useful schemes to solve coupled bi-domain models numerically. As we will point out later in Chapter 5, their schemes are not conservative and therefore not very useful.

In order to introduce this numerical coupling we consider the bi-domain diffusion equations as a first order system by introducing the fluxes $q_1 = \frac{\partial u}{\partial x}$, $q_2 = \frac{\partial v}{\partial x}$ as new variables. This gives the systems

$$\frac{\partial u}{\partial t} = \frac{\partial q_1}{\partial x}, \qquad q_1 = D_- \frac{\partial u}{\partial x} \quad \text{for } t > 0,\ x \in \Omega_1 \tag{4.6}$$

and

$$\frac{\partial v}{\partial t} = \frac{\partial q_2}{\partial x}, \qquad q_2 = D_+ \frac{\partial v}{\partial x} \quad \text{for } t > 0,\ x \in \Omega_2. \tag{4.7}$$

Let us consider the Dirichlet-Neumann coupling on the interface in the form

$$u(c,t) = v(c,t), \qquad D_- \frac{\partial u(c,t)}{\partial x} = D_+ \frac{\partial v(c,t)}{\partial x}. \tag{4.8}$$

The discretization of $q_1 = \frac{\partial u}{\partial x}$ with a backward difference method and $q_2 = \frac{\partial v}{\partial x}$ with a forward difference in space. For the the interface these will defined as

$$q^n_{m_-} := D_- \frac{u^n_m - u^n_{m-1}}{\Delta x}, \qquad q^n_{m_+} := D_+ \frac{v^n_{m+1} - v^n_m}{\Delta x}. \tag{4.9}$$

Now the discretization of $u_t = q_x$ at the interface, i.e. for $j = m$, is given by

$$\frac{u^{n+1}_m - u^n_m}{\Delta t} = \frac{q^n_{m+} - q^n_{m-}}{\Delta x}.$$

Inserting $q^n_{m_-}$ and $q^n_{m_+}$ from (4.9) to the above equation. This gives the following update

$$u^{n+1}_m = u^n_m + \nu_+(v^n_{m+1} - v^n_m) - \nu_-(u^n_m - u^n_{m-1}). \tag{4.10}$$

Our time step has to satisfy the CFL condition $\Delta t \leq \frac{(\Delta x)^2}{2\max\{D_-, D_+\}}$. The main steps are given in the following algorithm:

Algorithm A1, the explicit coupled scheme

The generic cycle of this algorithm for $M \in \mathbb{N}$ time steps is described below.

(1) Start from initial conditions u_0 and v_0 on the respective sub-domains to determine u^0_j for $j = 0, ..., m$ and v^0_j for $j = m+1, ..., 2m$. We assume that $v^0_m = u^0_m$ due to the Dirichlet condition in (4.8).

(2) We iterate for $n = 0, ..., M-1$ the following three steps:

(a) Compute u_0^{n+1} from (4.4) at node $j = 0$, i.e. on the left outer boundary. Then determine u_j^{n+1} on the interior nodes $j = 1, ..., m-1$ of the left sub-domain Ω_1 given (4.1). For $j = m$ we consider the Neumann condition at the interface corresponding to the left sub-domain u_m^{n+1} using (4.10).

(b) Impose the Dirichlet condition for v on the interface c, by setting $v_m^{n+1} = u_m^{n+1}$.

(c) Compute v_j^{n+1} on the interior nodes $j = m+1, ..., N-1$ of the right sub-domain Ω_2 from time t_n to t_{n+1} using (4.3) as well for the right outer boundary taking (4.5), i.e. for $j = N$.

(3) The iteration stops when computations under step (2) have been obtained for $n = M-1$. In order to determine v_m^M we set $v_m^M = u_m^M$.

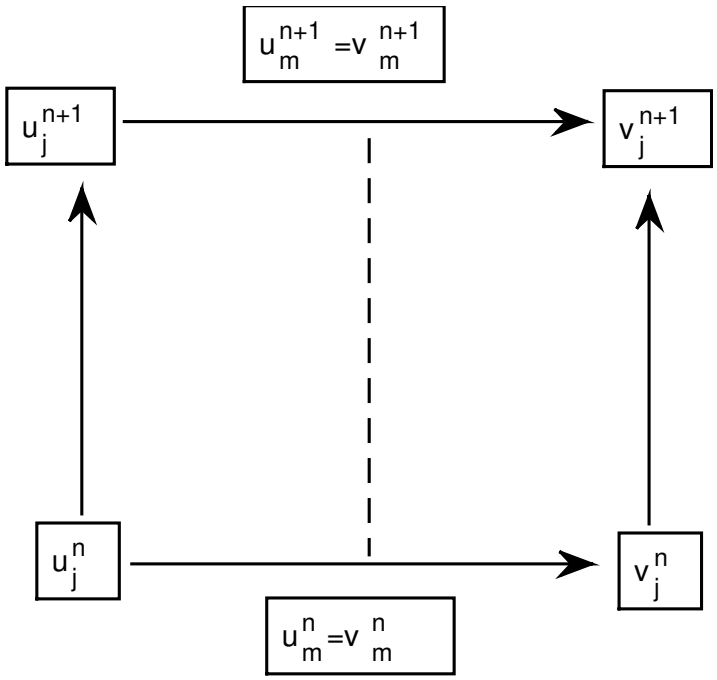

Figure 4.2: Graphical representation for the explicit coupled procedure for the Dirichlet-Neumann coupling

Now we write the fully discretized explicit form of the bi-domain diffusion model with Dirichlet-Neumann coupling conditions together in the following complete system

$$\begin{aligned}
u_0^{n+1} &= 2\nu_- u_1^n + (1-2\nu_-)u_0^n && \text{for } j=0\\
u_j^{n+1} &= \nu_- u_{j-1}^n + (1-2\nu_-)u_j^n + \nu_- u_{j+1}^n && \text{for } 0<j<m\\
u_m^{n+1} &= u_m^n + \nu_+(v_{m+1}^n - v_m^n) - \nu_-(u_m^n - u_{m-1}^n) && \text{for } j=m\\
v_m^{n+1} &= u_m^{n+1} && \text{for } j=m\\
v_j^{n+1} &= \nu_+ v_{j-1}^n + (1-2\nu_+)v_j^n + \nu_+ v_{j+1}^n && \text{for } m<j<N\\
v_N^{n+1} &= 2\nu_+ v_{N-1}^n + (1-2\nu_+)v_N^n && \text{for } j=N.
\end{aligned} \tag{4.11}$$

Alternatively, we can also write the explicit coupling system (4.11) in a matrix form $\mathbf{U}^{n+1} = \mathbf{A}\mathbf{U}^n$. Here $\mathbf{U}^{n+1}$ is the column matrix of the unknowns values, while $\mathbf{U}^n$ is the column matrix of the known values get from initial data. The coefficient matrix $\mathbf{A}$ is the following tri-diagonal block structure matrix

$$\mathbf{A} = \left(\begin{array}{ccccc|cccc}
1-2\nu_- & 2\nu_- & \dots & & 0 & & & & \\
\nu_- & 1-2\nu_- & \nu_- & & \vdots & & & & \\
\vdots & \ddots & \ddots & \ddots & & & & & \\
0 & \cdots & \nu_- & 1-2\nu_- & \nu_- & & & & \\
\hline
 & & & \nu_- & 1-\nu_- & -\nu_+ & +\nu_+ & & \\
 & & & & 1 & -1 & 0 & & \\
\hline
 & & & & & \nu_+ & 1-2\nu_+ & \nu_+ & \dots 0 \\
 & & & & & \vdots & \ddots & \ddots & \ddots \\
 & & & & & & \nu_+ & 1-2\nu_+ & \nu_+ \\
 & & & & & 0 & \dots & 2\nu_+ & 1-2\nu_+
\end{array}\right).$$

So for the numerical calculations either we can use directly the explicit formulas of the system (4.11) or the above matrix equation.

For the purpose of testing the coupling on known solutions we consider the special case $D_- = D_+ = D$. Then the coupling should give the single domain solutions. In this case using $\nu = \nu_- = \nu_+$ (4.10) becomes

$$u_m^{n+1} = u_m^n + \nu((v_{m+1}^n - v_m^n) - (u_m^n - u_{m-1}^n)). \tag{4.12}$$

The coupling scheme of Giles

Giles [10] considered heat diffusion with a heat capacity c and conductivity k, i.e. in our notation an equation of the form $cw_t - kw_{xx} = 0$. He further considered different mesh sizes $\Delta x_\pm$ in the two sub-domains.

Note that Giles [10, (26)] did not distinguish u and v in the bi-domain case. Therefore $v_m^{n+1} = u_m^{n+1}$ is automatically implied in his scheme. But he used for u_m^{n+1} the update

$$u_m^{n+1} = u_m^n + 2r\nu_+(v_{m+1}^n - v_m^n) - 2\nu_-(u_m^n - u_{m-1}^n) \tag{4.13}$$

where $r = \frac{c_-\Delta x_-}{c_+\Delta x_+}$ and $\nu_\pm = \frac{k_\pm \Delta t}{c_\pm(\Delta x_\pm)^2}$ for his stability analysis. We will consider $r \neq 1$ in Chapter 6. This discretization was obtained by an inconsistency in the time discretization which leads to the loss of conservativity, see Chapter 5.

For comparison to the single domain scheme we would choose $c = 1$, $k = D = D_- = D_+$ and $r = 1$. We do not get a scheme equivalent to the single domain diffusion equation as in our scheme (4.12). This is due to the factor of 2 in two terms.

Actually, before making his supposed simplification Giles [10, (26)] had derived a correct scheme [10, (16)]. It is given in our notation as

$$u_m^{n+1} = u_m^n + \frac{2r\nu_+}{1+r}(v_{m+1}^n - v_m^n) - \frac{2\nu_-}{1+r}(u_m^n - u_{m-1}^n). \tag{4.14}$$

We will later choose $c_\pm = 1$, $k_\pm = D_\pm$ and $r = 1$ in (4.14). This gives the correct scheme in the single domain case. Further it equals exactly to our formula for the DN-coupling (4.10).

Coupling with ghost points

Now we discuss the use of ghost point values in the schemes for interface coupling. The two mesh points $x_{m+1} = (m+1)\Delta x$ and $x_{m-1} = (m-1)\Delta x$ are used for the corresponding ghost point values u_{m+1}^n and v_{m-1}^n. To determine and eliminate these ghost values we use the various coupling conditions. We proceed in a manner analogous to the treatment of the outer boundary fluxes. We need to use a difference approximation for the coupling conditions in order to march forward in time. We use a one sided difference method, i.e. forward or backward difference, and the central difference approximation to discretize the coupling interface conditions such as (2.19), (2.21) and (2.22) to obtain the ghost point values u_{m+1}^n and v_{m-1}^n.

These coupling interface conditions to obtain the ghost point values are explained below for explicit and implicit discretization methods. We found that to use the central difference method for the coupling conditions does not maintain the conservation of mass property. The explanation is given in Chapter 5. Also we will discuss the case of coupling conditions without ghost point values.

Dirichlet-Neumann coupling condition via one sided differences

The explicit discretization for the left sub-domain was derived in (4.1). For the interface node at $j = m$ this can be written as

$$u_m^{n+1} = u_m^n + \nu_-(u_{m+1}^n - u_m^n) - \nu_-(u_m^n - u_{m-1}^n). \tag{4.15}$$

In the above equation we have the ghost point value u_{m+1}^n which will be not appear in the actual computations. To find this value we discretize the Neumann coupling defined in (2.11) via the forward difference method as follows

$$D_- \frac{u_{m+1}^n - u_m^n}{\Delta x} = D_+ \frac{v_{m+1}^n - v_m^n}{\Delta x}. \tag{4.16}$$

Solving the above equation for u^n_{m+1}, we obtain

$$u^n_{m+1} = u^n_m + \frac{D_+}{D_-}(v^n_{m+1} - v^n_m) \tag{4.17}$$

Substituting this in (4.15) we obtain

$$u^{n+1}_m = u^n_m + \nu_-\Big(u^n_m + \frac{D_+}{D_-}(v^n_{m+1} - v^n_m) - u^n_m\Big) - \nu_-(u^n_m - u^n_{m-1}).$$

Using $\nu_+ = \frac{D_+}{D_-}\nu_-$ and $v^n_m = u^n_m$. We obtain

$$u^{n+1}_m = u^n_m + \nu_+(v^n_{m+1} - u^n_m) - \nu_-(u^n_m - u^n_{m-1}). \tag{4.18}$$

This is the same formula that we obtained in (4.11). We will use the latter approach to derive other numerical coupling conditions. We find it to be more convenient.

4.1.3 Dirichlet-Neumann coupling condition in the finite volume discretization

Here we seek the approximations of u and v by a finite volume discretization as in Section 3.4. We use the cells and nodal values as defined there. The number of cells and nodes is always even in the coupling problems. We approximate u and v as follows

$$u^n_j \approx \frac{1}{\Delta x}\int_{x_{j-\frac{1}{2}}}^{x_{j+\frac{1}{2}}} u(x,t_n)\,dx, \qquad \text{for} \quad j = 1, ..., m,$$
$$v^n_j \approx \frac{1}{\Delta x}\int_{x_{j-\frac{1}{2}}}^{x_{j+\frac{1}{2}}} v(x,t_n)\,dx, \qquad \text{for} \quad j = m+1, ..., N = 2m.$$

For the discretization of the initial data we can use the integral averages. The integrals may be replaced by a quadrature rule.

Analogously, for the interior points of the left sub-domain as (3.33) we obtain

$$u^{n+1}_j = u^n_j + \nu_-(u^n_{j+1} - u^n_j) - \nu_-(u^n_j - u^n_{j-1}), \qquad j = 2, \ldots, m-1 \tag{4.19}$$

and for the interior of the right sub-domain

$$v^{n+1}_j = v^n_j + \nu_+(v^n_{j+1} - v^n_j) - \nu_+(v^n_j - v^n_{j-1}), \qquad j = m+1, \ldots, 2m-1. \tag{4.20}$$

For the bi-domain case we will use again the formulas for the outer boundaries, i.e. $j = 1$ and $j = 2m$ given in system (3.35) with $w = u$ and $w = v$ respectively.

Now we derive the discretization scheme for the Dirichlet-Neumann coupling (2.11) for a finite volume scheme of type (3.35) using ghost cell values v^n_m and u^n_{m+1}. We take the Dirichlet condition $u^n_m = v^n_m$ discretize the Neumann coupling condition via the central difference with respect to the boundary for the right hand domain follows. For the left hand domain

$$F_{m+1/2} = D_+\frac{v^n_{m+1} - v^n_m}{\Delta x} = D_-\frac{u^n_{m+1} - u^n_m}{\Delta x}. \tag{4.21}$$

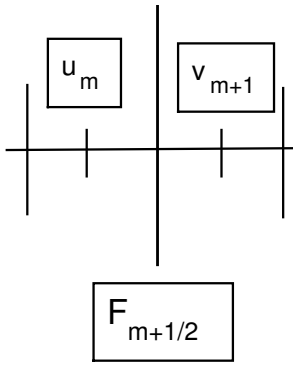

Figure 4.3: Graphical cell representation for Dirichlet-Neumann coupling conditions

This implies that $D_+(v^n_{m+1} - v^n_m) = D_-(u^n_{m+1} - u^n_m)$. Now we derive the scheme for the cell τ_m to the left of the interface. The discretization of the diffusion equation (4.19) for $j = m$ is as follows

$$u^{n+1}_m = u^n_m + \frac{D_-\Delta t}{\Delta x^2}(u^n_{m+1} - u^n_m) - \frac{D_-\Delta t}{\Delta x^2}(u^n_m - u^n_{m-1}). \tag{4.22}$$

Using both coupling conditions we can replace $D_-(u^n_{m+1} - u^n_m)$ by $D_+(v^n_{m+1} - u^n_m)$. We obtain the following scheme

$$\begin{aligned} u^{n+1}_m &= u^n_m + \frac{D_+\Delta t}{\Delta x^2}(v^n_{m+1} - u^n_m) - \frac{D_-\Delta t}{\Delta x^2}(u^n_m - u^n_{m-1}) \\ &= u^n_m + \nu_+(v^n_{m+1} - u^n_m) - \nu_-(u^n_m - u^n_{m-1}). \end{aligned} \tag{4.23}$$

Note that in the finite volume case the formulas for the interior nodes and the coupling are the same as in the nodal based case. A difference is seen only in the outer boundary conditions and the interpretation of the discrete values.

4.1.4 Heat flux coupling conditions via explicit discretization

Discretization of the heat flux coupling with ghost point values via one sided differences

We discretize the heat flux coupling conditions defined in (2.22) via an explicit discretization method with one sided differences. The heat flux coupling conditions are

$$D_-\frac{\partial u}{\partial x} = H(v - u), \qquad D_+\frac{\partial v}{\partial x} = H(v - u). \tag{4.24}$$

For the nodes $j \neq m$ we use the formulas in (4.11). Only the coupling conditions for $j = m$ will be replaced. Now for the interface node, i.e. $j = m$ the discretized scheme (4.1) will take the form

$$u^{n+1}_m = u^n_m + \nu_-(u^n_{m+1} - u^n_m) - \nu_-(u^n_m - u^n_{m-1}) \tag{4.25}$$

and the discretized scheme (4.3) will take the form

$$v_m^{n+1} = v_m^n + \nu_+(v_{m+1}^n - v_m^n) - \nu_+(v_m^n - v_{m-1}^n). \tag{4.26}$$

In these two formulas we have two ghost point values u_{m+1}^n and v_{m-1}^n. We calculate these values via using the coupling conditions (4.24).

We discretize the first equation of (4.24) via the forward difference approximation and the second equation of (4.24) via the backward difference approximation to obtain these ghost point values

$$D_-\frac{u_{m+1}^n - u_m^n}{\Delta x} = H(v_m^n - u_m^n), \qquad D_+\frac{v_m^n - v_{m-1}^n}{\Delta x} = H(v_m^n - u_m^n). \tag{4.27}$$

Solving the first equation for u_{m+1}^n we obtain $u_{m+1}^n = u_m^n + \frac{H\Delta x}{D_-}(v_m^n - u_m^n)$.

We substitute this value of u_{m+1}^n into (4.25). We obtain the following formula to determine u_m^{n+1} as follows

$$\begin{aligned} u_m^{n+1} &= u_m^n + \nu_-\Big(u_m^n + \frac{H\Delta x}{D_-}(v_m^n - u_m^n) - u_m^n\Big) - \nu_-(u_m^n - u_{m-1}^n) \\ &= u_m^n + \frac{D_-\Delta t}{H(\Delta x)^2}\frac{\Delta x}{D_-}(v_m^n - u_m^n) - \nu_-(u_m^n - u_{m-1}^n) \\ &= u_m^n - \nu_-(u_m^n - u_{m-1}^n) + \frac{H\Delta t}{\Delta x}(v_m^n - u_m^n). \end{aligned} \tag{4.28}$$

Solving the second equation of (4.27) for v_{m-1}^n we get $v_{m-1}^n = v_m^n - \frac{H\Delta x}{D_+}(v_m^n - u_m^n)$. Substituting this into (4.26) to obtain the following formula to determine v_m^{n+1} as

$$\begin{aligned} v_m^{n+1} &= v_m^n + \nu_+(v_{m+1}^n - v_m^n) - \nu_+(v_m^n - (v_m^n - \frac{H\Delta x}{D_-}(v_m^n - u_m^n)) \\ &= v_m^n + \nu_+(v_{m+1}^n - v_m^n) - \frac{H\Delta t}{\Delta x}(v_m^n - u_m^n). \end{aligned} \tag{4.29}$$

For the coupled scheme we proceed analogously as in algorithm A1. Only we are replacing the scheme for the Dirichlet-Neumann coupling conditions (4.11) by the new formulas (4.28) and (4.29) for the heat flux coupling conditions.

Heat flux coupling conditions with ghost point values via central differences

Now we discretize the heat flux coupling condition defined in (2.22) via central difference approximations are given as

$$D_-\frac{u_{m+1}^n - u_{m-1}^n}{2\Delta x} = H(v_m^n - u_m^n), \qquad D_+\frac{v_{m+1}^n - v_{m-1}^n}{2\Delta x} = H(v_m^n - u_m^n). \tag{4.30}$$

Solving the first equation for the ghost value $u^n_{m+1} = u^n_{m-1} + \frac{2H\Delta x}{D_-}(v^n_m - u^n_m)$. We substitute this into (4.25) to obtain the following formula to determine u^{n+1}_m as

$$\begin{aligned} u^{n+1}_m &= u^n_m + \nu_-(u^n_{m-1} + \frac{2H\Delta x}{D_-}(v^n_m - u^n_m) - u^n_m) - \nu_-(u^n_m - u^n_{m-1}) \\ &= u^n_m + \nu_- u^n_{m-1} + \frac{2H\Delta x}{D_-}\frac{D_-\Delta t}{(\Delta x)^2}(v^n_m - u^n_m) - \nu_- u^n_m - \nu_-(u^n_m - u^n_{m-1}) \\ &= u^n_m + \nu_- u^n_{m-1} + \frac{2H\Delta t}{\Delta x}(v^n_m - u^n_m) - \nu_- u^n_m - \nu_- u^n_m + \nu_- u^n_{m-1} \\ &= u^n_m - 2\nu_-(u^n_m - u^n_{m-1}) + \frac{2H\Delta t}{\Delta x}\Big(v^n_m - u^n_m\Big). \end{aligned} \tag{4.31}$$

Analogously we solve the second equation of (4.30) for the second ghost value $v^n_{m-1} = v^n_{m+1} - \frac{2H\Delta x}{D_-}(v^n_m - u^n_m)$. We substitute this into (4.26) to get the following formula to determine v^{n+1}_m as

$$v^{n+1}_m = v^n_m + 2\nu_+(v^n_{m+1} - v^n_m) - \frac{2H\Delta t}{\Delta x}\Big(v^n_m - u^n_m\Big). \tag{4.32}$$

For all coupled schemes we proceed analogously as in algorithm A1 replacing the Dirichlet-Neumann coupling conditions (4.11) by the new formulas (4.31) and (4.32) for the heat flux coupling condition. Note that the discretizations (4.31) and (4.32) are equal to the numerical homogeneous Neumann conditions, see (3.18), plus the heat flux term.

4.1.5 Channel pumping conditions

One-sided differences

The channel pumping conditions were defined in (2.16). We obtain the explicit discretization for these coupling conditions in the same way as derived for the heat flux coupling above. So, there is no need to repeat the whole derivation again. We just replace the right hand side of the heat flux coupling $-J = H(v^n_m - u^n_m)$ into $-J = \psi\frac{\alpha v^n_m - u^n_m}{\beta + \gamma u^n_m + \delta v^n_m}$ in the discretized schemes for the heat flux coupling via one sided difference method (4.28) and (4.29) to obtain the following formula for updates

$$u^{n+1}_m = u^n_m - \nu_-(u^n_m - u^n_{m-1}) + \frac{\Delta t}{\Delta x}\Big(\psi\frac{\alpha v^n_m - u^n_m}{\beta + \gamma u^n_m + \delta v^n_m}\Big) \tag{4.33}$$

and

$$v^{n+1}_m = v^n_m + \nu_+(v^n_{m+1} - v^n_m) - \frac{\Delta t}{\Delta x}\Big(\psi\frac{\alpha v^n_m - u^n_m}{\beta + \gamma u^n_m + \delta v^n_m}\Big). \tag{4.34}$$

Central difference

Analogously we can derive the updates for the coupling conditions via central difference method to make the setting again in the heat flux coupling $-J = H(v^n_m - u^n_m)$ into $-J =$

$\psi\frac{\alpha v_m^n - u_m^n}{\beta+\gamma u_m^n+\delta v_m^n}$ in the discretized schemes for the heat flux coupling via central difference method (4.31) and (4.32) to get the updates

$$u_m^{n+1} = u_m^n - 2\nu_-(u_m^n - u_{m-1}^n) + \frac{2\Delta t}{\Delta x}\Big(\psi\frac{\alpha v_m^n - u_m^n}{\beta+\gamma u_m^n+\delta v_m^n}\Big) \tag{4.35}$$

and

$$v_m^{n+1} = v_m^n + 2\nu_+(v_{m+1}^n - v_m^n) - \frac{2\Delta t}{\Delta x}\Big(\psi\frac{\alpha v_m^n - u_m^n}{\beta+\gamma u_m^n+\delta v_m^n}\Big). \tag{4.36}$$

4.1.6 Simplified channel pumping

One-sided differences

The simplified channel pumping conditions were defined (2.17). The explicit discretized form for these coupling conditions can be obtained in the same way as we derived above to set $\beta+\gamma u_m^n+\delta v_m^n = 1$ in the channel pumping conditions via one sided difference in (4.33) and (4.34). We will obtain the following updates

$$u_m^{n+1} = u_m^n - \nu_-(u_m^n - u_{m-1}^n) + \frac{\Delta t}{\Delta x}\Big(\psi(\alpha v_m^n - u_m^n)\Big) \tag{4.37}$$

and

$$v_m^{n+1} = v_m^n + \nu_+(v_{m+1}^n - v_m^n) - \frac{\Delta t}{\Delta x}\Big(\psi(\alpha v_m^n - u_m^n)\Big). \tag{4.38}$$

Central difference

Analogously we can derive the updates for the coupling conditions via central difference method to make the setting $\beta+\gamma u_m^n+\delta v_m^n = 1$ in (4.35) and (4.36) to obtain the updates

$$u_m^{n+1} = u_m^n - 2\nu_-(u_m^n - u_{m-1}^n) + \frac{2\Delta t}{\Delta x}\Big(\psi(\alpha v_m^n - u_m^n)\Big) \tag{4.39}$$

and

$$v_m^{n+1} = v_m^n + 2\nu_+(v_{m+1}^n - v_m^n) - \frac{2\Delta t}{\Delta x}\Big(\psi(\alpha v_m^n - u_m^n)\Big). \tag{4.40}$$

4.1.7 Membrane pumping coupling conditions via explicit discretization

One sided differences

The membrane pumping coupling conditions were defined in (2.19). Here, we derive their discretization via one sided differences. We will replace $H = P_l + P_{ch}(t)$ and add an extra term $P_p\frac{(v_m^n)^n}{k_d^2+(v_m^n)^n}$ in the discretized schemes of the heat flux conditions (4.28) and (4.29) to obtain the following updates

$$u_m^{n+1} = u_m^n - \nu_-(u_m^n - u_{m-1}^n) + \frac{\Delta t}{\Delta x}\Big((P_l + P_c(t))(v_m^n - u_m^n) + P_p\frac{(v_m^n)^2}{k_d^2+(v_m^n)^2}\Big). \tag{4.41}$$

and for v_m^{n+1} as

$$v_m^{n+1} = v_m^n + \nu_+(v_{m+1}^n - v_m^n) - \frac{\Delta t}{\Delta x}\Big((P_l + P_c(t))(v_m^n - u_m^n) + P_p\frac{(v_m^n)^2}{k_d^2 + (v_m^n)^2}\Big). \tag{4.42}$$

Central differences

Analogously, we are doing the same modification for the central difference discretization in the schemes for the heat flux coupling through the central difference method in (4.31) and (4.32) to get the following updates

$$u_m^{n+1} = u_m^n - 2\nu_-(u_m^n - u_{m-1}^n) + \frac{2\Delta t}{\Delta x}\Big((P_l + P_c(t))(v_m^n - u_m^n) + P_p\frac{(v_m^n)^2}{k_d^2 + (v_m^n)^2}\Big). \tag{4.43}$$

and for v_m^{n+1} as

$$v_m^{n+1} = v_m^n + 2\nu_+(v_{m+1}^n - v_m^n) - \frac{2\Delta t}{\Delta x}\Big((P_l + P_c(t))(v_m^n - u_m^n) + P_p\frac{(v_m^n)^2}{k_d^2 + (v_m^n)^2}\Big). \tag{4.44}$$

4.1.8 Simplified membrane pumping coupling conditions via one sided difference method with ghost point values

One sided differences

The simplified pumping coupling conditions were defined in (2.21). We know that by setting $P_l + P_c(t) = H$ and $P_p = P$ and $k_d = 1$ in (2.19) to obtain the simplified membrane pumping conditions. We substitute these in the discrete schemes for the membrane pumping conditions via one sided difference (4.41) and (4.42) to obtain the updat u_m^{n+1} as

$$u_m^{n+1} = u_m^n - \nu_-(u_m^n - u_{m-1}^n) + \frac{\Delta t}{\Delta x}\Big(H(v_m^n - u_m^n) + P\frac{(v_m^n)^2}{1 + (v_m^n)^2}\Big). \tag{4.45}$$

and for v_m^{n+1} as

$$v_m^{n+1} = v_m^n + \nu_+(v_{m+1}^n - v_m^n) - \frac{\Delta t}{\Delta x}\Big(H(v_m^n - u_m^n) + P\frac{(v_m^n)^2}{1 + (v_m^n)^2}\Big). \tag{4.46}$$

Central differences

Analogously, to do the above setting in the schemes for the membrane pumping conditions via central difference method (4.43) and (4.44) to get the updates

$$u_m^{n+1} = u_m^n - 2\nu_-(u_m^n - u_{m-1}^n) + \frac{2\Delta t}{\Delta x}\Big(H(v_m^n - u_m^n) + P\frac{(v_m^n)^2}{1 + (v_m^n)^2}\Big). \tag{4.47}$$

and for v_m^{n+1} as

$$v_m^{n+1} = v_m^n + 2\nu_+(v_{m+1}^n - v_m^n) - \frac{2\Delta t}{\Delta x}\Big(H(v_m^n - u_m^n) + P\frac{(v_m^n)^2}{1 + (v_m^n)^2}\Big). \tag{4.48}$$

4.1.9 Linearized membrane pumping coupling conditions

One sided differences

We know that the linearized membrane pumping coupling is the special case of the simplified channel pumping conditions for $\psi = 1$ and $\alpha = 3/2$. We substitute these into the discrete formulas for the simplified channel pumping (4.37) and (4.38) to obtain the updates

$$u_m^{n+1} = u_m^n - \nu_-(u_m^n - u_{m-1}^n) + \frac{\Delta t}{\Delta x}\Big(\frac{3}{2}v_m^n - u_m^n\Big). \tag{4.49}$$

and for v_m^{n+1} as

$$v_m^{n+1} = v_m^n + \nu_+(v_{m+1}^n - v_m^n) - \frac{\Delta t}{\Delta x}\Big(\frac{3}{2}v_m^n - u_m^n\Big). \tag{4.50}$$

Central differences

Analogously we substitute $\psi = 1$ and $\alpha = 3/2$ into (4.39) and (4.40) to obtain the schemes for the updates

$$u_m^{n+1} = u_m^n - 2\nu_-(u_m^n - u_{m-1}^n) + \frac{2\Delta t}{\Delta x}\Big(\frac{3}{2}v_m^n - u_m^n\Big). \tag{4.51}$$

and for v_m^{n+1} as

$$v_m^{n+1} = v_m^n + 2\nu_+(v_{m+1}^n - v_m^n) - \frac{2\Delta t}{\Delta x}\Big(\frac{3}{2}v_m^n - u_m^n\Big). \tag{4.52}$$

We remind that for all explicit coupled schemes we proceed analogously as in algorithm A1 for explicit discretization replacing the Dirichlet-Neumann coupling conditions in (4.11) by the new formulas (4.51) and (4.52) for the linearized membrane pumping coupling conditions.

4.2 Fully implicit formulation for the bi-domain diffusion equations with various coupling conditions

In this section we discretize the various coupling conditions using an implicit scheme. First we consider the Dirichlet-Neumann coupling and then the others. For these kinds of coupling schemes we are using two solution strategies, the monolithic and the partitioned iterative approach. In the monolithic approach we keep the whole system in one monolithic matrix and then solve via the direct method based on the Thomas algorithm, for this see the Subsection 3.3.2, because this system gives us a tridiagonal type matrix.

The second approach is the partitioned coupled iterative approach which is a bit more complicated as compared to the monolithic, because we solve for the two unknowns u and v separately in each time step. It is achieved via sub-iterations. We will explain this below. We use the monolithic solution as a reference solution for the partitioned coupling iterative approach. These two approaches are explained as follows.

4.2.1 Dirichlet-Neumann coupling via monolithic approach

Here, we derive the fully implicit discretization of the bi-domain diffusion equations with Dirichlet-Neumann coupling conditions. The implicit formulation for the single domain diffusion model was derived in (3.22). Now for the bi-domain diffusion model we replace $w_j^n = u_j^n$ for $j = 0, 1, ..., m-1$ and $w_j^n = v_j^n$ for $j = m+1, ..., 2m$.

Also, we derived the schemes for the left and right hand homogeneous Neumann boundary conditions in (3.23) and (3.24) respectively replace by $w_0^{n+1} = u_0^{n+1}$ and $w_N^{n+1} = v_{2m}^{n+1}$. Further, we derived the explicit scheme for the Dirichlet-Neumann coupling on the interface boundary in (4.10). Here for the implicit scheme we replace n by $n+1$ in the spatial discretization part. So, we write all these implicit formulations together in the following system

$$\begin{aligned}
(1+2\nu_-)u_0^{n+1} - 2\nu_- u_1^{n+1} &= u_0^n && \text{for } j = 0\\
-\nu_- u_{j-1}^{n+1} + (1+2\nu_-)u_j^{n+1} - \nu_- u_{j+1}^{n+1} &= u_j^n && \text{for } j < m\\
-\nu_- u_{m-1}^{n+1} + (1+\nu_-)u_m^{n+1} - \nu_+(v_{m+1}^{n+1} - v_m^{n+1}) &= u_m^n && \text{for } j = m\\
u_m^{n+1} - v_m^{n+1} &= 0 && \text{for } j = m\\
-\nu_+ v_{j-1}^{n+1} + (1+2\nu_+)v_j^{n+1} - \nu_+ v_{j+1}^{n+1} &= v_j^n && \text{for } j > m\\
-2\nu_+ v_{2m-1}^{n+1} + (1+2\nu_+)v_{2m}^{n+1} &= v_{2m}^n && \text{for } j = 2m
\end{aligned} \tag{4.53}$$

Now we give the detail for the monolithic approach. We can write the system (4.53) in a monolithic matrix equation

$$\mathbf{A}\mathbf{u}^{\mathbf{n+1}} = \mathbf{u}^{\mathbf{n}}. \tag{4.54}$$

Here $\mathbf{u}^{n+1} = (u_0^{n+1}, ..., u_m^{n+1}, v_m^{n+1}, , ..., v_{2m}^{n+1})^T$ is the unknown column matrix and the known vector $\mathbf{u}^n = (u_0^n, ..., u_m^n, 0, v_{m+1}^n, ..., v_{2m}^n)^T$ from the right hand side of the system (4.53). The monolithic matrix $\mathbf{A}$ has the following block structure

$$\mathbf{A} = \left(\begin{array}{cccc|cccc}
1+2\nu_- & -2\nu_- & \dots & 0 & & & & \\
-\nu_- & 1+2\nu_- & -\nu_- & \vdots & & & & \\
\vdots & \ddots & \ddots & \ddots & & & & \\
0 & \cdots & -\nu_- & 1+2\nu_- & -\nu_- & & & \\
\hline
 & & & -\nu_- & 1+\nu_- & \nu_+ & -\nu_+ & \\
 & & & & 1 & -1 & 0 & \\
\hline
 & & & & & -\nu_+ & 1+2\nu_+ & -\nu_+ & \dots 0 \\
 & & & & & \vdots & \ddots & \ddots & \ddots \\
 & & & & & & -\nu_+ & 1+2\nu_+ & -\nu_+ \\
 & & & & & 0 & \dots & -2\nu_+ & 1+2\nu_+
\end{array}\right).$$

In this matrix the block in the left upper side is the matrix from the interior of the left sub-domain with left hand boundary. The block in the middle two doted lines is for the Dirichlet-Neumann coupling, while the block in the lower right hand is the matrix for the interior of the right sub-domain with right hand boundary.

This will be a reference solution for the implicit partitioned iterative coupling approach. Now we can solve this linear algebraic system of equations via any linear algebraic

solvers. Here we are using the direct method based on the Thomas algorithm explained in Subsection 3.3.2.

Algorithm A2, for the Dirichlet-Neumann coupling via monolithic

The main steps of this algorithm are similar to the algorithm A1. We just have to insert the step for the solution of the implicit system (4.53) in each time step. Otherwise both are similar in practice.

4.2.2 Partitioned iterative coupling approach

In this approach we separate the domain into two sub-sets on which the equations have different diffusion constants, as represented in (4.53). We want to solve the separate matrix equations systems, that are coupled at the interface boundary. We use the Neumann condition for the left sub-domain and the Dirichlet condition for the other domain. We sub-iterate until the coupled convergence is reached.

The discretization for the left sub-domain together with homogeneous Neumann boundary condition and with Neumann coupling condition is given in the following sub-system

$$\begin{aligned}
(1+2\nu_-)u_0^{n+1} - 2\nu_- u_1^{n+1} &= u_0^n \qquad \text{for } j=0 \\
-\nu_- u_{j-1}^{n+1} + (1+2\nu_-)u_j^{n+1} - \nu_- u_{j+1}^{n+1} &= u_j^n \qquad \text{for } j<m \\
-\nu_- u_{m-1}^{n+1} + (1+\nu_-)u_m^{n+1} &= u_m^n + \nu_+(v_{m+1}^{n+1} - u_m^{n+1}) \qquad \text{for } j=m.
\end{aligned} \tag{4.55}$$

For the right sub-domain analogously we have the following sub-system

$$\begin{aligned}
v_m^{n+1} &= u_m^{n+1} \qquad \text{for } j=m \\
-\nu_+ v_{j-1}^{n+1} + (1+2\nu_+)v_j^{n+1} - \nu_+ v_{j+1}^{n+1} &= v_j^n \qquad \text{for } j>m \\
-2\nu_+ v_{2m-1}^{n+1} + (1+2\nu_+)v_{2m}^{n+1} &= v_{2m}^n \qquad \text{for } j=2m.
\end{aligned} \tag{4.56}$$

The systems (4.55) and (4.56) cannot be solved separately as long as the solution appears on the right hand side. There we replace the unknowns by the previous solution and alternate the solution of the sub-systems in order to approximate the solution to (4.53). For the convergence of the coupling interface condition we may check the residual equations at the interface

$$\begin{aligned}
R_1^{n+1} &= -\nu_- u_{m-1}^{n+1} + (1+\nu_-)u_m^{n+1} - u_m^n - \nu_+(v_{m+1}^{n+1} - u_m^{n+1}) \qquad \text{and} \\
R_2^{n+1} &= v_{m+1}^{n+1} - u_m^{n+1}.
\end{aligned}$$

They should become approximately zero. To achieve this we introduce the following sub-iterations. We set $u_m^{n,0} := u_m^n$, $v_m^{n,0} := v_m^n$ and $v_{m+1}^{n,0} := v_{m+1}^n$. Further we introduce the sub-iteration index $k = 0, 1, 2, ...$ With this we modify (4.55) and (4.56) to

$$\begin{aligned}
(1+2\nu_-)u_0^{n,k+1} - 2\nu_- u_1^{n,k+1} &= u_0^n \qquad \text{for } j=0 \\
-\nu_- u_{j-1}^{n,k+1} + (1+2\nu_-)u_j^{n,k+1} - \nu_- u_{j+1}^{n,k+1} &= u_j^n \qquad \text{for } j<m \\
-\nu_- u_{m-1}^{n,k+1} + (1+\nu_-)u_m^{n,k+1} &= u_m^n + \nu_+(v_{m+1}^{n,k} - u_m^{n,k}) \qquad \text{for } j=m
\end{aligned} \tag{4.57}$$

and

$$\begin{aligned} v_m^{n,k+1} &= u_m^{n,k} \qquad \text{for } j = m+1 \\ -\nu_+ v_{j-1}^{n,k+1} + (1+2\nu_+) v_j^{n,k+1} - \nu_+ v_{j+1}^{n,k+1} &= v_j^n \qquad \text{for } j > m \\ -2\nu_+ v_{2m-1}^{n,k+1} + (1+2\nu_+) v_{2m}^{n,k+1} &= v_{2m}^n \qquad \text{for } j = 2m. \end{aligned} \tag{4.58}$$

For the convergence of the coupling interface condition we check the residual equations at the interface

$$\begin{aligned} R_1^{n,k+1} &= -\nu_- u_{m-1}^{n,k+1} + (1+\nu_-) u_m^{n,k+1} - \nu_+ (v_{m+1}^{n,k+1} - u_m^{n,k+1}) - u_m^n \qquad \text{and} \\ R_2^{n,k+1} &= u_m^{n,k+1} - v_m^{n,k+1}. \end{aligned} \tag{4.59}$$

The above iteration process can be repeated. For $k \to \infty$ we expect $R_1^{n,k} \to 0$ and $R_2^{n,k} \to 0$ as well as $u_j^{n,k} \to u_j^{n+1}$ and $v_j^{n,k} \to v_j^{n+1}$, where u_j^{n+1} and v_j^{n+1} are the solutions of the system (4.53).

We prescribe some small tolerance $TOL > 0$ such that when we have achieved $|R_1^{n,k+1}| < TOL$ and $|R_2^{n,k+1}| < TOL$ we stop the sub iterations and start the next time step.

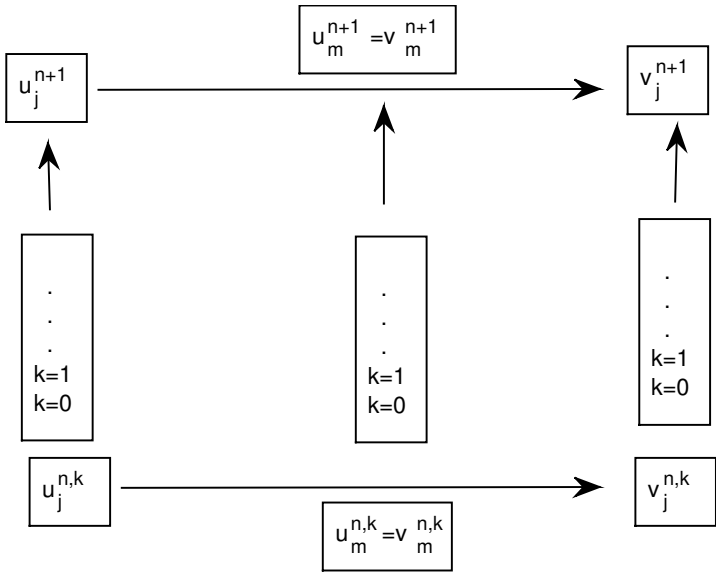

Figure 4.4: Graphical representation for the implicit partitioned iterative coupling.

Matrix representation of the two sub systems

We can write the first sub-system (4.55) in the matrix form $\mathbf{A}_1 \mathbf{u}^{n+1} = \mathbf{u}^n$, where $\mathbf{A}_1$ is a coefficient matrix and will take the following tridiagonal structure

$$\mathbf{A_1} = \begin{pmatrix} 1+2\nu_- & -2\nu_- & \dots & & 0 \\ -\nu_- & 1+2\nu_- & -\nu_- & & \vdots \\ \vdots & \ddots & \ddots & \ddots & \\ & & -\nu_- & 1+2\nu_- & -\nu_- \\ 0 & \dots & & -\nu_- & 1+\nu_- \end{pmatrix}.$$

The above matrix is a tri-diagonal matrix with the homogeneous Neumann boundary condition on the left hand boundary and the Neumann coupling at the interface. The matrix of unknown variables $\mathbf{u}^{n+1} = \mathbf{u}^{n,(k+1)} = (u_0^{n,k+1}, ..., u_m^{n,k+1})^T$ and $\mathbf{u}^n$ is the known vector of the initial data given as follows $\mathbf{u}^{n,k} = (u_0^{n,k}, ..., u_m^{n,k} + \nu_+(v_{m+1}^{n,k} - v_m^{n,k}))^T$.

Analogously, the second sub-system (4.56) can be expressed as $\mathbf{A}_2\mathbf{v}^{n+1} = \mathbf{v}^n$, where $\mathbf{A}_2$ is the coefficient matrix and will take the following structure

$$\mathbf{A_2} = \begin{pmatrix} 1 & 0 & \dots & & 0 \\ -\nu_+ & 1+2\nu_+ & -\nu_+ & & \vdots \\ \vdots & \ddots & \ddots & \ddots & \\ & & -\nu_+ & 1+2\nu_+ & -\nu_+ \\ 0 & \dots & & -2\nu_+ & 1+2\nu_+ \end{pmatrix}.$$

Again the above matrix is a tri-diagonal matrix. The first row is for the Dirichlet coupling condition and the last row is modified for the homogeneous Neumann boundary condition on the right hand boundary. The column matrix for the unknown variables $\mathbf{v}^{n+1} = \mathbf{v}^{n,(k+1)} = (v_m^{n,k+1}, ..., v_{2m}^{n,k+1})^T$ and $\mathbf{v}^n$ is the known vector from the initial data $\mathbf{v}^n = (u_m^{n,k}, v_{m+1}^{n,k}, ..., v_{2m-1}^{n,k}, v_{2m}^{n,k})^T$.

Now we want to achieve $|R_1^{n,k+1}| < TOL$ and $|R_2^{n,k+1}| < TOL$ for these two system respectively and for large k we expect $u_j^{n,k} \to u_j^{n+1}$ and $v_j^{n,k} \to v_j^{n+1}$.

Algorithm A3, for the Dirichlet-Neumann coupling via implicit partitioned iterative approach

This algorithm is basically overall the same as the algorithms A1 and A2. Only the solution procedure for the linear system to be solve in each time step is more complicated.

The generic cycles of the sub-iteration in this algorithm are given as follows:

(1) Start from the initial conditions $u_j^{n,0} = u_j^n$ for $j = 0, ..., m$ and $v_j^{n,0} = v_j^n$ for $j = m+1, ..., 2m$ on the respective sub-domain.

(2) Set up the two sub-systems (4.55) and (4.56).

(3) We achieve our required solution via sub-iterations using the following steps:

   (a) Using data $u_j^{n,k}$, $v_j^{n,k}$ solve to obtain $u_j^{n,k+1}$, $v_j^{n,k+1}$ and terminate the sub-iterate.

   (b) Check the residual conditions $|R_1^{n,k+1}| < TOL$ and $|R_2^{n,k+1}| < TOL$.

      (i) If satisfied, set $u_j^{n+1} = u_j^{n,k+1}$, $v_j^{n+1} = v_j^{n,k+1}$ and terminate the sub-iteration step.

      (ii) If not satisfied, then continue with next sub-iteration step.

   (c) Set the right hand sides in the last equation of the system (4.57) to be $u_m^n + \nu_+(v_{m+1}^{n,k+1} - u_m^{n,k+1})$ and in the first equation of the system (4.58) to be $u_m^{n,k+1}$. Now carry out (a) with index k increased by one.

We also tested this coupling algorithm for a known solution. We consider the special case of the identical diffusion coefficients $D_- = D_+ = D$. Then the coupling should give the known single domain solution. We will show this test case in Chapter 7 for the result and discussion. The scheme for $j = m$, i.e. the Dirichlet-Neumann coupling scheme in the system (4.53) will become

$$u_m^{n+1} + \nu((u_m^{n+1} - u_{m-1}^{n+1}) - (v_{m+1}^{n+1} - v_m^{n+1})) = u_m^n.$$

Clearly this is equivalent to the scheme of the single domain diffusion equation via implicit method.

4.2.3 Heat flux coupling conditions via implicit method

Here we give the implicit discretizations of the heat flux coupling conditions via monolithic as well as for the partitioned iterative approach.

Monolithic approach

First we derive the scheme for the implicit monolithic approach. Here we also show the schemes via one sided as well as for the central difference method.

One sided finite volume method

For the nodes $j \neq m$ we use the formulas in (4.53). Only the coupling conditions for $j = m$ will be replaced. For the implicit scheme we replace the time level n by $n+1$ in the spatial discretization derived for the heat flux coupling via explicit method via

one sided difference method in (4.28) and (4.29). The implicit formulas for the heat flux coupling conditions will take the following form

$$u_m^{n+1} = u_m^n - \nu_-(u_m^{n+1} - u_{m-1}^{n+1}) + H\frac{\Delta t}{\Delta x}\Big(v_m^{n+1} - u_m^{n+1}\Big)$$

and

$$v_m^{n+1} = v_m^n + \nu_+(v_{m+1}^{n+1} - v_m^{n+1}) - H\frac{\Delta t}{\Delta x}\Big(v_m^{n+1} - u_m^{n+1}\Big). \tag{4.60}$$

We re-arrange the formulas to obtain

$$-\nu_- u_{m-1}^{n+1} + \Big(1 + \nu_- + H\frac{\Delta t}{\Delta x}\Big)u_m^{n+1} - H\frac{\Delta t}{\Delta x}v_m^{n+1} = u_m^n \tag{4.61}$$

and

$$-H\frac{\Delta t}{\Delta x}u_m^{n+1} + \Big(1 + \nu_+ + H\frac{\Delta t}{\Delta x}\Big)v_m^{n+1} - \nu_+ v_{m+1}^{n+1} = v_m^n. \tag{4.62}$$

Central difference

Analogously we obtain the schemes via the central difference method are

$$-2\nu_- u_{m-1}^{n+1} + \Big(1 + 2\nu_- + 2H\frac{\Delta t}{\Delta x}\Big)u_m^{n+1} - 2H\frac{\Delta t}{\Delta x}v_m^{n+1} = u_m^n \tag{4.63}$$

and

$$-2H\frac{\Delta t}{\Delta x}u_m^{n+1} + \Big(1 + 2\nu_+ + 2H\frac{\Delta t}{\Delta x}\Big)v_m^{n+1} - 2\nu_+ v_{m+1}^{n+1} = v_m^n. \tag{4.64}$$

For the coupled scheme we proceed analogously as the implicit scheme for the Dirichlet-Neumann coupling (4.53). We replace the schemes of the Dirichlet-Neumann coupling conditions by the new formulas (4.61) and (4.62) for the the one sided and for the central difference (4.63) and (4.64). Note that we will show later in Chapter 5 that only the central difference maintains the conservativity for the nodal based method, while the one sided for the finite volume cell based scheme. But the one sided nodal based does not.

Partitioned iterative approach

Here we also follow the same procedure as we used in the implicit case of the Dirichlet-Neumann coupling. Now in the scheme (4.61) we need v_m^{n+1} which is not available for computing u_m^{n+1} so we set $v_m^{n+1} = v_m^{n,k}$ and we expect to achieve $v_m^{n,k} \to v_m^{n+1}$ via sub-iterations for $k \to \infty$. We set $v_m^{n,0} = v_m^n$. So the equation (4.63) will take the following form

$$-2\nu_- u_{m-1}^{n,k+1} + \Big(1 + 2\nu_- + 2H\frac{\Delta t}{\Delta x}\Big)u_m^{n,k+1} = u_m^n + 2H\frac{\Delta t}{\Delta x}v_m^{n,k} \tag{4.65}$$

and we set $u_m^{n,0} = u_m^n$. We are expecting to achieve $u_m^{n,k} \to u_m^{n+1}$ for $k \to \infty$. The scheme (4.64) will become

$$\Big(1 + 2\nu_+ + 2H\frac{\Delta t}{\Delta x}\Big)v_m^{n,k+1} - 2\nu_+ v_{m+1}^{n,k+1} = v_m^n + 2H\frac{\Delta t}{\Delta x}u_m^{n,k+1}. \tag{4.66}$$

For the numerical computation of the heat flux coupling the scheme for $j = m$ in the subsystem (4.55) will be replaced on (4.65) and in the second sub-system, i.e. for the right sub-domain in (4.56) for $j = m$ will be replaced in the scheme (4.66).

Further for the convergence of the heat flux coupling conditions we check the residual equations at the interface

$$R_1^{n,k+1} = -2\nu_- u_{m-1}^{n,k+1} + \Big(1 + 2\nu_- + 2H\frac{\Delta t}{\Delta x}\Big)u_m^{n,k+1} - u_m^n - 2H\frac{\Delta t}{\Delta x}v_m^{n,k+1} \qquad \text{and}$$
$$R_2^{n,k+1} = \Big(1 + 2\nu_+ + 2H\frac{\Delta t}{\Delta x}\Big)v_m^{n,k+1} - 2\nu_+ v_{m+1}^{n,k+1} - v_m^n - 2H\frac{\Delta t}{\Delta x}u_m^{n,k+1}.$$

The above iteration process can be repeated. For $k \to \infty$ we expect $R_1^{n,k} \to 0$ and $R_2^{n,k} \to 0$ as well as $u_j^{n,k} \to u_j^{n+1}$ and $v_j^{n,k} \to v_j^{n+1}$.

We prescribe some small tolerance $TOL > 0$ such that when we have achieved $|R_1^{n,k+1}| < TOL$ and $|R_2^{n,k+1}| < TOL$ we stop the sub iterations and start the next time step.

4.2.4 Simplified channel pumping coupling condition

Here we give the formulas for the simplified channel pumping conditions via one sided as well as for the central difference.

One sided finite volume method

The one sided finite volume formula for the simplified channel pumping conditions was derived for the explicit one sided difference in (4.37) and (4.38). We just replace the time level n in the spatial discretization which is given by

$$u_m^{n+1} + \nu_-(u_m^{n+1} - u_{m-1}^{n+1}) - \frac{\Delta t}{\Delta x}\Big(\psi(\alpha v_m^{n+1} - u_m^{n+1})\Big) = u_m^n \tag{4.67}$$

and

$$v_m^{n+1} - \nu_+(v_{m+1}^{n+1} - v_m^{n+1}) + \frac{\Delta t}{\Delta x}\Big(\psi(\alpha v_m^{n+1} - u_m^{n+1})\Big) = v_m^n. \tag{4.68}$$

The central difference method

The central difference formula for the simplified channel pumping conditions via explicit central difference method was derived in (4.39) and (4.40). We just replace the time level n by $n + 1$ in the spatial discretization as

$$u_m^{n+1} + 2\nu_-(u_m^{n+1} - u_{m-1}^{n+1}) - 2\frac{\Delta t}{\Delta x}\Big(\psi(\alpha v_m^{n+1} - u_m^{n+1})\Big) = u_m^n \tag{4.69}$$

and

$$v_m^{n+1} - 2\nu_+(v_{m+1}^{n+1} - v_m^{n+1}) + 2\frac{\Delta t}{\Delta x}\Big(\psi(\alpha v_m^{n+1} - u_m^{n+1})\Big) = v_m^n. \tag{4.70}$$

4.2.5 Linearized membrane pumping coupling conditions via implicit method

Here, we give the implicit discretization for the linearized membrane pumping conditions via monolithic as well as for partitioned coupling iterative approach. We know that only the discretization of the coupling via central difference method only maintains the discrete mass conservativity. So we show the schemes only for the central difference method.

Monolithic approach

We derived the explicit formulas for the linearized membrane pumping conditions in (4.51) and (4.52) via the central difference method. So, we replace n by $n+1$ in the spatial discretization to obtained the following schemes

$$-2\nu_- u_{m-1}^{n+1} + \Big(1 + 2\nu_- + \frac{2\Delta t}{\Delta x}\Big) u_m^{n+1} - \frac{3\Delta t}{\Delta x} v_m^{n+1} = u_m^n \tag{4.71}$$

and

$$-2\frac{\Delta t}{\Delta x} u_m^{n+1} + \Big(1 + 2\nu_+ + \frac{3\Delta t}{\Delta x}\Big) v_m^{n+1} - 2\nu_+ v_{m+1}^{n+1} = v_m^n. \tag{4.72}$$

For the coupled scheme we proceed analogously as we did in the implicit system (4.53) with Dirichlet-Neumann coupling. We replace the schemes of Dirichlet-Neumann coupling by the new formulas (4.71) and (4.72) for the linearized membrane pumping conditions.

Partitioned iterative approach

In the partitioned iterative approach for the implicit case we proceed analogously to achieve $u_m^{n,k+1} \to u_m^{n+1}$ and $v_m^{n,k+1} \to v_m^{n+1}$ via sub-iterations. We set $v_m^{n,0} = v_m^n$ in equations (4.71) and $u_m^{n,0} = u_m^n$ in (4.72) we obtain the following two schemes

$$-2\nu_- u_{m-1}^{n,k+1} + \Big(1 + 2\nu_- + \frac{2\Delta t}{\Delta x}\Big) u_m^{n,k+1} = u_m^n + \frac{3\Delta t}{\Delta x} v_m^{n,k} \tag{4.73}$$

and

$$\Big(1 + 2\nu_+ + \frac{3\Delta t}{\Delta x}\Big) v_m^{n,k+1} - 2\nu_+ v_{m+1}^{n,k+1} = v_m^n + \frac{2\Delta t}{\Delta x} u_m^{n,k}. \tag{4.74}$$

For the numerical computation of the linearized membrane pumping conditions the scheme for $j = m$ in the subsystem (4.55) will be replaced on (4.73) and in the second sub-system, i.e. for the right sub-domain in (4.56) for $j = m$ will be replaced on scheme (4.74).

Further for the convergence of the linearized coupling conditions we check the residual equations at the interface

$$R_1^{n,k+1} = -2\nu_- u_{m-1}^{n,k+1} + \Big(1 + 2\nu_- + \frac{2\Delta t}{\Delta x}\Big) u_m^{n,k+1} - u_m^n - \frac{3\Delta t}{\Delta x} v_m^{n,k+1} \qquad \text{and}$$
$$R_2^{n,k+1} = \Big(1 + 2\nu_+ + \frac{3\Delta t}{\Delta x}\Big) v_m^{n,k+1} - 2\nu_+ v_{m+1}^{n,k+1} - v_m^n - \frac{2\Delta t}{\Delta x} u_m^{n,k}.$$

The above iteration process can be repeated. For $k \to \infty$ we expect $R_1^{n,k} \to 0$ and $R_2^{n,k} \to 0$ as well as $u_j^{n,k} \to u_j^{n+1}$ and $v_j^{n,k} \to v_j^{n+1}$.

We prescribe some small tolerance $TOL > 0$ such that when we have achieved $|R_1^{n,k+1}| < TOL$ and $|R_2^{n,k+1}| < TOL$ we stop the sub iterations and start the next time step.

4.2.6 Membrane pumping conditions via implicit discretization

Monolithic approach

For the monolithic approach we have a monolithic matrix setting. Therefore the nonlinear coupling are not possible to implement in this case. While we use the partitioned iterative approach as follow.

Partitioned iterative approach

Here we give the discretized formulas for the membrane pumping conditions.

The central difference method (FD)

We derived the explicit discretization of the membrane pumping conditions via the central difference method in (4.43) and (4.44). Analogously, we replace there the time level n by $n+1$ in the spatial discretization part. Again we have u_n^{n+1} and v_m^{n+1}, so we proceed analogously to achieve $u_m^{n,k+1} \to u_m^{n+1}$ and $v_m^{n,k+1} \to v_m^{n+1}$ via sub-iterations. We set $v_m^{n,0} = v_m^n$ and $u_m^{n,0} = u_m^n$. The discretized scheme will become

$$-2\nu_- u_{m-1}^{n,k+1} + \Big(1+2\nu_- +2(P_l+P_c(t))\frac{\Delta t}{\Delta x}\Big)u_m^{n,k+1} = u_m^n + 2(P_l+P_c(t))\frac{\Delta t}{2\Delta x}v_m^{n,k} + P_p\frac{2\Delta t}{\Delta x}\frac{(v_m^{n,k})^2}{k_d^2+(v_m^{n,k})^2} \tag{4.75}$$

and

$$\Big(1+2\nu_+ +2(P_l+P_c(t))\frac{\Delta t}{\Delta x}\Big)v_m^{n,k+1} - 2\nu_+ v_{m+1}^{n,k+1} = v_m^n + 2(P_l+P_c(t))\frac{\Delta t}{2\Delta x}u_m^{n,k} - P_p\frac{2\Delta t}{\Delta x}\frac{(v_m^{n,k})^2}{k_d^2+(v_m^{n,k})^2}. \tag{4.76}$$

For the numerical computation of the membrane pumping conditions the scheme for $j = m$ in the subsystem (4.55) will be replaced on (4.75) and in the second sub-system, i.e. for the right sub-domain in (4.56) for $j = m$ will be replaced on scheme (4.76).

Further for the convergence of the membrane pumping conditions we check the residual equations at the interface

$$\begin{aligned} R_1^{n,k+1} &= -2\nu_- u_{m-1}^{n,k+1} + \Big(1+2\nu_- +2(P_l+P_c(t))\frac{\Delta t}{\Delta x}\Big)u_m^{n,k+1} - u_m^n - 2(P_l+P_c(t))\frac{\Delta t}{\Delta x}v_m^{n,k+1} \\ &\quad - P_p\frac{2\Delta t}{\Delta x}\frac{(v_m^{n,k})^2}{k_d^2+(v_m^{n,k})^2} \\ R_2^{n,k+1} &= \Big(1+2\nu_+ +2(P_l+P_c(t))\frac{\Delta t}{\Delta x}\Big)v_m^{n,k+1} - 2\nu_+ v_{m+1}^{n,k+1} - v_m^n - 2(P_l+P_c(t))\frac{\Delta t}{\Delta x}u_m^{n,k} \\ &\quad + P_p\frac{2\Delta t}{\Delta x}\frac{(v_m^{n,k})^2}{k_d^2+(v_m^{n,k})^2}. \end{aligned}$$

The above iteration process can be repeated. For $k \to \infty$ we expect $R_1^{n,k} \to 0$ and $R_2^{n,k} \to 0$ as well as $u_j^{n,k} \to u_j^{n+1}$ and $v_j^{n,k} \to v_j^{n+1}$.

We prescribe some small tolerance $TOL > 0$ such that when we have achieved $|R_1^{n,k+1}| < TOL$ and $|R_2^{n,k+1}| < TOL$ we stop the sub iterations and start the next time step.

Note that the simplified membrane pumping conditions is the special case of the membrane pumping conditions with $P_l + P_c(t) = H$ and $P_p = P$. There is no need to derive the complete derivation again.

Also note that the formulas for the coupling conditions in the case of one sided and the central difference is only differ by a factor of 2 with the term $\nu_{\pm}$. So, in the above two coupling conditions the one sided formulas can be easily obtained by dropping the factor of 2.

4.3 L_1 error and order of convergence for the bi-domain diffusion equations

We derived the L_1 error and order of convergence for the single domain diffusion equation in Chapter 3. Now here we will give formulas for the bi-domain diffusion equations with explicit, implicit and finite volume methods with coupling Dirichlet-Neumann coupling conditions with identical diffusion coefficients $D_- = D_+$.

Explicit (nodal based) and implicit method

For the explicit (nodal based) and implicit method the formula to calculate the L_1 error is given by

$$\begin{aligned} E_n(h) :&= \|u_h(t_n,\cdot) - u(t_n,\cdot)\|_{1,(a,c)} + \|v_h(t_n,\cdot) - v(t_n,\cdot)\|_{1,(c,b)} \\ &= \frac{\Delta x}{2}|u_0^n - \overline{u}_0^n| + \Delta x \sum_{i=1}^{m} |u_i^n - \overline{u}_i^n| + \Delta x \sum_{i=m+1}^{2m-1} |v_i^n - \overline{v}_i^n| + \frac{\Delta x}{2}|v_{2m}^n - \overline{v}_{2m}^n|. \end{aligned}$$

Here, $u_j^n = \frac{1}{\Delta x}\int_{x_{i-\frac{1}{2}}}^{x_{i+\frac{1}{2}}} u(t_n,x)\,dx$ and $v_j^n = \frac{1}{\Delta x}\int_{x_{i-\frac{1}{2}}}^{x_{i+\frac{1}{2}}} v(t_n,x)\,dx$. These error estimates tells us the order of convergence for our numerical schemes based of finite difference which is a finite element type method.

Finite volume method

Now we give the formula for the finite volume which is a cell based discretizations methods.

$$\begin{aligned} E_n(h) :&= \|u_h(t_n,\cdot) - u(t_n,\cdot)\|_{1,(a,c)} + \|v_h(t_n,\cdot) - v(t_n,\cdot)\|_{1,(c,b)} \\ &= \Delta x \sum_{i=0}^{m} |u_i^n - \overline{u}_i^n| + \Delta x \sum_{i=m+1}^{2m} |v_i^n - \overline{v}_i^n|. \end{aligned}$$

These estimates will give the L_1 error for the DN-coupling conditions with bi-domain diffusion equations. These results will show that how fast the error will decrease as we decrease the mesh size. The results for the L_1 error and for the order of convergence will show in Chapter 7 in Table 7.10 and the graphical interpretation will show in Figure 7.13.

Chapter 5

The discrete mass conservation property for single and bi-domain diffusion equations

Under homogeneous Neumann boundary conditions the diffusion equations conserve total mass for concentrations or total energy in the case of the heat equation. Since we assume there are no fluxes across the outer boundaries, the total change of discrete mass or energy in the domain should approximate zero up-to machine accuracy. This important property must be maintained by the scheme. In order to check whether the mass is conserved throughout the time interval, we compute the total mass C_{total} in the domain at each time step $t_n = n\Delta t$.

In this chapter we derive the discrete mass conservation property for the single domain diffusion equation with various discretization methods. These methods include the explicit, implicit and a finite volume discretization methods. Also, we derive this property for the various coupling interface conditions with bi-domain diffusion equations via explicit and implicit methods. These were implemented in the previous Chapter 4.

5.1 Conservation of discrete mass for the single domain diffusion equation

5.1.1 Explicit discretization (nodal based formulation)

It is necessary for the concentration problem that the total concentration diffused in the region must be conserved according to the law of mass conservation.

In the discretization of the initial data we are making a small error in the initial total concentration by approximating

$$\int_{x_{j-\frac{1}{2}}}^{x_{j+\frac{1}{2}}} w_0(x)\,dx \approx w_0(x_j)\Delta x = w_j^0 \Delta x \qquad \text{for} \qquad j = 1, 2, \ldots, N.$$

We are using quadrature by the midpoint rule for simplicity. One could also use a higher order quadrature for higher accuracy. Further we approximate $\int_{x_{0-\frac{1}{2}}}^{x_0} w(x)\,dx \approx w(x_0)\frac{\Delta x}{2} = w_0^0\frac{\Delta x}{2}$ on the cell $[x_0, x_{0+\frac{1}{2}}]$ and $\int_{x_{N-\frac{1}{2}}}^{x_N} w(x)\,dx \approx w(x_N)\frac{\Delta x}{2} = w_N^0\frac{\Delta x}{2}$ on the cell $[x_N, x_{N+\frac{1}{2}}]$, i.e. we use simple rectangle rules. Therefore we assume that our discrete initial total concentration is $\overline{C^0}_{total} = C^0_{total}\Delta x$ with

$$C^0_{total} = \frac{1}{2}w_0^0 + w_1^0 + \ldots + w_{N-1}^0 + \frac{1}{2}w_N^0 \tag{5.1}$$

The initial error in this term becomes smaller for $\Delta x \to 0$. Analogously, the total concentration for the later times t_n in the single domain diffusion equation is given by $C^n_{total}\Delta x$ with

$$C^n_{total} = \frac{1}{2}w_0^n + w_1^n + \ldots + w_{N-1}^n + \frac{1}{2}w_N^n. \tag{5.2}$$

First we consider the single domain diffusion equation (3.1) with the explicit discretization. We derived the discretization for the boundary conditions in (3.16) and (3.17). For homogeneous Neumann boundary conditions we took $J_L(t_n) = 0$ and $J_R(t_n) = 0$ and the discretizations are given as follows

$$w_0^{n+1} = 2\nu w_1^n + (1-2\nu)w_0^n, \qquad w_N^{n+1} = 2\nu w_{N-1}^n + (1-2\nu)w_N^n. \tag{5.3}$$

We have from (5.3)

$$\frac{1}{2}w_0^{n+1} = \frac{1}{2}(2\nu w_1^n + (1-2\nu)w_0^n) = \frac{1}{2}w_0^n + \nu(w_1^n - w_0^n) \tag{5.4}$$

and analogously for the right hand boundary

$$\frac{1}{2}w_N^{n+1} = \frac{1}{2}w_N^n - \nu(w_N^n - w_{N-1}^n). \tag{5.5}$$

For the interior points of the domain, i.e. for $j = 1, 2, ..., N-1$ the scheme (3.12) can be written as

$$w_j^{n+1} = w_j^n + \nu(w_{j+1}^n - w_j^n) - \nu(w_j^n - w_{j-1}).$$

Now the total concentration at the new time level $n+1$ is given by

$$\begin{aligned} C^{n+1}_{total} &= \frac{1}{2}w_0^n + \nu(w_1^n - w_0^n) + w_1^n - \nu(w_1^n - w_0^n) + \nu(w_2^n - w_1^n) + \ldots + w_{N-1}^n \\ &\quad - \nu(w_{N-1}^n - w_{N-2}^n) + \nu(w_N^n - w_{N-1}^n) + \frac{1}{2}w_N^n - \nu(w_N^n - w_{N-1}^n) \\ &= C^n_{total}. \end{aligned} \tag{5.6}$$

Due to conservativity of the scheme $C^n_{total} = C^0_{total}$ remains constant and deviations are due to rounding errors only.

We derived the boundary iteration (5.3) using a central difference method with ghost cells in order to obtain boundary conditions which are conservative. We could use one sided differences for the discretization of the outer boundary conditions as derived in (3.20) and (3.21). Then we obtain a non-conservative sum, i.e. $C^n_{total} \neq C^0_{total}$.

5.1.2 Implicit discretization (nodal based formulation)

Next, we consider the single domain diffusion equation (3.1) with the implicit discretization method. We derived the implicit discretization for the homogeneous Neumann boundary conditions in (3.23) and (3.24) and the discretizations are given as follows

$$w_0^n = w_0^{n+1} + 2\nu(w_0^{n+1} - w_1^{n+1}), \qquad w_N^n = w_N^{n+1} + 2\nu(w_N^{n+1} - w_{N-1}^{n+1}). \tag{5.7}$$

From equation (5.7) we have

$$\frac{1}{2}w_0^n = \frac{1}{2}w_0^{n+1} + \nu(w_0^{n+1} - w_1^{n+1}) \tag{5.8}$$

and analogously for the right hand boundary we have the following discretize scheme

$$\frac{1}{2}w_N^n = \frac{1}{2}w_N^{n+1} - \nu(w_{N-1}^{n+1} - w_N^{n+1}). \tag{5.9}$$

For $j = 1, 2, ..., N-1$ the scheme (3.12) gives

$$w_j^n = w_j^{n+1} - \nu(w_{j-1}^{n+1} - w_j^{n+1}) + \nu(w_j^{n+1} - w_{j+1}^{n+1}). \tag{5.10}$$

Using (5.2) the total concentrations $C_{total}^n \Delta x$ at the time levels n and $n+1$ satisfy

$$\begin{aligned} C_{total}^n &= \frac{1}{2}w_0^{n+1} + \nu(w_0^{n+1} - w_1^{n+1}) + w_1^{n+1} - \nu(w_0^{n+1} - w_1^{n+1}) + \nu(w_1^{n+1} - w_2^{n+1}) + \dots \\ &\quad + w_{N-1}^{n+1} - \nu(w_{N-2}^{n+1} - w_{N-1}^{n+1}) + \nu(w_{N-1}^{n+1} - w_N^{n+1}) + \frac{1}{2}w_N^{n+1} - \nu(w_{N-1}^{n+1} - w_N^{n+1}) \\ &= C_{total}^{n+1}. \end{aligned} \tag{5.11}$$

We obtain that the quantity $C_{total}^n = C_{total}^0$ remains constant and deviations are due to rounding errors only. Therefore the discretized scheme for the diffusion equation with homogeneous Neumann boundary conditions via the central difference method is conservative. While one sided differences as derived in (3.27) and (3.28) will lead to a non-conservative scheme.

5.1.3 Finite volume discretization (cell based formulation)

We derived the discretization of the single domain diffusion equation with the homogeneous Neumann boundary conditions via the finite volume discretization in Section 3.4. There we used the difference with a neighboring ghost cell value which is the central difference w.r.t. the boundary points a and b.

In this case the discrete initial total concentration is $C_{total}^0 \Delta x$ with

$$C_{total}^0 = w_1^0 + \dots + w_N^0. \tag{5.12}$$

Analogously, the total concentration for the later times t_n in the single domain diffusion model is given by $C_{total}^n \Delta x$ with

$$C_{total}^n = w_1^n + \dots + w_N^n. \tag{5.13}$$

Now we substitute the discrete values of $w_1^n, \ldots, w_N^n$ from (3.35) into (5.13) for time level $n+1$. Now the total concentration at the new time level $n+1$ is given by

$$\begin{aligned} C_{total}^{n+1} &= w_1^n + \nu(w_2^n - w_1^n) + w_2^n + \nu(w_3^n - w_2^n) - \nu(w_2^n - w_1^n) + \ldots + w_{N-1}^n \\ &\quad + \nu(w_N^n - w_{N-1}^n) - \nu(w_{N-1}^n - w_{N-2}^n) + w_N^n - \nu(w_N^n - w_{N-1}^n) \\ &= C_{total}^n. \end{aligned} \tag{5.14}$$

Again we obtain $C_{total}^n = C_{total}^0$. This implies that the discretized scheme of the diffusion equation with homogeneous boundary conditions is conservative. Any deviations are due to rounding errors.

5.2 Conservation of the discrete mass for the coupling conditions with bi-domain diffusion equation via explicit discretization method

In this section we derive the discrete mass conservation for the various coupling conditions via explicit discretization methods. First we derive them for the Dirichlet-Neumann coupling and then for the other coupling conditions.

Dirichlet-Neumann coupling

Now we consider the bi-domain diffusion equations with the Dirichlet-Neumann coupling conditions at the interface of the two sub-domains.

In the discretization of the initial data we are again making a small error in the initial total concentration by approximating

$$\int_{x_{j-\frac{1}{2}}}^{x_{j+\frac{1}{2}}} u(x)\,dx \approx u(x_j)\Delta x \qquad \text{for} \qquad j = 1, 2, \ldots, m-1$$

and analogously for v at $j = m+1, \ldots, N$.

For the outer boundary cells, i.e. for the left hand boundary we have $\int_{x_{0-\frac{1}{2}}}^{x_0} u(x)\,dx \approx u(x_0)\frac{\Delta x}{2} = u_0^0\frac{\Delta x}{2}$ on the cell $[x_0, x_{0+\frac{1}{2}}]$ and on the right hand boundary we approximate $\int_{x_{0-\frac{1}{2}}}^{x_0} v(x)\,dx \approx v(x_N)\frac{\Delta x}{2} = v_N^0\frac{\Delta x}{2}$ on the cell $[x_N, x_{N+\frac{1}{2}}]$ and for the interface boundary we approximate $\int_{x_{m-\frac{1}{2}}}^{x_m} u(x)\,dx \approx u(x_m)\frac{\Delta x}{2} = u_m^0\frac{\Delta x}{2}$ and $\int_{x_m}^{x_{m+\frac{1}{2}}} v(x)\,dx \approx v(x_m)\frac{\Delta x}{2} = v_m^0\frac{\Delta x}{2}$, on the cell $[x_{m-\frac{1}{2}}, x_{m+\frac{1}{2}}]$. Now our initial total concentration is $\overline{C^0}_{total} = C_{total}^0\Delta x$ with

$$C_{total}^0 = \frac{1}{2}u_0^0 + u_1^0 + \ldots + u_{m-1}^0 + \frac{1}{2}u_m^0 + \frac{1}{2}v_m^0 + v_{m+1}^0 + \ldots + v_{N-1}^0 + \frac{1}{2}v_N^0. \tag{5.15}$$

We will use this form of discretization with the splitting of the cell $[x_{m-\frac{1}{2}}, x_{m+\frac{1}{2}}]$ into two sub-cells in the later coupling conditions that do not involve the Dirichlet condition.

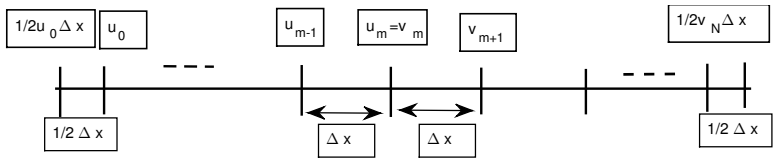

Figure 5.1: Sketch for the bi-domain with coupling interface conditions and with double nodes.

For the Dirichlet condition we modify the definitions of u_m^0 and v_m^0. We set $u_m^0 = v_m^0 = \int_{x_{m-\frac{1}{2}}}^{x_m} u_0(x)\,dx + \int_{x_m}^{x_{m+\frac{1}{2}}} v_0(x)\,dx$. In this special case we do not split the cell $[x_{m-\frac{1}{2}},\ x_{m+\frac{1}{2}}]$. Therefore, we define for $n \in \mathbb{N}_0$ the total concentration $C_{total}^n \Delta x$

$$C_{total}^n = \frac{1}{2}u_0^n + u_1^n + ...u_{m-1}^n + u_m^n + v_{m+1}^n + v_{m+2}^n ... + \frac{1}{2}v_N. \tag{5.16}$$

We derived the updates u_m^{n+1} for the Dirichlet-Neumann coupling in (4.11) to be due to the Dirichlet condition in (2.11) we have

$$v_m^{n+1} = u_m^{n+1}$$

and due to the Neumann coupling (4.10) we have

$$u_m^{n+1} = u_m^n + \nu_+(v_{m+1}^n - v_m^n) - \nu_-(u_m^n - u_{m-1}^n).$$

For the interior of the left sub-domain we have

$$u_j^{n+1} = u_j^n + \nu_-(u_{j+1}^n - u_j^n) - \nu_-(u_j^n - u_{j-1}^n) \tag{5.17}$$

and for the interior of the right sub-domain we have

$$v_j^{n+1} = v_j^n + \nu_+(v_{j+1}^n - v_j^n) - \nu_+(v_j^n - v_{j-1}^n). \tag{5.18}$$

So, the total concentration at time t_{n+1} is given by

$$\begin{aligned}
\overline{C}_{total}^{n+1} &= \frac{1}{2}u_0^{n+1} + u_1^{n+1} + ... + u_{m-1}^{n+1} + u_m^{n+1} + v_{m+1}^{n+1} + ... + \frac{1}{2}v_N^{n+1} \\
&= \frac{1}{2}u_0^n + \nu_-(u_1^n - u_0^n) + u_1^n + \nu_-(u_2^n - u_1^n) - \nu_-(u_1^n - u_0^n) + \ldots + u_{m-1}^n \\
&\quad + \nu_-(u_m^n - u_{m-1}^n) - \nu_-(u_{m-1}^n - u_{m-2}^n) + u_m^n + \nu_+(v_{m+1}^n - v_m^n) - \nu_-(u_m^n - u_{m-1}^n) \\
&\quad + v_{m+1}^n + \nu_+(v_{m+2}^n - v_{m+1}^n) - \nu_+(v_{m+1}^n - v_m^n) + \ldots \\
&\quad + v_{N-1}^n + \nu_+(v_N^n - v_{N-1}^n) - \nu_+(v_{N-1}^n - v_{N-2}^n) + \frac{1}{2}v_N^n + \nu_+(v_{N-1}^n - v_N^n).
\end{aligned}$$

After the cancellation of the identical terms in the above expression we obtain $\overline{C}_{total}^{n+1} = \overline{C}_{total}^n$. Due to conservativity of the scheme C_{total}^n remains constant and deviations are due to the rounding errors.

The Dirichlet-Neumann coupling considered by Giles

For comparison we choose $c_\pm = 1$, $k_\pm = D_\pm$ and $r = 1$ for the coupling scheme of Giles given in (4.13). Note for comparison that the correct scheme (4.14) with $r = 1$ gives our formula (4.10). This we have just shown to be conservative above.

In our notation his scheme (4.13) for the interface node $j = m$ and with $c_\pm = 1$ and $r = 1$ is given by

$$u_m^{n+1} = u_m^n + 2\nu_+(v_{m+1}^n - u_m^n) - 2\nu_-(u_m^n - u_{m-1}^n). \tag{5.19}$$

Further the schemes for the interior nodes of two sub-domains are identical. In our notation these are given in (5.17) and (5.18). So in this case the total concentration $C_{total}^{n+1}\Delta x$ is given by

$$\begin{aligned}
C_{total}^{n+1} &= \frac{1}{2}u_0^{n+1} + u_1^{n+1} + ... + u_{m-1}^{n+1} + u_m^{n+1} + v_{m+1}^{n+1} + ... + \frac{1}{2}v_N^{n+1} \\
&= \frac{1}{2}u_0^n + \nu_-(u_1^n - u_0^n) + u_1^n + \nu_-(u_2^n - u_1^n) - \nu_-(u_1^n - u_0^n) + \ldots + u_{m-1}^n \\
&\quad + \nu_-(u_m^n - u_{m-1}^n) - \nu_-(u_{m-1}^n - u_{m-2}^n) + u_m^n + 2\nu_+(v_{m+1}^n - v_m^n) - 2\nu_-(u_m^n - u_{m-1}^n) \\
&\quad + v_{m+1}^n + \nu_+(v_{m+2}^n - v_{m+1}^n) - \nu_+(v_{m+1}^n - v_m^n) + \ldots \\
&\quad + v_{N-1}^n + \nu_-(v_N^n - v_{N-1}^n) - \nu_-(v_{N-1}^n - v_{N-2}^n) + \frac{1}{2}v_N^n + \nu_+(v_{N-1}^n - v_N^n).
\end{aligned}$$

This will lead a non-conservative scheme since we have using the Dirichlet condition $u_m^n = v_m^n$

$$C_{total}^{n+1} = C_{total}^n - \nu_-(u_m^n - u_{m-1}^n) + \nu_+(v_{m+1}^n - u_m^n). \tag{5.20}$$

The schemes for the un-equal mesh sizes

Instead of (5.15) we have to consider the total concentration as

$$\overline{C}_{total}^0 = c_-\Delta x_-(\frac{1}{2}u_0^0 + u_1^0 + \ldots + u_{m-1}^0 + \frac{1}{2}u_m^0) + c_+\Delta x_+(\frac{1}{2}v_m^0 + v_{m+1}^0 + \ldots + v_{N-1}^0 + \frac{1}{2}v_N^0). \tag{5.21}$$

The scheme for the left hand boundary will be

$$\frac{1}{2}u_0^{n+1} = \frac{1}{2}u_0^n + \frac{D_-\Delta t}{c_-(\Delta x_-)^2}(u_1^n - u_0^n)$$

and the scheme for the interior of the left sub-domain is given by

$$u_j^{n+1} = u_j^n + \frac{D_-\Delta t}{c_-(\Delta x_-)^2}(u_{j+1}^n - u_j^n) - \frac{D_-\Delta t}{c_-(\Delta x_-)^2}(u_j^n - u_{j-1}^n).$$

Now the corrected Giles coupling scheme (4.14) has the form

$$u_m^{n+1} = u_m^n + \frac{2r\nu_+}{1+r}(v_{m+1}^n - v_m^n) - \frac{2\nu_-}{1+r}(u_m^n - u_{m-1}^n). \tag{5.22}$$

Further the scheme for the interior of the right sub-domain is

$$v_j^{n+1} = v_j^n + \frac{D_+\Delta t}{c_+(\Delta x_+)^2}(v_{j+1}^n - v_j^n) - \frac{D_+\Delta t}{c_+(\Delta x_+)^2}(v_j^n - v_{j-1}^n)$$

and for the right hand boundary condition we have

$$\frac{1}{2}v_N^{n+1} = \frac{1}{2}v_N^n + \frac{D_+\Delta t}{c_+(\Delta x_+)^2}(v_{N-1}^n - u_N^n).$$

Now we have to rewrite the scheme in the form that can be used in (5.21). We first consider the coupling condition (5.22)

$$u_m^{n+1} = u_m^n + \frac{2D_+\Delta t}{\Delta x_+(c_-\Delta x_- + c_+\Delta x_+)}(v_{m+1}^n - v_m^n) - \frac{2D_-\Delta t}{\Delta x_-(c_-\Delta x_- + c_+\Delta x_+)}(u_m^n - u_{m-1}^n). \tag{5.23}$$

This we rewrite in the following form

$$\frac{c_-\Delta x_- + c_+\Delta x_+}{2}u_m^{n+1} = \frac{c_-\Delta x_- + c_+\Delta x_+}{2}u_m^n + \frac{D_+\Delta t}{\Delta x_+}(v_{m+1}^n - v_m^n) - \frac{D_-\Delta t}{\Delta x_-}(u_m^n - u_{m-1}^n).$$

From the Dirichlet condition we have $u_m^{n+1} = u_m^{n+1}$ as well as $u_m^n = v_m^n$. Using these we can write

$$\frac{c_-\Delta x_- + c_+\Delta x_+}{2}u_m^{n+1} = \frac{c_-\Delta x_-}{2}u_m^{n+1} + \frac{c_+\Delta x_+}{2}v_m^{n+1} \tag{5.24}$$

and the same for time level n. Then we obtain

$$\frac{c_-\Delta x_-}{2}u_m^{n+1} + \frac{c_+\Delta x_+}{2}v_m^{n+1} = \frac{c_-\Delta x_-}{2}u_m^n + \frac{c_+\Delta x_+}{2}v_m^n + \frac{D_+\Delta t}{\Delta x_+}(v_{m+1}^n - v_m^n) - \frac{D_-\Delta t}{\Delta x_-}(u_m^n - u_{m-1}^n). \tag{5.25}$$

We will use this form of the scheme for the proof of the conservativity property.

Now we write the whole scheme in this form together in a system

$$\begin{aligned}
\frac{c_-\Delta x_-}{2}u_0^{n+1} &= \frac{c_-\Delta x_-}{2}u_0^n + \frac{D_-\Delta t}{c_-\Delta x_-}(u_1^n - u_0^n)\\
c_-\Delta x_- u_j^{n+1} &= c_-\Delta x_- u_j^n + \frac{D_-\Delta t}{\Delta x_-}(u_{j+1}^n - u_j^n) - \frac{D_-\Delta t}{\Delta x_-}(u_j^n - u_{j-1}^n)\\
\frac{c_-\Delta x_-}{2}u_m^{n+1} + \frac{c_+\Delta x_+}{2}v_m^{n+1} &= \frac{c_-\Delta x_-}{2}u_m^n + \frac{c_+\Delta x_+}{2}v_m^n + \frac{D_+\Delta t}{\Delta x_+}(v_{m+1}^n - v_m^n)\\
&\quad - \frac{D_-\Delta t}{\Delta x_-}(u_m^n - u_{m-1}^n)\\
c_+\Delta x_+ v_j^{n+1} &= c_+\Delta x_+ v_j^n + \frac{D_+\Delta t}{\Delta x_+}(v_{j+1}^n - v_j^n) - \frac{D_+\Delta t}{\Delta x_+}(v_j^n - v_{j-1}^n)\\
\frac{c_+\Delta x_+}{2}v_N^{n+1} &= \frac{c_+\Delta x_+}{2}v_N^n + \frac{D_+\Delta t}{\Delta x_+}(v_{N-1}^n - u_N^n).
\end{aligned} \tag{5.26}$$

Clearly after the summation of the above equations the identical terms will cancel out and again we obtain a conservative system $\overline{C}_{total}^{n+1} = \overline{C}_{total}^n$.

Heat flux coupling conditions via one sided difference method (nodal based)

Now we derive the conservativity for the heat flux coupling interface conditions via the one sided difference method by explicit nodal based discretization. The schemes for the coupling interface conditions are different for the interface node at $j = m$, we now consider the possibility $u_m^{n+1} \neq v_m^{n+1}$. For the other nodes the schemes are the same as in the Dirichlet-Neumann coupling.

The total concentration at time t_{n+1} for the bi-domain diffusion equation with zero flux boundary conditions on the outer boundaries and with heat flux coupling conditions is given by

$$\begin{aligned}
\overline{C}_{total}^{n+1} &= \frac{1}{2}u_0^{n+1} + u_1^{n+1} + ... + u_{m-1}^{n+1} + \frac{1}{2}u_m^{n+1} + \frac{1}{2}v_m^{n+1} + v_{m+1}^{n+1} + ... + \frac{1}{2}v_N^{n+1} \\
&= \frac{1}{2}u_0^n + \nu_-(u_1^n - u_0^n) + u_1^n + \nu_-(u_2^n - u_1^n) - \nu_-(u_1^n - u_0^n) + \ldots + u_{m-1}^n \\
&\quad + \nu_-(u_m^n - u_{m-1}^n) - \nu_-(u_{m-1}^n - u_{m-2}^n) + \frac{1}{2}u_m^n - \frac{\nu_-}{2}(u_m^n - u_{m-1}^n) + \frac{\Delta t}{2\Delta x}\Big(v_m^n - u_m^n\Big) \\
&\quad + \frac{1}{2}v_m^n - \frac{\nu_+}{2}(v_{m+1}^n - v_{m-1}^n) - \frac{\Delta t}{2\Delta x}\Big(v_m^n - u_m^n\Big) + v_{m+1}^n + \nu_+(v_{m+2}^n - v_{m+1}^n) \\
&\quad - \nu_+(v_{m+1} - v_m^n) + \ldots + \frac{1}{2}v_N^n + \nu_+(v_{N-1}^n - v_N^n).
\end{aligned}$$

After the cancellation of identical terms in the above expression we obtain

$$\overline{C}_{total}^{n+1} = \overline{C}_{total}^n + \frac{\nu_-}{2}\Big(u_m^n - u_{m-1}^n\Big) - \frac{\nu_+}{2}\Big(v_{m+1}^n - v_m^n\Big).$$

This implies that the total concentrations $\overline{C}_{total}^{n+1}$ does remain constant. This shows that the one sided difference approximating for the discretization of the coupling interface conditions is not conserved.

Heat flux coupling conditions via the central difference method

Analogously, here we derive the conservativity for the heat flux coupling interface conditions via the central difference method by explicit discretization. Only the schemes for the interface node are differnt, i.e. u_m^{n+1} and v_m^{n+1} and the rest of schemes are equal as we derived in the Dirichlet-Neumann coupling.

We derived the schemes for the heat flux conditions via central difference method u_m^{n+1} in (4.31) and v_m^{n+1} in (4.32). In this case the total concentration $C_{total}^{n+1}\Delta x$ is given by

$$\begin{aligned}
\overline{C}_{total}^{n+1} &= \frac{1}{2}u_0^n + \nu_-(u_1^n - u_0^n) + u_1^n + \nu_-(u_2^n - u_1^n) - \nu_-(u_1^n - u_0^n) + \ldots + u_{m-1}^n \\
&\quad + \nu_-(u_m^n - u_{m-1}^n) - \nu_-(u_{m-1}^n - u_{m-2}^n) + \frac{1}{2}u_m^n - \nu_-(u_m^n - u_{m-1}^n) + \frac{\Delta t}{\Delta x}\Big(v_m^n - u_m^n\Big) \\
&\quad + \frac{1}{2}v_m^n - \nu_+(v_{m+1}^n - v_m^n) - \frac{\Delta t}{\Delta x}\Big(v_m^n - u_m^n\Big) + v_{m+1}^n + \nu_+(v_{m+2}^n - v_{m+1}^n) \\
&\quad - \nu_+(v_{m+1}^n - v_m^n) + \ldots + \frac{1}{2}v_N^n + \nu_+(v_{N-1}^n - v_N^n).
\end{aligned}$$

After the cancellation of identical terms in the above expression we obtain $\overline{C}^{n+1}_{total} = \overline{C}^{n}_{total}$. This implies that the quantities C^n_{total} remains constant. This shows that the use of the central difference approximation for the discretization of the coupling conditions maintains the conservativity.

Heat flux coupling conditions via one sided difference method (cell based)

Now we derive the conservativity for the heat flux coupling interface conditions via the one sided difference method by explicit cell based discretization.

The total concentration at time t_{n+1} for the bi-domain diffusion equation with zero flux boundary conditions on the outer boundaries and with heat flux coupling conditions is given by

$$\begin{aligned}
\overline{C}^{n+1}_{total} &= \frac{1}{2}u_0^{n+1} + u_1^{n+1} + ... + u_{m-1}^{n+1} + u_m^{n+1} + v_{m+1}^{n+1} + ... + \frac{1}{2}v_N^{n+1} \\
&= \frac{1}{2}u_0^n + \nu_-(u_1^n - u_0^n) + u_1^n + \nu_-(u_2^n - u_1^n) - \nu_-(u_1^n - u_0^n) + \ldots + u_{m-1}^n \\
&\quad + \nu_-(u_m^n - u_{m-1}^n) - \nu_-(u_{m-1}^n - u_{m-2}^n) + u_m^n - \nu_-(u_m^n - u_{m-1}^n) + \frac{\Delta t}{\Delta x}\Big(v_m^n - u_m^n\Big) \\
&\quad + v_{m+1}^n + \nu_+(v_{m+2}^n - v_{m+1}^n) - \nu_+(v_{m+1} - v_m^n) + \ldots + \frac{1}{2}v_N^n + \nu_+(v_{N-1}^n - v_N^n).
\end{aligned}$$

After the cancellation of identical terms in the above expression we get the total concentrations remain constant, i.e. $\overline{C}^{n+1}_{total} = \overline{C}^{n}_{total}$. This shows that the one sided difference which is the central difference w.r.t. the boundary point in the cell based scheme maintain the conservativity.

So, we concluded that the central difference with nodal based scheme and the one sided finite volume cell based scheme maintain the conservativity, while the one sided differences with nodal based scheme does not.

5.3 Implicit discretization method

In this section we derive the mass conservation for the various coupling conditions. First we derive for the Dirichlet-Neumann coupling and then for the others.

Dirichlet-Neumann coupling

Here we derive the conservativity for the bi-domain diffusion equations and with Dirichlet-Neumann coupling via implicit discretization.

For the Dirichlet condition we again assume that $u_m^0 = v_m^0 = \int_{x_{m-\frac{1}{2}}}^{x_m} u_0(x)\,dx + \int_{x_m}^{x_m+\frac{1}{2}} v_0(x)\,dx$. Now for conservativity in the implicit case we prove that $C^n_{total} = C^{n+1}_{total}$. For this we need to calculate C^n_{total}. For the interior of the left sub-domain we derived the following scheme

$$u_j^n = u_j^{n+1} - \nu_-(u_{j-1}^{n+1} - u_j^{n+1}) + \nu_-(u_j^{n+1} - u_{j+1}^{n+1}).$$

and for the interior of the right sub-domain

$$v_j^n = v_j^{n+1} - \nu_+(v_{j-1}^{n+1} - v_j^{n+1}) + \nu_+(v_j^{n+1} - v_{j+1}^{n+1}).$$

Further, the scheme for the Dirichlet-Neumann coupling via the implicit method was derived in the system (4.53) for $j = m$ represented as

$$u_m^n = u_m^{n+1} + \nu_-(u_m^{n+1} - u_{m-1}^{n+1}) - \nu_+(v_{m+1}^{n+1} - v_m^{n+1}) \qquad \text{and} \qquad u_m^{n+1} = v_m^{n+1}.$$

Substituting all these values of $u_0^n, u_1^n \ldots, u_m^n, \ldots v_N^n$ in (5.16) we obtain

$$\begin{aligned}
\overline{C}_{total}^n = {} & \frac{1}{2}u_0^{n+1} + \nu_-(u_0^{n+1} - u_1^{n+1}) + u_1^{n+1} - \nu_-(u_0^{n+1} - u_1^{n+1}) + \nu_-(u_1^{n+1} - u_2^{n+1}) \\
& + \ldots + u_{m-1}^{n+1} - \nu_-(u_{m-2}^{n+1} - u_{m-1}^{n+1}) + \nu_-(u_{m-1}^{n+1} - u_m^{n+1}) + u_m^{n+1} - \nu_-(u_m^{n+1} - u_{m-1}^{n+1}) \\
& + \nu_+(v_{m+1}^{n+1} - v_m^{n+1}) + v_{m+1}^{n+1} - \nu_+(v_m^{n+1} - v_{m+1}^{n+1}) + \nu_+(v_{m+1}^{n+1} - v_{m+2}^{n+1}) + \ldots \\
& + v_{N-1}^{n+1} - \nu_+(v_{N-2}^{n+1} - v_{N-1}^{n+1}) - \nu_+(v_N^{n+1} - v_{N-1}^{n+1}) + \frac{1}{2}v_N^{n+1} + \nu_+(v_N^{n+1} - v_{N-1}^{n+1}).
\end{aligned}$$

After the cancellation of the identical terms in the above expression we obtain $\overline{C}_{total}^n = \overline{C}_{total}^{n+1}$. Due to conservativity of the scheme $\overline{C}_{total}^{n+1}$ remains constant. So, we concluded that the Dirichlet-Neumann coupling via implicit method is also conservation.

Heat flux coupling conditions via one sided difference method (nodal based)

Here, we derive the discrete conservation of mass for the heat flux coupling conditions via implicit discretization method. So, we replace only the schemes for the coupling interface nodes by new schemes of u_m^n and v_m^n were derived in (4.61) and in (4.62). In this case the total concentration $C_{total}^n \Delta x$ is give by

$$\begin{aligned}
\overline{C}_{total}^n = {} & \frac{1}{2}u_0^{n+1} + \nu_-(u_0^{n+1} - u_1^{n+1}) + u_1^{n+1} - \nu_-(u_2^{n+1} - u_1^{n+1}) - \nu_-(u_0^{n+1} - u_1^{n+1}) \\
& + \ldots + u_{m-1}^{n+1} - \nu_-(u_m^{n+1} - u_{m-1}^{n+1}) - \nu_-(u_{m-2}^{n+1} - u_{m-1}^{n+1}) + \frac{1}{2}u_m^{n+1} + \frac{\nu_-}{2}(u_m^{n+1} - u_{m-1}^{n+1}) \\
& - \frac{\Delta t}{2\Delta x}\left(v_m^{n+1} - u_m^{n+1}\right) + \frac{1}{2}v_m^{n+1} - \frac{\nu_+}{2}(v_{m+1}^{n+1} - v_m^{n+1}) + \frac{\Delta t}{2\Delta x}\left(v_m^{n+1} - u_m^{n+1}\right) \\
& + v_{m+1}^{n+1} + \nu_+(v_{m+1}^{n+1} - v_m^{n+1}) + \nu_+(v_m^{n+1} - v_{m+2}^{n+1}) + \ldots + v_{N-1}^{n+1} - \nu_+(v_N^{n+1} - v_{N-1}^{n+1}) \\
& - \nu_+(v_{N-2}^{n+1} - v_{N-1}^{n+1}) + \frac{1}{2}v_N^{n+1} + \nu_+(v_N^{n+1} - v_{N-1}^{n+1}).
\end{aligned}$$

After the cancellation of the identical terms in the above expression we obtain

$$\overline{C}_{total}^n = \overline{C}_{total}^{n+1} - \frac{\nu_-}{2}\left(u_m^{n+1} - u_{m-1}^{n+1}\right) + \frac{\nu_+}{2}\left(v_{m+1}^{n+1} - v_m^{n+1}\right)$$

This implies that the scheme $\overline{C}_{total}^n$ does not remains constant, which shows that the one sided difference approximation for the discretization of the coupling interface conditions is not conserved.

Heat flux coupling conditions via central difference method

Here, we dont want to repeat the whole derivation again. Therefore the discretization of the heat flux coupling via central difference method for the implicit discretization we obtain $\overline{C}^n_{total} = \overline{C}^n_{total}$. This implies that the quantities $\overline{C}^n_{total}$ is remains constant. This shows that the central difference approximation for the discretization of the coupling interface conditions is conserved.

5.3.1 Dirichlet-Neumann coupling via finite volume method (cell based formulation)

Here we derive the discrete mass conservation for the Dirichlet-Neumann coupling with bi-domain diffusion equation via cell based finite volume method. So, in this case the total concentration $\overline{C}^n_{total} = C^{n+1}_{total}\Delta x$ is given by

$$\begin{aligned}
\overline{C}^{n+1}_{total} &= u^{n+1}_1 + ... + u^{n+1}_{m-1} + u^{n+1}_m + v^{n+1}_{m+1} + ... + v^{n+1}_N \\
&= u^n_1 + \nu_-(u^n_2 - u^n_1) + u^n_2 + \nu_-(u^n_3 - u^n_2) - \nu_-(u^n_2 - u^n_1) + \ldots + u^n_{m-1} \\
&\quad + \nu_-(u^n_m - u^n_{m-1}) - \nu_-(u^n_{m-1} - u^n_{m-2}) + u^n_m + \nu_+(v^n_{m+1} - u^n_m) - \nu_-(u^n_m - u^n_{m-1}) \\
&\quad + v^n_{m+1} + \nu_+(v^n_{m+2} - v^n_{m+1}) - \nu_+(v^n_{m+1} - u^n_m) + \ldots \\
&\quad + v^n_{N-1} + \nu_-(v^n_N - v^n_{N-1}) - \nu_-(v^n_{N-1} - v^n_{N-2}) + v^n_N - \nu_+(v^n_N - v^n_{N-1}).
\end{aligned}$$

After the cancellation of the identical terms in the above expression we obtain $\overline{C}^{n+1}_{total} = \overline{C}^n_{total}$. Therefore, the coupled scheme is conservative.

5.4 Mass conservation of channel pumping, simplified channel pumping, linearized membrane pumping, membrane pumping coupling conditions (explicit and implicit discretization)

The discrete mass conservation for the channel pumping, simplified channel pumping, simplified membrane pumping, linearized membrane pumping and membrane pumping coupling interface conditions can be derived in the same way as for the heat flux coupling interface conditions via explicit as well with implicit discretization methods described above.

In the discretization of all these coupling conditions we see that in the two coupling schemes for u^{n+1}_m and v^{n+1}_m we have identical terms with opposite signs. Due to this in the conservation sum the extra terms cancel each other and give us conservativity via central difference method. They give non-conservativity with one sided differences.

5.5 Numerical tests for the discrete mass conservation

Here we give computational results for the discrete mass conservation for the single domain diffusion equation as well as for the bi-domain diffusion equations with various coupling

conditions. In the single domain case we give results for the explicit FTCS method and the finite volume method for comparison. For the bi-domain diffusion equations with various coupling conditions we give them only for the explicit FTCS method. In the implicit method the results were analogous to the explicit case, slightly worse. So there is no need to show them.

Note that for the numerical computations in this thesis we used two types of initial conditions the continuous cosine data and the constant data. In the case of cosine initial data the exact initial mass will be $\int_0^1[\cos(\pi x)+1]\,dx = 1$. The initial numerical mass for $\Delta x = 1/2000$ was $C^0_{total}\Delta x = 9.999999999999990e-01$. We used a constant data $u_0(x) = 0.06$. For this the initial numerical mass was $C^0_{total}\Delta x = 6.000000000000152e-02$ for $\Delta x = 1/2000$.

First we will show the results for the single domain diffusion equations with the above initial data. Then we present them for the bi-domain with the cosine initial data as well as piecewise constant initial data. For the piecewise constant data we took $u_0(x) = 0.06$ for $x \in [0, 1/2]$ and $v_0(x) = 700$ for $x \in [1/2, 1]$. The exact initial mass is $\frac{1}{2}(700 + 0.06) = 350.03$ and the initial numerical was $C^0_{total}\Delta x = 3.500300000000000e{+}02$ for $\Delta x = 1/2000$.

5.5.1 Single domain diffusion equation

Here we give the numerical results for the single domain diffusion equation with homogeneous Neumann boundary conditions. We obtained the results for the initial data given above with the diffusion coefficient $D = 0.001$ and fixed spatial step size $\Delta x = 1/2000$, time step $\Delta t = (\Delta x)^2/3D = 8.3333e-05$. For times t_n with $n = 0, 200, \ldots, 1200$ and $M = 1200$ the numerical total mass obtained via the FTCS scheme is given in the table in Figure 5.2. The results are plotted in Figure 5.3. For the same data we also calculated the result via the explicit finite volume cell based method. The result can be seen in table form in Figure 5.4 and plotted in Figure 5.5. Note that solution plots for the explicit FTCS and for the finite volume cell based in case are given in Figure 7.3.

We see that the conservation of mass is achieved up to some rounding error. This is also seen in the oscillatory behavior of the plots in Figures 5.3 and 5.5.

5.5.2 Discrete mass conservation for the bi-domain diffusion equations with various coupling conditions

Here we give the numerical results for the bi-domain diffusion equations with various coupling conditions.

DN-coupling

Here we give various possible test cases for the identical and distinct diffusion coefficients as well as with various initial conditions. As we explained in Chapter 4, for identical diffusion coefficients on the sub-domains the explicit, implicit monolithic and the finite volume methods give us the identical scheme to the single domain. The same observation we obtain here in the numerical computations of the discrete mass conservation. We get exactly the same values for the identical diffusion coefficients $D_- = D_+ = 0.001$ in the

Figure 5.2: **Single domain:** Table for the total concentration via explicit finite difference method (FTCS) with initial data $w_0(x) = cos(\pi x) + 1$ and a constant data $w_0(x) = 0.06$, with diffusion coefficient $D = 0.001$ and with $\Delta x = 1/2000$.

Number of time steps n	S-Domain FD (cosine data)	S-Domain FD (constant data)
0	9.999999999999990e-01	6.000000000000152e-02
200	1.000000000000002e+00	6.000000000000152e-02
400	1.000000000000002e+00	6.000000000000152e-02
600	1.000000000000003e+00	6.000000000000152e-02
800	1.000000000000003e+00	6.000000000000152e-02
1000	1.000000000000003e+00	6.000000000000152e-02
1200	1.000000000000006e+00	6.000000000000152e-02

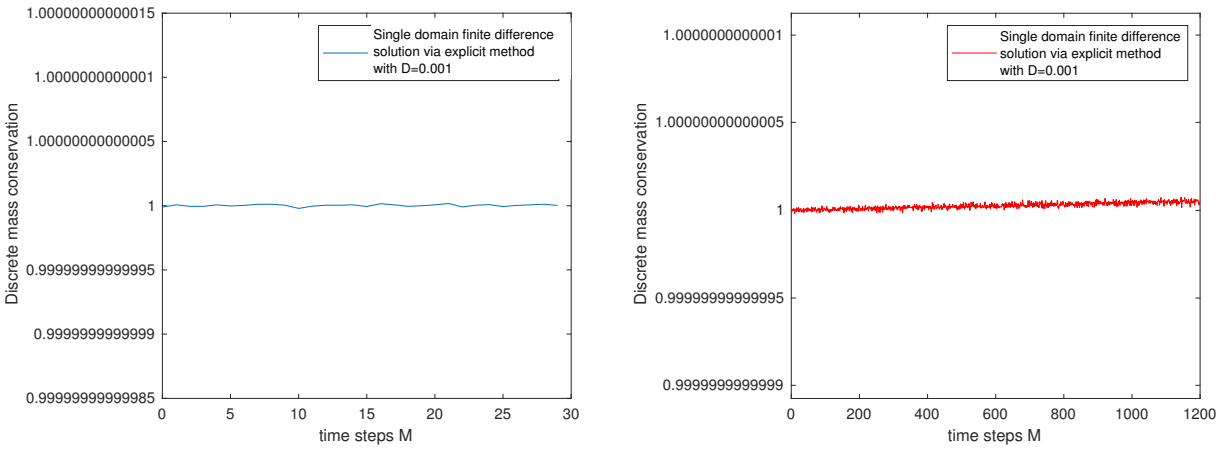

(a) (b)

Figure 5.3: **Single domain:** The figure in the left panel is the result for the the single domain diffusion equation via explicit nodal based method for the first 30 time steps and the figure in the right panel is for the number of time steps $M = 1200$, $\Delta x = 1/2000$, with initial data $w_0(x) = \cos(\pi x) + 1$ and the diffusion coefficient $D = 0.001$.

Figure 5.4: **Single domain:** Table for the total concentration via the finite volume method with initial data $w_0(x) = cos(\pi x)+1$ and a constant data $w_0(x) = 0.06$, with diffusion coefficient $D = 0.001$ and $\Delta x = 1/2000$.

Number of time steps n	S-Domain FV(cosine data)	S-Domain FV(constant data)
0	9.999999999999976e-01	6.000000000000152e-02
200	1.000000000000001e+00	6.000000000000152e-02
400	1.000000000000000e+00	6.000000000000152e-02
600	1.000000000000001e+00	6.000000000000152e-02
800	9.999999999999993e-01	6.000000000000152e-02
1000	9.999999999999993e-01	6.000000000000152e-02
1200	1.000000000000000e+00	6.000000000000152e-02

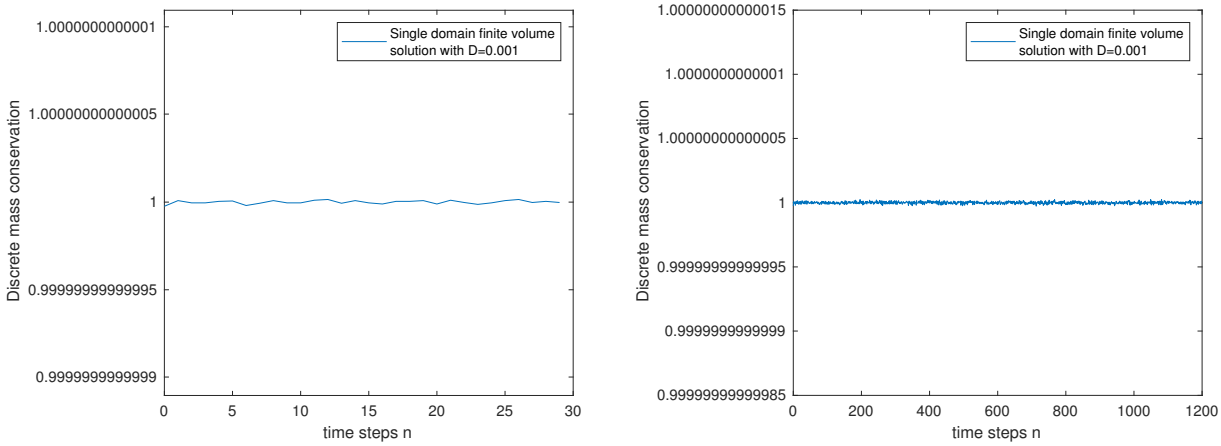

(a) (b)

Figure 5.5: **Single domain:** The figure in the left panel is the result for the the single domain diffusion equation via finite volume cell based method for the first 30 time steps and the figure in the right panel is for the number of time steps $M = 1200$, $\Delta x = 1/2000$, with initial data $w_0(x) = \cos(\pi x) + 1$ and the diffusion coefficient $D = 0.001$.

Figure 5.6: **Bi-domain with DN-coupling $D_- \neq D_+$:** Table for the total concentration for the DN-coupling of our scheme via explicit coupling method with initial data $u_0(x) = \cos(\pi x)+1$ and a constant data $u_0(x) = 0.06$, $v_0(x) = 700$ with distinct diffusion coefficients $D_- = 0.001$, $D_+ = 0.003$ and $\Delta x = 1/2000$.

Number of time steps n	Bi-domain(cosine data)	Bi-domain(constant data)
0	9.999999999999990e-01	3.500300000000000e+02
200	9.999999999999999e-01	3.500300000000001e+02
400	1.000000000000000e+00	3.500300000000001e+02
600	1.000000000000001e+00	3.500300000000003e+02
800	1.000000000000002e+00	3.500300000000004e+02
1000	9.999999999999992e-01	3.500300000000004e+02
1200	9.999999999999988e-01	3.500300000000007e+02

DN-coupling scheme via explicit finite difference coupled method which are given in table form shown in Figure 5.2. So there is no need to show again the identical table.

Now we give the results for un-equal diffusion coefficients $D_- = 0.001$, $D_+ = 0.003$. We will compare our results of the DN-coupling with the Giles scheme. These are given as follows.

DN-coupling of our scheme

First we give the results of our DN-coupling scheme for the initial data $u_0(x) = \cos(\pi x)+1$ and then for a piecewise continuous initial data $u_0(x) = 0.06$, $v_0(x) = 700$ with distinct diffusion coefficients $D_- = 0.001$, $D_+ = 0.003$ and with spatial step size $\Delta x = 1/2000$. The results are given in table form in Figure 5.6. The plot for the cosine initial data can be seen in Figure 5.7 and for the piecewise constant data in Figure 5.8. Note that solution plots for this case are given in Figure 7.8.

DN-coupling of the Giles scheme

We noticed in the derivation of conservativity for the DN-coupling in this chapter that the DN-coupling of the Giles scheme is not-conservative. Now analogously we calculated the total mass for the Giles scheme with cosine initial data $u_0(x) = \cos(\pi x) + 1$. We observed that for the equal diffusion coefficients we did not observe any difference to our scheme. The effect seems to small and there may be cancellation.

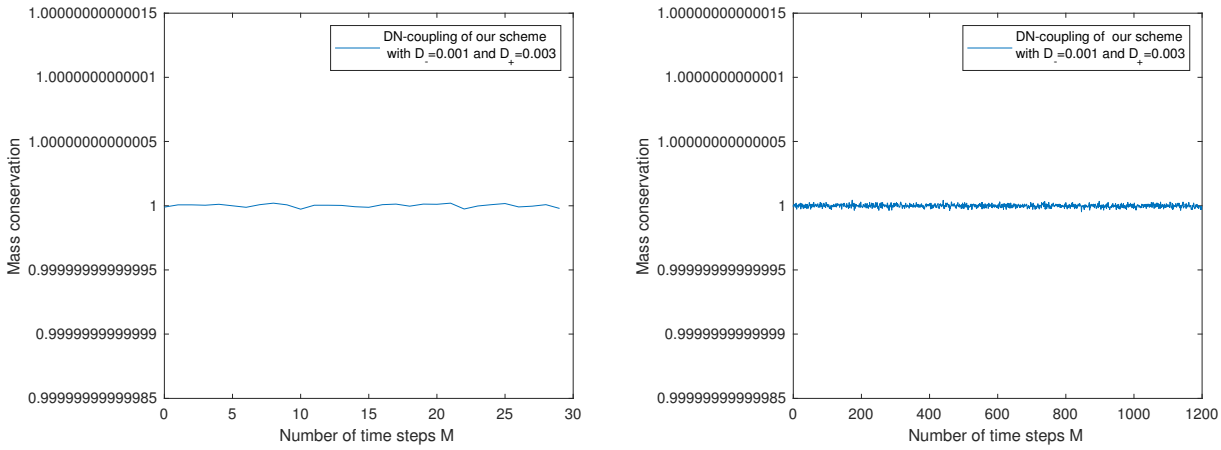

(a) (b)

Figure 5.7: **Bi-domain with DN-coupling $D_- \neq D_+$:** The figure in the left panel is the result for the DN-coupling of our scheme with initial data $u_0(x) = \cos(\pi x) + 1$ for the first 30 time steps and the figure in the right panel is for the number of time steps $M = 1200$, $\Delta x = 1/2000$ and with un-equal diffusion coefficients $D_- = 0.001$ and $D_+ = 0.003$.

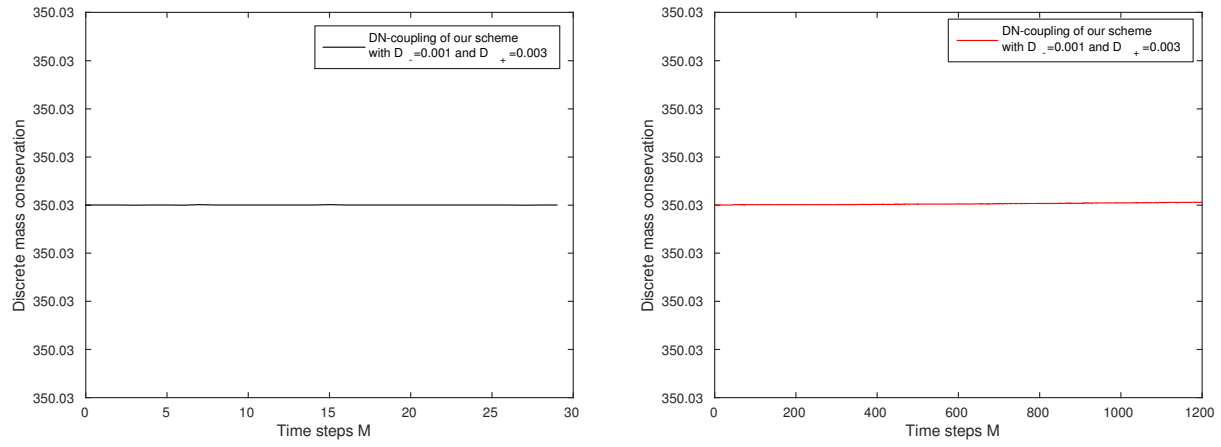

(a) (b)

Figure 5.8: **Bi-domain with DN-coupling $D_- \neq D_+$:** The figure in the left panel is the result for the DN-coupling of our scheme with initial data$u_0(x) = 0.06\ MOl$ for $x \in [0, 1/2]$ and $v_0(x) = 700$ for $x \in [1/2, 1]$ for the first 30 time steps and the figure in the right panel is for the number of time steps $M = 1200$, $\Delta x = 1/2000$ and with un-equal diffusion coefficients $D_- = 0.001$ and $D_+ = 0.003$.

Figure 5.9: **Bi-domain Giles scheme:** Table for the total concentration for the DN-coupling of the Giles scheme via explicit coupling method with initial data $u_0(x) = \cos(\pi x) + 1$ and a constant data $u_0(x) = 0.06$, $v_0(x) = 700$ with distinct diffusion coefficients $D_- = 0.001$, $D_+ = 0.003$ and with fixed $\Delta x = 1/2000$.

Number of time steps n	Bi-domain (cosine data)	Bi-domain (constant data)
0	9.999999999999990e-01	3.500300000000000e+02
200	9.999984188476869e-01	3.500539581974912e+02
400	9.999977857641400e-01	3.500538070485182e+02
600	9.999973002356525e-01	3.500537402329856e+02
800	9.999968911104437e-01	3.500537004361507e+02
1000	9.999965308296236e-01	3.500536732895834e+02
1200	9.999962052584714e-01	3.500536532564224e+02

With distinct diffusion coefficients $D_- = 0.001$, $D_+ = 0.003$ we get completely different results. They are given for the different number of time steps in the table in Figure 5.9. The plot of these results can be seen for the cosine initial data in Figure 5.10 and for the piecewise constant data in Figure 5.11. They show the non-conservativity of the scheme. Note that the solution plots for this case with comparison of our DN-coupling scheme are given in Figure 7.16.

In Figure 5.11 we observe that after initial strong deviation of the total concentration the non-conservativity become smaller. This becomes clear when looking at both the error in conservation in (5.20) together with the solution plot in Figure 7.16. We have $\nu_- < \nu_+$. But the slops of the solution concentration this difference since $u_m^n - u_{m-1}^n > v_{m+1}^n - v_m^n$. This makes the difference between $\nu_-(u_m^n - u_{m-1}^n)$ and $\nu_+(v_{m+1}^n - v_m^n)$ and thereby the error in conservativity much smaller.

Discrete mass conservation for the heat flux coupling

Here we give the results for the heat flux coupling conditions. We used both the one sided and the central difference method as numerical coupling conditions. As we explained in the derivation of the discrete mass conservation that the discretizations of the boundary conditions as well as the interface conditions via one sided methods does not maintain the conservativity, while the central difference method maintains the conservativity.

First we calculate the total mass for the heat flux conditions via one sided and central difference method for the initial data $u_0(x) = \cos(\pi x) + 1$. We took un-equal diffusion coefficients $D_- = 0.001$ and $D_+ = 0.003$, with $\Delta x = 1/2000$. The values for different

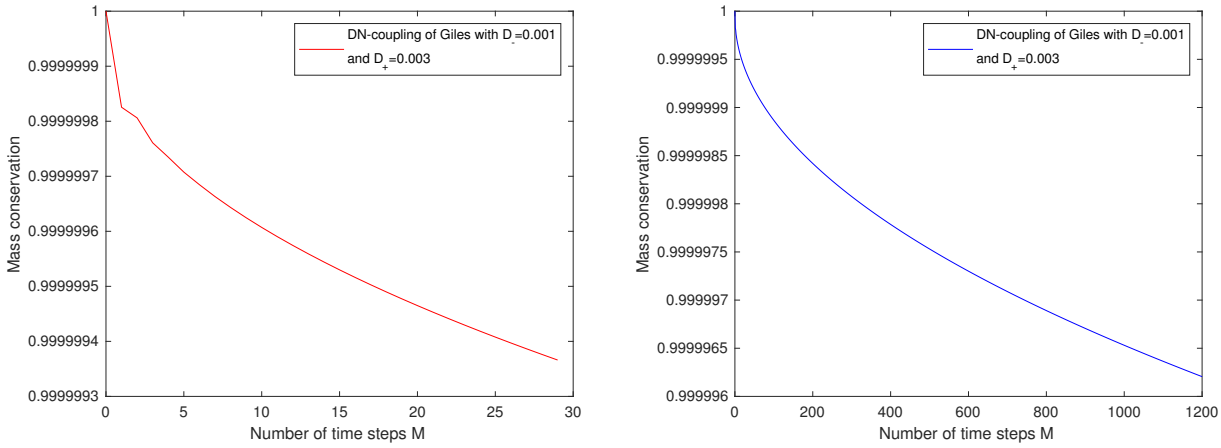

(a) (b)

Figure 5.10: **Bi-domain Giles scheme:** The figure in the left panel is the result of the DN-coupling of Giles scheme with initial data $u_0(x) = \cos(\pi x) + 1$ for the first 30 time steps and the figure in the right panel is for the number of time steps $M = 1200$ and $\Delta x = 1/2000$ with initial data $u_0(x) = \cos(\pi x) + 1$ and with un-equal diffusion coefficients $D_- = 0.001$ and $D_+ = 0.003$.

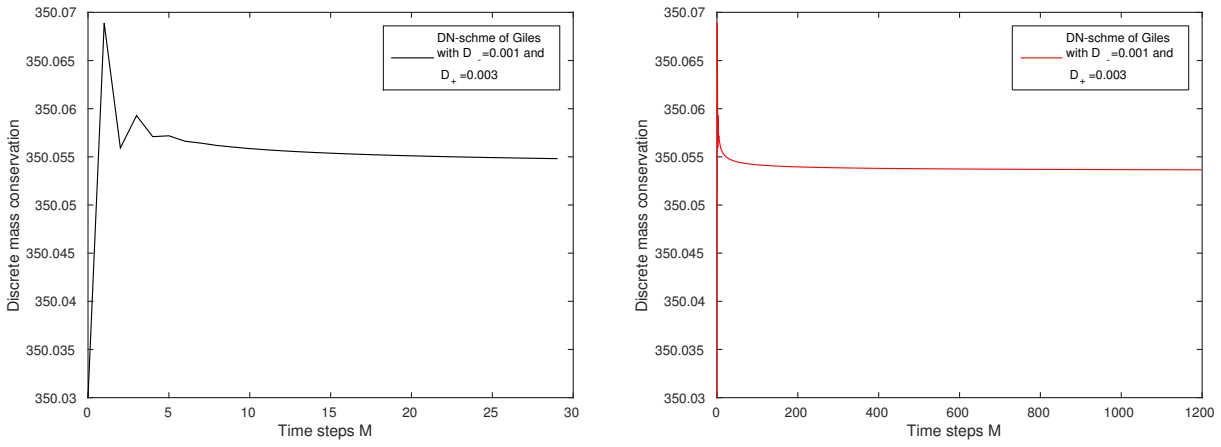

(a) (b)

Figure 5.11: **Bi-domain Giles scheme:** The figure in the left panel is the result for the DN-coupling of the Giles scheme for the first 30 time steps and the figure in the right panel is for the number of time steps $M = 1200$ with initial data $u_0(x) = 0.06\ MOl$ for $x \in [0, 1/2]$ and $v_0(x) = 700$ for $x \in [1/2, 1]$. These are for un-equal diffusion coefficients $D_- = 0.001$ and $D_+ = 0.003$.

Figure 5.12: **Bi-domain with heat flux conditions:** Table for the total concentration for the heat flux conditions via one sided and central difference methods with explicit coupling method with initial data $u_0(x) = \cos(\pi x)+1$, with distinct diffusion coefficients $D_- = 0.001$, $D_+ = 0.003$ and with $\Delta x = 1/2000$.

Number of time steps n	Bi-domain (cosine data one sided)	Bi-domain (cosine data with central)
0	9.999999999999990e-01	9.999999999999990e-01
200	1.000002556825716e+00	9.999999999999991e-01
400	1.000003801641210e+00	1.000000000000001e+00
600	1.000004763164191e+00	1.000000000000000e+00
800	1.000005575743941e+00	1.000000000000001e+00
1000	1.000006292459160e+00	1.000000000000001e+00
1200	1.000006940785814e+00	9.999999999999997e-01

time steps are given in table in Figure 5.12. The plots for the one sided method can be seen in Figure 5.14 and the plots for the central difference is given in Figure 5.15.

Also we used the piecewise continuous initial data $u_0(x) = 0.06$ and $v_0(x) = 700$ both methods. The numerical values for the different time steps are given in the table in Figure 5.13. The plots for the one sided difference are given in Figure 5.16 and for central difference method in Figure 5.17. Note that solution plots for this case via the central difference method are given in Figure 7.19 for the cosine initial data and for the discrete data in Figure 7.29. From these tables and graphical representations again we conclude that the one sided difference nodal based clearly does not maintain the conservativity, while the one sided finite volume cell based scheme maintains. Further central difference maintains discrete mass conservativity.

5.5.3 Discrete mass conservation of channel pumping, simplified channel pumping, linearized membrane pumping, membrane pumping coupling conditions (explicit and implicit discretization

Here, only we give a result for the membrane pumping conditions via one sided and central difference methods. The other coupling conditions are analogous to this for calculation of the discrete mass conservation. Also for this coupling conditions we use two kinds of initial data.

First we calculate the total mass via one sided and central difference method for the initial data $u_0(x) = \cos(\pi x) + 1$. We took un-equal diffusion coefficients $D_- = 0.001$ and

Figure 5.13: **Bi-domain with heat flux conditions:** Table for the total concentration for the heat flux conditions via one sided and central difference methods with explicit coupling method with constant data $u_0(x) = 0.06$, $v_0(x) = 700$ with distinct diffusion coefficients $D_- = 0.001$, $D_+ = 0.003$ and with $\Delta x = 1/2000$.

Number of time steps n	Bi-domain (constant data one sided)	Bi-domain(constant data with central)
0	3.500300000000000e+02	3.500300000000000e+02
200	3.499921275178879e+02	3.500300000000001e+02
400	3.499895408254793e+02	3.500300000000001e+02
600	3.499883762386270e+02	3.500300000000002e+02
800	3.499876776247660e+02	3.500300000000004e+02
1000	3.499871992418964e+02	3.500300000000004e+02
1200	3.499868453569094e+02	3.500300000000005e+02

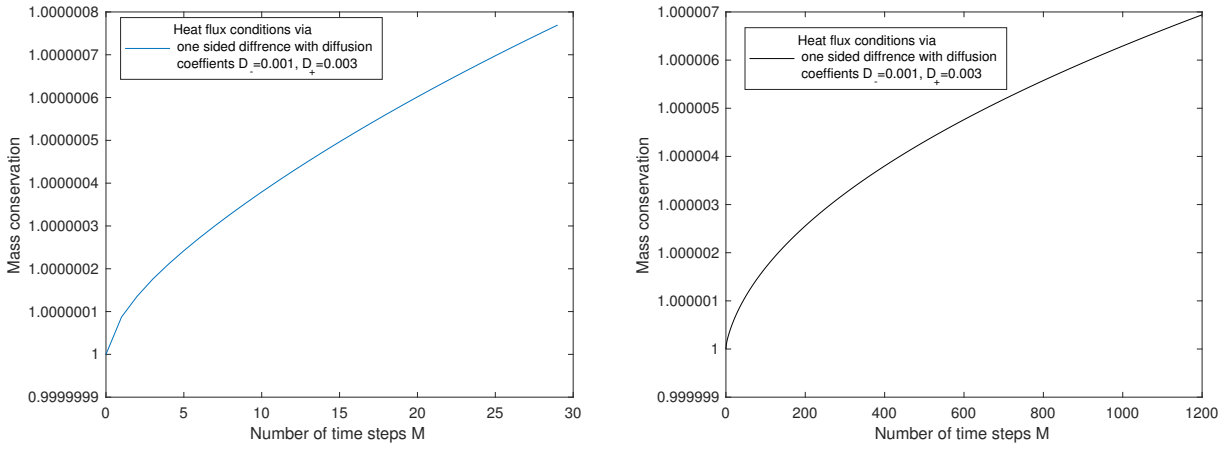

(a) (b)

Figure 5.14: **Bi-domain with heat flux conditions:** The figure in the left panel is for the heat flux conditions via one sided difference with $u_(0) = \cos(\pi x) + 1$ for the first 30 time steps and the figure in the right panel is for the number of time steps $M = 1200$ and $\Delta x = 1/2000$.

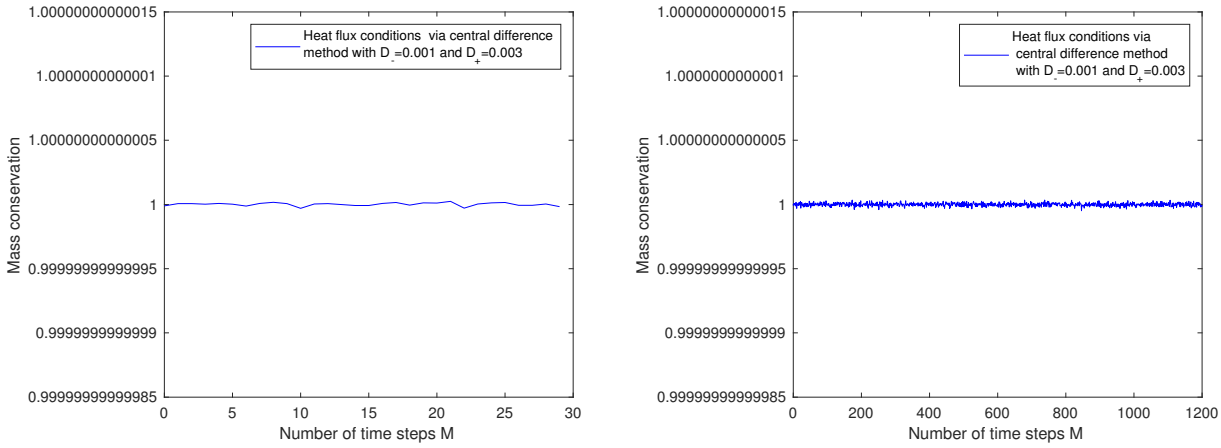

(a) (b)

Figure 5.15: **Bi-domain with heat flux conditions:** The figure in the left panel is for the heat flux conditions via central difference with piecewise constant $u_0(x) = \cos(\pi x) + 1$ for the first 30 time steps and the figure in the right panel is for the number of time steps $M = 1200$ and $\Delta x = 1/2000$.

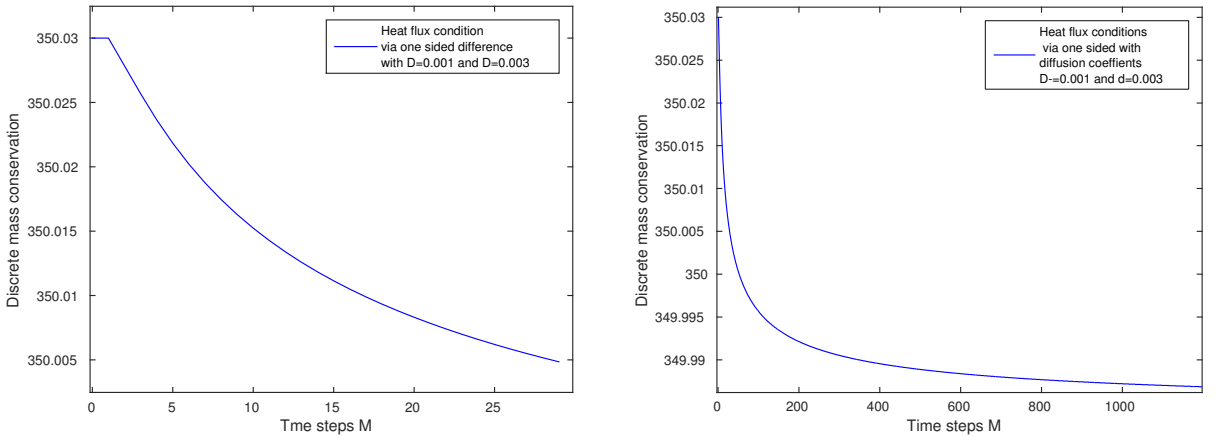

(a) (b)

Figure 5.16: **Bi-domain with heat flux conditions:** The figure in the left panel is for the heat flux conditions via one sided difference with piecewise constant initial data $u_0(x) = 0.06$ and $v_0(x) = 700$ for first 30 time steps and the figure in the right panel is for the number of time steps $M = 1200$ and $\Delta x = 1/2000$.

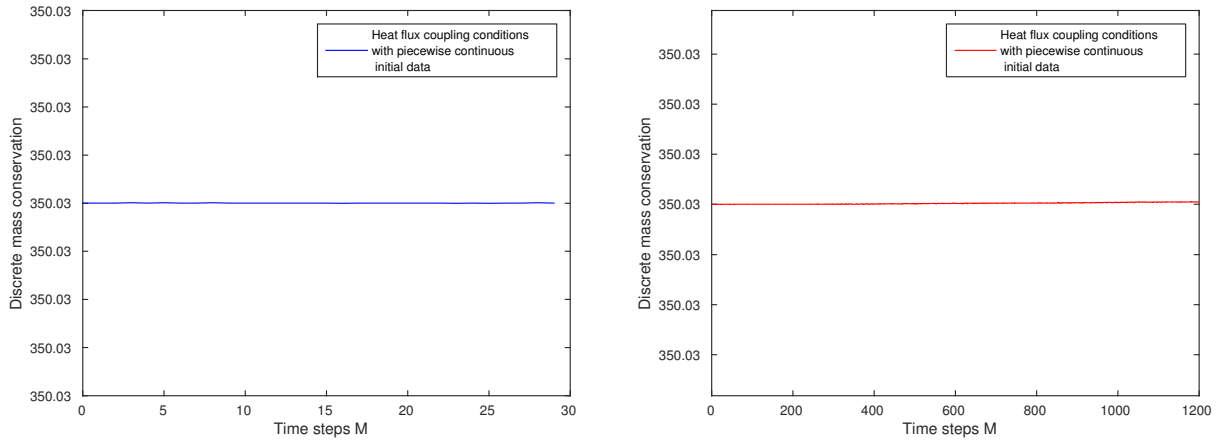

(a) (b)

Figure 5.17: **Bi-domain with heat flux conditions:** The figure in the left panel is for the heat flux conditions via central difference for the initial data $u_0(x) = 0.06$ and $v_0(x) = 700$ for first 30 time steps and the figure in the right panel is for the number of time steps $M = 1200$ and $\Delta x = 1/2000$.

$D_+ = 0.003$, with $\Delta x = 1/2000$. The values for the different time steps are given in the table in Figure 5.18. The plot for the one sided method can be seen in Figure 5.14 and the plots for the central difference gives us the similar oscillatory behavior plotted for the heat flux conditions in Figure 5.15.

Then we calculate for the piecewise constants data $u_0(x) = 0.06\ MOl$ for $x \in [0, 1/2]$ and $v_0(x) = 700$ for $x \in [1/2, 1]$ with diffusion coefficients $D_- = 0.001$, $D_+ = 0.003$ and the spatial step size $\Delta x = 1/2000$. The results for the various time steps are given in table in Figure 5.19. For the one sided difference method the plot is given in Figure 5.21. Again with central difference method we get an oscillatory behavior similar to the heat flux conditions given in Figure 5.17. So there is no need to give a repetitive figure. Note that solution plots for this case via central difference method are given in Figure 7.34.

Again we conclude that the one sided difference clearly does not maintain conservativity for the nodal based explicit method. But for the cell based finite volume maintain the conservativity. Further the central difference method maintains the conservativity for the discretization of the coupling interface conditions with nodal based discretization.

Figure 5.18: **Bi-domain with membrane pumping conditions:** Table for the total concentration for the membrane pumping conditions via one sided difference and central difference method via explicit coupling method with initial data $u_0(x) = \cos(\pi x) + 1$ with distinct diffusion coefficients $D_- = 0.001$, $D_+ = 0.003$ and with spatial step size $\Delta x = 1/2000$.

Number of time steps n	Bi-domain (cosine data one sided)	Bi-domain (cosine data with central)
0	9.999999999999990e-01	9.999999999999990e-01
200	9.999918858054577e-01	9.999999999999994e-01
400	9.999878828223312e-01	1.000000000000000e+00
600	9.999848044040148e-01	1.000000000000001e+00
800	9.999822067332306e-01	1.000000000000001e+00
1000	9.999799168706344e-01	9.999999999999997e-01
1200	9.999778458817771e-01	9.999999999999999e-01

Figure 5.19: **Bi-domain with membrane pumping conditions:** Table for the total concentration of the membrane pumping conditions via one sided and central difference with explicit coupling method with piecewise constant initial data $u_0(x) = 0.06$, $v_0(x) = 700$ with distinct diffusion coefficients $D_- = 0.001$, $D_+ = 0.003$ and with and with spatial step size $\Delta x = 1/2000$.

Number of time steps n	Bi-domain (constant data one sided)	Bi-domain (constant data central)
0	3.500300000000000e+02	3.500300000000000e+02
200	3.500255961726344e+02	3.500300000000001e+02
400	3.500268669222047e+02	3.500300000000001e+02
600	3.500274322830616e+02	3.500300000000002e+02
800	3.500277692893970e+02	3.500300000000003e+02
1000	3.500279989790556e+02	3.500300000000004e+02
1200	3.500281682206184e+02	3.500300000000005e+02

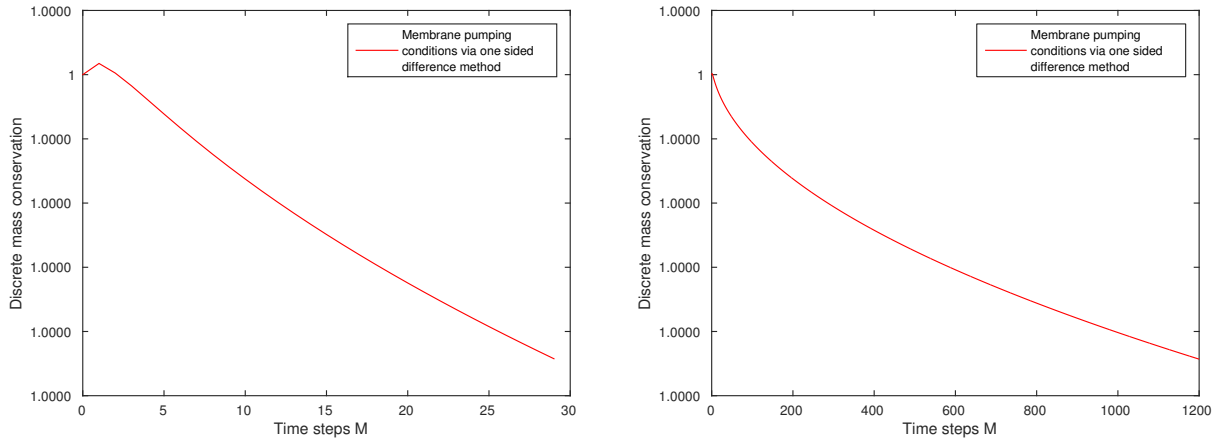

(a) (b)

Figure 5.20: **Bi-domain with membrane pumping conditions:** The figure in the left panel is for the membrane pumping condition via one sided difference method with cosine initial data $u_0(x) = \cos(\pi x) + 1$ for first 30 time steps and the figure in the right panel is for the number of time steps $M = 1200$ and with spatial step size $\Delta x = 1/2000$.

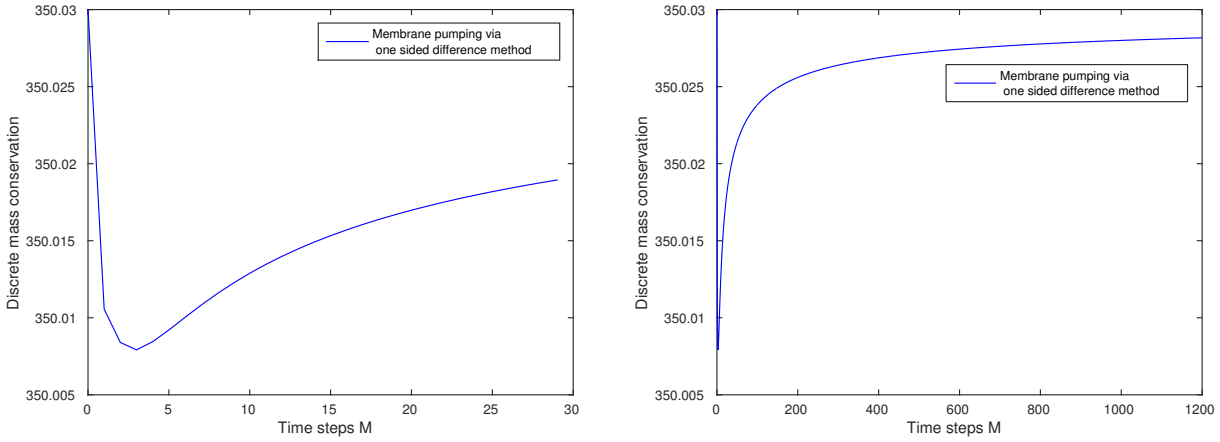

(a) (b)

Figure 5.21: **Bi-domain with membrane pumping conditions:** The figure in the left panel is for the membrane pumping conditions via one sided difference method for the initial piecewise constant data $u_0(x) = 0.06$ and $v_0(x) = 700$ for first 30 time steps and the figure in the right panel is for the number of time steps $M = 1200$ and with spatial step size $\Delta x = 1/2000$.

Chapter 6

Stability analysis

In this chapter we recall the von Neumann stability for the single domain diffusion equation and apply the Godunov-Ryabenkii stability analysis to boundary conditions as well as to various coupling conditions for the bi-domain diffusion equation as discussed in Chapter 3.

In the first section we discuss the well-known von Neumann stability analysis and the Godunov-Ryabenkii stability for the single domain diffusion equation with boundary conditions. In the second section we show the GR-stability for the Dirichlet-Neumann coupling conditions and in the third section for the heat flux coupling conditions. In fourth section we explain the GR-stability for the linearized membrane pumping coupling interface conditions. In Section 5 we discuss the GR-stability analysis for the implicit case.

6.1 The single domain case

The stability of numerical schemes is closely associated with the boundedness of numerical solutions, a necessary condition for convergence. For the time-dependent problems, stability guarantees that the numerical method produces a bounded solution whenever the solution of the exact differential equation is bounded. Numerical solutions to unstable schemes tend to blow up quite rapidly. Stability, in general, can be difficult to investigate. This is especially true when the equation under consideration is nonlinear.

6.1.1 Von Neumann interior stability (explicit case)

In order to determine the Courant-Friedrichs-Levy condition for the stability of an explicit solution of a time dependent PDE one uses the von Neumann stability analysis. To do this we assume that the solution is of the form $w_j^n = \lambda^n e^{i\alpha j}$ where λ represents the time dependence of the solution and the exponential represents the spatial dependence, α is a real parameter, see the book of Godunov and Ryabenkii [11, Ch. 8]. We substitute this into the finite difference formula (3.11). Using $\nu = D\frac{\Delta t}{\Delta x^2}$ we obtain the following form

$$\lambda - 1 = \nu(e^{-i\alpha} - 2 + e^{i\alpha}). \tag{6.1}$$

Noting that

$$\frac{e^{-i\alpha} - 2 + e^{i\alpha}}{4} = -\left(\frac{e^{i\frac{\alpha}{2}} - e^{-i\frac{\alpha}{2}}}{2i}\right)^2 = -\sin^2\frac{\alpha}{2} \tag{6.2}$$

we get

$$\lambda(\alpha) = 1 - 4\nu\sin^2\frac{\alpha}{2}. \tag{6.3}$$

As α varies the quantity $\lambda(\alpha)$ traverses the interval $1 - 4\nu \leq \lambda \leq 1$ of the real axis. For stability $|\lambda| \leq 1$ it is necessary that the left end of the interval lies in the unit circle so that we have $1 - 4\nu \geq -1$ or

$$0 < \nu \leq \frac{1}{2}. \tag{6.4}$$

If $\nu > \frac{1}{2}$, the point $\lambda(\alpha) = 1 - 4\nu\sin^2(\frac{\alpha}{2})$ corresponding to $\alpha = \pi$ lies to the left of the point -1 on the real axis. The harmonic $\exp(i\pi j) = (-1)^j$ gives rise to the unstable solution

$$w_j^n = (1 - 4\nu)^n(-1)^j$$

which does not satisfy the standard condition for the stability analysis $|\lambda| \leq 1$ for the interior domain, see Godunov and Ryabenkii [11] or Morton and Mayers [24].

6.1.2 Godunov-Ryabenkii (GR)-stability for the interior domain

The problem considered in our main study is not periodic, so we cannot apply the usual von Neumann stability analysis to boundary or coupling conditions. The stability analysis that we use for our boundary condition and the coupled interface equation is the so-called Godunov-Ryabenkii (GR)-stability. The GR-stability, see e.g. Godunov and Rybenkii [11], relies on a normal mode representation which generalizes the von Neumann stability by replacing Fourier modes with local modes as powers giving quasi-eigen vectors as explained in Godunov and Ryabenkii [11]. Also Gustafsson [12] gave details for the Godunov-Ryabenkii condition "The beginning of a new stability theory".

The same stability analysis has been used by Giles [10], Roe et al. [33] and Errera et al. [6] for coupling problems. We will give a more precise way of doing the analysis. We include for comparison the treatment of the outer boundary conditions which we handle first.

First, we recall the GR-stability for the single domain difference equation defined in (3.11) with the homogeneous Neumann boundary conditions $\frac{\partial w(0,t)}{\partial x} = 0$ and $\frac{\partial w(1,t)}{\partial x} = 0$, i.e. (3.16) and (3.17). We write the discretization of this boundary value problem together as the following system

$$\begin{aligned} w_0^{n+1} &= 2\nu w_1^n + (1 - 2\nu)w_0^n && \text{for } j = 0 \\ w_j^{n+1} &= \nu w_{j-1}^n + (1 - 2\nu)w_j^n + \nu w_{j+1}^n && \text{for } 0 < j < m \\ w_N^{n+1} &= 2\nu w_{N-1}^n + (1 - 2\nu)w_N^n && \text{for } j = N. \end{aligned} \tag{6.5}$$

We substitute as a preliminary step $w_j^n = c\lambda^n w_j$ with $c \neq 0$ into (6.5) for $0 < j < m$ to get the following second order difference equation

$$w_{j+1} + \left(\frac{1-(2\nu+\lambda)}{\nu}\right) w_j + w_{j-1} = 0. \tag{6.6}$$

Note that here the constant c drops out of the equation. In the analysis for some boundary and coupling conditions this will not be the case. To get the characteristic equation we substitute the normal solution $w_j^n = c\lambda^n q^j$ into the difference equation (6.5) for $0 < j < m$. After simplification we get the following characteristic equation

$$p(q) = q^2 + \left(\frac{1-\lambda}{\nu} - 2\right) q + 1 = 0. \tag{6.7}$$

Now we have to consider two cases.

If $|q| = 1$, then we may set $q = \exp(i\alpha)$ for $\alpha \in [0, 2\pi]$. This is the case of von Neumann stability. Inserting the mesh function $w_j^n = \lambda^n e^{i\alpha j}$ into (6.5) for $0 < j < m$ gives (6.1). This mesh function is bounded as $j \to \pm\infty$. The analysis leads to (6.3)

$$\lambda = 1 - 4\nu \sin^2(\frac{\alpha}{2}) \qquad \text{for } \ 0 \le \alpha \le 2\pi.$$

Thus again we obtain the bounds $1 - 4\nu \le \lambda \le 1$ on the real axis and (6.4) as stability condition.

The normal mode equation for the discretized diffusion equation and its roots

We will have to discuss the case with $|q_{1,2}| \neq 1$ in order to carry out the stability analysis for the boundary conditions and later the coupling conditions. For this we need to prove some results about the selection of the root that has modulus less than or equal to 1. This selection plays an important role in this whole analysis of the Godunov-Ryabenkii stability. We apply the stability theory to determine the existence of separable normal modes of the form $c\lambda^n q^j$ at nodal points j and time steps n.

We consider the scheme under the stability condition $0 < \nu \le \frac{1}{2}$. The quadratic equation (6.7) has the solutions

$$\begin{aligned} \widetilde{q}_{1,2}(\nu,\lambda) &= 1 - \frac{1-\lambda}{2\nu} \mp \frac{1}{2}\sqrt{(\frac{1-\lambda}{\nu} - 2)^2 - 4} \\ &= 1 - \frac{1-\lambda}{2\nu} \mp \frac{1}{2}\sqrt{\frac{(1-\lambda)^2}{\nu^2} - 4\frac{1-\lambda}{\nu}} \\ &= 1 + \frac{\lambda-1}{2\nu} \mp \frac{1}{2}\sqrt{\frac{\lambda-1}{\nu} \cdot \frac{\lambda+4\nu-1}{\nu}}. \end{aligned} \tag{6.8}$$

For the complex roots we take their principle value with angle $]-\pi, \pi]$, see Abramowitz and Stegun [1]. We reformulate (6.8) to

$$q_{1,2}(\nu,\lambda) = 1 + \frac{\lambda-1}{2\nu} \mp \frac{\sqrt{\lambda-1}}{2\nu}\sqrt{\lambda+4\nu-1} \tag{6.9}$$

where q_1 is the solution with the minus sign. Another useful reformulation of the roots was given by Giles [10]. We write it as

$$q_{1,2}(\nu,\lambda) = 1 + \frac{\lambda-1}{2\nu}\Big[1 \mp \sqrt{1+\frac{4\nu}{\lambda-1}}\Big]. \tag{6.10}$$

Due to the properties of the principal complex roots we have $q_1(\nu,\lambda) = \widetilde{q}_1(v,\lambda)$ from (6.8) only for $\mathrm{Re}\lambda \geq 0$ and $\lambda \neq iy$ for $y < 0$. On the complementary set $\mathrm{Re}\lambda \leq 0$ and $\lambda \neq iy$ for $y > 0$ we have $q_1(\nu,\lambda) = \widetilde{q}_2(\nu,\lambda)$.

Since $p(q) = (q-q_1)(q-q_2) = q^2 - (q_1+q_2)q + q_1q_2$ we have $q_1q_2 = 1$ or $q_2 = q^{-1}$ from (6.7). We prove the following lemma.

Lemma 1. *The solutions q_1, q_2 given by (6.9) satisfy $|q_1| \leq 1$ and $|q_2| \geq 1$ for all $\lambda \in \mathbb{C}$ and all $\nu > 0$. We have $|q_1| = |q_2| = 1$ iff $\lambda \in [1-4\nu, 1] \subset \mathbb{R}$. Further q_1, $q_2 \in \mathbb{C}\backslash\mathbb{R}$ holds if $\lambda \in]1-4\nu, 1[$ and q_1, $q_2 \in \mathbb{R}$ if $\lambda \in \mathbb{R}\backslash]1-4\nu, 1[$.*

Proof. First let us consider $\nu = \frac{1}{2}$. Then we have

$$q_{1,2} = \lambda \mp \sqrt{\lambda-1}\sqrt{\lambda+1}.$$

Since $q_2 = q_1^{-1}$ is suffices to prove the statements for q_2. We have for $\lambda \in \mathbb{C}\backslash]-\infty, 1[$

$$\begin{aligned} |q_2|^2 &= \left|\lambda + \sqrt{\lambda-1}\sqrt{\lambda+1}\right|^2 \\ &= |\lambda|^2 + |\lambda-1||\lambda+1| + 2\mathrm{Re}(\lambda\sqrt{\overline{\lambda}-1}\sqrt{\overline{\lambda}+1}). \end{aligned}$$

The restriction is due to the fact that $\overline{\sqrt{z}} = \sqrt{\overline{z}}$ holds only for $z \in \mathbb{C}\backslash]-\infty, 0[$. Let us set $\lambda = x + iy$. Then we first want to show that

$$|\lambda|^2 + |\lambda-1||\lambda+1| = x^2 + y^2 + \sqrt{(x-1)^2+y^2}\sqrt{(x+1)^2+y^2} \geq 1.$$

For $|\lambda| > 1$, i.e. $x^2 + y^2 > 1$, we have $|\lambda|^2 + |\lambda-1||\lambda+1| > 1$. For $|\lambda| \leq 1$ or $x^2 + y^2 \leq 1$ the above inequality is equivalent to

$$((x-1)^2+y^2)((x+1)^2+y^2) \geq (1-(x^2+y^2))^2 \quad = 1 + (x^2+y^2)^2 - 2(x^2+y^2).$$

Let us first consider the left hand side and multiply it out

$$\begin{aligned} (x^2-1)^2 + y^2((x+1)^2 + (x-1)^2) + y^4 &= x^4 + 1 - 2x^2 + y^2(x^2+1+2x) + y^2(x^2+1-2x) + y^4 \\ &= 1 + x^4 + y^4 - 2x^2 + 2y^2 + 2x^2y^2. \end{aligned}$$

Adding $2(x^2+y^2)$ to the inequality leads to

$$1 + x^4 + y^4 + 4y^2 + 2x^2y^2 \geq 1 + x^4 + y^4 + 2x^2y^2$$

or equivalently

$$4y^2 \geq 0.$$

So $|\lambda|^2 + |\lambda - 1||\lambda + 1| \geq 1$ for all $\lambda \in \mathbb{C}\backslash]-\infty, 1[$. Note that $1 < |\lambda|^2 + |\lambda - 1||\lambda + 1|$ holds for $\lambda \in \mathbb{C}\backslash]-\infty, 1]$.

Now we want to show that the remaining term satisfies

$$\mathrm{Re}(\lambda\sqrt{\overline{\lambda} - 1}\sqrt{\overline{\lambda} + 1}) \geq 0$$

for $\lambda \in \mathbb{C}\backslash]-\infty, 1[$. We introduce the function

$$\mathrm{sign}^+(y) = \begin{cases} 1 & \text{for } y \geq 0 \\ -1 & \text{for } y < 0. \end{cases}$$

Then we have the following formula, see e.g. Abramowitz and Stegun [1, 3.7.27] for the principal value of the square square root of any complex number $z = x + iy$

$$\sqrt{z} = \sqrt{\frac{|z| + x}{2}} + i\ \mathrm{sign}^+(y)\sqrt{\frac{|z| - x}{2}}$$

where all roots are real and positive. This gives for $\lambda = x + iy$

$$\begin{aligned} \sqrt{\overline{\lambda} - 1} &= \sqrt{\frac{|\lambda - 1| + x - 1}{2}} + i\ \mathrm{sign}^+(-y)\sqrt{\frac{|\lambda - 1| - (x - 1)}{2}}, \\ \sqrt{\overline{\lambda} + 1} &= \sqrt{\frac{|\lambda + 1| + x + 1}{2}} + i\ \mathrm{sign}^+(-y)\sqrt{\frac{|\lambda + 1| - (x + 1)}{2}}. \end{aligned}$$

The real part of the product $\lambda\sqrt{\overline{\lambda} - 1}\sqrt{\overline{\lambda} + 1}$ is the sum of four terms. The first is the product of the real parts. The other three are products of two imaginary parts with the respective other real part. This gives

$$\begin{aligned} \mathrm{Re}(\lambda\sqrt{\overline{\lambda} - 1}\sqrt{\overline{\lambda} + 1}) = {} & x\sqrt{\frac{|\lambda - 1| + x - 1}{2}}\sqrt{\frac{|\lambda + 1| + x + 1}{2}} \\ & - y\ \mathrm{sign}^+(-y)\Bigg(\sqrt{\frac{|\lambda - 1| + x - 1}{2}}\sqrt{\frac{|\lambda + 1| - (x + 1)}{2}} \\ & \qquad + \sqrt{\frac{|\lambda - 1| - (x - 1)}{2}}\sqrt{\frac{|\lambda + 1| + x + 1}{2}}\Bigg) \\ & - x\sqrt{\frac{|\lambda - 1| - (x - 1)}{2}}\sqrt{\frac{|\lambda + 1| - (x + 1)}{2}}. \end{aligned}$$

The second and third term are obviously non-negative. Also the first and last term together are always non-negative. For $x > 0$ the roots with the plus sign are larger than those multiplying $-x$. For $x < 0$ the situation is reversed. Therefore, we have shown that $|q_2| \geq 1$ and thereby $|q_1| \leq 1$, for $\lambda \in \mathbb{C}\backslash]-\infty, 1[$. For $\lambda \in \mathbb{C}\backslash [-\infty, 1]$ we have also just shown that $|q_2| > 1$ and $|q_1| < 1$.

For $\lambda \in [-1, 1]$ we have $|q_1| = |q_2| = 1$. This we can easily check since

$$q_2 = \lambda + \sqrt{\lambda - 1}\sqrt{\lambda + 1} = \lambda + \sqrt{\lambda^2 - 1} = \lambda + i\sqrt{1 - \lambda^2}.$$

This gives $|q_2|^2 = \lambda^2+1-\lambda^2 = 1$ and thereby $|q_1| = 1$. For $\lambda \in]-1, 1[$ we have $q_1, q_2 \in \mathbb{C}\backslash\mathbb{R}$. For $\lambda > 1$ we obtain $q_2 = \lambda + \sqrt{\lambda^2 - 1} \in \mathbb{R}$ giving $|q_2| = |\lambda + \sqrt{\lambda^2 - 1}| > \lambda > 1$ and thereby $|q_1| < 1$, this we have already shown above. Analogously, for $\lambda < -1$ not included above we have $q_2 = \lambda - \sqrt{\lambda^2 - 1} \in \mathbb{R}$ giving $|q_2| = |\lambda - \sqrt{\lambda^2 - 1}| > |\lambda| > 1$ and $|q_1| < 1$.

Now let us consider the general case $\nu > 0$. We set $w = \frac{\lambda-1}{2\nu} + 1$. Then $q_2(\nu, \lambda) = w + \sqrt{w-1}\sqrt{w+1}$. This is equivalent to the case discussed, only that λ is replaced by w. Since our transformation is a linear bijection from $\mathbb{C}$ to $\mathbb{C}$ the lemma is proven for all $\lambda \in \mathbb{C}$. We have e.g. $|q_1| = |q_2| = 1$ for $w \in [-1, 1]$ which is equivalent to $\lambda \in [1-4\nu, 1]$. □

On the unit circle with $|\lambda| = 1$ we have $q_1(\frac{1}{2}, 1) = 1$, $q_1(\frac{1}{2}, -1) = -1$ and $|q_1(\frac{1}{2}, \lambda)| < 1$ for $\lambda \neq -1, 1$. For $\nu \in]0, 1/2[$ we have $q_1(\nu, 1) = 1$ and $|q_1(\nu, \lambda)| < 1$ for $|\lambda| = 1$ and $\lambda \neq 1$.

For von Neumann stability one studies the case that $|q_1(\nu, \lambda)| = |q_2(\nu, \lambda)| = 1$. Such solutions exist only for $\lambda \in [1 - 4\nu, 1]$ due to Lemma 1. For $0 < \nu \leq \frac{1}{2}$ we have $\lambda \in [1 - 4\nu, 1] \subset [-1, 1]$ and stability. Instability for $\nu > \frac{1}{2}$ arises due to $\lambda \in [1 - 4\nu, -1[$.

6.1.3 GR-stability for boundary conditions

We have to rule out that there are bounded solutions in space that grow in time. In this case we have to consider the case of two roots q_1 and q_2 of (6.7) with $|q_{1,2}| \neq 1$. The product of the roots is equal to the constant term of (6.7) which is equal to 1, i.e. $q_1 q_2 = 1$. Since our calculations are real valued only $\lambda \in \mathbb{R}$ can appear in a computational instability. Since we assume that $0 < \nu \leq \frac{1}{2}$ holds, the values $|\lambda| > 1$ correspond to $q_{1,2} \in \mathbb{R}$ by Lemma 1. One of the roots of (6.7) then has modulus less than 1 and the second greater than 1. We had chosen $|q_1| < 1$ and $|q_2| > 1$. Then the general solution of (6.6) that is decreasing in modulus as $j \to +\infty$ has the form

$$w_j = c_1[q_1(\lambda)]^j \tag{6.11}$$

with $c_1 \neq 0$. The general solution of (6.6) tending to zero as $j \to -\infty$ has the form

$$w_j = c_2[q_2(\lambda)]^j \tag{6.12}$$

with $c_2 \neq 0$. In the GR-stability analysis for the boundary conditions these solutions are each used in a semi-infinite boundary value problem. They will also later both be used in coupling problems. Now we study outer boundary conditions. In these cases we are looking for such solutions with $|q_{1,2}| \neq 1$ for which $|\lambda| > 1$. If such solutions do not exist the scheme is stable

The outer boundary conditions with central differences for the homogeneous boundary conditions

First, we consider the difference scheme (3.12) for $j = 1, 2, ...$, i.e. the semi-infinite domain with only the left boundary. For $j = 0$ we have the left boundary condition $\frac{\partial w(0,t)}{\partial x} = 0$ given numerically by (3.15) with $q_L = 0$. The right boundary is moved to $+\infty$. See

the book of Godunov and Ryabenkii [11, Ch. 8] for further detail. To find a possible eigenvalue λ we substitute $w_j = c_1 q_1^j(\lambda)$ into the left hand boundary condition (3.15). We seek all the values of λ for which it is satisfied. Applying the left homogeneous Neumann boundary condition from (3.15) gives

$$c_1 q_1^{-1} = c_1 q_1^1$$

or $q_1^2 = 1$. This implies that $q_1 = \pm 1$ which is clearly a contradiction to our assumption $|q_1| \neq 1$.

Analogously, we could also use $q_1^{-1} = q_2$ leading to $q_2 = q_1$ as contradiction to $|q_1| < 1$, $|q_2| > 1$.

Analogously, we consider the right homogeneous Neumann boundary condition $\frac{\partial w(1,t)}{\partial x} = 0$ with (3.12) for $j = N-1, N-2, ...$ on the semi-infinite domain to the left of x_N. Using (6.12) this gives $q_2 = \pm 1$. This is again a contradiction to our consideration $|q_2| \neq 1$. So we obtain no further unstable solution due to the boundary conditions.

The scheme (6.5) with the discrete form of the homogeneous Neumann boundary conditions is stable under the CFL condition (6.4), which is a well known fact.

Alternatively for comparison we apply the normal mode solution to the scheme for the boundary conditions. For the left hand boundary scheme of the system (6.5) we obtain

$$\lambda = 2\nu q_1(\nu, \lambda) + 1 - 2\nu.$$

Taking the absolute value of the above equation leads to

$$\begin{aligned} |\lambda| &\leq |1 - 2\nu| + 2\nu |q_1(\nu, \lambda)| \\ &\leq 1 - 2\nu + 2\nu = 1 \end{aligned}$$

This gives us the stability condition under the CFL condition $0 < \nu \leq \frac{1}{2}$. The same stability condition is obtained for the scheme of the right hand boundary condition in the system (6.5).

The outer boundary conditions of the finite volume scheme

Analogously we derive the GR-stability for the schemes at the outer boundaries that were derived via finite volume method in system (3.35). To find a possible eigenvalue λ we substitute $w_j = c_1 q_1^j(\lambda)$ into the left hand boundary condition (3.34). We seek all the values of λ for which it is satisfied. This gives $q_1 - 1 = 0$ which implies that $q_1 = 1$. This is again a contradiction to our assumption that $|q_1| \neq 1$.

Again alternatively we apply the normal mode solutions to the first scheme of the system to obtain the following normal mode equation

$$\lambda = 1 - \nu + \nu q_1(\nu, \lambda).$$

Taking the absolute value of the above equation we obtain

$$\begin{aligned} |\lambda| &\leq |1 - \nu| + \nu |q_1(\nu, \lambda)| \\ &\leq 1 - \nu + \nu = 1. \end{aligned}$$

Also this gives us the stability condition under the CFL condition. The same stability condition can be obtained for the scheme of the right hand boundary in the system (3.35).

The outer boundary conditions with one sided differences

Now we discuss for the discretization of the homogeneous outer Neumann boundary conditions $w_x(0,t)=0$ and $w_x(1,t)=0$ via one sided differences derived in (3.20) and (3.21) as

$$\frac{w_0^n - w_{-1}^n}{\Delta x} = 0, \qquad \frac{w_{N+1}^n - w_N^n}{\Delta x} = 0.$$

This implies that the first condition is $w_0^n = w_{-1}^n$ and the second conditions is $w_{N+1}^n = w_N^n$.

To find a possible eigenvalue λ we substitute $w_j = c_1 q_1^j(\lambda)$ into the left hand boundary condition and $w_j = c_2 q_2^j(\lambda)$ into the right hand boundary. We obtain $1 = q_1^{-1}$ which implies that $q_1 = 1$. This is again a contradiction of our consideration $|q_1| \neq 1$. Analogously, we obtain $c_2 q_2^{N+1} = c_2 q_2^N$, this implies that $q_2 = 1$. This is again the contradiction of our consideration $|q_2| \neq 1$. So we conclude that the discrete form of homogeneous Neumann boundary condition via one sided differences is also stable under the CFL condition (6.4). Alternatively for the schemes of the outer boundaries we also get a stable solution under the CFL condition. But there is no need to repeat again because the procedure is analogous to the one derived above.

Note that later use of these stable boundary conditions depends on the interpretation of the difference scheme in connection with conservativity. The central difference is conservative for a finite element type scheme. The one sided difference is a central difference for the flux at the boundary in a finite volume type scheme.

The outer boundary conditions with central differences for the non-homogeneous boundary conditions

Now we consider a non-homogeneous Neumann boundary conditions $\frac{\partial w}{\partial x}(0,t) = J_L = H \in \mathbb{R}\backslash 0$ via the central difference method which implies that $\frac{w_1^n - w_{-1}^n}{2\Delta x} = J_L = H$. This gives

$$w_{-1}^n = w_1^n - 2H\Delta x.$$

Then the normal mode solution for this scheme will give $c_1 q_1^{-1} = c_1 q_1 - 2H\Delta x$. This implies that $c_1 q_2 = c_1 q_1 - 2H\Delta x$. By taking the absolute value of this normal mode equation and dividing by the non-zero constant c_1 we obtain

$$|q_2| = \Big| q_1 - \frac{2H}{c_1}\Delta x \Big|.$$

For Δx small enough this is a contradiction to the far-field assumption $|q_2| > 1$. Note that here and in the next case the constant c_1 does not cancel anymore.

Alternatively, we now apply the normal mode solution to the scheme for the left hand non-homogeneous Neumann boundary condition (3.16) for $J_L = H$. It gives

$$\lambda = 2\nu q_1(\nu,\lambda) + (1-2\nu) - \frac{2\nu H\Delta x}{c_1} = 2\nu\Big(q_1(\nu,\lambda) - \frac{H\Delta x}{c_1}\Big) + 1 - 2\nu.$$

Taking the absolute of the above normal mode equation we obtain

$$|\lambda| \leq 2\nu\Big|q_1(\nu,\lambda) - \frac{H\Delta x}{c_1}\Big| + 1 - 2\nu. \tag{6.13}$$

Now $\Big|q_1(\nu,\lambda) - \frac{H\Delta x}{c_1}\Big| \leq |q_1(\nu,\lambda)| + |\frac{H}{c_1}|\Delta x \leq 1$ for Δx small enough since $|q_1| < 1$. So we get an eigenvalue $|\lambda| \leq 1$, which is the required condition for the GR-stability. Note that such an inhomogeneous Neumann condition at the right boundary leads to an analogous result.

The outer boundary conditions with central differences for the heat flux boundary conditions

Here we consider the heat flux boundary conditions $\frac{w_1^n - w_{-1}^n}{2\Delta x} = H(\overline{w} - w_0)$ for a given value $\overline{w} \in \mathbb{R}$. This implies that

$$w_{-1}^n = w_1^n - 2H\Delta x(\overline{w} - w_0).$$

Then the normal mode equation for this scheme will give us $c_1 q_2 = c_1 q_1 - 2H\Delta x(\overline{w} - w_0)$. Now we divide this equation by the non-zero constant c_1. This leads to

$$q_2(\nu,\lambda) = q_1(\nu,\lambda) - \frac{2H}{c_1}\overline{w}\Delta x + 2\Delta x.$$

By taking the absolute value of above normal mode equation we obtain

$$|q_2(\nu,\lambda)| = \Big|q_1(\nu,\lambda) + 2(1 - \frac{H}{c_1}\overline{w})\Delta x\Big|.$$

For Δx small enough this is again a contradiction to the far-field assumption $|q_2| > 1$.

Alternatively, we consider the scheme for the heat flux boundary condition at the left boundary in (3.16). It will take the form for $J_L = H(\overline{w} - w_0)$ and obtain

$$w_0^{n+1} = 2\nu w_1^n + (1 - 2\nu)w_0^n + 2\nu\Delta x H(w_0^n - \overline{w}). \tag{6.14}$$

Now we apply the normal mode solutions to the above equation to obtain

$$\begin{aligned}
\lambda &= 2\nu q_1(\nu,\lambda) + 1 - 2\nu + 2\nu H\Delta x - 2\nu\frac{H}{c_1}\overline{w}\Delta x \\
&= 2\nu q_1(\nu,\lambda) + 1 - 2\nu + 2\nu H(1 - \frac{\overline{w}}{c_1})\Delta x \\
&= 2\nu\Big(q_1 + H(1 - \frac{\overline{w}}{c_1})\Delta x\Big) + 1 - 2\nu.
\end{aligned}$$

Taking the absolute of the above normal mode equation we get an eigenvalue $|\lambda| \leq 1$ with $\Big|q_1 + H\Big(1 - \frac{\overline{w}}{c_1}\Big)\Delta x\Big| < 1$ for Δx small enough. This is the required condition for the GR-stability.

6.1.4 Von Neumann stability for the implicit method

We derived the implicit scheme with homogenous outer boundaries conditions in (3.25). Here we derive the von Neumann stability for the implicit scheme of single domain diffusion equation. We re-write the system as follows

$$\begin{aligned} w_0^n &= (1+2\nu)w_0^{n+1} - 2\nu w_1^{n+1} && \text{for } j=0 \\ w_j^n &= -\nu w_{j+1}^{n+1} + (1+2\nu)w_j^{n+1} - \nu w_{j-1}^{n+1} && \text{for } 0<j<N \\ w_N^n &= (1+2\nu)w_N^{n+1} - 2\nu w_{N-1}^{n+1} && \text{for } j=N. \end{aligned} \tag{6.15}$$

We recall the derivation given in the book of Godunov and Ryabenkii [134]. Analogously we substitute $w_j^n = \lambda^n \exp^{i\alpha j}$ in the scheme for the interior nodes, i.e. the second equation in the above system

$$1 = \lambda(1+2\nu - \nu(e^{-i\alpha} + e^{i\alpha})) \qquad \text{or} \qquad \lambda = \frac{1}{1-\nu(e^{-i\alpha}+e^{i\alpha}-2)}.$$

Using the formula (6.2) lead to the following expression

$$\lambda(\alpha) = \frac{1}{1+4\nu\sin^2(\frac{\alpha}{2})}.$$

The spectrum for this problem gives us the following stability bound

$$(1+4\nu\sin^2(\frac{\alpha}{2}))^{-1} \leq \lambda \leq 1 \tag{6.16}$$

of the real axis and the condition $|\lambda| \leq 1$ is satisfied for all positive value of ν. So, this method is unconditionally stable.

The outer boundary conditions with central differences

For the implicit case we get the same stability conditions for the outer boundaries as we obtained in case of explicit discretization. This implies that for the left hand boundary we obtain $q_1 = \pm 1$ and for the right hand boundary $q_2 = \pm 1$.

The outer boundary conditions with one sided differences

Also in this case we get the same stability condition as we obtained in case of explicit discretization method. For the left hand boundary we obtain $q_1 = 1$ and for the right hand boundary $q_2 = 1$.

6.2 GR-stability for the Dirichlet-Neumann coupling conditions (explicit case)

For the stability analysis of the coupling interface condition we apply the method introduced by Godunov and Ryabenkii for boundary conditions, see e.g. [11]. It seems that

such an application was first made by Giles [10]. We have to determine whether the coupling conditions give rise to unstable modes even though the CFL condition (6.4) is satisfied.

Further, first we derive the GR-stability for the Dirichlet-Neumann coupling and then for the other coupling conditions with and without ghost point values.

The procedure we use is simpler than the one in Giles [10], Roe et al. [33] and Errera et al. [6]. Therefore, we obtain more precise GR-stability results in direct way. The complete coupling system with homogeneous Neumann outer boundary conditions with the bi-domain diffusion equation can be re-written as follows

$$\begin{aligned}
u_0^{n+1} &= 2\nu_- u_1^n + (1-2\nu_-)u_0^n && \text{for } j=0\\
u_j^{n+1} &= \nu_- u_{j-1}^n + (1-2\nu_-)u_j^n + \nu_- u_{j+1}^n && \text{for } 0<j<m\\
&\quad \text{the coupling conditions} && \text{for } j=m\\
v_j^{n+1} &= \nu_+ v_{j-1}^n + (1-2\nu_+)v_j^n + \nu_+ v_{j+1}^n && \text{for } m<j<N\\
v_N^{n+1} &= 2\nu_+ v_{N-1}^n + (1-2\nu_+)v_N^n && \text{for } j=N.
\end{aligned} \tag{6.17}$$

We consider the following separable normal mode solution for the GR-stability in the case of coupled case

$$\begin{aligned}
u_j^n &= c_2 \lambda^n q_2^{j-m}(\nu_-,\lambda) \qquad \text{if } j \le m\\
v_j^n &= c_1 \lambda^n q_1^{j-m}(\nu_+,\lambda) \qquad \text{if } j \ge m.
\end{aligned} \tag{6.18}$$

Here λ is the temporal amplification factor and $q_1(\nu_+,\lambda)$ as well as $q_2(\nu_-,\lambda)$ are the spatial amplification factors. For the left and right hand boundaries we discussed the GR-stability in the previous subsection. In the right sub-domain, i.e. for $j>m$ the amplitude of the mode $q_1^{j-m}(\nu_+)$ remains bounded as $j\to\infty$ due to $|q_1(\nu_-,\lambda)|<1$. Analogously for the left sub-domain we use $|q_2(\nu_-,\lambda)|>1$. The discretization is unstable if the difference equation admits such a solutions which gives exponential growth in time, i.e. $|\lambda|>1$.

For the stability analysis we take the unit open ball $\mathbb{B}=\{z\in\mathbb{C}:|z|<1\}$, where $q_1(\nu_-,\lambda)=q_2^{-1}(\nu_-,\lambda)\in\mathbb{B}$, $q_1(\nu_+,\lambda)=q_2^{-1}(\nu_+,\lambda)\in\mathbb{B}$.

In system (6.17) we have six types of equations. We derived the GR-stability for the outer boundary conditions as well for the interior points via von Neuman stability in the preceding section. So, now we only need to derive the GR-stability for the Dirichlet-Neumann coupling conditions and other coupling conditions.

6.2.1 Dirichlet-Neumann coupling with ghost point value

The Dirichlet-Neumann coupling condition was defined in (4.8). We use the ghost point values u_{m+1}^n. We discretize the Dirichlet-Neumann coupling via $u_m^n=v_m^n$ and one sided differences given as

$$D_-\frac{u_{m+1}^n-u_m^n}{\Delta x}=D_+\frac{v_{m+1}^n-v_m^n}{\Delta x}=D_+\frac{v_{m+1}^n-u_m^n}{\Delta x}.$$

or

$$u_{m+1}^n = u_m^n + \frac{D_+}{D_-}(v_{m+1}^n - u_m^n). \tag{6.19}$$

Applying the separable normal mode solutions defined in (6.18) to the Dirichlet condition $u_m^n = v_m^n$ we obtain $u_m^n = c_2\lambda^n = v_m^n = c_1\lambda^n$. So, the constants c_1 and c_2 have to be equal, i.e. $c_1 = c_2 = c$.

For simplicity at first we take the identical diffusion coefficients $D_- = D_+ = D$. Now we apply the separable normal mode solutions to (6.19) to obtain the following normal mode equation

$$q_2(\nu, \lambda) = 1 + q_1(\nu, \lambda) - 1 = q_1(\nu, \lambda).$$

This is a contradiction to the far-field assumptions $|q_2(\nu, \lambda)| > 1$ and $|q_1(\nu, \lambda)| < 1$. So, there is no such solution and the coupling condition gives us a stable solution under the CFL condition $0 < \nu \leq \frac{1}{2}$.

Case with un-equal diffusion coefficients $D_- \neq D_+$

Now for the case $D_- \neq D_+$ we can write (6.19) as

$$\nu_-(u_{m+1}^n - u_m^n) = \nu_+(v_{m+1}^n - u_m).$$

We apply the normal mode solutions to the above scheme to obtain

$$\nu_-(q_2(\nu_-, \lambda) - 1) = \nu_+(q_1(\nu_+, \lambda) - 1).$$

Into this equation we insert the formula (6.10) for the roots. This gives

$$\frac{\lambda - 1}{2}\Big[1 + \sqrt{1 + \frac{4\nu_-}{\lambda - 1}}\Big] = \frac{\lambda - 1}{2}\Big[1 - \sqrt{1 + \frac{4\nu_+}{\lambda - 1}}\Big]$$

or equivalently

$$\sqrt{1 + \frac{4\nu_-}{\lambda - 1}} = -\sqrt{1 + \frac{4\nu_+}{\lambda - 1}}.$$

Since the square roots are positive this implies that

$$0 = 1 + \frac{4\nu_\pm}{\lambda - 1}$$

which gives $\lambda = 1 - 4\nu_+ = 1 - 4\nu_-$. This is a contradiction to the assumption that $\nu_+ \neq \nu_-$. Therefore we have stability.

Alternatively, we proceed as follows using the discretized scheme of the DN-coupling that was derived in (4.18). It is given by

$$u_m^{n+1} = u_m^n + \nu_+(v_{m+1}^n - u_m^n) - \nu_-(u_m^n - u_{m-1}^n). \tag{6.20}$$

Substituting the separable normal mode solution (6.18) into the above equation leads to the following normal mode equation

$$\lambda = 1 + \nu_+(q_1(\nu_+, \lambda) - 1) - \nu_-(1 - q_2^{-1}(\nu_-, \lambda)). \tag{6.21}$$

We take the modulus of the above equation and use the CFL condition $0 \leq \nu_{\pm} \leq \frac{1}{2}$. This implies that $0 \leq \nu_- + \nu_+ \leq 1$ which gives us $1 - (\nu_+ + \nu_-) \geq 0$. Further we have $q_2^{-1}(\nu_-, \lambda) = q_1(\nu_-, \lambda)$. Then we obtain

$$\begin{aligned}|\lambda| &= |1 - (\nu_+ + \nu_-) + \nu_+ q_1(\nu_+, \lambda) + \nu_- q_1(\nu_-, \lambda)| \\ &\leq |1 - (\nu_+ + \nu_-)| + \nu_+ |q_1(\nu_+, \lambda)| + \nu_- |q_1(\nu_-, \lambda)| \\ &\leq 1 - (\nu_+ + \nu_-) + \nu_+ + \nu_- \\ &\leq 1.\end{aligned}$$

Therefore, this coupling condition does not introduce instabilities when the CFL condition is satisfied.

Note that in all cases we could alternatively do the stability analysis for the discrete coupling condition itself as well as for its use in a modification of the scheme. Here we are not able to prove the stability for the coupling itself using only the properties $|q_1| < 1$ and $|q_2| > 1$. We have to use the more specific formula (6.10) for the roots.

Note on the maximum principle

The stability analysis is closely related to the maximum principle for our diffusion equations as long as the coupling conditions allow for the maximum principle. For the interior nodes we have under the CFL condition $0 \leq v_- \leq \frac{1}{2}$

$$\begin{aligned}\max_{j=1,\dots,m-1} |u_j^{n+1}| &= \max_{j=1,\dots,m-1} |(1 - 2\nu_-)u_j^n + \nu_- u_{j+1} + \nu_- u_{j+1}| \\ &\leq (1 - 2\nu_-) \max_{j=1,\dots,m-1} |u_j^n| + \nu_- \max_{j=1,\dots,m-1} |u_{j+1}^n| + \nu_- \max_{j=1,\dots,m-1} |u_{j-1}^n| \\ &\leq \max_{j=0,\dots,m} |u_j^n|,\end{aligned} \tag{6.22}$$

for the left boundary we have

$$|u_0^{n+1}| \leq 2\nu_- |u_1^n| + (1 - 2\nu_-)|u_0^n| \tag{6.23}$$

as well as for the coupling condition (6.20)

$$|u_m^{n+1}| \leq (1 - (\nu_+ + \nu_-))|u_m^n| + \nu_+ |v_{m+1}^n| + \nu_- |u_{m-1}^n|. \tag{6.24}$$

Proceeding analogously for v_j^{n+1} we obtain

$$\max_{j=0,\dots,m} |u_j^{n+1}| + \max_{j=m+1,\dots,2m} |v_j^{n+1}| \leq \max_{j=0,\dots,m} |u_m^n| + \max_{j=m+1,\dots,2m} |v_m^n|. \tag{6.25}$$

So, the discrete maximum principle holds under the CFL condition $0 \leq \nu_{\pm} \leq \frac{1}{2}$.

6.2.2 GR-stability for the cell based scheme of the Dirichlet-Neumann coupling

In the cell based formulation we derived the schemes for the left interior nodes in (4.19), for the Dirichlet-Neumann coupling in (4.23) and for the interior of the right sub-domain

in (4.20). The formulas for these schemes are the same as in the nodal based case treated above. So, there is no need to repeat the stability analysis again. The schemes for the outer boundary conditions are different. But, for them we already discussed the normal mode analysis in Subsection 6.1.3.

6.2.3 Comparison and discussion with the coupling of Giles

We used a slightly different procedure than Giles [10] in our formulation. In deriving his coupling term Giles [10, p. 426] omitted a term in the time difference making his scheme inconsistent with the time derivative and non conservative, as will be shown further on. His coupling term is given as

$$u_m^{n+1} = u_m^n + 2r\nu_+(v_{m+1}^n - u_m^n) - 2\nu_-(u_m^n - u_{m-1}^n). \tag{6.26}$$

This coupling scheme is missing factors of $\frac{1}{1+r}$ that appear in (4.14). Note that Roe et al. [33] also used this incorrect scheme. Repeating the above stability analysis leads to a much sharper CFL restriction, namely $0 \le 2r\nu_+ + 2\nu_- \le 1$ or $0 \le r\nu_+ + \nu_- \le \frac{1}{2}$. So, the instabilities that Giles [10] observed are due to his modification that makes his scheme inconsistent as we remarked in Chapter 4 and non-conservative as shown in Chapter 5.

Taking $r = 1$ and comparing to our coupling formula (6.20) we see that Giles produced a factor of two in the flux terms.

6.2.4 Corrected Giles coupling condition

We recall the corrected Giles coupling scheme in (4.14)

$$u_m^{n+1} = u_m^n + \frac{2r\nu_+}{1+r}(v_{m+1}^n - v_m^n) - \frac{2\nu_-}{1+r}(u_m^n - u_{m-1}^n).$$

In Chapter 5 we have shown that it is conservative. We apply the normal mode solutions to the above scheme

$$\lambda = 1 + \frac{2r}{1+r}\nu_+(q_1(\nu_+,\lambda) - 1) - \frac{2}{1+r}\nu_-(1 - q_1(\nu_-,\lambda)).$$

After re-arranging we obtain

$$\lambda = 1 - \Big(\frac{2r}{1+r}\nu_+ + \frac{2}{1+r}\nu_-\Big) + \frac{2r}{1+r}\nu_+ q_1(\nu_+,\lambda) + \frac{2}{1+r}\nu_- q_1(\nu_-,\lambda). \tag{6.27}$$

Now for the stability we need to $\frac{2r}{1+r}\nu_+ + \frac{2}{1+r}\nu_- \le 1$. Under the CFL condition $0 < \nu_\pm \le \frac{1}{2}$ we have

$$\frac{2r}{1+r}\nu_+ + \frac{2}{1+r}\nu_- \le \frac{r}{1+r} + \frac{1}{1+r} = 1.$$

So we do not have a further restriction. Now we take the absolute value of the normal mode equation (6.27)

$$\begin{aligned} |\lambda| &\le \Big|1 - \Big(\frac{2r}{1+r}\nu_+ + \frac{2}{1+r}\nu_-\Big)\Big| + \frac{2r}{1+r}\nu_+\Big|q_1(\nu_+,\lambda)\Big| + \frac{2}{1+r}\nu_-\Big|q_1(\nu_-,\lambda)\Big| \\ &\le 1 - \Big(\frac{2r}{1+r}\nu_+ + \frac{2}{1+r}\nu_-\Big) + \frac{2r}{1+r}\nu_+ + \frac{2}{1+r}\nu_- = 1. \end{aligned}$$

We obtain the GR-stability condition $|\lambda| \le 1$ under the CFL condition.

6.3 GR-stability for the heat flux coupling

We discretized the heat flux coupling condition in Chapter 4 via one sided differences and with central differences. Here, we derive the GR-stability for the heat flux coupling conditions and for scheme of the heat flux coupling conditions as follows.

Heat flux coupling conditions via one sided differences for the finite volume scheme

First we derive the GR-stability for the one sided finite volume schemes. The discretized coupling scheme for the heat flux coupling conditions was derived in (4.28)

$$u_m^{n+1} = u_m^n - \nu_-(u_m^n - u_{m-1}^n) + \frac{H\Delta t}{\Delta x}(v_m^n - u_m^n). \tag{6.28}$$

In order to continue the result just obtained we applying the separable normal mode solutions defined in (6.18) to the above scheme. Using $\nu_- = \frac{D_-\Delta t}{(\Delta x)^2}$ gives

$$\begin{aligned} \lambda &= 1 - \nu_-\Big(1 - q_2^{-1}(\nu_-, \lambda)\Big) + \frac{H\Delta t}{\Delta x}\frac{(c_1 - c_2)}{c_2} \\ &= 1 - \nu_- + \nu_-\Big(q_1(\nu_-, \lambda) + \frac{H\Delta x}{D_-}\frac{(c_1 - c_2)}{c_2}\Big) \end{aligned} \tag{6.29}$$

We take the modulus of the above normal mode equation under the CFL condition. Using $q_2^{-1}(\nu_-, \lambda) = q_1(\nu_-, \lambda)$ we obtain

$$\begin{aligned} |\lambda| &\leq |1 - \nu_-| + \nu_-\Big|q_1(\nu_-, \lambda) + \frac{H\Delta x}{D_-}\frac{(c_1 - c_2)}{c_2}\Big| \\ &\leq 1 - \nu_- + \nu_-\Big|q_1(\nu_-, \lambda) + \frac{H\Delta x}{D_-}\frac{(c_1 - c_2)}{c_2}\Big|. \end{aligned} \tag{6.30}$$

Now $\Big|q_1(\nu_-, \lambda) + \frac{H\Delta x}{D_-}\frac{(c_1-c_2)}{c_2}\Big| \leq |q_1(\nu_-, \lambda)| + |\frac{H(c_1-c_2)}{c_2}\Big|\frac{\Delta x}{D_-} \leq 1$ for Δx small enough. So we get the required condition $|\lambda| \leq 1$ for the GR-stability under the CFL condition.

Analogously, now we find the GR-stability for the second scheme of the heat flux coupling condition given as

$$v_m^{n+1} = v_m^n + \nu_+(v_{m+1}^n - v_m^n) - H\frac{\Delta t}{\Delta x}(v_m^n - u_m^n). \tag{6.31}$$

Now apply the normal mode solution to the above scheme and using $\nu_+ = \frac{D_+\Delta t}{(\Delta x)^2}$ we obtain

$$\begin{aligned} \lambda &= 1 + \nu_+(q_1(\nu_+, \lambda) - 1) + \frac{H\Delta t}{\Delta x}\frac{(c_2 - c_1)}{c_1} \\ &= 1 - \nu_+ + \nu_+\Big(q_1(\nu_+, \lambda) + \frac{H\Delta x}{D_+}\frac{(c_2 - c_1)}{c_1}\Big) \end{aligned}$$

Taking the absolute value of the above equation

$$\begin{aligned} |\lambda| &\leq |1-\nu_+| + \nu_+ \Big| q_1(\nu_+,\lambda) + \frac{H\Delta x}{D_+}\frac{(c_2-c_1)}{c_1}\Big| \\ &\leq 1 - \nu_+ + \nu_+ \Big| q_1(\nu_+,\lambda) + \frac{H\Delta x}{D_+}\frac{(c_2-c_1)}{c_1}\Big|. \end{aligned} \tag{6.32}$$

Now $\Big| q_1(\nu_+,\lambda) + \frac{H\Delta x}{D_+}\frac{(c_2-c_1)}{c_1}\Big| \leq |q_1(\nu_+,\lambda)| + |\frac{H(c_2-c_1)}{c_1}\Big|\frac{\Delta x}{D_+} \leq 1$ for Δx small enough. So we get the required condition $|\lambda| \leq 1$ for the GR-stability under the CFL condition.

Heat flux coupling conditions via central differences

Now we use the heat flux coupling condition for u_m^{n+1} that was derived in (4.31)

$$u_m^{n+1} = u_m^n - 2\nu_-(u_m^n - u_{m-1}^n) + \frac{2H\Delta t}{\Delta x}\Big(v_m^n - u_m^n\Big).$$

After applying the normal mode solutions to the above scheme we obtain the following normal mode equation

$$\begin{aligned} |\lambda| &\leq |1-2\nu_-| + 2\nu_- \Big| q_1(\nu_-,\lambda) + \frac{H\Delta x}{D_-}\frac{(c_1-c_2)}{c_2}\Big| \\ &\leq 1 - 2\nu_- + 2\nu_- \Big| q_1(\nu_-,\lambda) + \frac{H\Delta x}{D_-}\frac{(c_1-c_2)}{c_2}\Big|. \end{aligned} \tag{6.33}$$

To follow the same argument which is used just above here too. Then we obtain the GR-stability condition $|\lambda| \leq 1$.

Analogously, we derive the GR-stability for the second scheme of the heat flux coupling conditions which was derived in (4.32) via central difference method

$$v_m^{n+1} = v_m^n + 2\nu_+(v_{m+1}^n - v_m^n) - \frac{2H\Delta t}{\Delta x}(v_m^n - u_m^n). \tag{6.34}$$

Now apply the normal mode solution to the above scheme we obtain the following normal mode equation

$$\begin{aligned} |\lambda| &\leq |1-2\nu_+| + 2\nu_+ \Big| q_1(\nu_+,\lambda) + \frac{H\Delta x}{D_+}\frac{(c_2-c_1)}{c_1}\Big| \\ &\leq 1 - 2\nu_+ + 2\nu_+ \Big| q_1(\nu_+,\lambda) + \frac{H\Delta x}{D_+}\frac{(c_2-c_1)}{c_1}\Big|. \end{aligned}$$

Similarly again we used the argument just used above we obtain the stability condition $|\lambda| \leq 1$ under the CFL condition here too with the same argument given above. Therefore, this coupling condition does not introduce instabilities with further restrictions when the CFL condition is satisfied.

6.3.1 Channel pumping condition

The channel pumping conditions (2.16) have the constant term β in the denominator which introduce a term λ^n in the denominator of β. Then we can not easily find the GR-stability.

6.3.2 Simplified channel pumping conditions and linearized membrane pumping

Here we derive the GR-stability for the simplified channel pumping conditions and its special case linearized membrane pumping conditions. In implementations we use the one sided and central difference methods. So, we derive for both as follows.

One sided difference method for the finite volume scheme

First we derive the GR-stability for the one sided differences for the finite volume scheme. Then for the central differences. The schemes of the simplified channel pumping conditions via the one sided difference method. The schemes were derived in (4.37) and (4.38). First, we consider (4.37)

$$u_m^{n+1} = u_m^n - \nu_-(u_m^n - u_{m-1}^n) + \frac{\Delta t\psi}{\Delta x}\Big(\alpha v_m^n - u_m^n\Big).$$

We apply the separable normal mode solutions defined in (6.18) to the above scheme. We obtain

$$\begin{aligned}\lambda &= 1 - \nu_-(1 - q_2^{-1}(\nu_-, \lambda)) + \frac{\psi\Delta t}{\Delta x}\frac{(\alpha c_1 - c_2)}{c_2}\\ &= 1 - \nu_-(1 - q_1(\nu_-, \lambda)) + \frac{\psi\Delta t}{\Delta x}\frac{(\alpha c_1 - c_2)}{c_2}.\end{aligned}$$

We know that $\nu_- = \frac{\Delta t D_-}{(\Delta t)^2}$, $\alpha \geq 1$ and $\psi > 0$. This gives

$$\begin{aligned}\lambda &= 1 - \nu_-(1 - q_1(\nu_-, \lambda)) + \nu_-\frac{\psi\Delta x}{D_+}\frac{(\alpha c_1 - c_2)}{c_2}\\ &= 1 - \nu_- + \nu_-\Big(q_1(\nu_-, \lambda) + \frac{\psi\Delta x}{D_-}\frac{(\alpha c_1 - c_2)}{c_2}\Big).\end{aligned} \tag{6.35}$$

Now $\Big|q_1(\nu_-, \lambda) + \frac{\psi\Delta x}{D_-}\frac{(\alpha c_1 - c_2)}{c_2}\Big| \leq |q_1(\nu_-, \lambda)| + \frac{\psi\Delta x}{D_-}\Big|\frac{\alpha c_1 - c_2}{c_2}\Big| \leq 1$. Now by taking the absolute value of the (6.35) we get the stability condition $|\lambda| \leq 1$ under the CFL condition.

Analogously, we follow the same procedure for the second formula of the simplified channel pumping conditions (4.38) that was derived via one sided difference

$$v_m^{n+1} = v_m^n + \nu_+(v_{m+1}^n - v_m^n) - \frac{\Delta t}{\Delta x}\Big(\psi(\alpha v_m^n - u_m^n)\Big). \tag{6.36}$$

Now we apply the separable normal mode solutions to the above scheme. We obtain

$$\begin{aligned}\lambda &= 1+\nu_+(q_1(\nu_+,\lambda)-1)-\frac{\Delta t}{\Delta x}(\psi(\alpha-1))\\ &= 1-\nu_++\nu_+\Big(q_1(\nu_+,\lambda)+\frac{\psi\Delta x}{D_+}\frac{(c_2-\alpha c_1)}{c_1}\Big).\end{aligned} \tag{6.37}$$

Now $\Big|q_1(\nu_+,\lambda)+\frac{\psi\Delta x}{D_-}\frac{(c_2-\alpha c_1)}{c_1}\Big| \leq |q_1(\nu_+,\lambda)|+\frac{\psi\Delta x}{D_+}\Big|\frac{c_2-\alpha c_1}{c_1}\Big| \leq 1$. Now by taking the absolute value of the (6.37) we get the stability condition $|\lambda| \leq 1$ under the CFL condition.

Central difference method

Here, we derive the GR-stability for the simplified coupling conditions via the central difference method.

The schemes of the simplified channel pumping conditions via the central difference method in (4.35) and (4.36). First, we consider (4.35)

$$u_m^{n+1} = u_m^n - 2\nu_-(u_m^n-u_{m-1}^n)+\frac{2\Delta t}{\Delta x}\Big(\psi(\alpha v_m^n-u_m^n)\Big).$$

We apply the separable normal mode solutions defined in (6.18) to the above scheme. We obtain

$$\begin{aligned}\lambda &= 1-2\nu_-(1-q_2^{-1}(\nu_-,\lambda))+\frac{2\Delta x}{D_+}(\psi(\alpha-1))\\ &= 1-2\nu_-(1-q_1(\nu_-,\lambda))+\frac{2\Delta x}{D_+}(\psi(\alpha-1))\end{aligned}$$

We know that $\nu_- = \frac{\Delta t D_-}{(\Delta t)^2}$, $\alpha \geq 1$ and $\psi > 0$. This gives

$$\begin{aligned}\lambda &= 1-2\nu_-(1-q_1(\nu_-,\lambda))+2\nu_-\frac{\psi\Delta x}{D_+}\frac{(\alpha c_1-c_2)}{c_2}\\ &= 1-2\nu_-+2\nu_-\Big(q_1(\nu_-,\lambda)+\frac{\psi\Delta x}{D_-}\frac{(\alpha c_1-c_2)}{c_2}\Big).\end{aligned} \tag{6.38}$$

Now $\Big|q_1(\nu_-,\lambda)+\frac{\psi\Delta x}{D_-}\frac{(\alpha c_1-c_2)}{c_2}\Big| \leq |q_1(\nu_-,\lambda)|+\frac{\psi\Delta x}{D_-}\Big|\frac{\alpha c_1-c_2}{c_2}\Big| \leq 1$. Now by taking the absolute value of the (6.38) we get the stability condition $|\lambda| \leq 1$ under the CFL condition.

Analogously, using the same procedure for the second formula of the simplified channel pumping conditions via central difference method in (4.36) as

$$v_m^{n+1} = v_m^n + 2\nu_+(v_{m+1}^n-v_m^n)-\frac{2\Delta t}{\Delta x}\Big(\psi(\alpha v_m^n-u_m^n)\Big).$$

We apply the separable normal mode solutions to the above scheme. We obtain the following normal mode equation

$$\begin{aligned}\lambda &= 1+2\nu_+(q_1(\nu_+,\lambda)-1)-2\frac{\Delta t}{\Delta x}(\psi(\alpha-1))\\ &= 1-2\nu_++2\nu_+\Big(q_1(\nu_+,\lambda)+\frac{\psi\Delta x}{D_+}\frac{(c_2-\alpha c_1)}{c_1}\Big).\end{aligned} \tag{6.39}$$

Now $\Big|q_1(\nu_+,\lambda)+\frac{\psi\Delta x}{D_-}\frac{(c_2-\alpha c_1)}{c_1}\Big| \leq |q_1(\nu_+,\lambda)|+\frac{\psi\Delta x}{D_+}\Big|\frac{c_2-\alpha c_1}{c_1}\Big| \leq 1$. Now by taking the absolute value of the (6.39) we get the stability condition $|\lambda| \leq 1$ under the CFL condition.

Linearized pumping coupling condition (special case)

The linearized membrane pumping conditions is the special case of the simplified channel pumping conditions. Note that for $\psi = 1$ and $\alpha = 3/2$ we get the linearized pumping condition. By substitution of these values we can get the conditions for stability derived above.

6.3.3 GR-stability for the simplified membrane pumping conditions

The simplified membrane pumping as a perturbation of the stable heat flux coupling. The perturbation smaller as Δx becomes smaller.

One sided difference method

We derived the scheme for the simplified pumping membrane conditions via one sided difference for the finite volume scheme in (4.45) as given

$$u_m^{n+1} = u_m^n - \nu_-(u_m^n - u_{m-1}^n) + \frac{\Delta t}{\Delta x}\Big(H(v_m^n - u_m^n) + P\frac{(v_m^n)^2}{1+(v_m^n)^2}\Big).$$

Now we apply the normal mode solutions (6.18) to the above scheme. We obtain

$$\lambda = 1 - \nu_-(1 - q_2^{-1}(\nu_-,\lambda)) + \nu_-\frac{\Delta x}{D_-}\Big(\frac{H(c_1-c_2)}{c_2} + \frac{P}{c_2}\frac{c_1^2(q_1(\nu_+,\lambda))^2}{1+c_1^2(q_1(\nu_+,\lambda))^2}\Big).$$

This implies that

$$\lambda = 1 - \nu_- + \nu_- q_1(\nu_-,\lambda) + \nu_-\frac{\Delta x}{D_-}\Big(\frac{H(c_1-c_2)}{c_2} + \frac{P}{c_2}\frac{c_1^2(q_1(\nu_+,\lambda))^2}{1+c_1^2(q_1(\nu_+,\lambda))^2}\Big).$$

Now we take the absolute value of the above equation

$$|\lambda| \leq 1 - \nu_- + \nu_-\Big[|q_1(\nu_-,\lambda)| + \frac{\Delta x}{D_-}\Big(\Big|\frac{H(c_1-c_2)}{c_2}\Big| + \frac{P}{|c_2|}\frac{c_1^2(q_1(\nu_+,\lambda))^2}{1+c_1^2(q_1(\nu_+,\lambda))^2}\Big)\Big]. \quad (6.40)$$

In a real valued computation an instability could only produce a $\lambda \in \mathbb{R}$. From Lemma 1 we know that $q_1(\nu_+,\lambda) \in \mathbb{R}$ for $\lambda \in \mathbb{R}\backslash]1-4\nu_+, 1[$. Clearly the non-linear function in the above equation is bounded as

$$\frac{c_1^2(q_1(\nu_+,\lambda))^2}{1+c_1^2(q_1(\nu_+,\lambda))^2} \leq 1.$$

This implies that

$$|\lambda| \leq 1 - \nu_- + \nu_-\Big[|q_1(\nu_-,\lambda)| + \frac{\Delta x}{D_-}\Big(H\Big|\frac{(c_1-c_2)}{c_2}\Big| + \frac{P}{|c_2|}\Big)\Big].$$

Now suppose that we had $\lambda \in \mathbb{R}$ with $|\lambda| > 1$. Then for Δx small enough we obtain the contradiction $|\lambda| \leq 1$ due to $|q_1(\nu_-, \lambda)| < 1$. This implies stability for this coupling condition.

Analogously, we derive the stability condition for the second formula of the simplified coupling condition derived in (4.46) as

$$v_m^{n+1} = v_m^n + \nu_+(v_{m+1}^n - v_m^n) - \frac{\Delta t}{\Delta x}\Big(H(v_m^n - u_m^n) + P\frac{(v_m^n)^2}{1+(v_m^n)^2}\Big).$$

Now we apply the normal mode solutions to the above scheme we get the following normal mode equation

$$\lambda = 1 - \nu_+(1 - q_1(\nu_+, \lambda)) - \nu_+\frac{\Delta x}{D_+}\Big(\frac{H(c_1 - c_2)}{c_1} - \frac{P}{c_1}\frac{c_1^2(q_1(\nu_+,\lambda))^2}{1 + c_1^2(q_1(\nu_+,\lambda))^2}\Big).$$

This gives the condition for stability as above

$$|\lambda| \leq 1 - \nu_+ + \nu_+\Big[|q_1(\nu_+,\lambda)| + \frac{\Delta x}{D_+}\Big(H\Big|\frac{(c_2 - c_1)}{c_1}\Big| - \frac{P}{|c_1|}\Big)\Big].$$

This implies that $|\lambda| \leq 1$ for Δx sufficiently small as above, which is the required condition for the GR-stability.

Central difference method

Analogously we obtain the following normal mode equation for the scheme u_m^{n+1} via central difference method. Because we know that the scheme of the central difference is only differ with a factor of 2

$$\lambda = 1 - 2\nu_- + 2\nu_- q_1(\nu_-, \lambda) + 2\Delta x\frac{\nu_-}{D_-}\Big(\frac{H(c_1 - c_2)}{c_2} + \frac{P}{c_2}\frac{c_1^2(q_1(\nu_+,\lambda))^2}{1 + c_1^2(q_1(\nu_+,\lambda))^2}\Big) \tag{6.41}$$

and for the second scheme v_m^{n+1} as

$$\lambda = 1 - 2\nu_+ + 2\nu_+ q_1(\nu_+, \lambda) + 2\Delta x\frac{\nu_-}{D_+}\Big(\frac{H(c_2 - c_1)}{c_1} - \frac{P}{c_1}\frac{c_1^2(q_1(\nu_+,\lambda))^2}{1 + c_1^2(q_1(\nu_+,\lambda))^2}\Big). \tag{6.42}$$

The argument given above for the stability of the one sided normal mode equations will be followed here too because the formulas only differ by a factor of 2 with $\nu_\pm$.

6.3.4 GR-stability for the membrane pumping conditions

Here we derive the GR-stability for the membrane pumping condition via the one sided finite volume cell based and the nodal based central difference method.

One sided difference finite volume cell based method

First we consider the one sided finite volume cell based method which was derived in (4.41) and (4.42). We derive the GR-stability for the formula derived for the coupling conditions corresponding to the left sub-domain (4.41)

$$u_m^{n+1} = u_m^n - \nu_-(u_m^n - u_{m-1}^n) + \frac{\Delta t}{\Delta x}\Big((P_l + P_c(t))(v_m^n - u_m^n) + P_p\frac{(v_m^n)^2}{k_d^2 + (v_m^n)^2}\Big).$$

The simplified membrane pumping is a special case of the membrane pumping containing the essential features. So, we can follow the same steps taken above to obtain the following normal mode equation

$$|\lambda| \leq 1 - \nu_- + \nu_-|q_1(\nu_-,\lambda)| + \Delta x\frac{\nu_-}{D_-}\Big((P_l + P_c(t))\Big|\frac{(c_1 - c_2)}{c_2}\Big| + \frac{P_p}{|c_2|}\frac{c_1^2(q_1(\nu_+,\lambda))^2}{k_d^2 + c_1^2(q_1(\nu_+,\lambda))^2}\Big).$$

Again the nonlinear function is bounded as

$$\frac{c_1^2(q_1(\nu_+,\lambda))^2}{k_d^2 + c_1^2(q_1(\nu_+,\lambda))^2} \leq 1.$$

With this condition we obtain

$$|\lambda| \leq 1 - \nu_- + \nu_-\Big[|q_1(\nu_-,\lambda)| + \frac{\Delta x}{D_-}\Big((P_l + P_c(t))\Big|\frac{(c_1 - c_2)}{c_2}\Big| + \frac{P_p}{|c_2|}\Big)\Big].$$

If we assume $P_c(t)$ to be a bounded function, this implies stability for this coupling condition with Δx sufficiently small as above.

The second formula (4.42) of the membrane pumping conditions via one sided difference is given by

$$v_m^{n+1} = v_m^n + \nu_+(v_{m+1}^n - v_m^n) - \frac{\Delta t}{\Delta x}\Big((P_l + P_c(t))(v_m^n - u_m^n) + P_p\frac{(v_m^n)^2}{k_d^2 + (v_m^n)^2}\Big).$$

The stability follows analogously as above.

Central difference method

Analogously, we obtain the normal mode solution for u_m^{n+1} via the central difference method

$$\lambda = 1 - 2\nu_- + 2\nu_-q_1(\nu_-,\lambda) + 2\nu_-\frac{\Delta x}{D_-}\Big(\frac{(P_l + P_c(t))(c_1 - c_2)}{c_2} + \frac{P_p}{c_2}\frac{c_1^2(q_1(\nu_+,\lambda))^2}{k_d^2 + c_1(q_1(\nu_+,\lambda))^2}\Big). \tag{6.43}$$

and the normal mode equation for the second formula, i.e. for v_m^{n+1}

$$\lambda = 1 - 2\nu_+ + 2\nu_+q_1(\nu_-,\lambda) + 2\nu_+\frac{\Delta x}{D_+}\Big(\frac{(P_l + P_c(t)(c_2 - c_1)}{c_1} - \frac{P_p}{c_1}\frac{c_1^2(q_1(\nu_+,\lambda))^2}{k_d^2 + c_1(q_1(\nu_+,\lambda))^2}\Big). \tag{6.44}$$

The argument given above for the stability of the one sided normal mode equations of the membrane pumping conditions will be followed here too because the formulas only differ by a factor of 2 with the $\nu_{\pm}$.

6.4 GR-stability for the fully implicit discretization

Here we derive the GR-stability for the coupling conditions via an implicit discretization method. We derived the unconditional von Neumann stability for the interior points as well the GR-stability for the boundary conditions in Subsection 6.1.4 for the implicit discretization method. The fully implicit discretization system together with boundary conditions and the coupling conditions is given by

$$\begin{aligned}
(1+2\nu_-)u_0^{n+1} - 2\nu_- u_1^{n+1} &= u_0^n \qquad \text{for } j=0 \\
-\nu_- u_{j-1}^{n+1} + (1+2\nu_-)u_j^{n+1} - \nu_- u_{j+1}^{n+1} &= u_j^n \qquad \text{for } j<m \\
\text{the coupling conditions} \quad \text{for } j&=m \\
-\nu_+ v_{j-1}^{n+1} + (1+2\nu_+)v_j^{n+1} - \nu_+ v_{j+1}^{n+1} &= v_j^n \qquad \text{for } j>m \\
-2\nu_+ v_{2m-1}^{n+1} + (1+2\nu_+)v_{2m}^{n+1} &= v_{2m}^n \qquad \text{for } j=2m.
\end{aligned} \tag{6.45}$$

Normal mode equation for the interior nodes

Here we consider the second equation of the above system, which is for the interior nodes of the left sub-domain

$$u_j^n = -\nu_- u_{j+1}^{n+1} + (1+2\nu_-)u_j^{n+1} - \nu_- u_{j-1}^{n+1}. \tag{6.46}$$

Now we apply the normal mode solution $u_j^{n+1} = c\lambda^{n+1}q^j$ to the above formula. We obtain

$$\lambda^{-1} = -\nu_- q^{-1} + (1+2\nu_-) - q.$$

After re-arranging terms we get the following quadratic equation

$$q^2 + \Big(\frac{1-\lambda}{\nu_-\lambda} - 2\Big)q + 1 = 0.$$

The two roots of the above equation are given by

$$\widetilde{q}_{1,2} = \frac{2 - (\frac{1-\lambda}{\nu_-\lambda}) \mp \sqrt{(\frac{1-\lambda}{\nu_-\lambda} - 2)^2 - 4}}{2}.$$

A more convenient but not identical reformulation is

$$q_{1,2} = 1 + \frac{\lambda - 1}{2\nu_-\lambda}\Big[1 \mp \sqrt{1 + \frac{4\nu_-\lambda}{\lambda - 1}}\Big]. \tag{6.47}$$

This formula for the two roots is equivalent to the one derived in Giles [10, (30)] for the implicit discretization. The same formula for the roots can be derived for the right

sub-domain which will only differ by replacing ν_- by ν_+. Note that the roots $q_{1,2}$ in the implicit case are not equal to ones derived for the explicit case, but we use the same notation $q_{1,2}$ for the remaining part of this chapter.

In this case we follow Giles that for the roots with the minus sign is less 1 in absolute the solution exist so we will use $|q_1(\nu_\pm, \lambda)| \leq 1$ and the roots with the plus sign, i.e. $|q_2(\nu_\pm, \lambda)| \geq 1$.

6.4.1 Dirichlet-Neumann coupling

Let us consider the scheme of the implicit formula with Dirichlet-Neumann coupling conditions. We derived it in (4.53). For $j = m$ we have

$$u_m^n = -\nu_- u_{m-1}^{n+1} + (1 + \nu_-)u_m^{n+1} - \nu_+(v_{m+1}^{n+1} - v_m^{n+1}). \tag{6.48}$$

Again we have the Dirichlet condition $u_m^{n+1} = v_m^{n+1}$. To apply the normal modes to this we get $u_m^{n+1} = c_2\lambda^{n+1} = v_m^{n+1} = c_1\lambda^{n+1}$. So, the constants c_1 and c_2 have to be equal, i.e. $c_1 = c_2 = c$. These cancel as before in the calculation for the Dirichlet-Neumann coupling.

Inserting the separable normal mode solutions (6.18) into the above scheme we obtain the following normal mode equation

$$\begin{aligned} 1 &= -\nu_-\lambda q_2^{-1}(\nu_-, \lambda) + (1 + \nu_-)\lambda - \nu_+\lambda(q_1(\nu_+, \lambda) - 1) \\ &= \lambda\Big(1 + \nu_-(1 - q_1(\nu_-, \lambda)) + \nu_+(1 - q_1(\nu_+, \lambda))\Big). \end{aligned}$$

For an instability we would need to find a $|\lambda| > 1$ and $\lambda \in \mathbb{R}$. By Lemma 1 this implies $q_1(\nu_\pm, \lambda) \in \mathbb{R}$ and $|q_1(\nu_{\pm,\lambda})| \leq 1$. We define $\xi =: \Big(1+\nu_-(1-q_1(\nu_-, \lambda))+\nu_+(1-q_1(\nu_+, \lambda))\Big)$. Clearly we have $1 - q_1(\nu_\pm) \geq 0$. This implies that $\xi \geq 1$. This gives us $|\lambda| = \frac{1}{|\xi|} \leq 1$. This is a contradiction to $|\lambda| > 1$. We obtain a stable solution for the implicit case of Dirichlet-Neumann coupling scheme under the CFL condition (6.4).

Chapter 7

Numerical results and discussion

In this chapter we discuss the numerical results for the single domain diffusion equation as well as for the various coupling conditions with bi-domain diffusion equations considered in this thesis. We used an explicit as well an implicit discretization methods for the single as well as for the bi-domain diffusion equations. In the first section we discuss the numerical results for the single domain diffusion equation. In the second section we give for the Dirichlet-Neumann (DN) coupling with error in the L_1 norm as well the order of convergence. In the third section we explain the various test cases for the stable and unstable solutions for the heat flux coupling conditions. In the fourth section we give a comparison of the results for the heat flux, membrane pumping as well as for the simplified membrane pumping.

We explain the results for the channel pumping conditions and its special case simplified channel pumping conditions in section five. Section 6 contains the results for the membrane pumping conditions, its special case simplified membrane pumping and the linearized membrane pumping condition. The details for the solution times and iterations counts will present in Section 7.

We will consider single and bi-domain diffusion problems on the interval $[0, 1]$. The basic details of the discretization were discussed in Sections 3.2 and 4.1. The spatial mesh size is given as $\Delta x = 1/N$. We choose the CFL-number 1/3, this leads to the time step size $\Delta t = \frac{(\Delta x)^2}{3\max(D_1,D_2)}$. For a given time T the number of time steps is $M = T/\Delta t$. In our calculations we choose $T = 6.666666666666667e-01$. The table for all the necessary parameters w.r.t. the different mesh sizes and with corresponding number of time steps are given in Figure 7.1.

7.1 Results of the single domain computations

Here we give the numerical results for the various discretization methods used for the single domain diffusion equation with homogeneous Neumann boundary conditions that were derived in Chapter 3. The numerical scheme for the explicit FTCS was given in (3.18), for the implicit BTCS in (3.25) and for the explicit finite volume scheme in (3.35).

As our test case we consider the non-negative exact solution $w(t, x) = e^{-D\pi^2 t}\cos(\pi x) + 1$ on the spatio-temporal domain $[0, T] \times [0, 1]$ for the diffusion equation. It satisfies the

Figure 7.1: Table for number of nodal values N, number of time steps M, time step size $\Delta t = \frac{(\Delta x)^2}{3\max(D_1,D_2)}$, spatial mesh size Δx and for $T = M\Delta t$.

Nodes N	time steps $M = T/\Delta t$	Δt	$\Delta x = 1/N$
200	80	0.0083	0.005
400	320	0.0021	0.0025
600	720	9.25e-04	0.0017
800	1280	5.20e-04	0.0013
1000	2000	3.33e-04	1.0000e-03
1200	2880	2.314e-04	8.3333e-04
1400	3920	1.700e-04	7.1429e-04

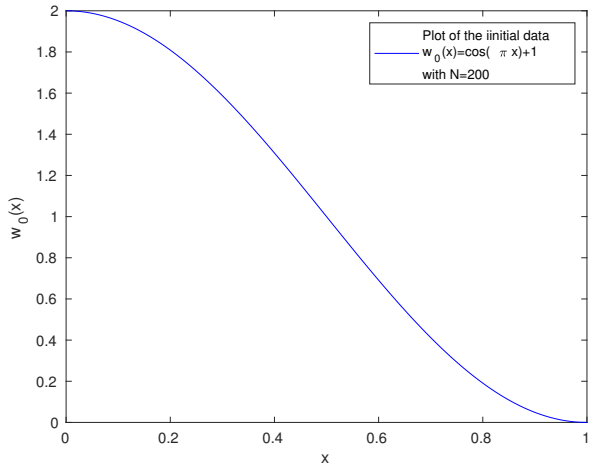

Figure 7.2: **Initial data:** Plot of the initial data $w_0(x) = \cos(\pi x) + 1$.

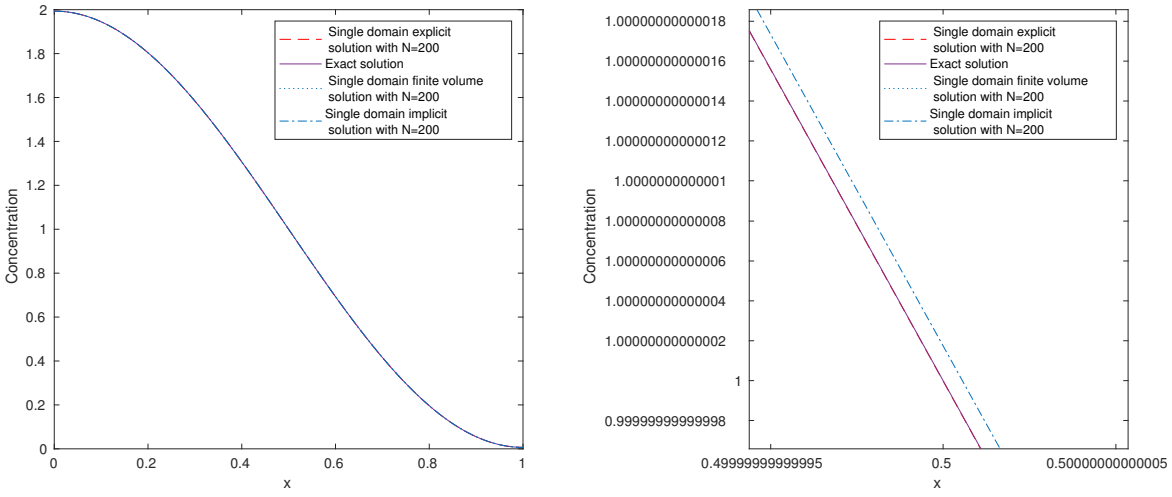

Figure 7.3: **Single domain:** Comparison of the exact, explicit, implicit and finite volume solution for the single domain diffusion equation, while the right figure is the zoom at the mid point of the internal, i.e. on 0.5.

initial data $w_0(x) = \cos(\pi x) + 1$ plotted in Figure 7.2 and the homogeneous Neumann boundary conditions, i.e. $w_x(0) = w_x(1) = 0$. We will present the comparisons of this solution with the numerical solutions obtained via the explicit, implicit and finite volume discretization methods. The diffusion coefficient $D = 0.001\ m^2 s^{-1}$, mesh size $\Delta x = 1/N = 1/200$ and with corresponding number of time steps $M = 80$ are used. The choice is somewhat arbitrary since e.g. Thul and Falcke [38] used much smaller values and Zhang et al. [40] much larger ones. The results for all methods together with the exact solution are shown in Figure 7.3 with the zoom at the mid point 0.5. These results are close to each other. So we give zooms at the left and on the right boundary which are given in Figure 7.4.

We observed that the finite volume scheme gives a less exact solution than the explicit FTCS and implicit BTCS. Clearly this can be seen in the graphs of Figure 7.3. Also this difference is seen in the L_1 error in Figure 7.6.

7.1.1 L_1 error computations

We know an exact solution of the diffusion equation (3.1). So, we can compute the L_1 error, see the formulations in Section 3.6. Here we compute this error for the single domain diffusion equation for various discretization methods namely the explicit FTCS, implicit BTCS and explicit cell based finite volume method. The parameters, for which we compute the error, are given in Figure 7.1.

All these error computations for the FTCS and BTCS using the exact solver in each time step are arranged in table form in Figure 7.5. For the explicit finite volume method they are given in Figure 7.6. The errors were computed at the final time $T = 6.66666e{-}01$

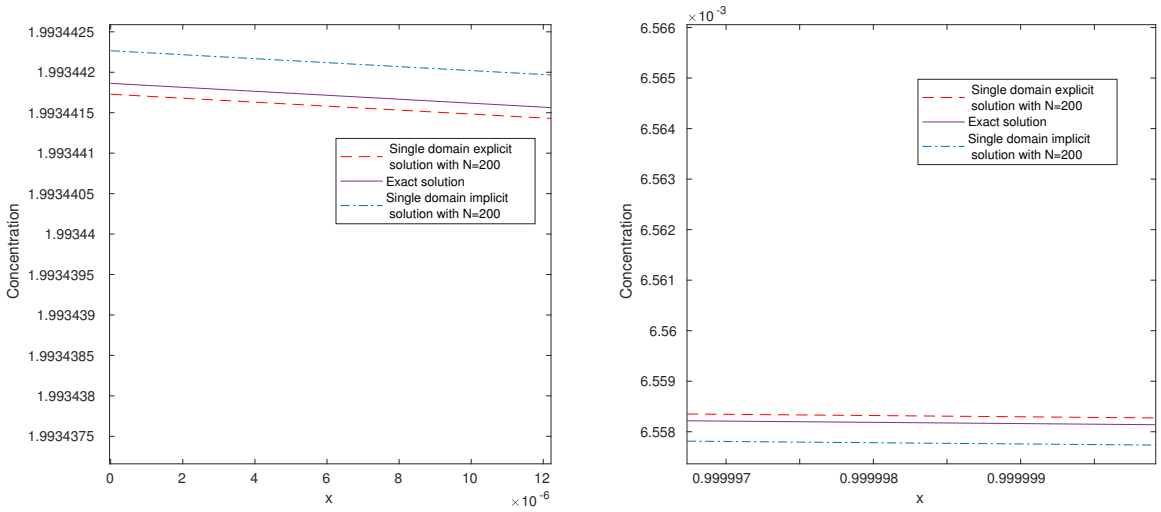

Figure 7.4: **Zoom of the Figure 7.3:** The left panel is the zoom of left end of the boundary of Figure 7.3 and the right panel is the zoom of the right end boundary

and the diffusion coefficient used above. The implicit scheme has a larger error than the explicit scheme. The finite volume scheme gives slightly worse results than the finite difference explicit scheme. A comparison for the log of the L_1 error, i.e. $\log(E_M(h))$ for these three methods, is plotted in the left panel of the Figure 7.7, while the order of convergence can be seen in the right panel.

7.2 Dirichlet-Neumann coupling computations

In Chapter 4 we derived the schemes for the Dirichlet-Neumann (DN) coupling for the bi-domain diffusion equations with various coupling discretization methods including the explicit nodal based coupling, the explicit finite volume cell based coupling and the implicit coupling methods. The explicit nodal based scheme was derived in (4.11), for the explicit finite volume cell based in (4.23) and for the implicit coupling method in (4.53).

The numerical procedures of these various coupling methods are given in algorithms $A1$, $A2$ and $A3$. These can be found in the Subsections 4.1.2, 4.2.1 and 4.2.2 respectively. We give numerical results for these algorithms. All results for these methods are obtained for the spatial domain $[0, 1]$ with the interface at $x = 0.5$. We have the zero flux Neumann outer boundary conditions, i.e. $u_x(0) = 0$. We use again the initial data $u_0(x) = \cos(\pi x/L) + 1$ for $x \in [0, 1/2]$ and $v_0(x) = \cos(\pi x/L) + 1$ for $x \in [1/2, 1]$ which are plotted in Figure 7.2. We consider identical as well as un-equal diffusion coefficients for these three methods. Results are given in the following three subsections.

Figure 7.5: **Single domain:** Table of L_1-error and numerical order of convergence (NOC) for single domain diffusion equation computed via explicit FTCS, implicit FTCS methods.

N	$E_M(h)$-FTCS (explicit)	NOC	$E_M(h)$-BTCS (implicit)	NOC
200	8.556498810833192e-08		2.566687725217643e-07	
400	2.139100654452614e-08	2.000016	6.417142470268746e-08	1.99990
600	9.507094722562578e-09	2.00000	2.852105819638663e-08	1.99996
800	5.347737733092669e-09	2.00000	1.604328622745763e-08	1.99995
1000	3.422545358139610e-09	2.00000	1.026772952039765e-08	1.99998
1200	2.376773246719804e-09	1.99998	7.130697937340753e-09	1.99974
1400	1.746202345499005e-09	1.99999	5.239139725389993e-09	1.99967

Figure 7.6: **Single domain:** Table of L_1-error and numerical order of convergence (NOC) for the single domain diffusion equation computed via the finite volume cell based method.

N	$E_M(h)$-FV-scheme (explicit)	NOC
200	8.556762708040664e-08	
400	2.139117129657063e-08	2.0000496
600	9.507127133935071e-09	2.0000155
800	5.347747843576079e-09	2.0000077
1000	3.422549401822966e-09	2.0000072
1200	2.376775105666832e-09	1.9999891
1400	1.746202929372229e-09	1.999996

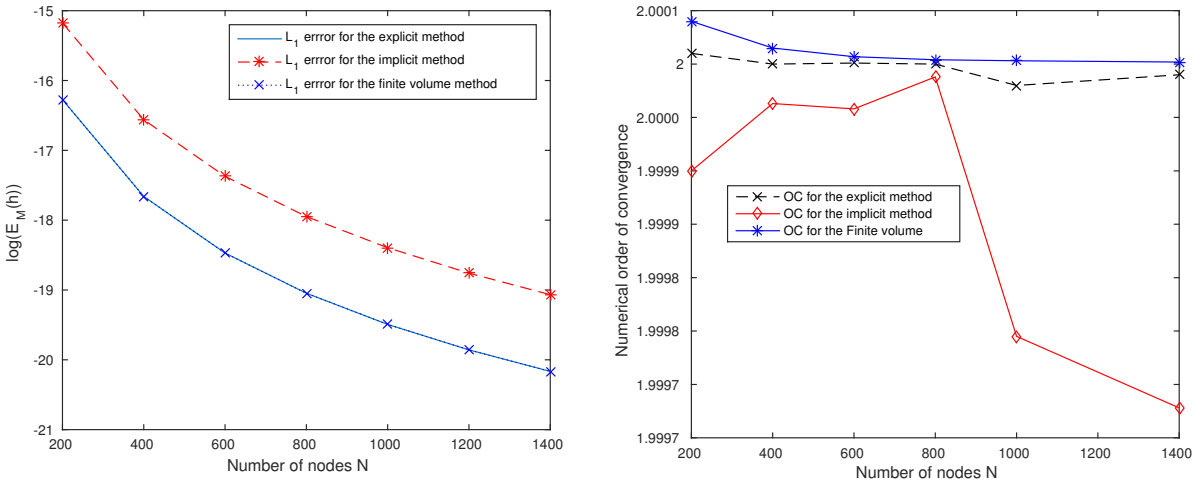

Figure 7.7: **Single domain:** The left panel shows $\log(E_M(h))$ for the single domain diffusion equation over the number of nodes via the explicit, the implicit method and the finite volume scheme, while the right panel gives the numerical order of convergence.

7.2.1 DN-coupling with bi-domain diffusion equation for the identical diffusion coefficients

Here we calculate the numerical solution for the DN-coupling scheme with the identical diffusion coefficients $D_- = D_+ = 0.001$ via the explicit, implicit monolithic, implicit partitioned iterative approach and for the scheme of Giles. We know from Chapter 4 that in the case of our explicit DN-coupling scheme for the same diffusion coefficients we obtain a scheme identical to the one for the single domain diffusion equation. In our implementation of both schemes we observed identical results. Also we have an exact solution for comparison.

We use the initial data given above, with mesh size $\Delta x = 1/N = 1/200$. The solutions are given in Figure 7.8 with a zoom at the left boundary in the right panel. We compare with the exact solution. From now on we only show a zoom at the left boundary. The solutions at the right boundary are symmetric in reverse order as was seen in Figure 7.4.

In these computations we observed that the exact solution lies between the explicit and implicit solutions. Both implicit solutions, monolithic and partitioned iterative, are also not distinguishable with a stronger zoom. We know that the formulas for the left and right hand boundaries of our explicit scheme and the Giles scheme are same. They differ only at the interface. So they are also on the top of each other at the boundaries. As we observed in the single domain computations the finite volume is a bit worse here too.

Further we calculated the numerical values of the L_1 error for clear insight. For the explicit methods the numerical values for the L_1 error are given in a table given in Figure 7.10. For the implicit methods it is given in Figure 7.11 and for the Giles scheme in Figure 7.12.

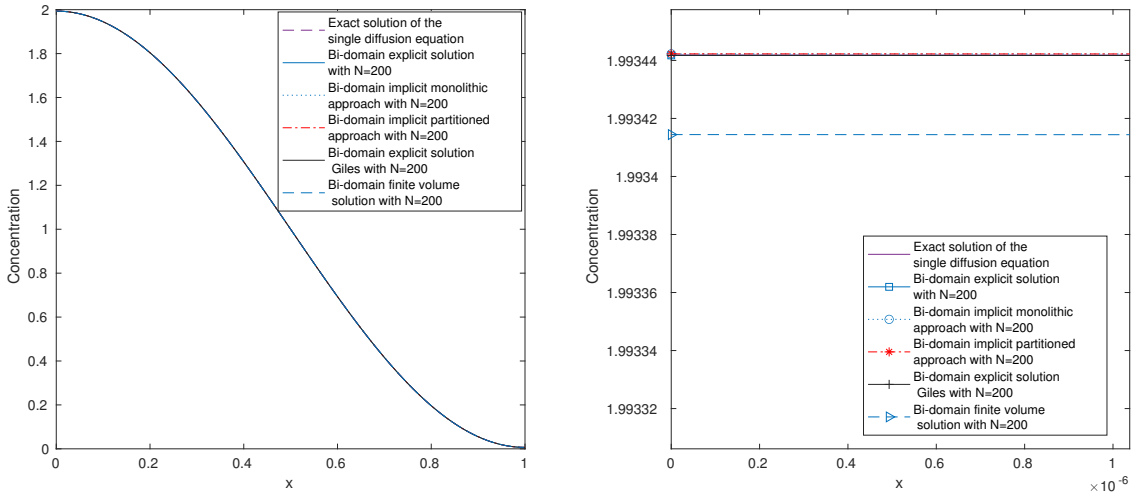

(a) (b)

Figure 7.8: **Single and bi-domain diffusion equations:** with DN-coupling via explicit, implicit monolithic, implicit partitioned and Giles coupling scheme with the identical diffusion coefficients $D_- = D_+$, while the figure in the right panel is the zoom on the left boundary.

These L_1 errors are too small which are not distinguishable so we take a *log* of the errors. These are plotted in the left panel of the Figure 7.13, while the corresponding numerical order of convergence are given in the right panel.

7.2.2 DN-coupling with un-equal diffusion coefficients

Now we give the numerical results for the DN-coupling via explicit, implicit methods with bi-domain diffusion equations for un-equal diffusion coefficients $D_- = 0.001$ and $D_+ = 0.003$.

Test case 1, for the cosine initial data

Here we compute the solution of DN-coupling for un-equal diffusion coefficients via explicit and implicit discretization methods. The results are computed for the parameters given in Figure 7.1. The results are given for the cosine initial data with explicit method are given in Figure 7.14.

For the comparison we also compute the solution via implicit monolithic as well as for the implicit partitioned coupling iterative coupling approach and for the Giles scheme (4.13). These results are plotted in Figure 7.15 with the same data given above with mesh size $\Delta x = 1/1400$.

Again the results are not clearly distinguishable. So, we zoom in at the interface of the figure given in the left panel. It is given in the right panel of the Figure 7.15. The three solutions of our DN-coupling schemes are near to each other while the the Giles one is a bit away. This can be seen in Figure 7.15. Therefore we show another zoom of the

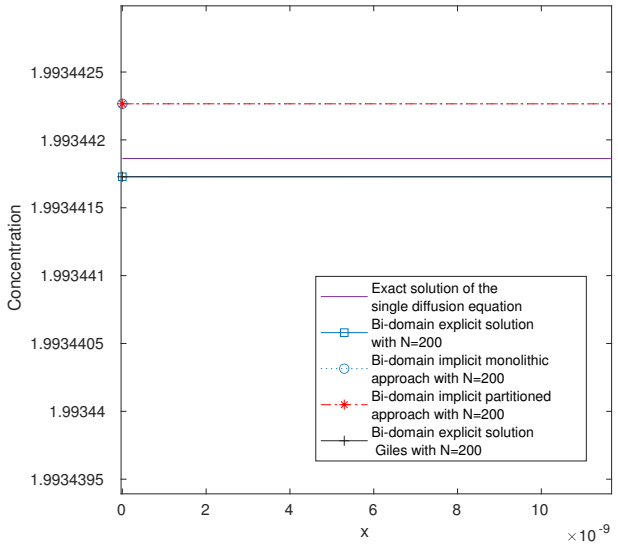

Figure 7.9: **Further zoom of Figure 7.8** without finite volume solution.

Figure 7.10: **Bi-domain with DN-coupling via explicit methods for $D_- = D_+$:** Table for the L_1 error and numerical order of convergence (NOC) for the bi-domain diffusion equations with Dirichlet-Neumann coupling via explicit nodal based and explicit finite volume (cell based) schemes with $D_- = D_+ = 0.001\ m^2 s^{-1}$ and initial data $u_0(x) = \cos(\pi x) + 1$ for $x \in [0, 1/2]$ and $v_0(x) = \cos(\pi x) + 1$ for $x \in [1/2, 1]$.

N	Explicit (nodal based)	NOC	Explicit finite volume(cell based)	NOC
200	8.556498810562790e-08		8.489560814769387e-08	
400	2.139100637520629e-08	2.00001	2.130716922972956e-08	1.99435
600	9.507094796064251e-09	2.00000	9.482237650850574e-09	1.99677
800	5.347737808639870e-09	2.000001	5.337247600968709e-09	1.99772
1000	3.422545398932502e-09	2.00000	3.417173263687602e-09	1.99824
1200	2.376773342011054e-09	1.99998	2.373663919416076e-09	1.99856
1400	1.746202354509961e-09	1.99999	1.744243691333185e-09	1.99878

Figure 7.11: **Bi-domain diffusion equations with DN-coupling via implicit methods for $D_- = D_+$:** Table for the L_1 error and numerical order of convergence (NOC) for the bi-domain diffusion equations with Dirichlet-Neumann coupling via implicit monolithic and implicit partitioned with $D_- = D_+ = 0.001\ m^2 s^{-1}$ and initial data $u_0(x) = \cos(\pi x) + 1$ for $x \in [0, 1/2]$ and $v_0(x) = \cos(\pi x) + 1$ for $x \in [1/2, 1]$.

N	Implicit monolithic approach	NOC	Implicit partitioned approach	NOC
200	2.566687726083617e-07		4.392006789042615e-07	
400	6.417142485006956e-08	1.999904	1.073150103537145e-07	2.033028
600	2.852105841991153e-08	1.99996	4.733602945757239e-08	2.018661
800	1.604328660326812e-08	1.99995	2.652673643867433e-08	2.013050
1000	1.026772963264120e-08	1.999988	1.693892546605989e-08	2.010091
1200	7.130698464696688e-09	1.999745	1.174585371987267e-08	2.008067
1400	5.239140283911478e-09	1.99967	8.620629839927151e-09	2.006751

Figure 7.12: **Bi-domain:** Table of L_1-error and numerical order of convergence (NOC) for bi-domain diffusion equation with DN-coupling of Giles scheme computed via the explicit coupling method.

N	$E_M(h)$-Giles-scheme(explicit)	NOC
200	8.556498810562790e-08	
400	2.139100636826739e-08	2.00001
600	9.507094791253282e-09	2.000004
800	5.347737828207554e-09	2.000001
1000	3.422545399154546e-09	2.000008
1200	2.376773350337728e-09	1.999986
1400	1.746202359585267e-09	1.99999

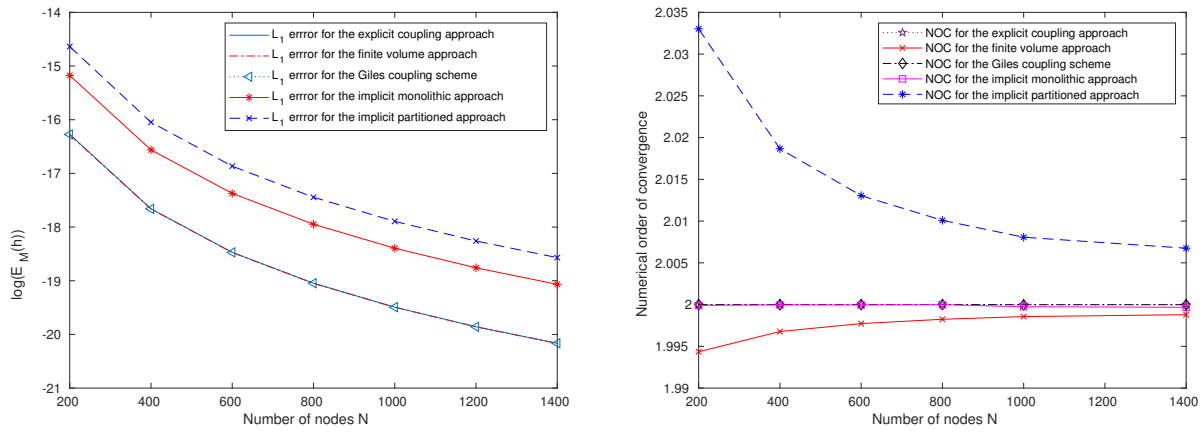

(a) (b)

Figure 7.13: **Bi-domain with DN-coupling via explicit and implicit methods for $D_- = D_+$:** The figure in the left panel is the log of the L_1 error, i.e. $\log(E_m(h))$, while the right panel is given for the numerical order of convergence (NOC) with $D_- = D_+ = 0.001$.

three solutions in Figure 7.16.

This difference of the solutions were explained for the discrete mass conservation previously in the subsection 5.5.2.

Test case 2, for the piecewise constant initial data

Also we plot the solution of the DN-coupling via explicit, implicit coupling methods and the Giles coupling scheme for the piecewise constant initial data $u_0(x) = 0.06$ for $x \in [0, 1/2]$ and $v_0(x) = 700$ for $x \in [1/2, 1]$. The remaining data for these computations are the same as used above. The results are given in Figure 7.17. We observed that the results of the Giles scheme is away from the results of our three coupling schemes. So we zoom in at the interface of the solutions obtained via three coupling methods. It is given in Figure 7.18.

7.3 Results of the heat flux coupling conditions

We concluded in Chapter 5 that the discretization of the heat flux coupling conditions via one sided difference method does not maintain the discrete mass conservation while the central difference maintains it. So, here we show only the numerical results for the conservative central difference method. The explicit formulas for the heat flux coupling conditions via the central difference method were derived in (4.31) and (4.32). The schemes for the the implicit monolithic method were derived in (4.63) and (4.64) and for the implicit partitioned iterative approach in (4.65) and (4.66). Unless mentioned otherwise the computations use the value $H = 1$. Here we present some test cases to discuss the solution of the heat flux coupling conditions. We used different initial data namely cosine initial

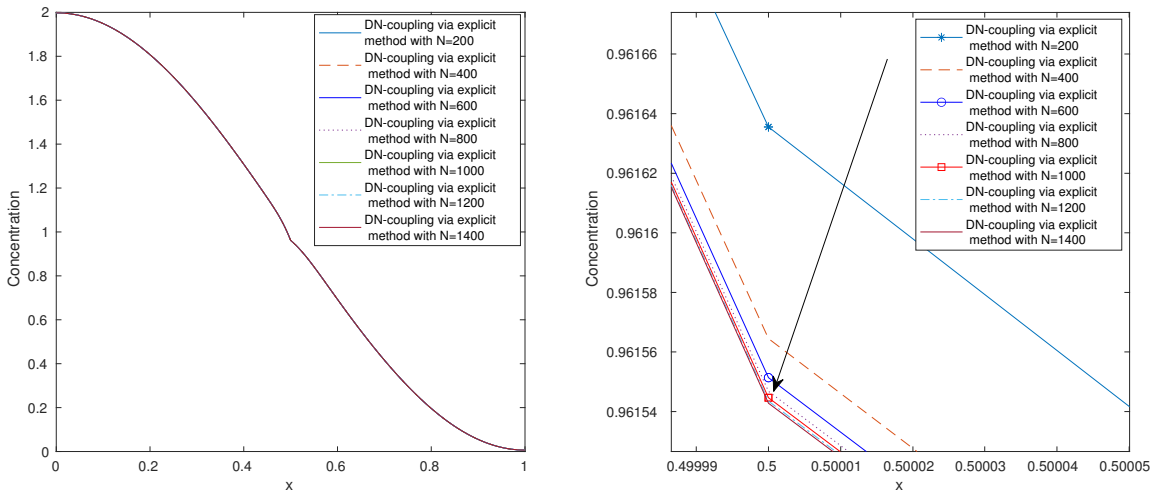

(a) (b)

Figure 7.14: **Bi-domain diffusion equation:** with DN-coupling via explicit method with diffusion coefficients $D_- \neq D_+$ and cosine initial data, while the figure in the right is the zoom at the interface of the figure given in the left.

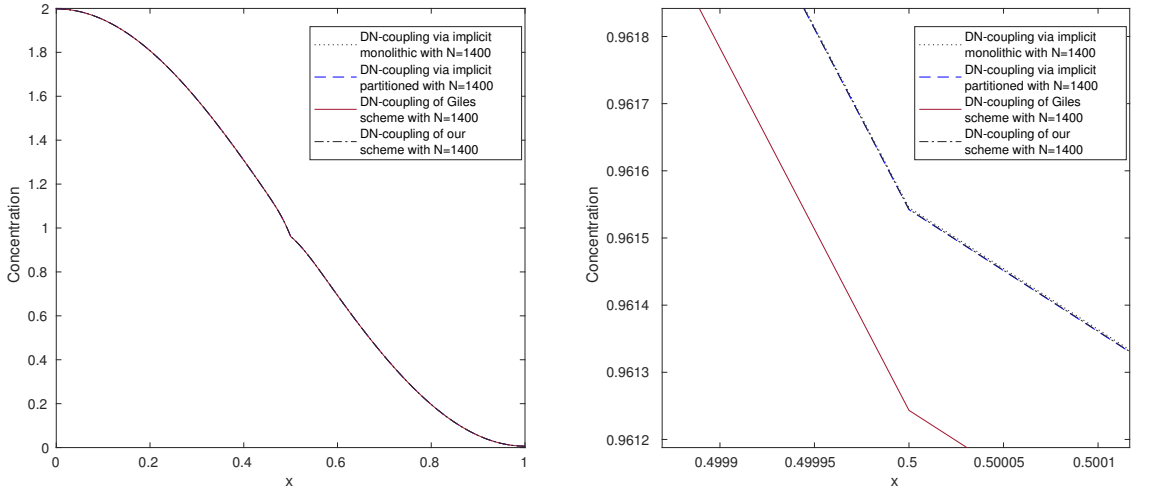

(a) (b)

Figure 7.15: **Comparison of the bi-domain diffusion equations:** with DN-coupling conditions via the explicit, implicit monolithic, implicit partitioned iterative coupling approach and for the DN-coupling of Giles with un-equal diffusion coefficients $D_- \neq D_+$ for the cosine initial data.

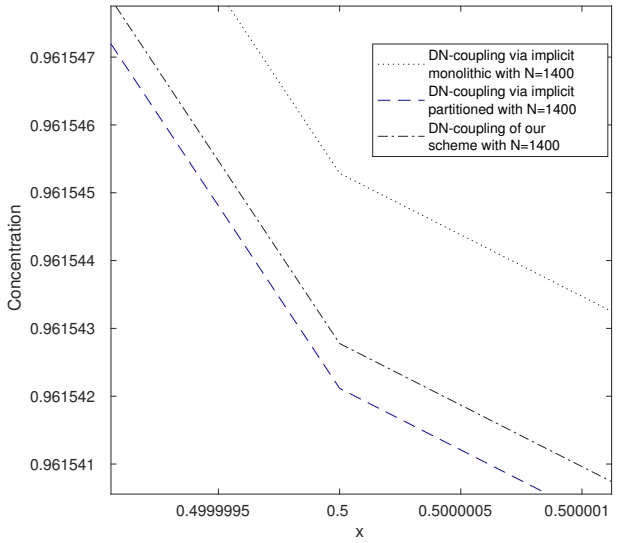

Figure 7.16: **Further zoom:** zoom into the upper numerical solutions in Figure 7.15 (b).

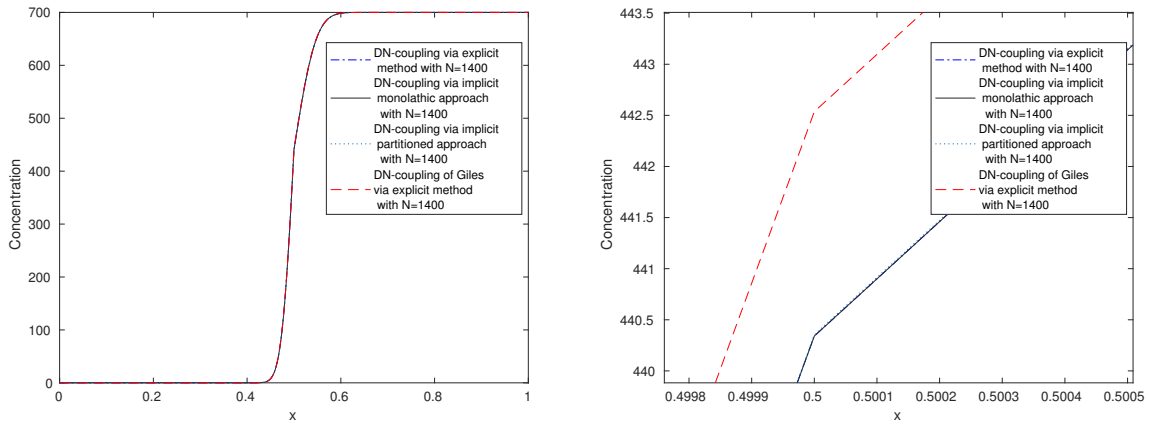

Figure 7.17: **Comparison of the bi-domain diffusion equations:** with DN-coupling conditions via the explicit, implicit monolithic, implicit partitioned iterative coupling approach and for the DN-coupling of Giles with un-equal diffusion coefficients $D_- \neq D_+$ for the cosine initial data, while the figure in the right panel is zoom into the numerical solutions near $x = 0.5$.

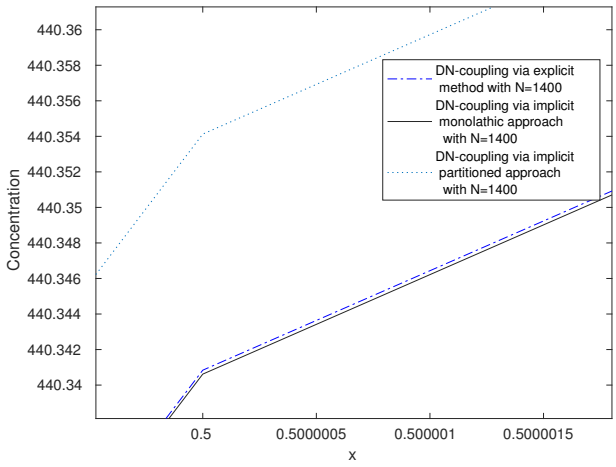

Figure 7.18: **Further zoom:** into the lower numerical solutions in Figure 7.17 (b) at $x = 0.5$.

data and piecewise constant data. Also we show a stable and unstable solutions for this coupling conditions with different diffusion coefficients.

Test case 1, cosine data

In this case we choose the initial data $u_0(x) = \cos(\pi x/L) + 1$ for $x \in [0, 1/2]$ and $v_0(x) = \cos(\pi x/L) + 1$ for $x \in [1/2, 1]$, the diffusion coefficients, $D_- = 0.001$ and $D_+ = 0.003$. Here, we calculate the results for the heat flux coupling conditions by using the parameters given 7.1 via the explicit method.

Note that for the mesh size $\Delta x = 1/200$ we obtain an unstable solution, which is shown in the left panel of the Figure 7.19. While stable solutions for Δx other than $1/200$ which are shown in the right panel of Figure 7.19. These results in the right panel are not clearly distinguishable so we take a zoom in at the interface. The zoom near to the interface can be seen in the Figure 7.20.

For the same data given above we also use an implicit monolithic coupling approach. For this the schemes were derived in (4.63) and (4.64). Here we get a stable solution even in a larger $\Delta x = 1/200$. The obtained results are plotted in Figure 7.21 with zoom at the interface.

Computations with smaller diffusion coefficients and with different values of H

In these computations we fixed the mesh size $\Delta x = 1/1400$. Here we use un-equal smaller diffusion coefficients $D_- = 200 \times 10^{-06}$ and $D_+ = 200 \times 10^{-05}$ taken from Chamakuri [26].

We show the results for different values of H. We consider $H = 1$ to $H = 3$ and $H = P_l + P_c(t) = 6.3613E{-}12$ to see the behavior of the solution. The second value for H comes from taking only the linear part of the membrane condition (2.20) with the values given in Table 2.1. For these computations we used the explicit coupling method. For these values of H we made a time evolution study by taking $M = 80, 320, 720, 1280, 2000, 2820, 3920$.

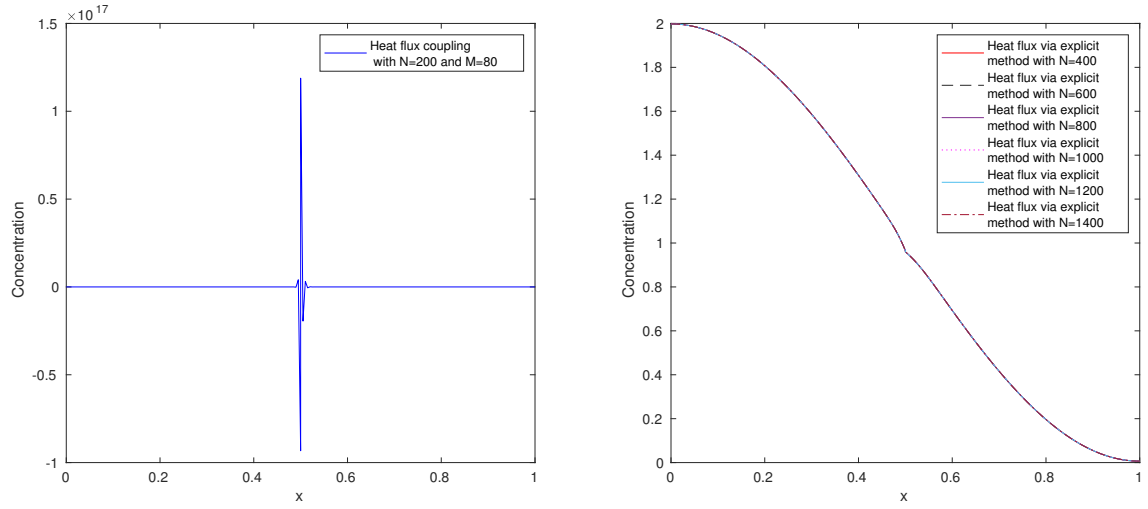

(a) (b)

Figure 7.19: **Unstable and stable solution:** the bi-domain diffusion equations with heat flux conditions via the explicit method.

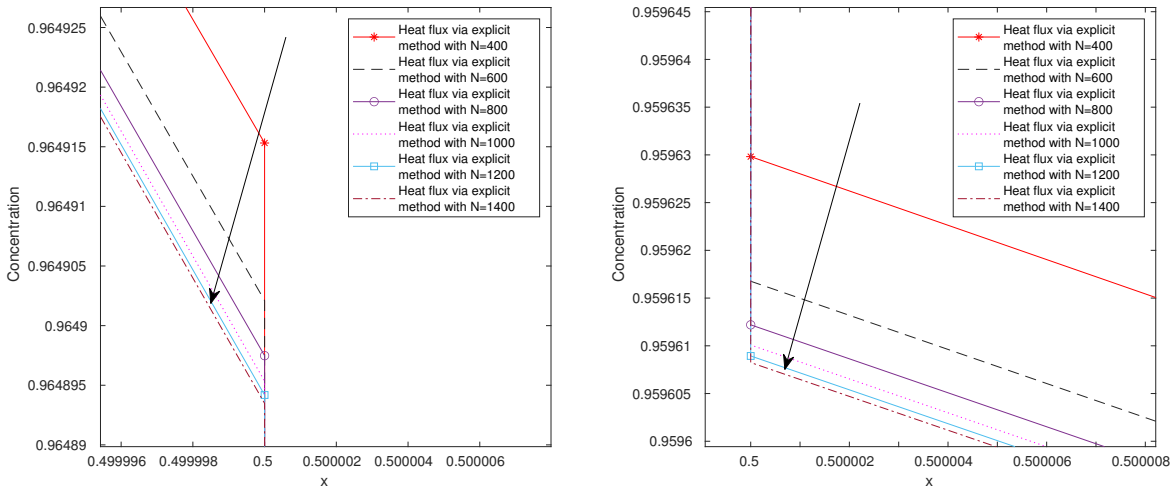

(a) (b)

Figure 7.20: **Zoom of the right panel of Figure 7.19:** The left panel is the zoom of the upper part of the kink and the right panel is the lower part of the kink at the interface. The arrows in the figure points in the direction of increasing value of N.

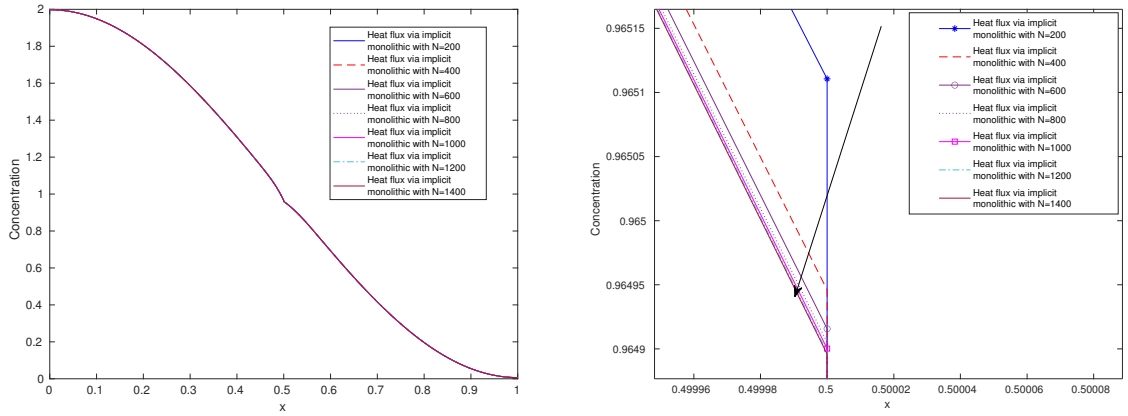

(a) (b)

Figure 7.21: **Bi-domain diffusion equations:** with heat flux conditions via implicit monolithic approach with cosine initial data, while the figure in the right panel is the zoom at the interface.

First we show the numerical results for $H = 1$ which are given in Figure 7.22. The results of a second computation for $H = 3$ are shown in the Figure 7.23. We observed a similar behavior for $H = 1$ to $H = 3$ while we obtain an unstable solution for values of H larger than 3. Note that in this case an increasing jump discontinuity arises at the interface.

Then we calculate the results for $H = 6.3613E - 12$ which is a small positive real number. The results are shown in the Figure 7.24.

Computations with different diffusion coefficients and H

The conditional stability of the heat flux coupling depends on the term $\frac{H\Delta x}{D_\pm}$. We observed instability when these terms become too large. For this purpose we made numerical studies in which we varied only one of three parameters.

We computed the various solutions for the heat flux coupling condition via the explicit discretization method with various diffusion coefficients used in the literature for the similar problems and some values we have chosen. For the diffusion coefficients $D_- = 0.001$, $D_+ = 0.003$ and $D_- = 200E - 05$ and $D_+ = 200E - 06$ as in Thul [37] and $H = 1$ we get an unstable solution for larger mesh sizes Δx, i.e. $\Delta x = 1/200$ and $1/400$. A stable solution is obtained for smaller values than these.

Then for larger diffusion coefficient as $D_- = 0.01$, $D_+ = 0.03$ or $D_- = 0.1$, $D_+ = 0.2$ or $D_- = 1$, $D_+ = 2$ or $D_- = 222$, $D_+ = 223$ as in Zhang et al. [40] and $H = 1$ we get a stable solution even for larger $\Delta x = 1/200$ and $1/400$.

Further for smaller $H = 0.06$ with $D_- = 0.001$, $D_+ = 0.003$ and $D_- = 200E - 05$, $D_+ = 200E - 06$ we get a stable solution for the mesh sizes $\Delta x = 1/200$ and $1/400$ as well as for ones smaller than these.

So we conclude that the stability for heat flux coupling conditions with the explicit discretization depends on mesh size Δx, diffusion coefficients $D_\pm$ and on heat flux coefficients

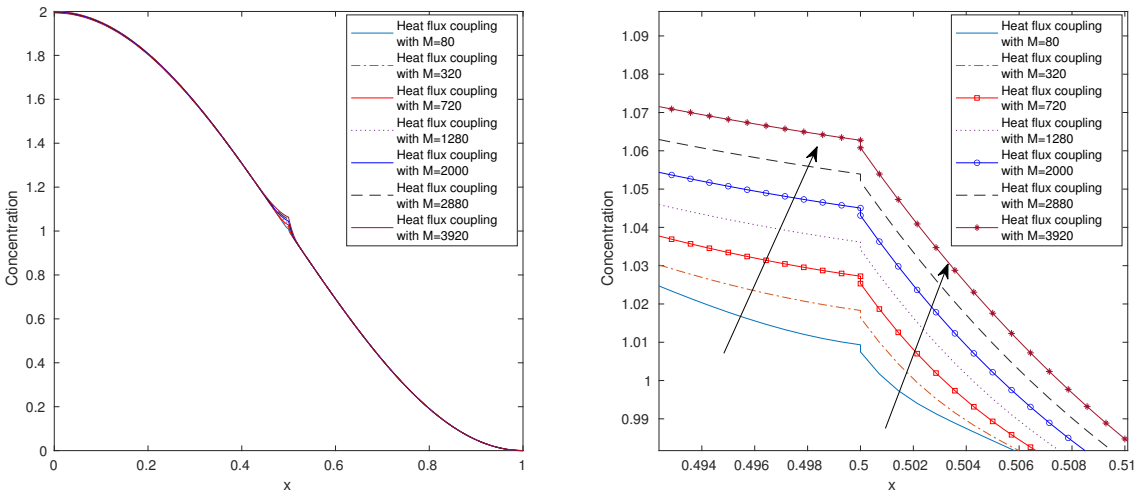

(a) (b)

Figure 7.22: **Bi-domain diffusion:** with heat flux conditions via explicit method with $H = 1$, while the right figure is the zoom at the interface.

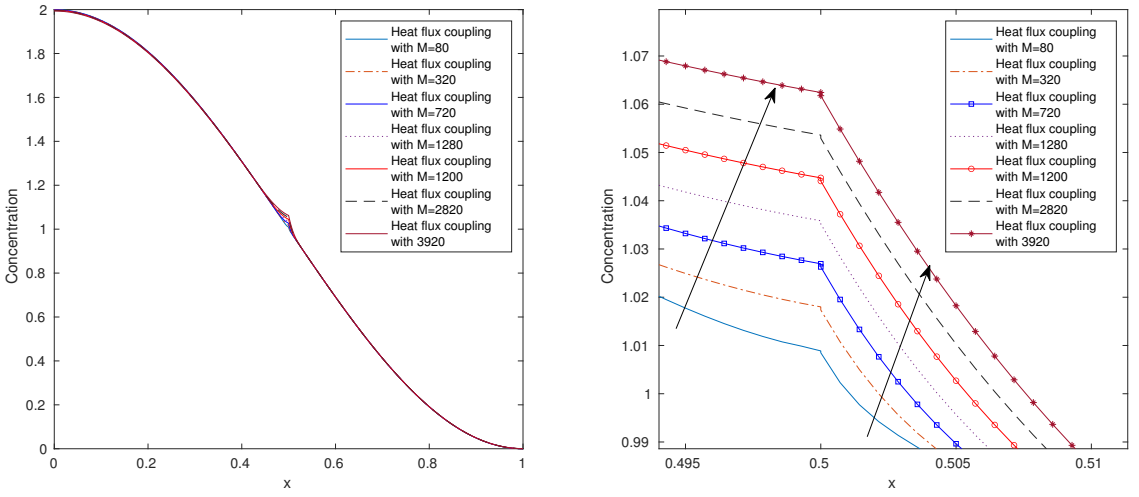

(a) (b)

Figure 7.23: **Bi-domain diffusion equations:** with heat flux conditions via explicit method with $H = 3$, while the right figure is the zoom at the interface.

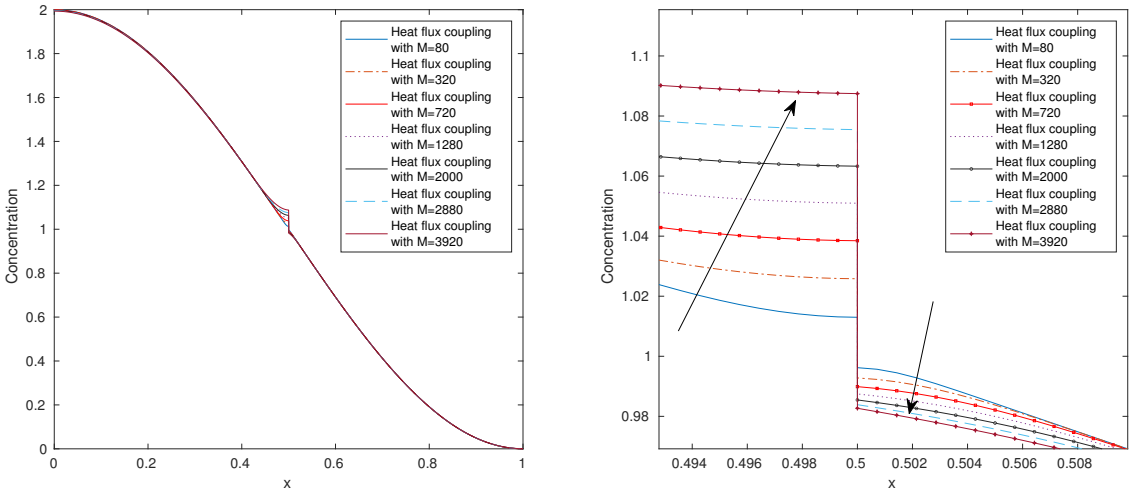

(a) (b)

Figure 7.24: **Bi-domain diffusion equations:** The figure in the left panel is for $H = P_l + P_c(t) = 6.3613E-12$ with heat flux conditions via explicit method, while the figure in the right panel is the zoom at the interface of the left figure.

H are in a manner consistent with the stability analysis in Section 6.3.

In this computations we fixed the mesh size $\Delta x = 1/1400$, the number of time steps $M = 3920$ and varies the value of H from $H = 1$ to $H = 4.4$. So, we obtained the stable solutions from 1 to 4.3 and unstable solution for $H = 4.4$. These solutions are plotted in Figure 7.25.

Test case 2, double cosine data

Here we used the initial data $u_0(x) = \frac{1}{4}\cos(2\pi x) + \frac{3}{4}$ for $x \in [0, 1/2]$ and $v_0(x) = \frac{1}{4}\cos(2\pi x - \pi) + \frac{1}{4}$ for $x \in [1/2, 1]$ in order to reduce to zero the slope of the initial data at the coupling interface $x = 1/2$. The plot of the initial data is given in Figure 7.26. We use the parameters as in test case 1 and the explicit discretization method. Again we obtained an unstable solution for the mesh size $\Delta x = 1/200$ and a stable solution for the Δx smaller than this. The unstable solution is shown in the left panel of Figure 7.27 while the stable solutions are plotted in the right panel. The different stable solutions are not distinguishable, the zoom is given at the interface in Figure 7.28.

Test case 3, piecewise constant data

In this test we show the results of the heat flux coupling conditions for the piecewise constants initial data via explicit coupling method. We use the diffusion coefficients $D_- = 0.001$ and $D_+ = 0.003$ with constant initial data $u_0(x) = 0.06$ for $x \in [0, 1/2]$ and $v_0(x) = 700$ for $x \in [1/2, 1]$.

We calculate the results with parameters given in Figure 7.1. Again we obtain an

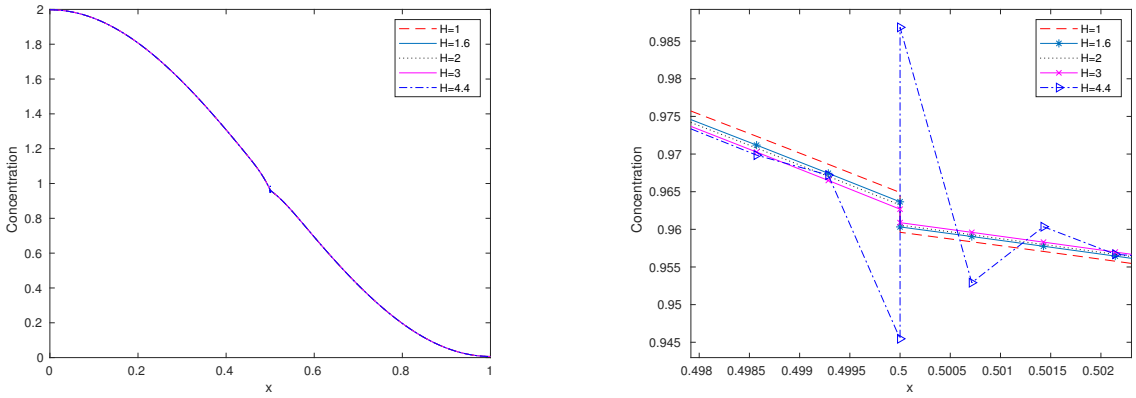

Figure 7.25: Stable and unstable solutions for the heat flux coupling conditions with variation of H.

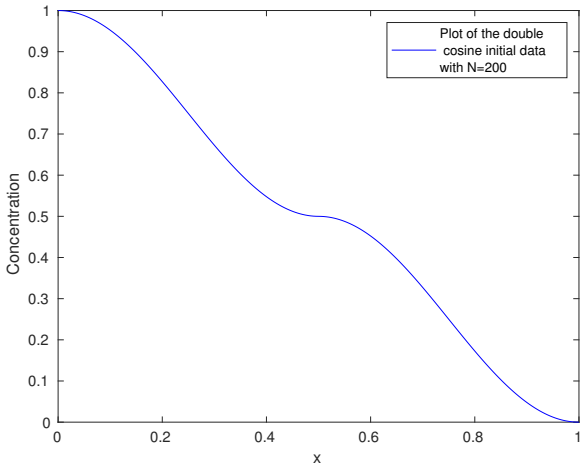

Figure 7.26: **Plot of the double cosine initial data.**

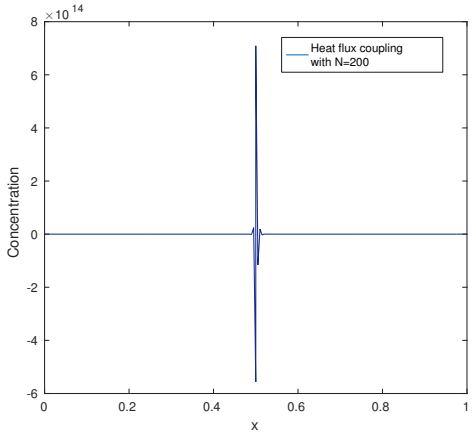

(a)

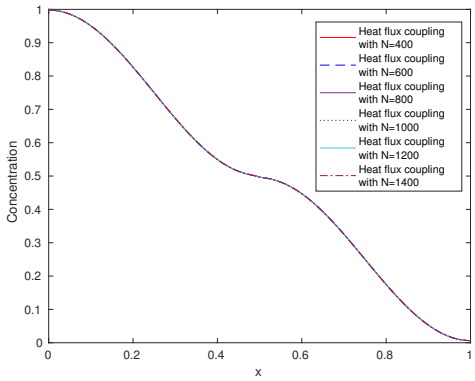

(b)

Figure 7.27: **Unstable and stable solution:** the bi-domain diffusion equations with heat flux conditions via the explicit method.

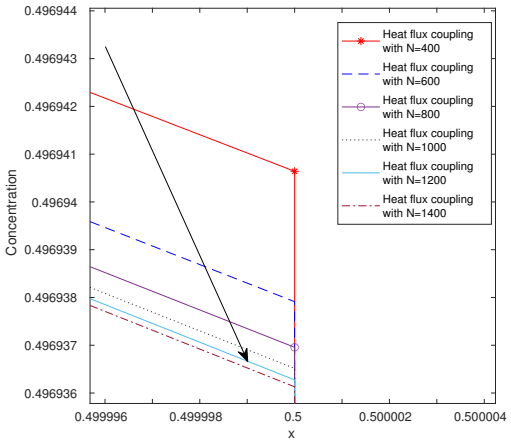

(a)

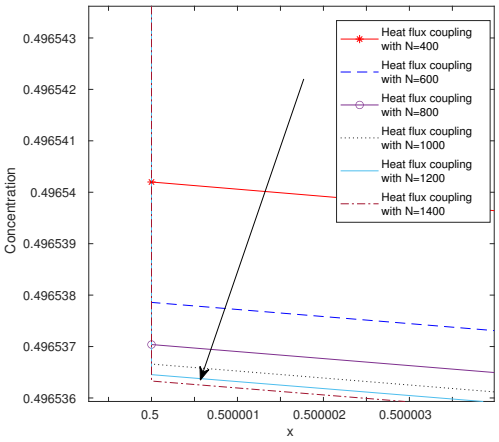

(b)

Figure 7.28: **Zoom of the Figure given in the right panel of 7.27:** at the interface on the left and right hand side.

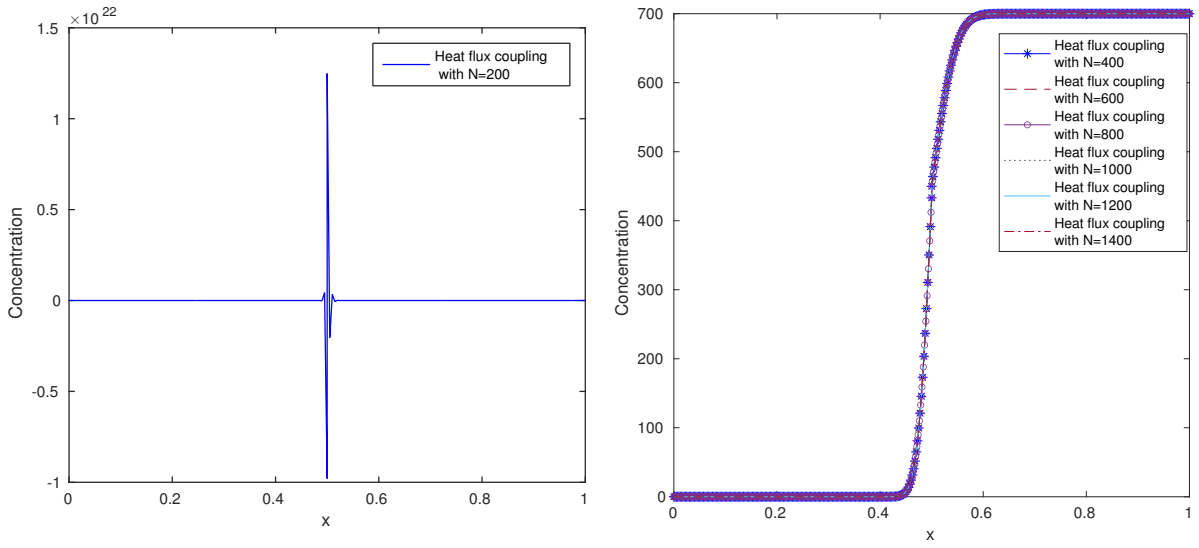

(a) (b)

Figure 7.29: **Unstable and stable solution:** of the bi-domain diffusion equations with heat flux conditions via explicit method with piecewise constants data.

unstable solution for the mesh size $\Delta x = 1/N = 1/200$ which is shown in the left of Figure 7.29 and for the others in the right panel. These results are not clearly distinguishable. So, we give the zooms at the interface shown in Figure 7.30.

Comparison of the explicit, implicit monolithic and implicit partitioned approach using test case 1

Here we give the comparison of the solution for heat flux coupling conditions via the explicit, implicit monolithic and implicit partitioned coupling iterative approach via using the data given in test case 1. The results are plotted for the mesh size $\Delta x = 1/N = 1/1400$ with corresponding number of time steps $M = 3920$.

The results are shown in the left panel of Figure 7.31, while the zoom at the interface is shown in the right panel. The explicit and monolithic solution are near to each other shown in the dashed and dotted lines while the partitioned solution is represented by the solid line.

7.4 Channel pumping conditions and its special case simplified channel conditions

The discretizations schemes for the channel pumping conditions via the central difference method were derived in (4.35) and (4.36) and for the simplified channel pumping conditions in (4.39) and (4.40). We compute the numerical results for the cosine and constant initial data.

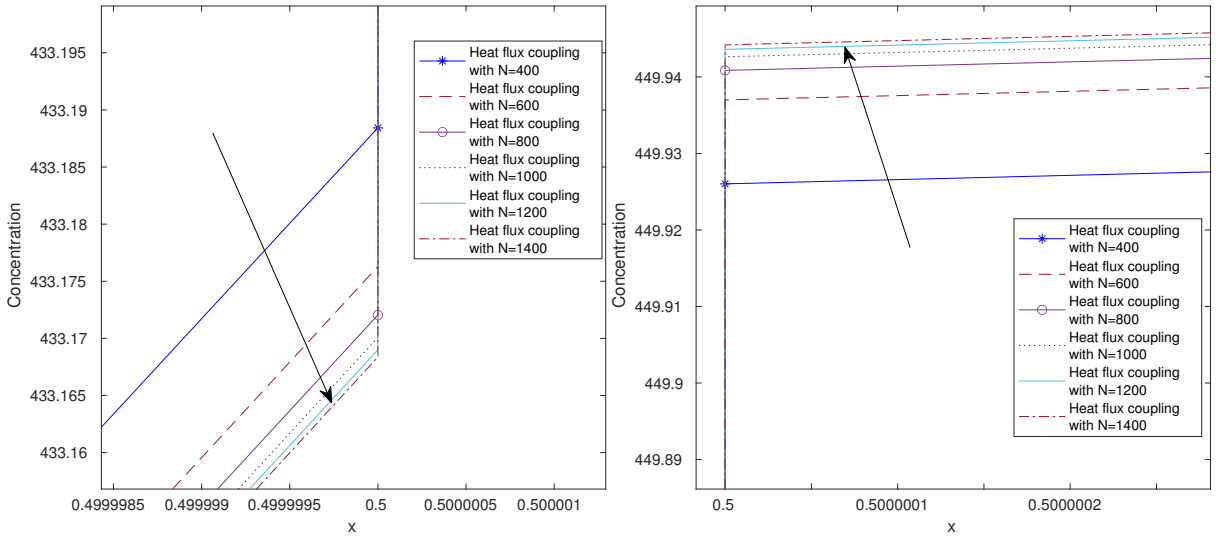

(a) (b)

Figure 7.30: **Zoom of the Figure 7.29 given in the right panel:** Figure in left panel is the zoom near to the interface in the left sub-domain and the right panel is the zoom near to the interface of the right sub-domain.

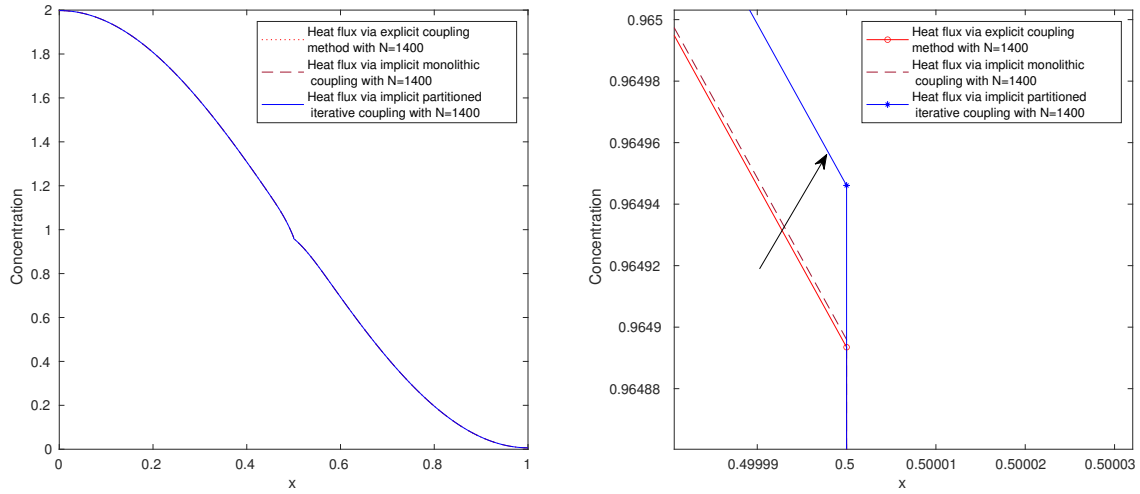

(a) (b)

Figure 7.31: **Comparison:** of the bi-domain diffusion equations with heat flux conditions via the explicit, the implicit monolithic and implicit partitioned approach with cosine initial data.

For these test cases we take the values of the diffusion coefficients from Thul and Falcke [38], $D_- = 222$, $D_+ = 223$, $\psi = 9.3954$, $\alpha = 1.497$, $\beta = 1.1949 \times 10^{-04}$, $\gamma = 1.1444 \times 10^{-07}$ and $\delta = 1.1556 \times 10^{-07}$.

Test case 1, cosine Initial data

Here we give the numerical results for the channel pumping conditions. This test is perform for the initial data $u_0(x) = \cos(\pi x/L)+1$ for $x \in [0, 1/2]$ and $v_0(x) = \cos(\pi x/L)+1$ for $x \in [1/2, 1]$. Further, we used the necessary parameters for the channel pumping conditions given above and the parameters for the computations given in Figure 7.1. The results are given in Figure 7.32. Again these results are not clearly distinguishable, so we make a zoom in at the interface given in the right panel of Figure 7.32. Again we observed the same behavior with changing $\Delta x = 1/N$ as above.

Note that the simplified channel pumping conditions give us unstable solutions for $\psi = 9.3954$ and $\alpha = 1.497$. Then we fixed the value of $\alpha = 1.497$ and changing the values of ψ from 1 to 4. So, for $\psi = 1$ we get the unstable solution for $\Delta x = 1/200$ and $\Delta x = 1/400$, while the stable solutions for Δx smaller than these. The graphical results are similar to the channel pumping conditions. So, there is no need to repeat again.

Further for $\psi = 2$ we get more unstable solutions, i.e. for $\Delta x = 1/200$, $1/400$, $1/600$ and $1/800$, while the stable solutions for $\Delta x = 1/1000$, $1/1200$ and $1/1400$. For $\psi = 3$ we get only a stable solutions $\Delta x = 1/1400$ and smaller than this. It is observed that the parameter ψ in this case play a role like the heat flux coefficient H in the case of heat flux coupling conditions. Finally for $\psi = 4$ and greater than this we get unstable solutions for the mesh sizes given in the table in Figure 7.1 with the fixed α used above. We conclude that, as we increase the value of ψ we will get more unstable solutions.

So the stability for the simplified channel coupling conditions with the explicit discretization depends on mesh size Δx and ψ are in a manner consistent with the stability analysis given in Subsection 6.3.2.

Test case 2, piecewise constant data

This test is performed for the piecewise constant initial data $u_0(x) = 0.06$ for $x \in [0, 1/2]$ and $v_0(x) = 700$ for $x \in [1/2, 1]$. The necessary parameters for the coupling conditions are given above and for the numerical calculation given in Figure 7.1.

The results is shown in the left of Figure 7.33. Again the results are not distinguishable so we make a zoom at the the interface given in the right panel of Figure 7.33. It is observed for the simplified channel pumping conditions we get the same stability as given above for the cosine initial data.

7.5 Membrane pumping coupling computations

The discretized schemes for membrane pumping conditions via the central difference method were derived in (4.43) and (4.44). Here, we only show the comparison of the explicit and implicit partitioned iterative coupling approach for the cosine initial data and for the piecewise constant data. The parameters for these coupling conditions are, the leak

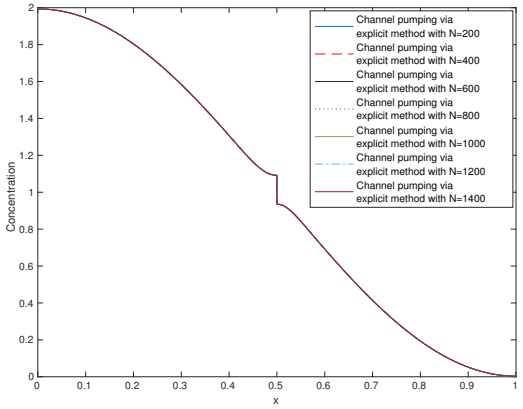

(a)

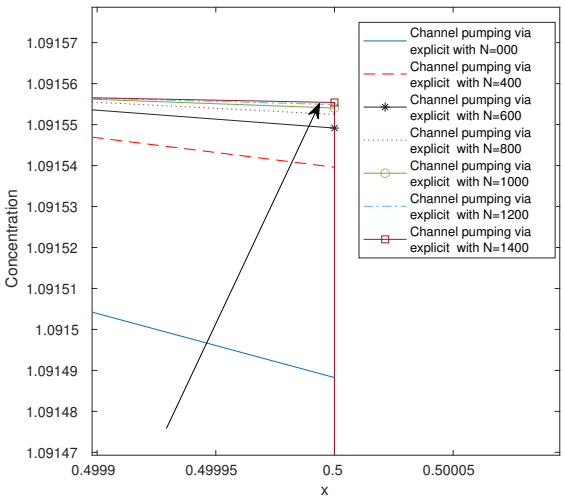

(b)

Figure 7.32: **Bi-domain diffusion equations:** with simplified channel pumping conditions via the explicit method with cosine initial data, while the figure in the right panel is the zoom near to the interface.

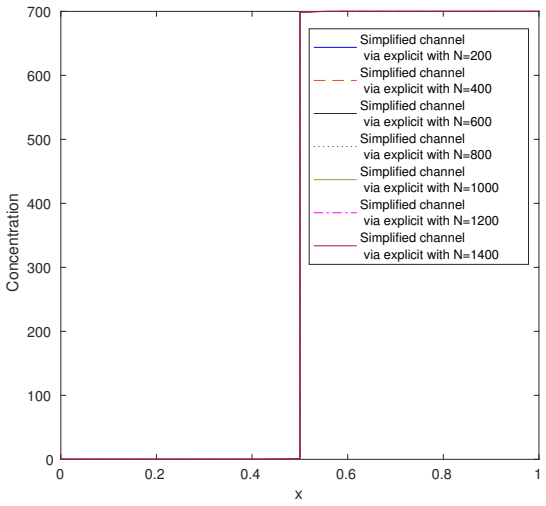

(a)

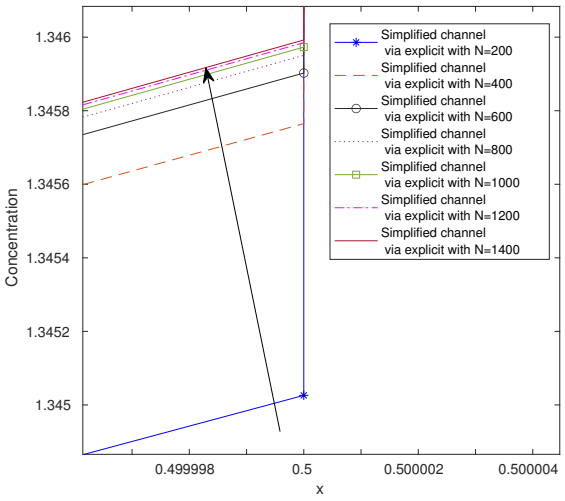

(b)

Figure 7.33: **Bi-domain diffusion equations:** with simplified channel pumping conditions via explicit method with piecewise constant initial data, while the figure in the right panel is the zoom at the interface.

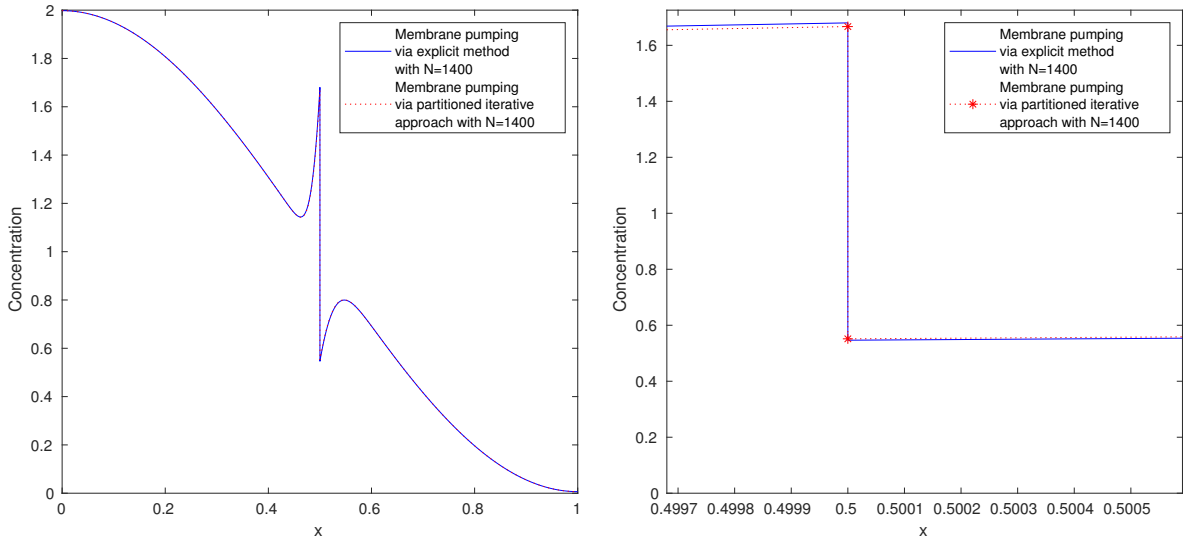

(a) (b)

Figure 7.34: **Comparison:** of the results for the membrane pumping conditions with bi-domain diffusion equations via explicit and implicit partitioned coupling iterative approach, while the right panel is the zoom at the interface.

and other pumping parameters are $P_p = 40000 \times 10^{-6}$, $k_d = 0.2 \times 10^{-6}$, $P_l = 3.3613 \times 10^{-9}$ and $P_c(t) = 3 \times 10^{-3}$. These are taken from Chamakuri [26].

Test case 1, cosine initial data

In this test case we show the comparison of the membrane pumping conditions via explicit coupling and implicit implementation with inital data $u_0(x) = \cos(\pi x/L) + 1$ for $x \in [0, 1/2]$ and $v_0(x) = \cos(\pi x/L) + 1$ for $x \in [1/2, 1]$. We use the diffusion coefficients $D_- = 0.001$, $D_+ = 0.003$, with mesh size $\Delta x = 1/N = 1/1400$ and corresponding number of time steps $M = 3920$. The comparison is given in Figure 7.34.

Test case 2, piecewise constant data

Here, we show the result for the piecewise constant data given above with mesh size $\Delta x = 1/N = 1/1400$ and the corresponding number of time steps $M = 2880$. We make the comparison of the membrane pumping conditions via explicit coupling and implicit partitioned iterative coupling approach. The diffusion coefficients in the ER domain $D_- = 200 \times 10^{-05}$ and in cytosolic sub-domain $D_+ = 200 \times 10^{-06}$. The comparison is given in Figure 7.35.

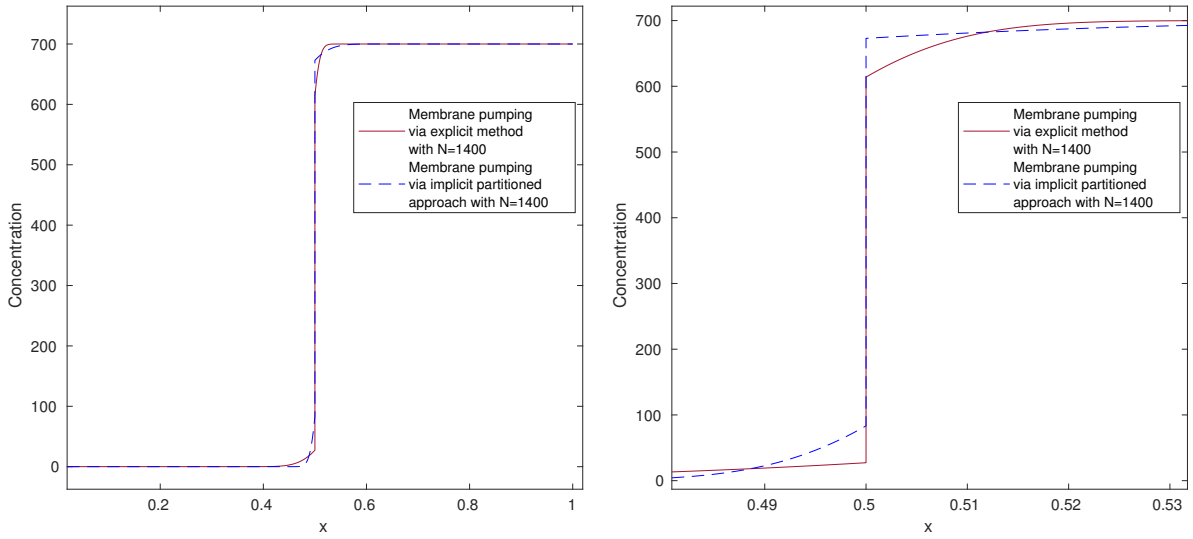

(a) (b)

Figure 7.35: **Comparison:** of the results for the membrane pumping conditions with bi-domain diffusion equations via explicit and implicit partitioned coupling iterative approach, while the figure in the right panel is the zoom at the interface of the left panel.

7.5.1 Results of the simplified membrane pumping coupling condition

The schemes for the membrane conditions were derived in (4.47) and (4.48) via the central difference method. Here show the numerical results for the cosine and constant initial data in the following two tests.

Test case 1, cosine initial data

First, we calculate the solution for the cosine initial data given above. In this case we used the diffusion coefficients, $D_- = 0.001$, $D_+ = 0.003$, with mesh sizes and other parameters given in Figure 7.1. For mesh sizes $\Delta x = 1/200$ and $1/400$ we obtained unstable solutions, while for the mesh sizes smaller than this we obtained the stable solutions. These solutions are plotted in Figure 7.36. The solutions in the right panel are not distinguishable, so we give the zoom in Figure 7.37.

Test case 2, piecewise constant data

This test case is performed for the piecewise constant initial data $u_0(x) = 0.06$ for $x \in [0, 1/2]$ and $v_0(x) = 700$ for $x \in [1/2, 1]$ and the diffusion coefficients $D_- = 200 \times 10^{-05}$ and $D_+ = 200 \times 10^{-06}$ are used. The results are calculated for the different mesh sizes given in Figure 7.1. Again for the mesh sizes $\Delta x = 1/200$ and $1/400$ we obtained unstable solutions, while for the mesh sizes smaller than this we obtained the stable solutions. These solutions are plotted in Figure 7.38. The solutions in the right panel are not clearly

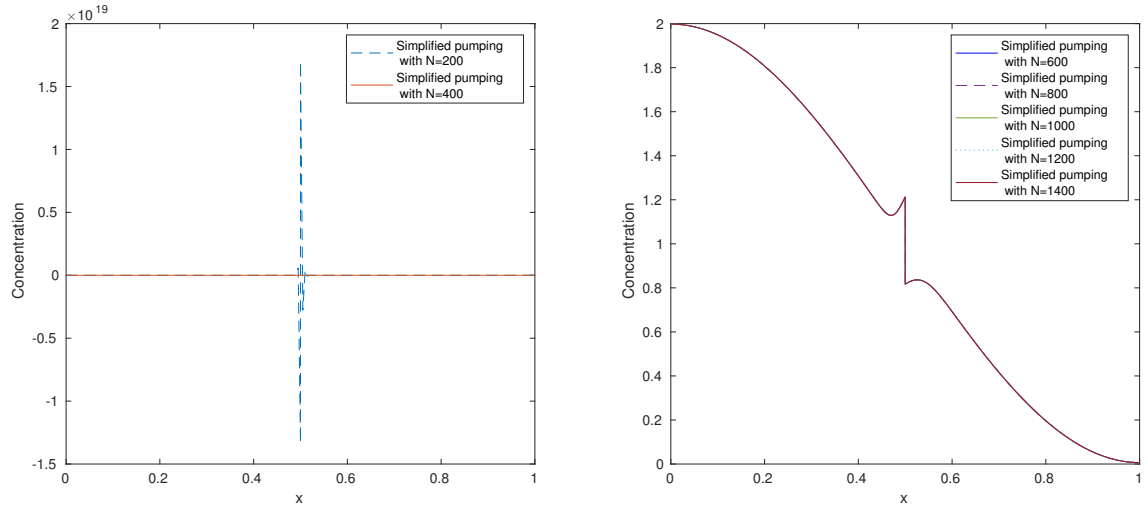

(a) (b)

Figure 7.36: **Bi-domain diffusion equations:** Unstable and stable solution of the simplified membrane pumping conditions via explicit discretization for the cosine initial data.

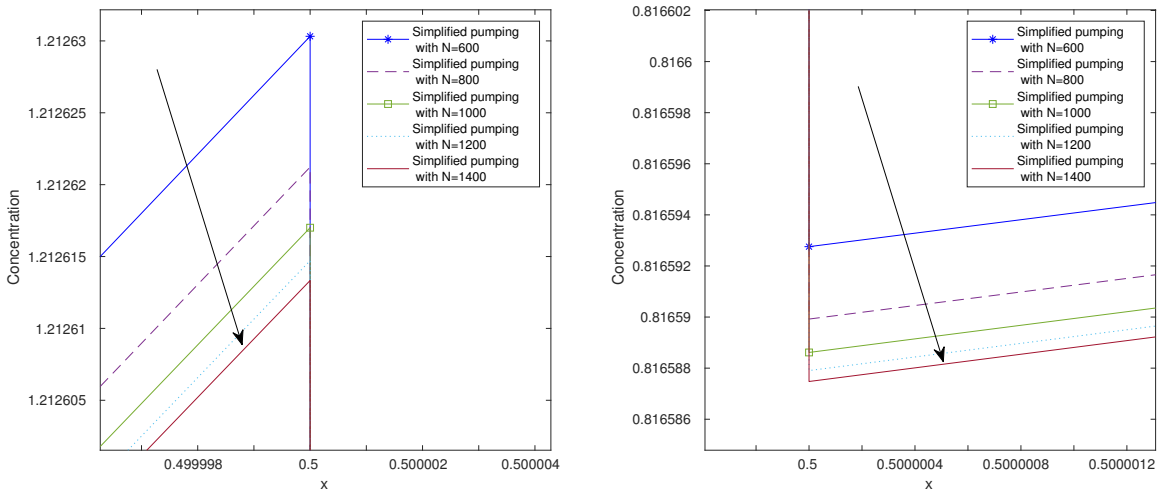

(a) (b)

Figure 7.37: **Zoom of the right panel (b) of Figure 7.36**.

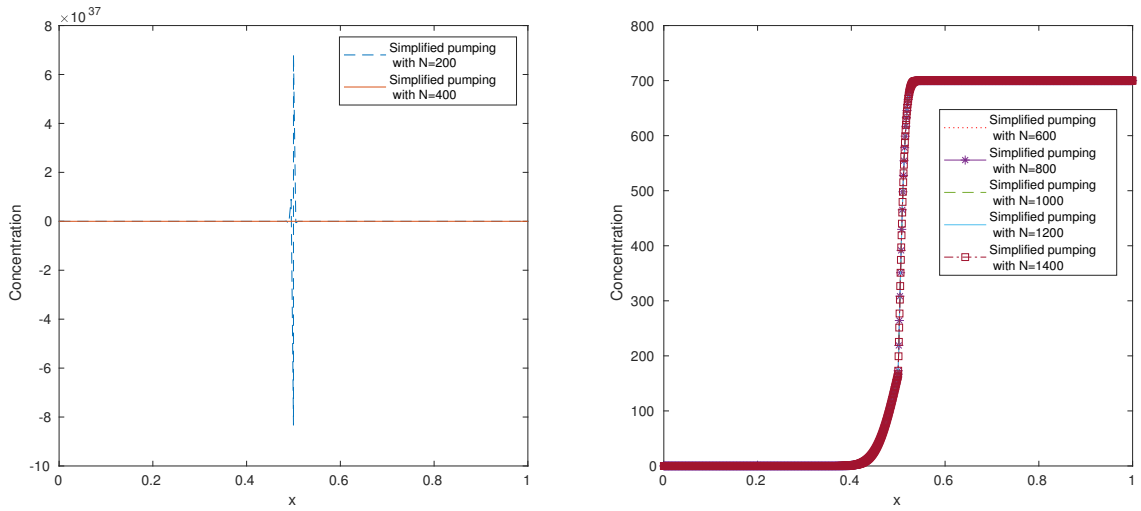

(a) (b)

Figure 7.38: **Bi-domain diffusion equations:** Unstable and stable solution of the simplified membrane pumping conditions via explicit discretization for the piecewise constant initial data.

distinguishable, so we give the zoom in Figure 7.39.

7.6 Combined results for the heat flux, simplified membrane pumping and membrane pumping coupling conditions

The discretized schemes for the heat flux coupling conditions via the central difference method were derived in (4.31) and (4.32). For the membrane pumping conditions in (4.43) and (4.44) and for the simplified membrane pumping conditions in (4.47) and (4.48). We give the numerical results for the cosine and piecewise constant initial data in the following two test cases.

Test case 1, cosine initial data

This test case is performed for the cosine initial data $u_0(x) = \cos(\pi x/L)+1$ for $x \in [0, 1/2]$ and $v_0(x) = \cos(\pi x/L) + 1$ for $x \in [1/2, 1]$. We used the diffusion coefficients $D_- = 0.001$ and $D_+ = 0.003$ with mesh size $\Delta x = 1/N = 1400$ and with corresponding number of time steps $M = 3920$.

The comparison is given in the left panel of Figure 7.40, while the figure in the right panel is the zoom of the solution at the interface of the figure in the left panel. We observed in these coupling conditions the membrane pumping conditions gives more oscillatory behavior as compare to the other two.

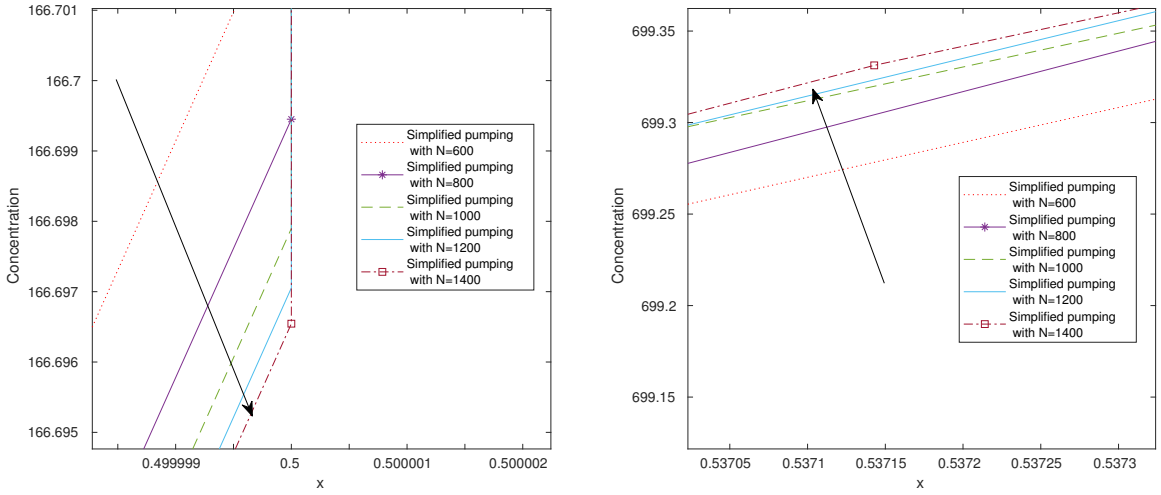

(a) (b)

Figure 7.39: **Zoom of the panel (b) in Figure 7.38.**

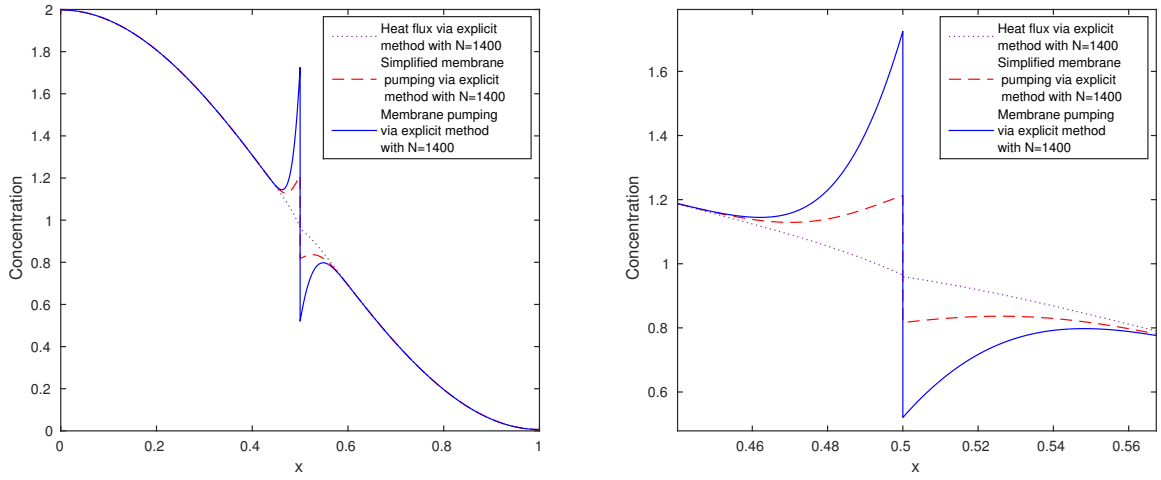

(a) (b)

Figure 7.40: **Comparison:** of the heat flux, simplified membrane pumping and membrane pumping conditions with cosine initial data.

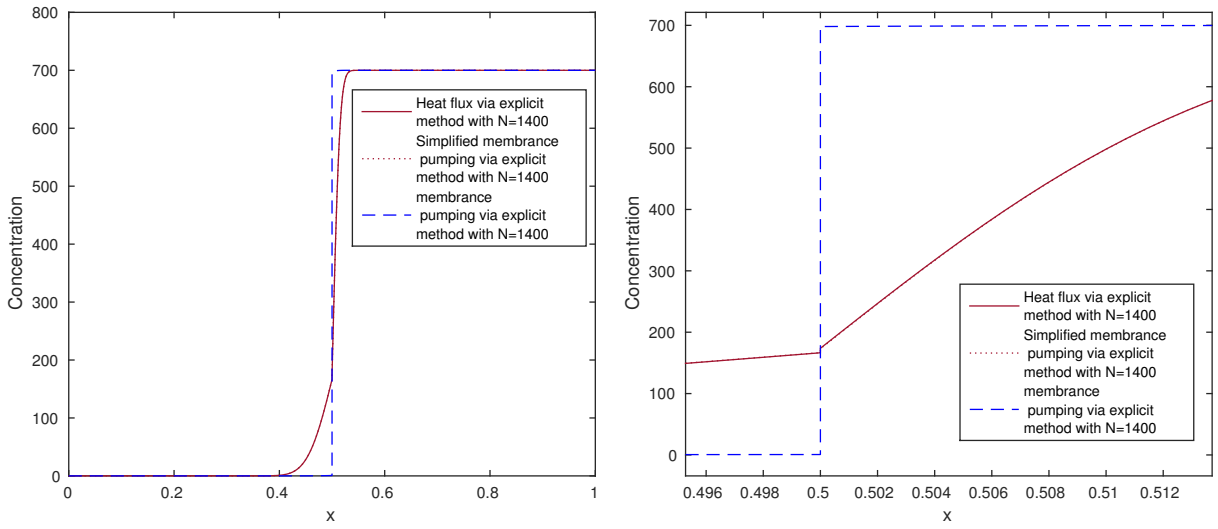

(a) (b)

Figure 7.41: **Comparison:** of the heat flux coupling, simplified membrane pumping and membrane pumping coupling conditions with piecewise constant initial data.

Test case 2, piecewise constant data

The second test case is performed for the piecewise constants values $u_0(x) = 0.6$ and $v_0(x) = 700$ with diffusion coefficients $D_- = 200 \times 10^{-06}$ and $D_+ = 200 \times 10^{-05}$. We plotted the results for the mesh size $\Delta x = 1/N = 1/1400$ and the corresponding number of time steps $M = 3920$.

The comparison is given in Figure 7.41 with zoom at the interface in the right panel. Again we observed that the solution of the membrane pumping conditions is approaches to the solution faster as compare to the other two. The result for the membrane pumping conditions is clearly seen in the figure, while the other two are on the top of each other. Note that in a very higher zoom these two can be also distinguishable.

7.6.1 Results of the linearized membrane pumping coupling

The schemes for the linearized membrane conditions via the central difference method with explicit discretization were derived in (4.51) and (4.52) for the implicit monolithic approach in (4.71) and (4.72) and for the implicit partitioned iterative approach in (4.73) and (4.74). Here show the numerical results for the cosine and piecewise constant initial data and with various diffusion coefficients.

Test case 1, cosine initial data

This test is performed for the cosine initial data $u_0(x) = \cos(\pi x/L) + 1$ for $x \in [0, 1/2]$ and $v_0(x) = \cos(\pi x/L) + 1$ for $x \in [1/2, 1]$ and the diffusion coefficients $D_- = 0.001$ and $D_+ = 0.003$ are used.

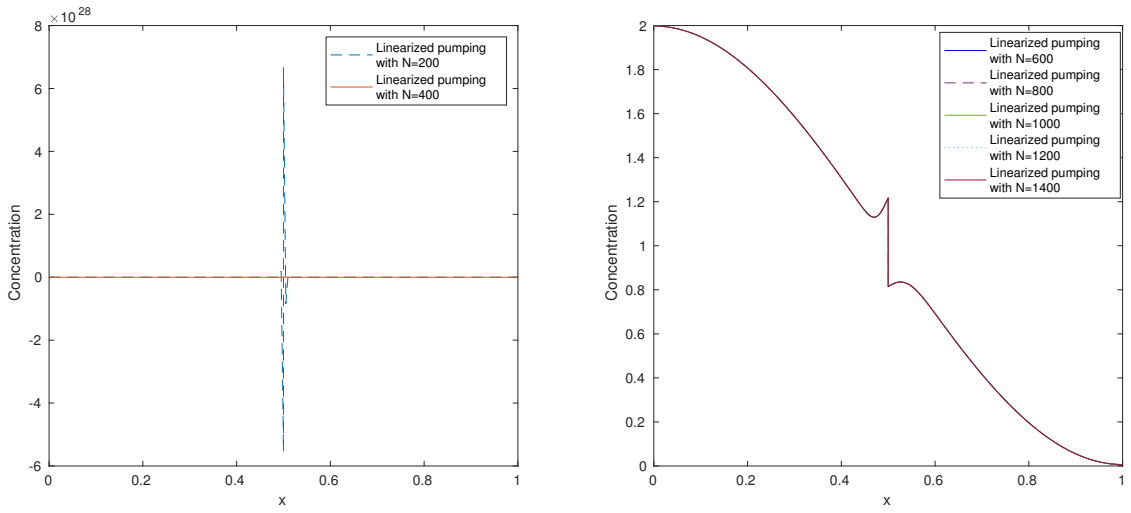

(a) (b)

Figure 7.42: **Unstable and stable solutions:** of the linearized membrane conditions via explicit method.

Note that for the mesh size $\Delta x = 1/N = 200$ and $1/400$ we get unstable solutions. This is shown in the Figure 7.42. While we get the stable solutions for the remaining values of Δx given in Figure7.1, i.e. $\Delta x = 1/N = 600$ to $1/1400$. These stable solutions are given in the Figure 7.43 with the zoom at the interface. The detail for this were explained in the stability Chapter 6 in the in Section 6.3.2.

Also we calculate the results via implicit monolithic and partitioned coupling iterative approach for the same data used above. The results are plotted for the necessary parameters given in Figure 7.1. We observed that the implicit solution is always stable and have no restriction on the the spatial mesh size Δx. While the explicit method have a restriction on the size of Δx for the stability.

The stable solutions are plotted for the implicit monolithic approach in Figure 7.44. Analogously we get the same observation for the implicit partitioned coupling iterative approach. But there is no need to show the repetitive results again. But we show a comparison for the solutions obtained via the three methods, namely explicit, implicit monolithic and implicit partitioned iterative method.

Comparison via explicit, implicit monolithic and implicit partitioned approach

Here we give the comparison via an explicit, an implicit monolithic approach and an implicit partitioned coupling approaches. The comparison is plotted for the diffusion coefficients $D_- = 0.001$, $D_+ = 0.003$ and with cosine initial data used above and with mesh size $\Delta x = 1/N = 1/1400$. The results are shown in the Figure 7.45 with zoom at the interface. Also we found a very good agreement between these three methods.

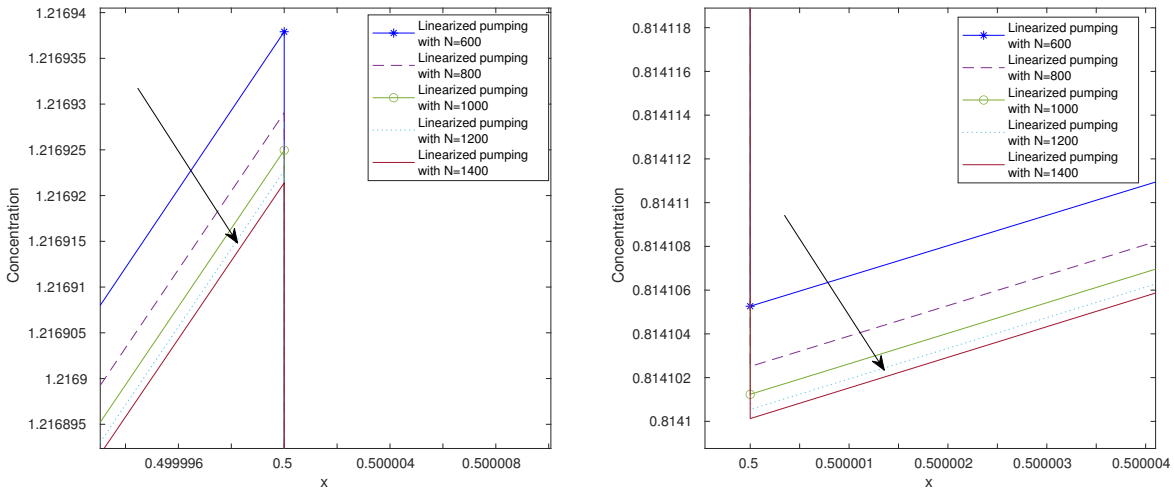

(a) (b)

Figure 7.43: **Zoom of the Figure 7.42 (b)**

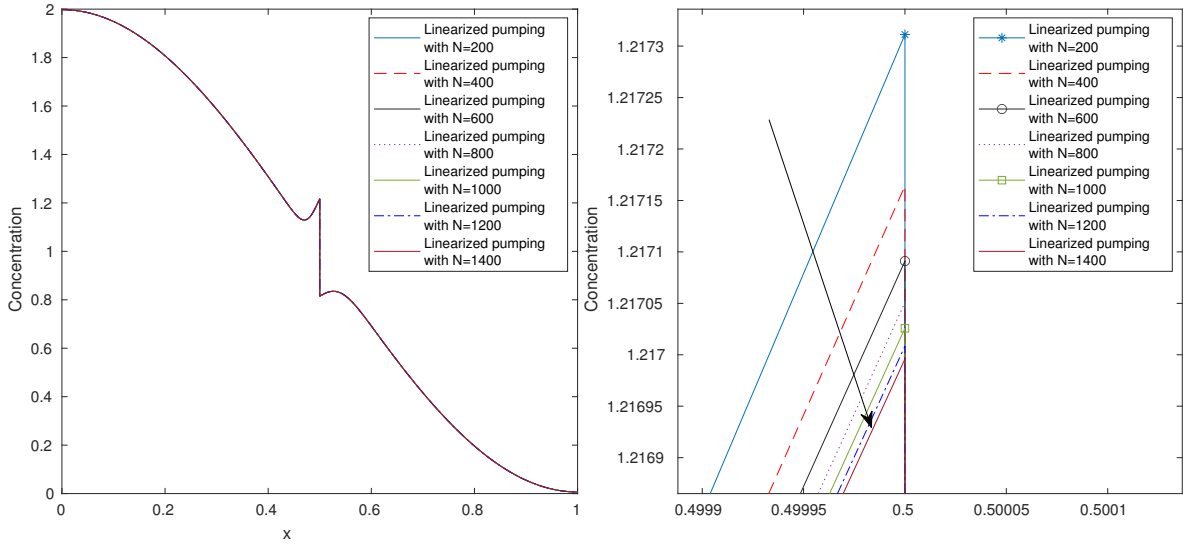

(a) (b)

Figure 7.44: **Bi-domain diffusion equation:** results of the linearized membrane pumping coupling conditions via implicit monolithic coupling approach, while the figure in the right is the zoom at the interface.

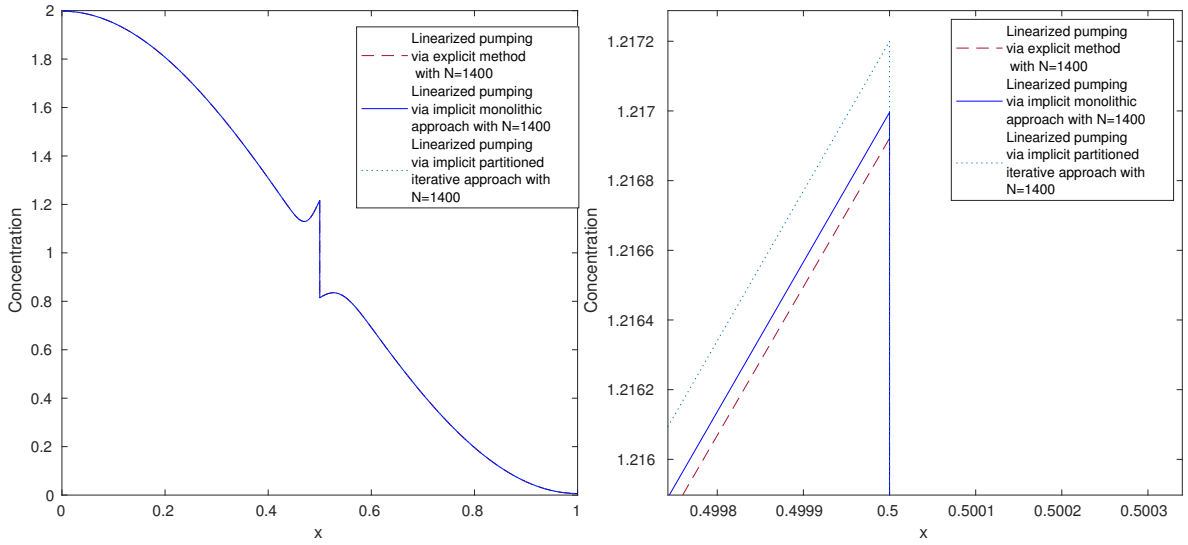

(a) (b)

Figure 7.45: **Comparison:** the left panel represents the result of the linearized membrane pumping coupling conditions with bi-domain diffusion equations via explicit, implicit monolithic and implicit partitioned coupling iterative approaches, while the panel is the zoom at the interface of the left.

Test case 2, piecewise constants initial data and smaller diffusion coefficients

In this case we give the results for the piecewise constant initial data $u_0(x) = 0.06$ for $x \in [0, 1/2]$ and $v_0(x) = 700$ for $x \in [1/2, 1]$. In this computation we used the diffusion coefficients $D_- = 200 \times 10^{-05}$ and $D_+ = 200 \times 10^{-06}$.

Analogously, here we also get an unstable solution for the large value of Δx, i.e. $\Delta x = 1/N = 200$ and $N = 1/400$. While we get the stable solutions for the mesh size $\Delta x = 1/N = 1/600$ to $1/1400$, i.e. for smaller enough . The results of the stable solutions are shown in Figure 7.46 with the zoom at the interface. The comparison shows the result is converging with increasing the value of N means to decrease the value of mesh size Δx.

In this case we also obtained a stable solution even for a large value of $\Delta x = 1/200$ via implicit monolithic approach and implicit partitioned iterative coupling approach. While there is no need to give repetitive results again.

Comparison

In this test case we show the comparison of the results for linearized membrane pumping coupling conditions via explicit, implicit monolithic and implicit partitioned coupling iterative approaches for the piecewise constant data used above with mesh size $\Delta x = 1/1400$. We used the diffusion coefficients $D_- = 200 \times 10^{-06}$ and $D+ = 200 \times 10^{-05}$. Again, we found a good agreement between these three methods shown in Figure 7.48 with the zoom near to the interface.

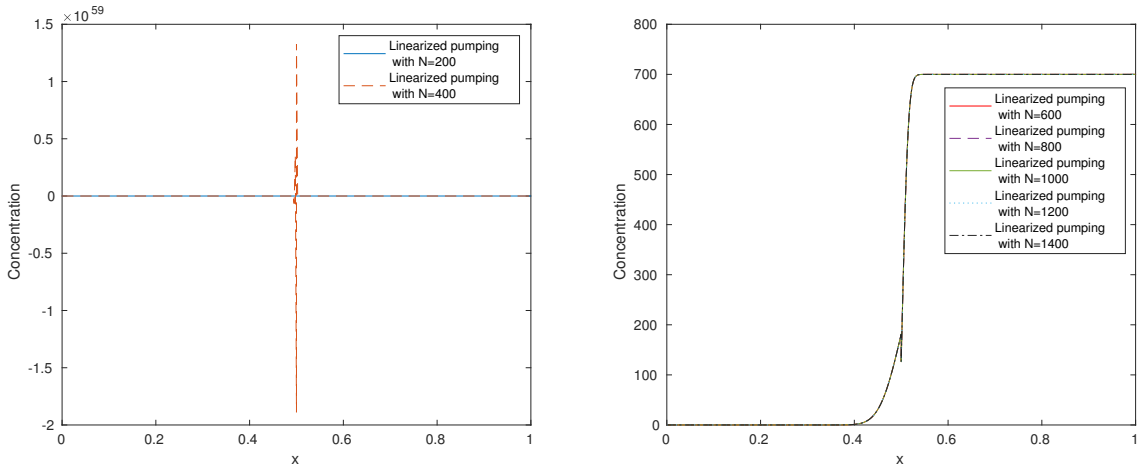

(a) (b)

Figure 7.46: **Unstable and stable solutions:** of the linearized membrane pumping coupling interface conditions via explicit discretization method with piecewise constant data, while the right panel is the zoom at the interface.

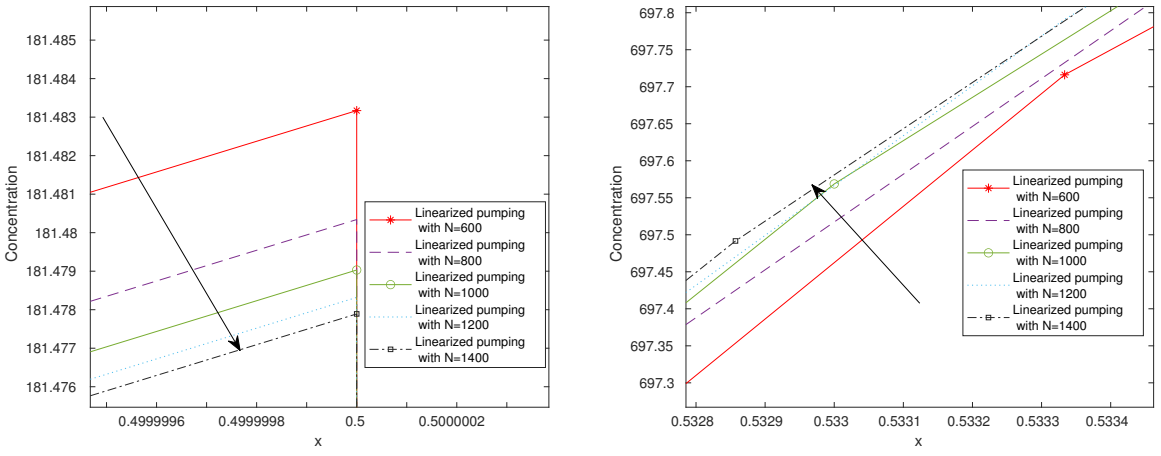

(a) (b)

Figure 7.47: **Zoom of the Figure 7.46 of panel (b)**.

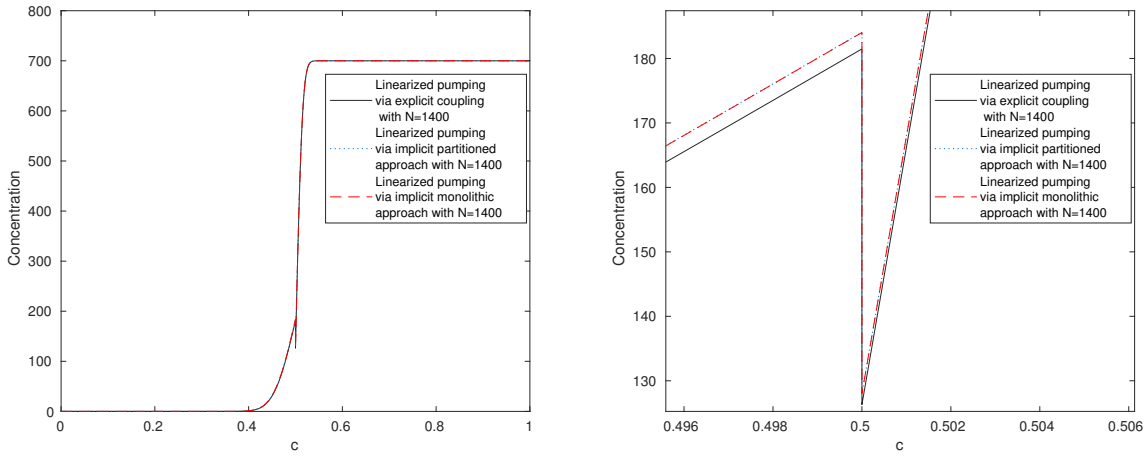

(a) (b)

Figure 7.48: **Comparison:** of the linearized membrane pumping coupling conditions via the explicit, the implicit monolithic and the implicit partitioned coupling iterative approaches with constant data, while the right panel is the zoom near to the interface.

7.7 Solution times and iteration counts

Here we calculate the solution times and for the explicit, implicit monolithic and implicit partitioned iterative approaches for the various coupling conditions. These coupling conditions include the Dirichlet-Neumann coupling, heat flux, linearized pumping and membrane pumping conditions with bi-domain diffusion equations. The solution time comprises the total time of computation. Also we obtain the iteration number for the partitioned iterative approach to achieve the the residual for the prescribe tolerance TOL. We used a tolerance $TOL = 0.00001$ for the partitioned iterative coupling approach. Also, we calculate the number of iteration for the partitioned iterative method. We calculate the computation for the mesh size $\Delta x = 1/N = 1/2000$ with corresponding time steps $M = 8000$ and for the cosine initial data. As we know that the explicit solution take less time as compare to the implicit but this have a restriction on time steps. Because there is no such iteration required to obtained the required solution in the explicit method.

Further, we concluded in Table 7.1 that the implicit partitioned iterative coupling approach take less time as compare to the implicit monolithic approach. This depends on the size of a matrix because in the monolithic approach we keep all the data in a one big matrix which take more time in the terms of storage and computational work. The counterpart is the partitioned iterative approach. That solves two different matrix sub-systems which calculate the solutions faster than the monolithic approach. Also we concluded that when we decrease the tolerance TOL then we need more iterations to achieve the required solution. These results are shown in the Table 7.1 for the computational time and the iteration counts. Moreover for the nonlinear membrane pumping we did not calculate the implicit monolithic solution because we put the entries corresponding to the each unknown in a matrix. Here this not possible. But surely we calculated the

solution of its special case a linearized membrane pumping case via monolithic approach.

In Table 7.1 DN-coupling is for the Dirichlet-Neumann coupling, (s) represents the computational time in seconds, Lin: pum: for the linearized pumping, Mem: pum: is for the membrane pumping , Implicit (M) is the implicit monolithic and Implicit (P) is for the implicit partitioned coupling iterative approach.

For these numerical computations and all others in this thesis we used a CPU systems, Intel xeon(R) CPU E5640.

Table 7.1: Solution times and iteration counts of the explicit, implicit monolithic and implicit partitioned coupling iterative solvers for the Dirichlet-Neumann coupling, heat flux, linearized pumping and membrane pumping conditions with the bi-domain diffusion equation. The solution time comprises the total time of computation.

Solver	DN-coupling (s)	Heat flux (s)	Linearized mem: pum (s)	Membrane pum:(s)	Iterations
Explicit	52.12	52.45	52.21	53.51	–
Implicit(M)	347.30	332.78	331.78	–	–
Implicit(P)	147.78	153.87	153.36	311.31	10

Chapter 8

Summary and conclusion

The aim of this thesis was to study various coupling conditions with bi-domain diffusion equations. We modified a 3D model of Falcke [7] to one dimensional bi-domain equations with various coupling interface conditions. The coupling conditions are linear and non-linear coupling conditions. The major achievements of this thesis are given as follows.

- Three algorithms are discussed: namely explicit coupling algorithm (A1), implicit monolithic coupling algorithm (A2) and the implicit partitioned iterative coupling algorithm (A3). These algorithms are implemented for the various coupling conditions that were considered in Chapter 4.

- The discrete mass conservation for the single as well as for the bi-domain diffusion equations with various numerical coupling conditions has been derived for various discretization methods. It was found that in case of finite volume discretizations the one sided difference maintains the discrete mass conservativity. While the central difference approach maintains discrete mass conservativity in the nodal based case.

- The well known Godunov-Ryabenkii stability conditions have been studied for the various coupling conditions in this thesis. We obtained stable and unstable cases for these coupling conditions. We also studied the stability conditions for the single domain diffusion equation via von Neumann analysis and the GR-stability for the explicit, implicit as well as for the finite volume discretization methods.

- For the stability analysis of the coupling conditions we extended an approach from previous studies of Giles [10], Roe et al. [33], Errera and Chemin [6] and Zhang et al. [40]. We implement the procedure used by Godunov-Ryabenkii [11] to derive the stability analysis. Also many previous studies are based on the procedure of Giles [10]. In the study of Giles the selection of the roots of the quadratic equation of the normal mode equation was unclear. We proved the selection of the roots q_1 and q_2 such that $|q_1| \leq 1$ and $|q_2| \geq 1$ in Chapter 7. One can follow our procedure or the procedure of Giles [10] for further investigation. The Giles one gives the stability asymptotically. While our procedure gives an exact condition for stability.

- The truncation error, L_1 error and the numerical order of convergence have been discussed for the single as well as for the bi-domain diffusion equations with Dirichlet-

Neumann coupling with the identical diffusion coefficients $D_1 = D_2$ have been computed in order to check the coupling.

- The computational time for the above three proposed algorithms has been calculated.

Chapter 9

Open problems

In this chapter we summarize various questions or problems that arise in this work. Some of them might be easily solvable, whereas others may need thorough investigations.

Problem 1

So far we included the explicit and implicit discretization methods for the bi-domain diffusion equations together with the boundary and coupling interface conditions. Other discretization methods can be used, such as semi-implicit coupling, for further investigation.

Problem 2

Three algorithms were used in this thesis, namely explicit coupling, implicit monolithic coupling and implicit partitioned coupling approach for the one dimensional case of the 3D model of Falcke [7]. This work can be extended to the two and three dimensional cases together with the coupling conditions. Also we discuss the implementation and other necessary properties of the numerical analysis such as discrete mass conservativity, stability and error analysis. These properties can be used and extended to the two and three dimensional cases.

Problem 3

We obtain the discrete mass conservativity for all the coupling conditions that we considered. In this work we concluded that to discretize the Dirichlet-Neumann coupling conditions via one sided differences maintains conservativity in finite volume schemes . While in the case of nodal based schemes central differences maintain conservativity. Maybe some other strategies such as FEM-FVM etc. can be considered for further investigation.

Problem 4

In this thesis we considered a calcium dynamics model taking realistic values of parameters from Chamakuri [26], and Thul [37]. This can be further studied with the reaction and kinetic terms and compared with the experimental results.

Bibliography

[1] M. Abramowitz and I. A. Stegun. *Handbook of mathematical functions. Dover Publications Inc. New York*, 1972.

[2] F. Blom. A monolithic fluidstructure interaction algorithm applied to the piston problem. *Computer Methods in Applied Mechanics and Engineering*, 167:369–391, 12 1998.

[3] K. E. Brenan, S. L. Campbell, and L. R. Petzold. *Numerical solution of initial-value problems in differential-algebraic equations*. SIAM, 1995.

[4] E. Carr and N. March. Semi-analytical solution of multilayer diffusion problems with time-varying boundary conditions and general interface conditions. *Applied Mathematics and Computation*, 333:286–303, 09 2018.

[5] B. N. Datta. *Numerical linear algebra and applications*, volume 116. SIAM, 2010.

[6] M.-P. Errera and S. Chemin. Optimal solutions of numerical interface conditions in fluid–structure thermal analysis. *Journal of Computational Physics*, 245:431–455, 2013.

[7] M. Falcke. On the role of stochastic channel behavior in intracellular Ca2+ dynamics. *Biophysical journal*, 84(1):42–56, 2003.

[8] C. Felippa, K. C. Park, and C. Farhat. Partitioned analysis of coupled system. *Computer Methods in Applied Mechanics and Engineering*, 190:32473270, 03 2001.

[9] M. Fernndez, J. Mullaert, and M. Vidrascu. Explicit Robin-Neumann schemes for the coupling of incompressible fluids with thin-walled structures. *Computer Methods in Applied Mechanics and Engineering*, 267:566–593, 12 2013.

[10] M. B. Giles. Stability analysis of numerical interface conditions in fluid–structure thermal analysis. *International journal for numerical methods in fluids*, 25(4):421–436, 1997.

[11] S. K. Godunov and V. S. Ryabenki. *Theory of difference schemes-an introduction. North Holland, Amsterdam*, 1964.

[12] B. Gustafsson. The Godunov-Ryabenkii condition: The beginning of a new stability theory. In *Godunov Methods*, pages 425–443. Springer, 2001.

[13] B. Gustafsson, H.-O. Kreiss, and A. Sundström. Stability theory of difference approximations for mixed initial boundary value problems. II. *Mathematics of Computation*, pages 649–686, 1972.

[14] S. Heikkila and V. Lakshmikantham. *Monotone iterative techniques for discontinuous nonlinear differential equations*, volume 181. CRC Press, 1994.

[15] W. D. Henshaw and K. K. Chand. A composite grid solver for conjugate heat transfer in fluid–structure systems. *Journal of Computational Physics*, 228(10):3708–3741, 2009.

[16] N. J. Higham. *Accuracy and stability of numerical algorithms*, volume 80. SIAM, 2002.

[17] S. Hu. Differential equations with discontinuous right-hand sides. *Journal of Mathematical Analysis and Applications*, 154:377390, 01 1991.

[18] J. C. Jaeger and H. S. Carslaw. *Conduction of heat in solids*. Clarendon Press Oxford, 1959.

[19] J. Koivumäki, T. Korhonen, and P. Tavi. Impact of sarcoplasmic reticulum calcium release on calcium dynamics and action potential morphology in human atrial myocytes: A computational study. *PLoS computational biology*, 7:e1001067, 01 2011.

[20] D. Kuhl. *Modellierung und Simulation von Mehrfeldproblemen der Strukturmechanik*. PhD thesis, Ruhr-Universität Dortmund, 2005.

[21] S. Lang. *Parallele Numerische Simulation instationärer Probleme mit adaptiven Methoden auf unstrukturierten Gittern*. PhD thesis, Universität Stuttgart, 2007.

[22] F. Lemarié, E. Blayo, and L. Debreu. Analysis of ocean-atmosphere coupling algorithms: consistency and stability. *Procedia Computer Science*, 51:2066–2075, 2015.

[23] R. Moretti, M.-P. Errera, V. Couaillier, and F. Feyel. Stability, convergence and optimization of interface treatments in weak and strong thermal fluid-structure interaction. *International Journal of Thermal Sciences*, 126:23–37, 2018.

[24] K. Morton and D. Mayers. *Numerical solution of partial differential equations An introduction*. Cambridge University Press Cambridge, 1994.

[25] S. Müthing. *A flexible framework for multi-physics and multi-domain PDE simulation*. PhD thesis, University of Stuttgart, February 2015.

[26] C. Nagaiah. *Adaptive numerical simulation of reaction-diffusion systems*. PhD thesis, University of Magdeburg, 2007.

[27] L. Olsen-Kettle. Numerical solution of partial differential equations. *Lecture notes at University of Queensland, Australia*, 2011.

[28] J. W. Putney Jr. and G. S. J. Bird. The inositol phosphate-calcium signaling system in nonexcitable cells. *Endocrine Reviews*, 14(5):610–631, 1993.

[29] A. Quarteroni and S. Quarteroni. *Numerical models for differential problems*, volume 2. Springer, 2009.

[30] A. Quarteroni, F. Saleri, and P. Gervasio. *Scientific computing with MATLAB and Octave*, volume 2. Springer, 2006.

[31] A. Quarteroni and A. Valli. *Domain decomposition methods for partial differential equations*. Oxford University Press, Oxford, 1999.

[32] B. Roe, A. Haselbacher, and P. H. Geubelle. Stability of fluid–structure thermal simulations on moving grids. *International journal for numerical methods in fluids*, 54(9):1097–1117, 2007.

[33] B. Roe, R. Jaiman, A. Haselbacher, and P. H. Geubelle. Combined interface boundary condition method for coupled thermal simulations. *International journal for numerical methods in fluids*, 57(3):329–354, 2008.

[34] H. Seppo. On functional-differential equations with discontinuous right-hand side in ordered banach spaced. *Funkcialaj Ekvacioj*, 33:519–526, 01 1990.

[35] A. Spencer. Constitutive theory for strongly anisotropic solids. *Continuum Theory of the Mechanics of Fibre-Reinforced Composites*, 282, 01 1984.

[36] C. Taylor. Inositol trisphosphate receptors: Ca2+-modulated intracellular Ca2+ channels. *Biochimica et biophysica acta*, 1436:19–33, 01 1999.

[37] R. Thul. *Analysis of intracellular reaction diffusion systems: The stochastic medium Calcium*. PhD thesis, Free University, Berlin, November, 2004.

[38] R. Thul and M. Falcke. Release currents of IP3 receptor channel clusters and concentration profiles. *Biophysical journal*, 86(5):2660–2673, 2004.

[39] G. Wanner and E. Hairer. *Solving ordinary differential equations II*. Springer, Berlin Heidelberg, 1996.

[40] H. Zhang, Z. Liu, E. Constantinescu, and R. Jacob. Stability analysis of interface conditions for ocean-atmosphere coupling. *arXiv preprint arXiv:1909.00916*, 2019.

[41] O. Zienkiewicz, R. Taylor, and P. Nithiarasu. *The Finite Element Method Vol 3 Fluid Dynamics*. Butterworth-Heinemann, Oxford, 2005.